

Electronic Properties of Single-layered Transition Metal Dichalcogenides

João Eduardo Henriques Braz

Thesis to obtain the Master of Science Degree in

Engineering Physics

Advisors: Prof. Eduardo Filipe Vieira de Castro
Prof. Nuno Miguel Reis Peres

Examination Committee

Chairperson: Prof.^a Susana Isabel Pinheiro Cardoso de Freitas
Advisor: Prof. Eduardo Filipe Vieira de Castro

Members of the Committee: Prof. Pedro Domingos Santos do Sacramento
Prof. Balázs Dóra

November 2015

Acknowledgments

First and foremost, I thank my parents and my family for their unerodable support, and for making it possible for me to comfortably pursue my dreams and ambitions.

I thank Ana Lúcia, for her love and its byproducts, especially the patience and support, and for inspiring me to always do better.

I thank my friends and colleagues, for being able to get my mind completely off of work just as well as they are able to make me think deeply about it.

Last, but not least, I thank my advisor, for his remarkable guidance, support and cooperation.

Abstract

The now decade-old discovery of two-dimensional materials has originated a wealth of new physics to explore and apply. Although the star of this discovery has been graphene, other materials have accompanied it since the beginning of the isolation and study of these novel systems. A class of such materials are the transition metal dichalcogenides, sharing features such as a honeycomb lattice and topologically non-trivial Dirac cones. These materials, however, possess a band gap and, due to the high atomic number of transition metals, display sizeable effects of spin-orbit coupling.

The research work presented here has been an effort to further understand the nature and consequences of electronic interactions to the single-electron description and the existence of a possible broken symmetry phase.

To that end, the study and review of an established effective band model for these systems has been carried out, from which a low-energy description was derived.

Using this theory, the self-energy correction to the bare propagator in the Hartree-Fock approximation was computed. Due to the expectedly feeble screening in a gapped 2D material, a long-range Coulomb interaction was considered. A renormalization of the gap was estimated for both the undoped and the hole doped system.

A Hubbard model for this theory was then used to predict the possible existence of a spin and valley polarized phase in the hole doped system. It is shown that this phase displays an anomalous Hall response.

Keywords: 2D materials, transition metal dichalcogenides, electron interactions, self-energy correction, Hubbard model, spin-valley physics

Resumo

A descoberta, de há uma década, de materiais bidimensionais originou um vasto leque de nova física para explorar e aplicar. Apesar de a estrela desta descoberta ter sido o grafeno, outros materiais o têm acompanhado desde o início da isolação e estudo destes novos sistemas. Uma classe destes materiais são os dicalcogenetos de metais de transição, que partilham características com o grafeno tais como uma rede hexagonal e cones de Dirac topologicamente não-triviais. Estes materiais, porém, possuem um hiato e, devido ao elevado número atómico dos metais de transição, demonstram efeitos de acoplamento spin-órbita assinaláveis. O trabalho de investigação apresentado foi um esforço para aprofundar a compreensão da natureza e consequências das interacções electrónicas para a descrição de bandas e da existência de possíveis fases de simetria quebrada.

Com essa finalidade, levou-se a cabo o estudo e revisão de um modelo efectivo de três bandas já estabelecido, a partir do qual uma descrição de baixa energia foi obtida.

Com esta teoria calculou-se a correcção de auto-energia para o propagador desrido, na aproximação de Hartree-Fock. Devido à fraca blindagem num material 2D com hiato, considerou-se uma interacção de Coulomb de longo-alcance. Estimou-se uma renormalização para os sistemas não-dopado bem como dopado de lacunas.

Finalmente, usou-se um modelo de Hubbard nesta teoria para prever a possível existência de uma fase polarizada em spin e valley no sistema dopado de lacunas. Mostrou-se que esta fase possui uma resposta de Hall anómala.

Keywords: materiais 2D, dicalcogenetos de metal de transição, interacções electrónicas, correcção de auto-energia, modelo de Hubbard, física de spin-valley

Contents

List of Tables	xi
List of Figures	xiii
I Introduction and Band Structure	1
1 State of the art	3
1.1 The discovery of graphene and the rise of 2D-materials	3
1.2 The superlatives and the shortcomings of graphene	4
1.3 A companion family: Group-VI transition metal dichalcogenides	6
1.4 Outline	12
2 An effective three-band tight-binding Hamiltonian	13
2.1 Spinless tight-binding model	14
2.1.1 Discrete symmetries of the Hamiltonian and Group Theory analysis	14
2.1.2 Representations and computation of hopping matrices	17
2.2 Spinful tight-binding Hamiltonian	21
2.2.1 Basis states and tight-binding Hamiltonian with spin-orbit coupling	21
3 Continuum limit and Berry curvature	23
3.1 Computation of the Dirac Hamiltonian	24
3.1.1 Taylor expansion of the TB Hamiltonian	24
3.1.2 1st and 2nd order Perturbation Theory for the spinless TB-Hamiltonian . .	26
3.1.3 1st and 2nd order Perturbation Theory for the SOC-TB Hamiltonian . .	32
3.1.4 Effective masses	33
3.2 Hall effects in inversion symmetry broken honeycomb lattices	35
3.2.1 Berry connection and Berry curvature	35
3.2.2 Hall conductivity	37

II Electron-Electron Interactions	43
4 Perturbation Theory and self-energy correction to the electronic structure	45
4.1 1st order self-energy in the continuum limit	45
4.1.1 Tight-binding description of electronic interactions	45
4.1.2 Evaluation of the matrix elements of the interaction	48
4.2 Gap renormalization	52
4.2.1 Undoped system	52
4.2.2 Hole-doped system	54
5 Broken symmetry phases - Hubbard model	57
5.1 General formulation for TMDCs	57
5.1.1 Intra- and inter-orbital couplings, validity of the Hubbard model	58
5.1.2 Path-integral formulation	59
5.2 Low-energy theory	61
5.2.1 Saddle-point solution	62
5.2.2 Action expansion	65
5.2.3 Anomalous Hall effect in the spin-valley-polarized phase	72
5.3 Dependence on the Fermi level	76
5.3.1 Intermediate doping regime: $\mu_B < \mu_0 < \mu_A$	77
5.3.2 High doping regime: $\mu_0 < \mu_B$	79
6 Conclusions and future work	83
Bibliography	85
A Perturbation theory for the tight-binding Hamiltonian	97
B Quantum adiabatic theorem and Berry curvature	101
B.1 Adiabatic time evolution of a quantum system	101
B.1.1 Quantum adiabatic theorem	101
B.1.2 Berry phase and Berry curvature	103
B.1.3 1st order adiabatic approximation	106
B.2 Bloch bands and Hall effects	107
B.2.1 Brillouin zone as a parameter space	107
B.2.2 Velocity under adiabatic evolution	108
B.2.3 Bloch electrons in an electric field	109
C Perturbation theory for the electron propagator, self-energy correction	113
C.1 Path Integral approach to Statistical Quantum Mechanics	113
C.1.1 Grand-partition function of a non-interacting theory	114
C.1.2 Green's functions - bare propagator	115

C.1.3	Matsubara frequency sums	119
C.2	Green's functions - Perturbation Theory	121
C.2.1	1st order contribution to the propagator	122
C.2.2	Dyson's equations, self-energy correction of the bare propagator	125
C.3	Conservation of crystal momentum from the Coulomb potential	126
D	The Gibbs-Bogoliubov-Feynman inequality and the Hubbard-Stratonovich action approaches to the mean-field problem	129
D.1	Mean-field from a variational free energy using the Gibbs-Bogoliubov-Feynman inequality	129
D.2	Perturbative expansion of the fermionic term in the Hubbard-Stratonovich action	135

List of Tables

2.1	Multiplication table of the subset of Eq. (2.5). Elements of the top row are multiplied by elements of the leftmost column.	15
2.2	Hopping matrices and representations of operations relevant to their computation. (Read: upper sign, left index; lower sign, right index).	19
2.3	Parameters of the three-band TB model as presented in Ref. [1], obtained by fitting the model to FP calculations. This particular set of values is that obtained using the generalized-gradient approximation (GGA), as indicated in the reference. (Energy units: eV)	20
3.1	Energies of states at the K -point and the Fermi energy, gap and inter-band hoppings to 1st order in aq , base on the numerical values of Table 2.3. (Units: eV)	26
3.2	Band concavity contributions and inter-band hoppings to 2nd order in aq , based on the numerical values of Tables 2.3 and 3.1. (Units: eV)	30
3.3	Numerical values of the effective masses to both 1st and 2nd order for the conduction band, degenerate valence band and spin-split valence band. (Units: m_e)	35
4.1	Renormalization of the half-band-gaps for the spin-split valence band, for $\varepsilon_r = 1$. The renormalization of the half-spin-gap can be inferred from $\delta\lambda = \delta\Delta^< - \delta\Delta^>$. (Units: eV)	53
4.2	Thomas-Fermi vector q_{TF} and the associated hole surface density ρ_{TF} in hole-doped TMDCs.	56
4.3	Ratio of gap shift to hole surface density $\delta\Delta_h/\rho$ in hole-doped TMDCs, for $\varepsilon_r = 1$. (Units: eV cm ²)	56
5.1	DOS of the high-lying cones $D^>$ and critical value U_c for the various TMDCs - low doping. (Units: eV)	69
5.2	Hole surface density ρ_A for the intermediate threshold for the different TMDCs. (Units: cm ⁻²)	75
5.3	Critical value U_c for the various TMDCs - high doping. (Units: eV)	80

List of Figures

1.1 Monolayers of NbSe_2 (a), graphene (b), $\text{Bi}_2\text{Sr}_2\text{CaCu}_2\text{O}_x$ (c) and MoS_2 (d). Figures (a) and (b) were obtained by AFM, (c) by electron microscopy and (d) by optical microscope. Lighter regions correspond to regions raised above the supporting surface, pleated or folded. [2]	4
1.2 (a) Unit cell of bulk 2H- MoS_2 . (b) Top view of the MoS_2 . \mathbf{R}_i are the vectors connecting the Mo atoms. (c) Schematic drawing of the band structure at the band edges located at the K points. [3]	7
1.3	9
1.4 Valley and spin optical transition selection rules. $\sigma \pm$ denote circular polarizations of the optical field while $\omega_{u,d}$ denote, respectively, the transition frequencies from the two split valence-band tops to the conduction band bottom. [3]	11
2.1 Top view of monolayered MX_2 . Gray spheres are M atoms, otherwise are X atoms. \mathbf{R}_i , $i = 1, \dots, 6$ are the lattice vectors between $M - M$ nearest-neighbours. The green region is the unit cell with lattice constant a . [1]	16
2.2 Plot along the path $\Gamma \rightarrow K \rightarrow M \rightarrow \Gamma$ of the band structure yielded by the three-band effective model with NN hoppings, using the numerical values presented in Table 2.3.	21
3.1 Plot of the Berry curvature of Eq. (3.31) in units of the lattice constant a . Values used for the parameters $t \equiv {}_1t_{vc}$ and Δ are those of Table 3.1. (Note: The curves for MoS_2 and MoSe_2 coincide).	39
4.1 Feynman diagram for the electron-electron Coulomb interaction.	46
4.2 Feynman diagram contributing the 1st order exchange self-energy operator.	47
5.1 Magnetic bands, according to Eq. 5.25, for (a) the normal phase, $D > U < 1$, and (b) the magnetic phase, $D > U > 1$. In (b) we have assumed $\xi > 0$.	72
5.2 Schematic of the electric-field effect apparatus.	74

Part I

Introduction and Band Structure

Chapter 1

State of the art

1.1 The discovery of graphene and the rise of 2D-materials

Two dimensional (2D) materials have faced a challenging existence, in theory as well as in laboratories. It has been almost 80 years since both Landau and Peierls separately argued that 2D crystalline systems are thermodynamically unstable and could not exist [4, 5]. This argument was later extended by Mermin and Wagner [6, 7], to what is now a well-known theorem of statistical mechanics [8], strongly supported by numerous experimental observations [9].

Indeed, atomic monolayers had been known, until recently, only as an integral part of larger 3D structures due to the rapid decrease of melting temperature of thin films with decreasing thickness, and to their instability (segregating into islands or decompose) at thicknesses below, typically, dozens of atomic layers [10, 11]. As such, 2D materials were presumed not to exist without a 3D base, until the 2004 experimental discovery of graphene along with other free-standing 2D materials [2, 12].

Although graphene is the basis of most widely known allotropes of carbon, such as fullerenes, carbon nanotubes and graphite, its isolation has not been trivial [12]. This may be accounted for by the fact that, as already pointed out, 2D layers of materials were not expected to exist isolated from a 3D base, though there is also much accountability in that it was practically unfeasible to search for single atom thick layers amidst debris of graphite covering macroscopic areas [9, 13].

A range of experimental procedures have been carried out in attempting to obtain isolated graphene, such as chemical exfoliation [14], epitaxial growth by chemical vapour deposition of hydrocarbons on metal substrates [15, 16] and by thermal decomposition of SiC [17–19]. However, micromechanical cleavage was the technique that allowed for successful controlled isolation of graphene for the first time [2, 12]. Roughly speaking, this technique amounts to drawing a trace with a piece of graphite and repeatedly peeling with adhesive tape until finding the thinnest flakes [9].

The problem was then to find several micrometer-size samples over an area of about 1 cm^2 ,

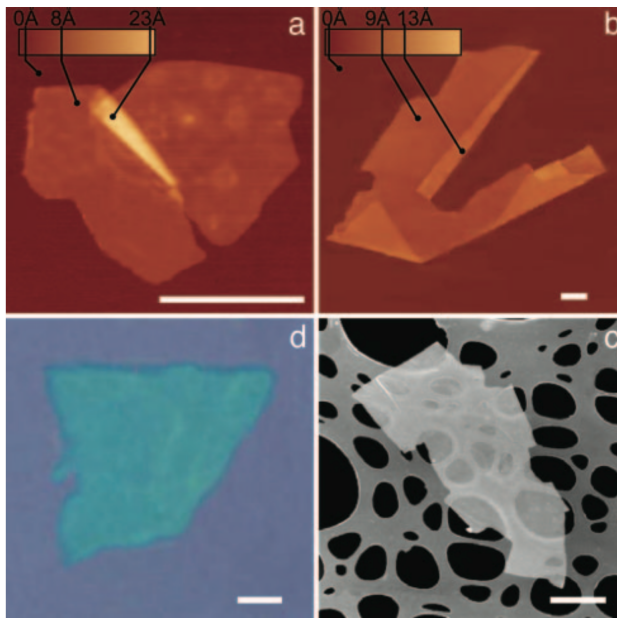


Figure 1.1: Monolayers of NbSe_2 (a), graphene (b), $\text{Bi}_2\text{Sr}_2\text{Ca}\text{Cu}_2\text{O}_x$ (c) and MoS_2 (d). Figures (a) and (b) were obtained by AFM, (c) by electron microscopy and (d) by optical microscope. Lighter regions correspond to regions raised above the supporting surface, pleated or folded. [2]

which modern techniques for studying atomically thin materials could not cope with [2, 9]. Instead, the solution was found by placing the peeled samples of graphite on top of an oxidized Si wafer [2, 9]. Despite the reduced thickness, the layers of graphene managed to produce a slight interference, observable against the bare surface with an optical microscope [2, 9] (Fig. 1.1).

Although graphene attracted the spotlight among the brand new class of 2D materials, certainly owing both to its vast new landscape of physics as well as to its potential for device applications [20], it has been in exceedingly good company since as early as 2005 [2, 21], namely alongside BN, $\text{Bi}_2\text{Sr}_2\text{Ca}\text{Cu}_2\text{O}_x$, NbSe_2 and MoS_2 . The last two belong in the family of transition metal dichalcogenides (TMDCs), which have increasingly attracted interest in the past few years [3, 21–28].

1.2 The superlatives and the shortcomings of graphene

Due to its truly outstanding properties, graphene has attracted widespread interest from physicists, chemists and engineers alike since its very discovery.

For physics, in particular, graphene stands as a system with a wealth of properties of rather dihcotomic character. First, it is a semiconductor, in the sense that it has zero density-of-states (DOS) at the Fermi level, while having a metallic gaplessness in its dispersion. Second,

graphene possesses flexural phonons, i.e. out-of-plane vibration modes, leading to crumpling instabilities characteristic of soft membranes, thus bringing together issues of soft condensed matter and hard condensed matter physics. Third, its charge carriers are described in terms of Dirac fermions in flat space, bringing together issues of condensed matter physics and particle physics. The outstanding electrical and thermal conductivities of graphene reflects their insensitivity to disorder and owes much to the Dirac-nature of its charge carriers, since it is essentially a manifestation of the Klein paradox: a phenomenon that prevents backscattering of particles by a potential barrier, restricted to relativistic fermions. Additionally, graphene stands as an extremely versatile system in condensed-matter, since its standard properties can be easily modified by application of electric and magnetic fields, addition of layers, control of its geometry and chemical doping, which can be directly probed by various scanning probe techniques over a range of microscopic scales. A thorough account of the electronic properties of graphene can be found in Ref. [20].

Despite all its impressive properties, graphene shows limitations concerning some electronic applications, namely the opening of a band gap, and the existence and robustness of different phases such as intrinsic magnetism, superconductivity and topological phases.

Band gap An early renormalization group analysis of electro-electron interactions showed no opening of the band in single-layer graphene, a result which has been experimentally verified [29]. Although it has been shown that bilayer graphene has a gap tunable by electric field-effect [30], this gap is limited to hundreds of meV which, coupled with a reduced transport gap due to disorder [31], leads to very small on/off ratios [32]. Other methods include nanostructuring [33–35] and chemical functionalization [36], but all these methods add complexity and further diminish mobility [27]. Note that the existence of a band gap is a prime requirement for rather important devices in modern technology such as transistors.

Intrinsic Magnetism Although the electronic correlations in graphene are not as strong as in materials with partially filled d-shells [20], a strong magnetic response can emerge from an enhanced DOS at the Fermi level in monolayer [37, 38] as well as bilayer graphene, under similar conditions [39]. One of the most effective ways to increase the DOS at the Dirac point is by making vacancies in the carbon lattice, inducing zero energy states [40, 41]. However, single-layer graphene with vacancies has proved to be only paramagnetic [42]. Parameters which are difficult to control experimentally, in single-layer graphene, are thought to have an important role, such as the imbalance between vacancies of the two sub-lattices of the honeycomb [43].

Superconductivity A superconducting phase has been predicted for graphene doped to the vicinity of a Van Hove singularity, inducing d-wave superconductivity due to repulsive electron-electron interactions [44]. However, this realization requires prohibitive doping levels [45].

Topological Phases Topological phases have spurred a wealth of new physics and have thus attracted a wave of interest since their prediction and experimental observation [46–50], both for fundamental physics as for device applications [51, 52]. A particular topological phase in 2D materials is the Quantum Spin Hall (QSH) insulator. In general, the signature trait of such phases is the existence of a gap in the 2D bulk and topologically protected gapless 1D edge states which, in QSH insulators, carry a spin hall current [46]. This phase attracts particular interest due to having dissipationless transport [51], with special potential for spintronic applications [51]. Although the first predictions of a topological insulator were made for graphene [53], the weak spin-orbit coupling (SOC) of carbon diminishes this effect [54, 55].

1.3 A companion family: Group-VI transition metal dichalcogenides

Faced with the shortcomings of single-layer graphene and motivated by the prospect of intriguing new physics, interest has begun to shift to its 2D companions, namely to the family of transition-metal dichalcogenides (TMDCs) [3, 21–28].

TMDCs form 3D structures in many ways similar to carbon: they are composed of stacked sheets of monolayers bonded by weak van der Waals forces, they are well-known, documented and studied materials [56–59], naturally found in layered forms and used primarily as solid lubricants [21]. This work shall focus primarily on group-VI transition metals , namely molybdenum (Mo) and tungsten (W), compounded with two chalcogens sulphur (S), selenium (Se). From here, TMDCs shall be referred to generically as MX_2 , where M represents the transition metal and X the chalcogen.

A monolayer can be seen as a triangular lattice of M atoms. Each M atom becomes coordinated with six X atoms. Two different unit cells can figure in these materials that, depending on the geometry of the coordination of M atom with the X atoms. The type of unit cell determines which one of three polytypes the stacked structure may occur in: the coordination may be trigonal prismatic, in which case the stacked structure may be of the type 2H (hexagonal symmetry) or 3R (rhombohedral symmetry), whereas for a octahedral coordination the structure will be 1T (tetragonal symmetry). Note that this structure is not as strictly two-dimensional as, say, graphene: the X atoms are at an angle with the M -atom plane [3, 22, 27]. In practice, the lattice is usually referred to as hexagonal, with sites M and X . Figure 1.2.b shows a top-down view of the monolayer crystal structure.

Since this discussion shall be focused on monolayers, special care must be taken towards the geometry of the coordination. As such, further analysis shall be restricted to the trigonal prismatic coordination. This distinction is not at all pedantic, since a trigonal prismatic coordination, unlike octahedral, has no inversion symmetry relatively to the M atom, a crucial ingredient in the electronic properties of interest in monolayer TMDCs [3]. Figure 1.2.a shows schematic

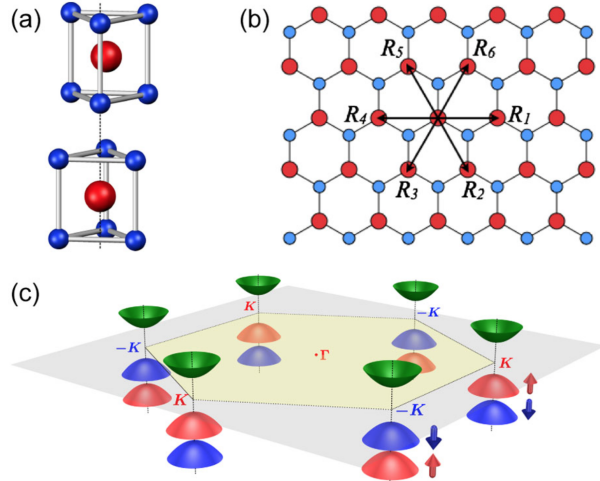


Figure 1.2: (a) Unit cell of bulk 2H-MoS₂. (b) Top view of the MoS₂. \mathbf{R}_i are the vectors connecting the Mo atoms. (c) Schematic drawing of the band structure at the band edges located at the K points. [3]

representations of the bulk atomic structure with 2H stacking order.

A thorough account of the electronic structure of TMDCs can be found in Ref. [60]. Monolayers are direct gap semiconductors with the gap lying at the inequivalent K points of the hexagonal BZ. Valence bands result of the hybridization of the d_{xy} and $d_{x^2-y^2}$ orbitals of transition metal M with the p_x and p_y orbitals of chalcogenide X , whereas conduction bands have a major contribution from the orbital $d_{3z^2-r^2}$ of M with a minor contribution of the orbitals p_x and p_y of X [22, 60]. There is thus a remarkable difference between graphene and monolayer TMDCs, in that the latter have an intrinsic band gap, thus opening the possibility for important application that graphene, as previously noted, cannot cover on its own [21, 26, 27].

Band structures obtained from DFT calculations [22] are shown in Figure 1.3b. The noticeable band splittings are due to the strong SOC in these compounds [61]. Compounds of W or Se have more pronounced splittings due to their greater mass, relatively to Mo and S, respectively, thus having a greater SOC [22]. Moreover, time-reversal symmetry implies that the SOC induced splitting must switch sign between opposing K points [3, 22]. This is schematically represented in Figure 1.2.c.

There is already a catalogue of demonstrated production methods of atomically thin TMDCs [27], both top-down and bottom-up. Top-down methods include micromechanical cleavage [2, 25, 26], liquid-phase preparations [62–65] and intercalation by ionic species [66–70]. Bottom-up methods include mostly chemical vapour deposition [71–74] and also hydrothermal synthesis [75].

A very important advantage of the chosen class of TMDCs is their chemical and thermal stability as monolayers. Indeed, as previously pointed out, parameters such as melting temper-

atures rapidly decrease with decreasing thickness of the material and, as a matter of fact, most materials only resist ambient conditions due to natural passivation of their surfaces [10, 11, 76]. Thus, the possibility of exfoliating or growing a 2D material is a necessary but not sufficient condition of existence: stability under ambient conditions is necessary as well, for all practical purposes [76].

It must be required then that the parent 3D material have a high thermal and chemical stability. For instance, graphite has both [76], which allowed for the isolation of graphene. Group-VI TMDCs monolayers composed of Mo, W and S, Se are indeed the only 2D chalcogenides known to be stable under ambient conditions [76] and are therefore the most viable to be studied.

It is now appropriate to discuss and overview the structural and electronic properties predicted or observed, until now, in multilayers or monolayers of the chosen class of TMDCs. Note that there are two differences to graphene that have a preponderant role in these materials' properties: breaking of inversion symmetry (in monolayers) due to the trigonal prismatic geometry and a strong SOC provided by transition metals Mo and W.

Henceforth, when referring to TMDCs it is implicit the restriction to the aforementioned compounds, unless otherwise noted.

Superconductivity

It has been shown that a superconducting transition with a critical temperature T_c strongly dependent on the carrier density n occurs in multilayered MoS₂, with the observation of a concave region in the T_c vs n phase diagram, commonly known as a superconducting dome (Figure 1.3a) [22, 77, 78], with a critical temperature $T_c \sim 10.8$ K for an optimal carrier density $n \sim 1.2 \times 10^{14} \text{ cm}^{-2}$ [22].

A theoretical analysis of heavily-doped MoS₂ has been carried out [79], accounting for electron-electron as well as electron-phonon interactions, which has suggested that the phase observed in Refs. [77] is preponderantly induced by electron-electron interactions [22]. This superconducting phase has exotic properties, such as gaps of opposite signs in the opposing valleys of the conduction band [79]. Density-functional theory (DFT) calculations of the phase diagram suggest also that a superconducting phase based on electron-phonon interactions is possible within a range of electron doping [22]. However, no hole-doped regime has been studied yet.

The strong SOC in MoS₂ induces a pronounced spin-splitting in the valence band [3], thus topological superconductivity stands as a possibility [51]. Recently, it has been proposed that some superconducting states can be realized due to Rashba spin-orbit coupling [22, 80].

Magnetism

Recent reports indicate the existence of ferromagnetism in proton irradiated multilayered MoS₂ [81, 82] with a tendency to produce vacancy sites exclusively on the S sublattice [83]. From a

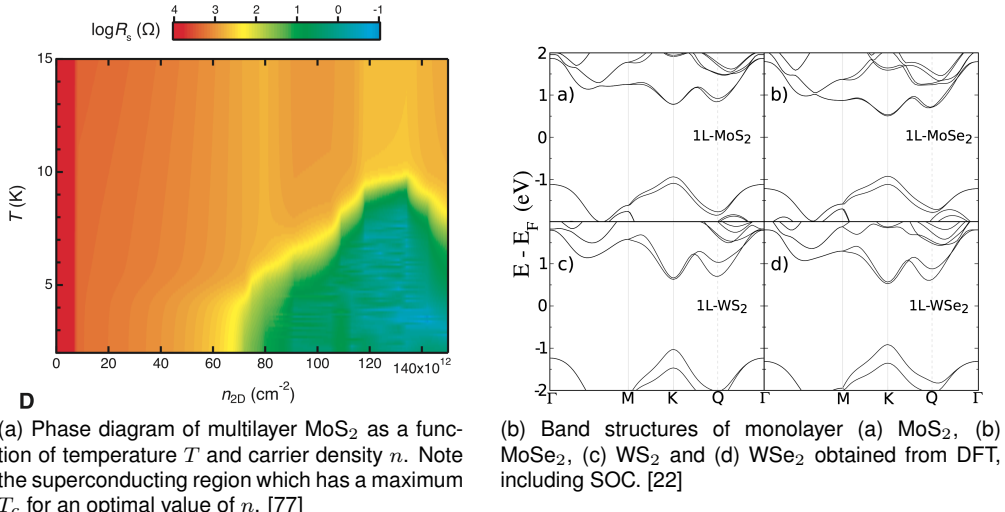


Figure 1.3

theoretical point of view, due to the lack of a realistic tight-binding model, one which would be amenable to perform simulations of large lattices with different densities yet would be complex enough to incorporate disorder, there was no knowledge on the effect of varying density and distribution of vacancies in the system.

Recently, however, such a tight-binding model has been put forward [60] and successfully applied to study the effect of strain on monolayer MoS₂ [84] as well as the electronic and optical properties of monolayers of MoS₂ and WS₂ in the presence of vacancies [85]. Besides mean-field and perturbative treatments, this model is apt for studies using Quantum Monte Carlo methods [86].

Strain and topological phases

The electronic structure and phonon modes of TMDCs suggest that band structure engineering, such as strain, can be used for electronic and optoelectronic applications [22, 87]. Indeed, a proposal to induce topological phases in TMDCs, particularly the 2D quantum spin hall (QSH) effect, via strain engineering has recently been put forward [28]. TMDCs stand as apt platforms for this implementation as their ability to sustain elastic deformations of up to 11% without breaking has been shown [22, 87].

It has been predicted [88] and experimentally shown [89] that strain induces pseudo-magnetic fields in 2D crystals, producing Landau levels (LL) in the electronic spectrum of 2D crystals such as graphene [90]. It is thus possible to exploit these pseudo-magnetic fields to induce topological phases in other 2D materials, such as TMDCs [28].

Experimentally, it has been shown [88, 89] that strain produces fields $B_0 \sim 10 - 10^2 \text{ T}$, leading to LL gaps of up to $\approx 100 \text{ K}$ [28], in clear contrast with the gaps achievable of strained,

say, GaAs, which are in the range of tens of mili-Kelvin (CIT). What truly sets TMDCs apart from other multi-valley systems, such as graphene, is that due to the spin-splitting resulting from SOC, LLs will be spin-polarized in different valleys [28], opening the possibility of realizing time-reversal invariant topological phases [51].

Moreover, due to the character of the electronic structure of TMDCs and to the poor screening of the Coulomb interaction in 2D, electron-electron interactions may have unexpected effects in the aforementioned topological phases [28].

Valleytronics and coupled spin-valley physics

Valleytronics, the use of valley index of charge carriers as a potential information carrier, became of great interest with the emergence of graphene [91–94]. The basic idea is founded on the binary relation between inequivalent K valleys and the fact that they have a large separation in momentum space (of the order of the BZ), meaning each valley state is robust against scattering into the other by smooth deformations and long wavelength phonons [92]. Thus two inequivalent valleys may constitute a binary index for low energy carriers, akin to the role of spin in spintronics.

However, relevant use of the valley index can only be made if there is some valley-contrasting physics. Such may appear as a consequence of bulk symmetry properties, particularly inversion symmetry breaking in 2D materials [92]. For instance, there will be a non-zero valley Hall conductivity, resulting in a valley current of carriers from inequivalent valleys flowing into opposing transverse edges upon application of an in-plane electric field [92], and inequivalent valleys will have helicity-dependent optical selection rules [93].

Although valley physics was first studied in monolayer graphene with broken inversion symmetry due to the substrate potential [92, 95], TMDCs open a whole new venue for valley physics, due to their intrinsic inversion symmetry breaking and non-vanishing SOC which, as previously noted, leads to sizable spin-splitting in the valence band [3]. Additionally, the aforementioned time-reversal symmetry induced sign change of the spin-splitting constitutes a valley-contrasting mechanism, since flipping the valley index will require flipping the spin index as well due to breaking of spin degeneracy. Thus, valley and spin states become strongly coupled [3].

Perhaps the most important implication of this new physics is the possibility of directly controlling spin and valley degrees of freedom via helicity and frequency-dependent optical selection rules [3]. Indeed, spin-valley coupling suggests that it is possible to exclusively excite carriers of a specific combination of spin and valley with optical fields of specific frequencies (according to spin-split band gaps) and circular polarization (according to valley index), as schematically depicted in Figure 1.4.

Moreover, the spin-valley coupling allows for photoinduced charge Hall, spin Hall and valley Hall effects [3]. Particularly, the suppressed relaxation of spin and valley states due to the robustness of the coupling causes the spin Hall and valley Hall effects to generate long lived spin and valley carrier accumulation on the edges of the monolayer [3].

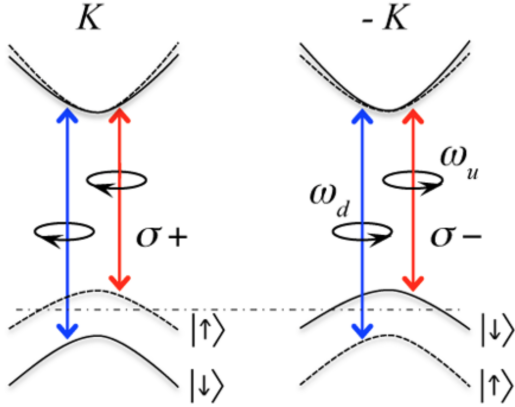


Figure 1.4: Valley and spin optical transition selection rules. σ^\pm denote circular polarizations of the optical field while $\omega_{u,d}$ denote, respectively, the transition frequencies from the two split valence-band tops to the conduction band bottom. [3]

These predictions have been experimentally observed [22], including the valley Hall effect [96, 97], spin and valley control with optical helicity selection rules [96, 98] as well as determination of spin relaxation times [98, 99].

Excitons

Due to the weak screening of the Coulomb interaction in 2D materials, strong excitonic effects become apparent. The existence and stability of both neutral and charged excitons has been shown experimentally [100–102], consisting of optically excited electrons and holes bound together via Coulomb interaction [22].

An important particularity of excitons in TMDCs is that they occur at the K and K' points of the BZ [22]. Thus, these are so called valley excitons, providing a means for controlling the valley index through optical probes, as previously noted. Moreover, due to the large spin-splitting of the valence band at the K point, two excitonic features are found in the photo-absorption spectrum [25].

Also as a signature of the strong Coulomb interactions, large binding energies of charged excitons (also known as trions) have been measured [100–102], with values of 18 meV for MoSe₂ and 30 meV for both MoSe₂ and WSe₂. Further measurements [103] have revealed an even larger exciton binding energy of ~ 0.32 eV in WS₂, representing a significant deviation from the conventional hydrogenic model of Wannier excitons [22]. A correction to the functional form of the Coulomb interaction under the nonlocal nature of the effective dielectric screening [22] has been put forward [103].

Taking on this problem, however, requires going beyond the usual approach of DFT calculations [22]. A number of treatments have been attempted [104–106] and in Ref. [22] a summary table of theoretical and experimental binding energies can be found.

1.4 Outline

It is clear that single-layered TMDCs have a vast landscape of physics and potential applications to explore. In particular, the many-body physics of these systems, and its implications to their electronic structure and non-interactive ground state, are yet to be known and may render desirable properties to these materials, from a point of view of both fundamental physics and applications. As such, the basic consequences of electron-electron interactions within a low-energy theory shall be the primary focus of this work, which is outlined as follows:

- **Chapter 2** presents an established effective model for the band structure of TMDCs, using only 3 of the 11 orbitals per unit cell. These are the orbitals that majorly compose the edges of the valence and conduction bands and, thus, this model lends itself to the derivation of a low-energy theory. This tight-binding model is symmetry-based, in the sense that it is obtained using a group theory analysis of the discrete symmetries of the lattice;
- In **Chapter 3**, the low-energy electronic structure is derived to both 1st and 2nd order. Since the aim is to obtain a two-level description for the valence-conduction band subspace, we complement the power expansion of the tight-binding Hamiltonian with the projection onto the relevant subspace, which induces a rather preponderant perturbative expansion. This is topped off with a brief description and analysis of the topological properties of the massive Dirac cones and their physical implications, namely, those in virtue of the spin-valley coupling;
- **Chapter 4** moves on to the electronic many-body problem in this system. A perturbative expansion is developed in order to determine the self-energy correction to the bare propagator. Although this is carried out within a Hartree-Fock approximation, we consider a strictly long-range Coulomb interaction, which renders the computation of the full self-energy correction a numerically challenging problem. For simplicity, we restricted the analysis to the renormalization of the band gap, for both undoped and hole doped systems;
- **Chapter 5** explores the Hubbard model of the low-energy theory and the existence of a possible symmetry broken ground state, namely, a spin- and valley-polarized phase. Based on the path integral formulation, a Hubbard-Stratonovich transformation is applied and the resulting action is analyzed by first taking the saddle-point and then expanding around this solution. This phase displays a remarkable feature that is the existence of an anomalous Hall conductivity, in virtue of the topological character of the cones;
- Finally, in **Chapter 6** we present our conclusions and proposals for future work.

Additionally, the Appendix contains relevant derivations and auxiliary results.

Chapter 2

An effective three-band tight-binding Hamiltonian

This chapter reviews the method employed by Liu *et al.* [1] for obtaining a minimal symmetry-based three-band tight-binding (TB) model for monolayers of group-VI TMDCs (MX_2) with trigonal prismatic coordination.

The basis behind this approach is twofold: On one hand, previous theoretical studies and calculations revealed that orbital contributions to the band edges stem mostly from M atoms' d -orbitals, namely, $d_{3z^2-r^2} \equiv d_{z^2}$, d_{xy} and $d_{x^2-y^2}$, with negligible contributions from X atoms' p -orbitals. On the other hand, monolayers of MX_2 with trigonal prismatic coordination have D_{3h} point-group symmetry, and the three sets of M atom d -orbitals $\{d_{z^2}\}$, $\{d_{xy}, d_{x^2-y^2}\}$ and $\{d_{xz}, d_{yz}\}$ constitute basis of irreducible representations of this symmetry group. This means that an orbital will only mix with orbitals within its set under any symmetry operation of the group. An important symmetry of this group is the reflection by the $x - y$ plane (denoted $\hat{\sigma}_h$), which implies that hybridization can only take place between orbitals of the first two sets.

A model which neglects the p -orbital contributions from X atoms is, evidently, an approximation. However, given the intent of this work – which is to ultimately arrive at the continuum (low-energy) description of single-layered MX_2 – it is reasonable to construct an effective model based on the three d -orbitals d_{z^2} , d_{xy} and $d_{x^2-y^2}$.

2.1 Spinless tight-binding model

2.1.1 Discrete symmetries of the Hamiltonian and Group Theory analysis

Following the group theory motivated notation used in Ref. [1], we define the basis for the TB hamiltonian as the Wannier states

$$\langle \mathbf{x} | \phi_1^1(\mathbf{r}) \rangle = d_{z^2}(\mathbf{x}-\mathbf{r}), \quad \langle \mathbf{x} | \phi_1^2(\mathbf{r}) \rangle = d_{xy}(\mathbf{x}-\mathbf{r}), \quad \langle \mathbf{x} | \phi_2^2(\mathbf{r}) \rangle = d_{x^2-y^2}(\mathbf{x}-\mathbf{r}), \quad \forall \mathbf{r} \in \text{lattice} \quad (2.1)$$

where each $|\phi_\mu^j\rangle$ stands for the μ -th element of the j -th basis set of the irreducible representation. The functional form of the d orbitals can be obtained from the spherical harmonics $Y_l^m(\theta, \varphi)$ for $l = 2$ and, particularly, for $m = 0, \pm 2$. To see it, note that

$$\begin{aligned} Y_2^0 &= \frac{1}{2} \sqrt{\frac{5}{4\pi}} (3 \cos^2 \theta - 1) & Y_2^{\pm 2} &= \frac{1}{4} \sqrt{\frac{15}{2\pi}} \sin^2 \theta e^{\pm 2i\varphi} \\ &= \frac{1}{2} \sqrt{\frac{5}{4\pi}} (3 \bar{z}^2 - 1), & &= \frac{1}{4} \sqrt{\frac{15}{2\pi}} (\bar{x}^2 - \bar{y}^2 \pm 2i\bar{x}\bar{y}), \end{aligned}$$

where $\bar{x}_i \equiv x_i / \|\mathbf{r}\|$ and transformation between spherical and cartesian coordinates was used. We may write the normalized d -functions in terms of spherical harmonics as:

$$\begin{aligned} d_{x^2-y^2} &\propto \frac{1}{\sqrt{2}} (Y_2^{-2} + Y_2^2) & d_{xy} &\propto \frac{-i}{\sqrt{2}} (Y_2^{-2} - Y_2^2) & d_{z^2} &\equiv d_{3z^2-r^2} \propto Y_2^0 \\ &= \frac{1}{4} \sqrt{\frac{15}{4\pi}} (\bar{x}^2 - \bar{y}^2) & &= -\frac{1}{4} \sqrt{\frac{15}{4\pi}} 2\bar{x}\bar{y} & &= \frac{1}{2} \sqrt{\frac{5}{4\pi}} (3 \bar{z}^2 - 1) \\ &= \frac{1}{4} \sqrt{\frac{15}{4\pi}} \sin^2 \theta \cos 2\varphi, & &= -\frac{1}{4} \sqrt{\frac{15}{4\pi}} \sin^2 \theta \sin 2\varphi, & &= \frac{1}{2} \sqrt{\frac{5}{4\pi}} (3 \cos^2 \theta - 1). \end{aligned} \quad (2.2)$$

The computation of the TB Hamiltonian matrix will be based on the basic relation for the single-electron Hamiltonian,

$$\hat{g} \hat{H} \hat{g}^\dagger = \hat{H}, \quad (2.3)$$

i.e., that the Hamiltonian (essentially, the free-particle operator plus the potential from the lattice) is invariant under any symmetry operation $\hat{g} \in D_{3h}$ prismatic symmetry [107]. The matrix elements of \hat{H} yield the hopping integrals between sites, which, according to the basis of Eq. (2.1), read

$$E_{\mu\nu}^{ij}(\mathbf{R}_l) = \langle \phi_\mu^i(\mathbf{r}) | \hat{H} | \phi_\nu^j(\mathbf{r} - \mathbf{R}_l) \rangle. \quad (2.4)$$

Since we are interested in the low-energy limit of this model, a NN hopping model will suffice. Therefore, the \mathbf{R}_l are restricted to nearest-neighbour lattice vectors, as shown in Figure 2.1.

We now intend to arrive at a systematic method for obtaining the TB Hamiltonian following the symmetry group approach developed so far. As so, note that all the \mathbf{R}_l involved in NN

Table 2.1: Multiplication table of the subset of Eq. (2.5). Elements of the top row are multiplied by elements of the leftmost column.

\hat{E}	\hat{C}_3	\hat{C}_3^2	$\hat{\sigma}_v$	$\hat{\sigma}'_v$	$\hat{\sigma}''_v$
\hat{C}_3	\hat{C}_3^2	\hat{E}	$\hat{\sigma}''_v$	$\hat{\sigma}_v$	$\hat{\sigma}'_v$
\hat{C}_3^2	\hat{E}	\hat{C}_3	$\hat{\sigma}'_v$	$\hat{\sigma}''_v$	$\hat{\sigma}_v$
$\hat{\sigma}_v$	$\hat{\sigma}'_v$	$\hat{\sigma}''_v$	\hat{E}	\hat{C}_3	\hat{C}_3^2
$\hat{\sigma}'_v$	$\hat{\sigma}''_v$	$\hat{\sigma}_v$	\hat{C}_3^2	\hat{E}	\hat{C}_3
$\hat{\sigma}''_v$	$\hat{\sigma}_v$	$\hat{\sigma}'_v$	\hat{C}_3	\hat{C}_3^2	\hat{E}

hoppings are related by a subset of the symmetry operations of D_{3h} , namely

$$\hat{g} \in \{\hat{E}, \hat{C}_3, \hat{C}_3^2, \hat{\sigma}_v, \hat{\sigma}'_v, \hat{\sigma}''_v\}. \quad (2.5)$$

Here, \hat{E} is the identity, \hat{C}_3 is rotation by $2\pi/3$ around the z axis and $\hat{\sigma}_v$ is the reflection through the plane defined by the z axis and the angular bisector of \mathbf{R}_1 and \mathbf{R}_6 . The remaining operations can be inferred from the multiplication table of the subset, as shown in Table 2.1. These symmetry operations, when acted upon an orbital, produce a linear combination of the elements of the basis set to which the operated orbital belongs. If the operator associated to the operation \hat{g} acting on the orbitals $\langle \mathbf{x} | \phi_\mu^i(\mathbf{r}) \rangle$ is denoted by $O_{\hat{g}}$, that statement reads

$$\begin{aligned} O_{\hat{g}} \langle \mathbf{x} | \phi_\mu^i(\mathbf{r} + \mathbf{R}_l) \rangle &= \langle \hat{g}^\dagger \mathbf{x} | \phi_\mu^i(\mathbf{r} + \mathbf{R}_l) \rangle \\ &= \langle \mathbf{x} | \hat{g} | \phi_\mu^i(\mathbf{r} + \mathbf{R}_l) \rangle \\ &= \sum_{\mu'} D_{\mu\mu'}^i(\hat{g}) \langle \mathbf{x} | \phi_{\mu'}^i(\mathbf{r} + \hat{g} \mathbf{R}_l) \rangle, \end{aligned} \quad (2.6)$$

where the third equality implies that

$$\hat{g} | \phi_\mu^i(\mathbf{r} + \mathbf{R}_l) \rangle = \sum_{\mu'} D_{\mu\mu'}^i(\hat{g}) | \phi_{\mu'}^i(\mathbf{r} + \hat{g} \mathbf{R}_l) \rangle. \quad (2.7)$$

Here, $D_{\mu\mu'}^i(\hat{g})$ are the matrix elements of the symmetry operation \hat{g} in the i -th irreducible representation, \mathbf{r} is the center of symmetry of the operation and \mathbf{R}_l is a lattice vector. Eqs. (2.7) and (2.6) are particular to our problem, in which we want to compare orbitals at different positions of the lattice. However, taking \mathbf{R}_l to zero reduces them to the general expressions found in group theory textbooks (for instance, see Ref. [108]).

Special attention should be given to the meaning of Eq. (2.6). The symmetry operation \hat{g} acting on a function defined on the lattice site \mathbf{R}_l relatively to the center of symmetry at the lattice site \mathbf{r} takes it to a different function at a relative lattice site $\hat{g} \mathbf{R}_l$. In turn, the fact that the original function belongs to the basis of an irreducible representation of the point-group means that the new function can be written as a linear combination of the functions belonging to the

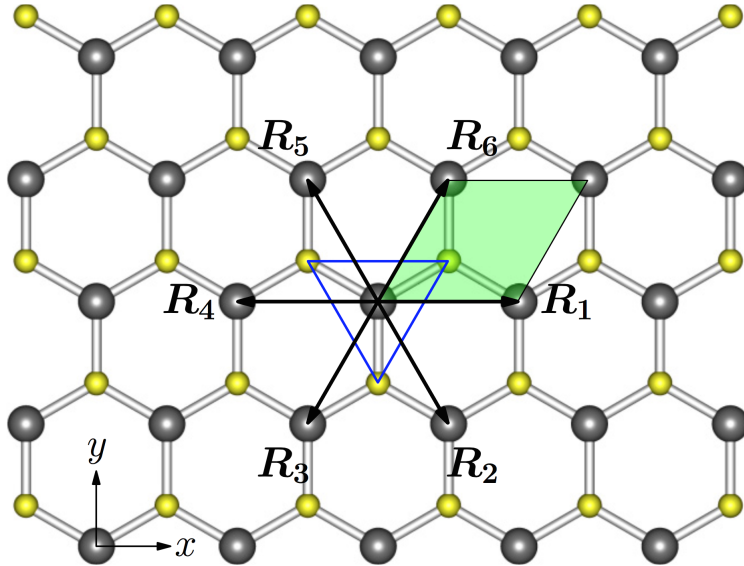


Figure 2.1: Top view of monolayered MX_2 . Gray spheres are M atoms, otherwise are X atoms. R_i , $i = 1, \dots, 6$ are the lattice vectors between $M - M$ nearest-neighbours. The green region is the unit cell with lattice constant a . [1]

same basis. However, in this case we are not dealing with functions which origin are at the center of symmetry. Thus, it only makes sense to define these functions at the relative lattice site to which the operation transported the original function, hence Eq. (2.7).

This argument can be better understood by establishing a loose analogy with the rotation of a rigid body in classical mechanics, in which a well-known theorem states that the rotation of a rigid body relatively to an arbitrary point in space can be decomposed into a rotation of the body about its center of mass and the rotation of the body as a point-particle about the center of rotation. The same basic principle can be interpreted here: the operation induces a transformation of the function about its origin and a transformation of the origin to a different point in space. The nuance is that, in order to determine the representation of the operation, we need only to compare the change of the function about its origin, independently of the position of the origin before and after the transformation. Note also that the analogy is only loose since the considered subset of the point-group involves inversions, besides rotations.

Also, it has become clearer why the sets $\{d_{z^2}\}$ and $\{d_{xy}, d_{x^2-y^2}\}$ are basis sets of irreducible representations of the symmetry group: acting a symmetry operation upon them generates the respective irreducible representation.

Given the functional form of the d -functions in Eq. (2.2), the effects of every transformation of the point-group on the on the TB basis states amount to affine transformations of the angular coordinates. Particularly, the subset of interest induces affine transformations of the kind $(\theta, \varphi) \xrightarrow{\hat{g}} (\theta', \varphi') = (\theta, \varphi_0 \pm \varphi)$, where the plus signs applies to rotations and the minus sign to

inversions, whereas φ_0 is some characteristic angle, specific to the transformation.

These results allow us to derive a generating equation which will allow us to arrive at the hopping matrix for any lattice vector. Consider a lattice vector related to \mathbf{R}_l by a symmetry operation of the subset of Eq. (2.5), $\hat{g}\mathbf{R}_l$. The matrix elements of its hopping matrix are given by

$$\begin{aligned}
E_{\mu\nu}^{ij}(\hat{g}\mathbf{R}_l) &= \langle \phi_\mu^i(\mathbf{r}) | \hat{H} | \phi_\nu^j(\mathbf{r} - \hat{g}\mathbf{R}_l) \rangle \\
&\stackrel{(2.3)}{=} \langle \phi_\mu^i(\mathbf{r}) | \hat{g} \hat{H} \hat{g}^\dagger | \phi_\nu^j(\mathbf{r} - \hat{g}\mathbf{R}_l) \rangle \\
&\stackrel{(2.7)}{=} \left[\sum_\beta \langle \phi_\beta^i(\mathbf{r}) | D_{\mu\beta}^i(\hat{g}) \right] \hat{H} \left[\sum_\delta D_{\nu\alpha}^j(\hat{g}^\dagger) | \phi_\alpha^j(\mathbf{r} - \mathbf{R}_l) \rangle \right] \\
&= \sum_\beta \sum_\alpha D_{\mu\beta}^i(\hat{g}) \langle \phi_\beta^i(\mathbf{r}) | \hat{H} | \phi_\alpha^j(\mathbf{r} - \mathbf{R}_l) \rangle D_{\alpha\nu}^j(\hat{g})^* \\
&= \sum_\beta \sum_\alpha D_{\mu\beta}^i(\hat{g}) E_{\beta\alpha}^{ij}(\mathbf{R}_l) D_{\alpha\nu}^j(\hat{g})^* \\
&= [D^i(\hat{g}) E^{ij}(\mathbf{R}_l) D^j(\hat{g})^\dagger]_{\mu\nu}.
\end{aligned}$$

This is equivalent to the matricial equation

$$E^{ij}(\hat{g}\mathbf{R}_l) = D^i(\hat{g}) E^{ij}(\mathbf{R}_l) D^j(\hat{g})^\dagger. \quad (2.8)$$

2.1.2 Representations and computation of hopping matrices

Equation (2.8) provides a systematic method of obtaining the hopping matrix for any lattice vector in terms of the hopping matrix elements of a single lattice vector. In practice, we will consider the total hopping matrix $E(\mathbf{R}_l)$, given by

$$E(\mathbf{R}_l) = \begin{pmatrix} E^{11}(\mathbf{R}_l) & E^{12}(\mathbf{R}_l) \\ E^{21}(\mathbf{R}_l) & E^{22}(\mathbf{R}_l) \end{pmatrix},$$

so that Eq. (2.8) becomes

$$E(\hat{g}\mathbf{R}_l) = D(\hat{g}) E(\mathbf{R}_l) D(\hat{g})^\dagger, \quad D(\hat{g}) = D^1(\hat{g}) \oplus D^2(\hat{g}). \quad (2.9)$$

Taking the lattice vector \mathbf{R}_l as a reference, we define

$$E(\mathbf{R}_1) = \begin{pmatrix} E^{11}(\mathbf{R}_1) & E^{12}(\mathbf{R}_1) \\ E^{21}(\mathbf{R}_1) & E^{22}(\mathbf{R}_1) \end{pmatrix} = \begin{pmatrix} E_{11}^{11}(\mathbf{R}_1) & E_{11}^{12}(\mathbf{R}_1) & E_{12}^{12}(\mathbf{R}_1) \\ E_{11}^{21}(\mathbf{R}_1) & E_{11}^{22}(\mathbf{R}_1) & E_{12}^{22}(\mathbf{R}_1) \\ E_{21}^{21}(\mathbf{R}_1) & E_{21}^{22}(\mathbf{R}_1) & E_{22}^{22}(\mathbf{R}_1) \end{pmatrix} = \begin{pmatrix} t_0 & t_{01} & t_{02} \\ t_{10} & t_{11} & t_{12} \\ t_{20} & t_{12} & t_{22} \end{pmatrix}.$$

We are now in position to compute all the necessary hopping matrices. We can start by reducing the number of free parameters. Consider the lattice vector \mathbf{R}_4 , related to \mathbf{R}_1 by $\hat{g} = \hat{\sigma}_v''$. In

angular coordinates, the transformation is $(\theta, \varphi) \rightarrow (\theta, \pi - \varphi)$ which, when applied to the d -functions of the TB basis, yields the representation

$$D(\hat{\sigma}_v'') = \begin{pmatrix} 1 & 0 & 0 \\ 0 & -1 & 0 \\ 0 & 0 & 1 \end{pmatrix},$$

which, substituting in Eq. (2.9), gives the hopping matrix

$$E(\hat{\sigma}_v'' \mathbf{R}_1) = E(-\mathbf{R}_1) = E(\mathbf{R}_4) = \begin{pmatrix} t_0 & -t_{01} & t_{02} \\ -t_{10} & t_{11} & -t_{12} \\ t_{20} & -t_{12} & t_{22} \end{pmatrix}.$$

On the other hand, we can relate the hopping matrices for \mathbf{R}_4 and \mathbf{R}_1 from the definition:

$$\begin{aligned} E_{\mu\nu}^{ij}(\mathbf{R}_4) &= E_{\mu\nu}^{ij}(-\mathbf{R}_1) \\ &= \langle \phi_\mu^i(\mathbf{r}) | \hat{H} | \phi_\nu^j(\mathbf{r} + \mathbf{R}_1) \rangle \\ &= \langle \phi_\mu^i(\mathbf{r}' - \mathbf{R}_1) | \hat{H} | \phi_\nu^j(\mathbf{r}') \rangle, \quad \mathbf{r}' = \mathbf{r} + \mathbf{R}_1 \\ &= \langle \phi_\nu^j(\mathbf{r}') | \hat{H} | \phi_\mu^i(\mathbf{r}' - \mathbf{R}_1) \rangle^* \\ &= E_{\nu\mu}^{ji}(\mathbf{R}_1)^* \\ \Leftrightarrow E(\mathbf{R}_4) &= E(\mathbf{R}_1)^\dagger. \end{aligned}$$

Considering that the elements of the hopping matrices are real, we find:

$$t_1 \equiv t_{01} = -t_{10}, \quad t_2 \equiv t_{02} = t_{20}, \quad t_{12} = -t_{21}.$$

A summary of the representations of the relevant operations and of the resulting hopping matrices can be found in Table 2.2.

Tight-binding Hamiltonian

In order to arrive at the TB Hamiltonian, consider the total second-quantized Hamiltonian in 2 dimensions

$$\hat{\mathcal{H}} = \int d^2x \hat{\psi}^\dagger(\mathbf{x}) \left[-\frac{\hbar^2}{2m} \frac{\partial^2}{\partial \mathbf{x}^2} + V(\mathbf{x}) \right] \hat{\psi}(\mathbf{x}), \quad V(\mathbf{x}) = \sum_I V_{ei}(\mathbf{x} - \mathbf{R}_I), \quad (2.10)$$

where $V_{ei}(\mathbf{x} - \mathbf{R}_I)$ is the potential on an electron at the point \mathbf{x} of configuration space due to the ion at the point \mathbf{R}_I and $V(\mathbf{x})$ is, thus, the potential due to the entire lattice on an electron at the point \mathbf{x} . Since the Wannier states of Eq. (2.1) over all lattice sites \mathbf{r} form a complete, orthonormal (in the tight-binding approximation) basis, we can expand the field operators $\hat{\psi}^\dagger(\mathbf{x})$

Table 2.2: Hopping matrices and representations of operations relevant to their computation.
(Read: upper sign, left index; lower sign, right index).

Representation	Hopping Matrix
—	$E(\mathbf{0}) = \begin{pmatrix} \varepsilon_1 & 0 & 0 \\ 0 & \varepsilon_2 & 0 \\ 0 & 0 & \varepsilon_2 \end{pmatrix}$
$D(\hat{\sigma}_v'') = \begin{pmatrix} 1 & 0 & 0 \\ 0 & -1 & 0 \\ 0 & 0 & 1 \end{pmatrix}$	$E(\mathbf{R}_{1,4}) = \begin{pmatrix} t_0 & \pm t_1 & t_2 \\ \mp t_1 & t_{11} & \pm t_{12} \\ t_2 & \mp t_{12} & t_{22} \end{pmatrix}$
$D(\hat{C}_3) = \begin{pmatrix} 1 & 0 & 0 \\ 0 & -1/2 & -\sqrt{3}/2 \\ 0 & \sqrt{3}/2 & -1/2 \end{pmatrix}$	$E(\mathbf{R}_{2,5}) = \begin{pmatrix} t_0 & \pm \frac{1}{2}t_1 - \frac{\sqrt{3}}{2}t_2 & \mp \frac{\sqrt{3}}{2}t_1 - \frac{1}{2}t_2 \\ \mp \frac{1}{2}t_1 - \frac{\sqrt{3}}{2}t_2 & \frac{1}{4}(t_{11} + 3t_{22}) & \frac{\sqrt{3}}{4}(t_{22} - t_{11}) \mp t_{12} \\ \pm \frac{\sqrt{3}}{2}t_1 - \frac{1}{2}t_2 & \frac{\sqrt{3}}{4}(t_{22} - t_{11}) \pm t_{12} & \frac{1}{4}(3t_{11} + t_{22}) \end{pmatrix}$
$D(\hat{\sigma}_v) = \begin{pmatrix} 1 & 0 & 0 \\ 0 & 1/2 & \sqrt{3}/2 \\ 0 & \sqrt{3}/2 & -1/2 \end{pmatrix}$	$E(\mathbf{R}_{6,3}) = \begin{pmatrix} t_0 & \pm \frac{1}{2}t_1 + \frac{\sqrt{3}}{2}t_2 & \pm \frac{\sqrt{3}}{2}t_1 - \frac{1}{2}t_2 \\ \mp \frac{1}{2}t_1 + \frac{\sqrt{3}}{2}t_2 & \frac{1}{4}(t_{11} + 3t_{22}) & -\frac{\sqrt{3}}{4}(t_{22} - t_{11}) \mp t_{12} \\ \mp \frac{\sqrt{3}}{2}t_1 - \frac{1}{2}t_2 & -\frac{\sqrt{3}}{4}(t_{22} - t_{11}) \pm t_{12} & \frac{1}{4}(3t_{11} + t_{22}) \end{pmatrix}$

and $\hat{\psi}(\mathbf{x})$ as

$$\hat{\psi}^\dagger(\mathbf{x}) = \sum_i \langle \phi_\alpha(\mathbf{r}_i) | \mathbf{x} \rangle \hat{a}_{i\alpha}^\dagger, \quad \hat{\psi}(\mathbf{x}) = \sum_j \langle \mathbf{x} | \phi_\beta(\mathbf{r}_j) \rangle \hat{a}_{j\beta}, \quad (2.11)$$

where α and β are indices representing any set of quantum numbers which, in our case, are the orbital indices of Eq. (2.1) and the spin index. Summation over repeated greek indices is implied. Eq. (2.10) becomes

$$\hat{\mathcal{H}} = \sum_i \sum_j \hat{a}_{i\alpha}^\dagger E_{\alpha\beta}(\mathbf{r}_{ij}) \hat{a}_{j\beta}, \quad \mathbf{r}_{ij} = \mathbf{r}_i - \mathbf{r}_j. \quad (2.12)$$

The matrix elements depend only on the difference in position of the lattice in virtue of the lattice vector translation invariance of the system, reading

$$E_{\alpha\beta}(\mathbf{r}_i - \mathbf{r}_j) = \int d^2x \langle \phi_\alpha(\mathbf{r}_i) | \mathbf{x} \rangle \left[-\frac{\hbar^2}{2m} \frac{\partial^2}{\partial \mathbf{x}^2} + V(\mathbf{x}) \right] \langle \mathbf{x} | \phi_\beta(\mathbf{r}_j) \rangle = \langle \phi_\alpha(\mathbf{r}_i) | \hat{H} | \phi_\beta(\mathbf{r}_j) \rangle,$$

which, as expected, are simply hopping integrals as defined in Eq. (2.4). The Hamiltonian of Eq. (2.12) can be diagonalized by taking the Fourier transform from lattice sites to crystal momenta in the Brillouin Zone:

$$\hat{a}_{\mathbf{r}} = \frac{1}{\sqrt{N}} \sum_{\mathbf{k}} e^{-i\mathbf{k}\cdot\mathbf{r}} \hat{a}_{\mathbf{k}}, \quad N = \text{number of lattice sites},$$

which, substituting into the Hamiltonian yields

$$\hat{\mathcal{H}} = \sum_{\mathbf{k}} \hat{a}_{\mathbf{k},\alpha}^\dagger [H_{tb}(\mathbf{k})]_{\alpha\beta} \hat{a}_{\mathbf{k},\beta}, \quad H_{tb}(\mathbf{k}) = \sum_{\forall i:j} E(\mathbf{r}_{ij}) e^{i\mathbf{k}\cdot\mathbf{r}_{ij}}. \quad (2.13)$$

Since, in our approximation, hoppings further than NN are suppressed, we can write the summation in the second equality of Eq. (2.13) as a sum over nearest-neighbours,

$$H_{tb}(\mathbf{k}) = \sum_{\langle i,j \rangle} E(\mathbf{r}_{ij}) e^{i\mathbf{k} \cdot \mathbf{r}_{ij}} = \sum_{l=1}^6 E(\mathbf{R}_l) e^{i\mathbf{k} \cdot \mathbf{R}_l},$$

where we have set $\mathbf{r}_{ij} = \mathbf{R}_l$, $\forall i, j, l = 1, \dots, 6$ the NN lattice vectors as shown in Fig. 2.1. Note that the Fourier transform of the creation and annihilation operators induces a Fourier transform from Wannier states to Bloch states of the orbitals, so that the TB Hamiltonian is written in the basis $\{|\varphi_\alpha(\mathbf{k})\rangle\}_{\forall \mathbf{k}, \alpha}$ given by

$$|\varphi_\alpha(\mathbf{k})\rangle = \frac{1}{\sqrt{N}} \sum_{\mathbf{r}} e^{i\mathbf{k} \cdot \mathbf{r}} |\phi_\alpha(\mathbf{r})\rangle.$$

Finally, using the hopping matrices of Table 2.2, the tight-binding Hamiltonian $H_{tb}(\mathbf{k})$ can be written as:

$H_{tb}(\mathbf{k}) = \begin{pmatrix} h_0 & h_1 & h_2 \\ h_1^* & h_{11} & h_{12} \\ h_2^* & h_{12}^* & h_{22} \end{pmatrix}, \quad (\alpha, \beta) = \left(\frac{1}{2}k_x a, \frac{\sqrt{3}}{2}k_y a \right),$	$\begin{aligned} h_0 &= \epsilon_1 \\ &\quad + 2t_0(\cos 2\alpha + 2 \cos \alpha \cos \beta) \\ h_{11} &= \epsilon_2 + 2t_{11} \cos 2\alpha \\ &\quad + (t_{11} + 3t_{22}) \cos \alpha \cos \beta \\ h_{22} &= \epsilon_2 + 2t_{22} \cos 2\alpha \\ &\quad + (3t_{11} + t_{22}) \cos \alpha \cos \beta \end{aligned} \quad \begin{aligned} h_1 &= -2\sqrt{3}t_2 \sin \alpha \sin \beta \\ &\quad + 2it_1(\sin 2\alpha + \sin \alpha \cos \beta) \\ h_2 &= 2t_2(\cos 2\alpha - \cos \alpha \cos \beta) \\ &\quad + 2\sqrt{3}it_1 \cos \alpha \sin \beta \\ h_{12} &= \sqrt{3}(t_{22} - t_{11}) \sin \alpha \sin \beta \\ &\quad + 4it_{12} \sin \alpha (\cos \alpha - \cos \beta) \end{aligned} \quad (2.14)$
---	--

Figure 2.2 shows a plot of the band structure along the path $\Gamma \rightarrow K \rightarrow M \rightarrow \Gamma$ for various MX_2 as given by this model. Numerical values for orbital energies and hopping integrals can be checked in Table 2.3. These are taken from Ref. [1].

Table 2.3: Parameters of the three-band TB model as presented in Ref. [1], obtained by fitting the model to FP calculations. This particular set of values is that obtained using the generalized-gradient approximation (GGA), as indicated in the reference. (Energy units: eV)

MX_2	a (Å)	λ	ϵ_1	ϵ_2	t_0	t_1	t_2	t_{11}	t_{12}	t_{22}
MoS ₂	3.190	0.073	1.046	2.104	-0.184	0.401	0.507	0.218	0.338	0.057
WS ₂	3.191	0.211	1.130	2.275	-0.206	0.567	0.536	0.286	0.384	-0.061
MoSe ₂	3.326	0.091	0.919	2.065	-0.188	0.317	0.456	0.211	0.290	0.130
WSe ₂	3.325	0.228	0.943	2.179	-0.207	0.457	0.486	0.263	0.329	0.034

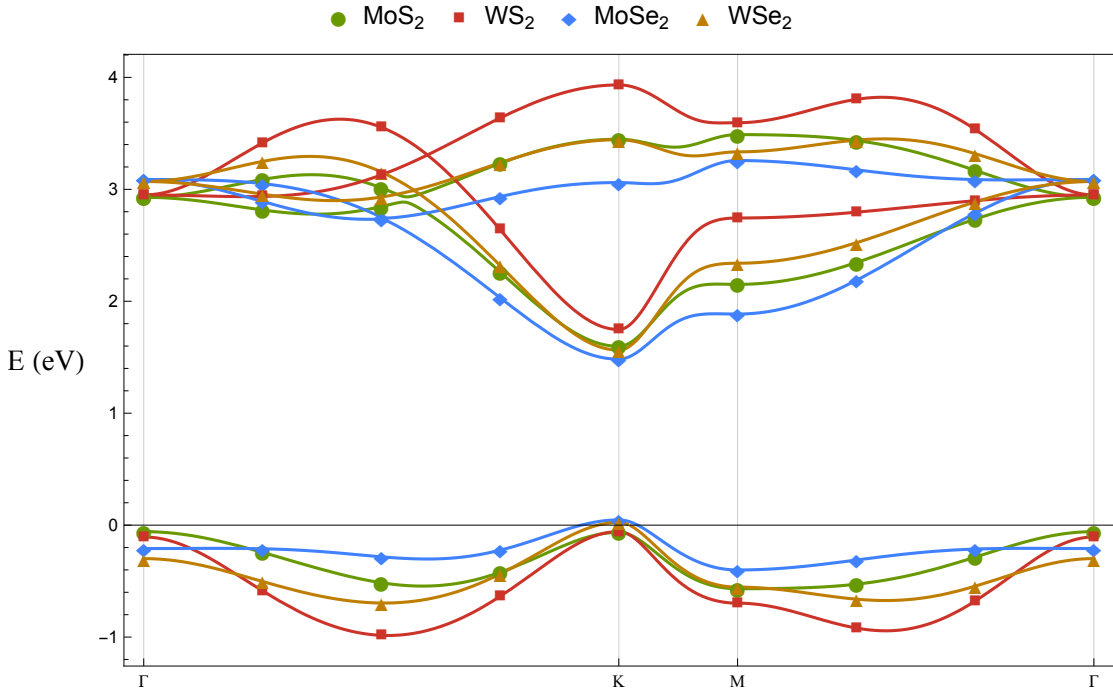


Figure 2.2: Plot along the path $\Gamma \rightarrow K \rightarrow M \rightarrow \Gamma$ of the band structure yielded by the three-band effective model with NN hoppings, using the numerical values presented in Table 2.3.

2.2 Spinful tight-binding Hamiltonian

2.2.1 Basis states and tight-binding Hamiltonian with spin-orbit coupling

Consider now the Hilbert space defined by the ordered basis

$$\begin{aligned} \mathcal{H} &= \mathcal{H}_{orb} \otimes \mathcal{H}_{spin} \\ &= \{ |\phi_1^1(\mathbf{r}), \uparrow\rangle, |\phi_1^2(\mathbf{r}), \uparrow\rangle, |\phi_2^2(\mathbf{r}), \uparrow\rangle, |\phi_1^1(\mathbf{r}), \downarrow\rangle, |\phi_1^2(\mathbf{r}), \downarrow\rangle, |\phi_2^2(\mathbf{r}), \downarrow\rangle \}, \end{aligned} \quad (2.15)$$

where the $|\phi_j^\mu(\mathbf{r})\rangle$ describe the same as orbitals as in the spinless model and $|\uparrow\rangle, |\downarrow\rangle$ are the spin-1/2 states in the eigenbasis of the σ_3 Pauli matrix. In order to incorporate the SOC in the Hamiltonian \hat{H} with the symmetry of Eq. (2.3), the usual prescription is made

$$\hat{H} \rightarrow \hat{H}_{SOC} = \hat{H} + \lambda \hat{\mathbf{L}} \cdot \hat{\mathbf{s}},$$

where $\hat{\mathbf{L}}$ and $\hat{\mathbf{s}}$ are, respectively, the adimensional orbital and spin angular momentum operators. This model is approximated by considering only the on-site contribution of this interaction to the hopping matrices, so that the spinless hopping terms of Eq. (2.4) are modified as

$$E_{\mu\nu,\alpha\beta}^{ij}(\mathbf{0}) = \langle \phi_\mu^i(\mathbf{r}), \alpha | \hat{H} | \phi_\nu^j(\mathbf{r}), \beta \rangle + \langle \phi_\mu^i(\mathbf{r}), \alpha | \lambda \hat{\mathbf{L}} \cdot \hat{\mathbf{s}} | \phi_\nu^j(\mathbf{r}), \beta \rangle = E_{\mu\nu}^{ij}(\mathbf{0}) \delta_{\alpha\beta} + \Delta E_{\mu\nu,\alpha\beta}^{ij},$$

$$E_{\mu\nu,\alpha\beta}^{ij}(\mathbf{R}_l) = E_{\mu\nu}^{ij}(\mathbf{R}_l) \delta_{\alpha\beta},$$

where α, β are indices in spin space. Thus, it is not necessary to repeat the group theory analysis carried out for the spinless model. In order to evaluate the matrix elements of the SOC term, note that it can be written as (implying tensor products)

$$\hat{\mathbf{L}} \cdot \hat{\mathbf{s}} = \hat{L}_0 \hat{s}_0 + \hat{L}_1 \hat{s}_1 + \hat{L}_2 \hat{s}_2 = \hat{L}_0 \hat{s}_0 + \frac{1}{2} (\hat{L}_- \hat{s}_+ + \hat{L}_+ \hat{s}_-), \quad (2.16)$$

where the operators $\hat{J}_+ = \hat{J}_1 - i\hat{J}_2$ and $\hat{J}_- = \hat{J}_+^\dagger$ were defined. These are the raising and lowering operators of the projection of angular momentum which, for a generic spin- j system, read [109]

$$\hat{J}_\pm |j, m_j\rangle = \sqrt{(j \mp m_j)(j \pm m_j + 1)} |j, m_j \pm 1\rangle.$$

The basis states of Eq. (2.15) can be written as a linear combination of eigenstates of angular momentum, according to Eq. (2.2), which, upon applying the SOC operator Eq. (2.16), yield

$$\begin{cases} |\phi_1^1, m\rangle \propto |2, 0\rangle \otimes |1/2, m\rangle \\ |\phi_1^2, m\rangle \propto i(|2, +2\rangle - |2, -2\rangle) \otimes |1/2, m\rangle \\ |\phi_2^2, m\rangle \propto (|2, +2\rangle + |2, -2\rangle) \otimes |1/2, m\rangle \end{cases} \Rightarrow \begin{cases} \hat{\mathbf{L}} \cdot \hat{\mathbf{s}} |\phi_1^1, m\rangle \propto 0 \times |\phi_1^1, m\rangle + \sqrt{6} |2, \pm 1\rangle |1/2, m\rangle \\ \hat{\mathbf{L}} \cdot \hat{\mathbf{s}} |\phi_1^2, m\rangle \propto +m(2i) |\phi_2^2, m\rangle \mp 2i |2, \mp 1\rangle |1/2, m\rangle \\ \hat{\mathbf{L}} \cdot \hat{\mathbf{s}} |\phi_2^2, m\rangle \propto -m(2i) |\phi_1^2, m\rangle + 2 |2, \mp 1\rangle |1/2, m\rangle \end{cases}$$

It is no surprise that the application of the operator produces states outside of the Hilbert space considered. However, it is safe to project the transformed states back to the Hilbert space of Eq. (2.15), according to the arguments presented in the introduction of the present chapter. Note that this approximation is equivalent to the 1st order of the perturbation theory developed in Appendix A: it amounts to projecting the operator $\lambda \hat{\mathbf{L}} \cdot \hat{\mathbf{s}}$ onto the subspace of interest, in this case, that of Eq. (2.15). Thus, we arrive at

$$\Delta E_{\mu\nu,\alpha\beta}^{ij} = \langle \phi_\mu^i(\mathbf{r}), \alpha | \lambda \hat{\mathbf{L}} \cdot \hat{\mathbf{s}} | \phi_\nu^j(\mathbf{r}), \beta \rangle = \lambda \langle \alpha | \hat{s}_0 | \beta \rangle \otimes \langle \phi_\mu^i(\mathbf{r}) | \hat{L}_0 | \phi_\nu^j(\mathbf{r}) \rangle,$$

which implies that the new TB Hamiltonian can be written as, with $H_{tb}(\mathbf{k})$ the TB Hamiltonian of Eq. (2.14),

$$H_{soc}(\mathbf{k}) = \hat{1} \otimes H_{tb}(\mathbf{k}) + \Delta E = \begin{pmatrix} H_{tb}(\mathbf{k}) + \frac{\lambda}{2} L_0 & 0 \\ 0 & H_{tb}(\mathbf{k}) - \frac{\lambda}{2} L_0 \end{pmatrix},$$

$$\Delta E = \lambda s_0 \otimes L_0 = \frac{\lambda}{2} \begin{pmatrix} L_0 & 0 \\ 0 & -L_0 \end{pmatrix}, \quad L_0 = \begin{pmatrix} 0 & 0 & 0 \\ 0 & 0 & 2i \\ 0 & -2i & 0 \end{pmatrix}. \quad (2.17)$$

Chapter 3

Continuum limit and Berry curvature

Before proceeding, a brief analysis of the Brillouin Zone (BZ) is in order. The low-energy limit of the TB Hamiltonian (2.14) is obtained at the edges of the valence and conduction bands, namely, at the K point of the BZ, as an analysis of $H_{tb}(\mathbf{k})$ can prove. Thus, in order to determine the coordinates of the K point, we shall compute the reciprocal lattice vectors. We can define a pair of primitive vectors from lattice vectors \mathbf{R}_1 and \mathbf{R}_2 :

$$\begin{aligned}\mathbf{R}_1 &= a\mathbf{e}_x, \\ \mathbf{R}_2 &= \frac{1}{2}a\mathbf{e}_x - \frac{\sqrt{3}}{2}a\mathbf{e}_y,\end{aligned}$$

and use the fundamental relation

$$\mathbf{R}_i \cdot \mathbf{G}_j = 2\pi\delta_{ij},$$

where \mathbf{G}_j are reciprocal lattice primitive vectors. In 2D this derivation is straightforward, and a possible solution is

$$\left. \begin{aligned}\mathbf{G}_1 &= \frac{2\pi}{a}\mathbf{e}_x + \frac{2\pi}{\sqrt{3}a}\mathbf{e}_y \\ \mathbf{G}_2 &= \frac{4\pi}{\sqrt{3}a}\mathbf{e}_y\end{aligned}\right\} \Rightarrow \cos(\mathbf{G}_1 \wedge \mathbf{G}_2) = \frac{1}{2}.$$

The BZ is thus a hexagon with side $4\pi/(3a)$ with two of its vertices on the x -axis. We consider the $\pm K$ points on the x -axis. Taking the symbol τ to be the signs plus or minus, according to the respective K -point, these have coordinates

$$\tau\mathbf{K} = \left(\tau \frac{4\pi}{3a}, 0 \right). \quad (3.1)$$

Our interest in studying the electronic structure of the material at the K point of the BZ is due to the fact that most of the physical processes that define the properties of the system take place in the vicinity of the Fermi level. Since electrons are constrained to the vicinity of the Fermi level, in virtue of the Pauli exclusion principle or, more succinctly, due to the fermionic statistic, low-energy (or, equivalently, low-momentum) excitations will be responsible for most of the electronic properties of the material.

Thus, we consider momenta $\mathbf{k} = \mathbf{K} + \mathbf{q}$, such that $\|a\mathbf{q}\| \ll \|a\mathbf{K}\|$, where a is the lattice constant, and Taylor expand the TB Hamiltonian $H_{tb}(\mathbf{k})$ in Taylor series up to n -th order, which can be written as:

$$H_{tb}(\mathbf{K} + \mathbf{q}) = H_{tb}(\mathbf{K}) + \sum_{m=1}^n H^{(m)}(\mathbf{q}) + \mathcal{O}(aq)^{n+1}, \quad H^{(m)}(\mathbf{q}) = \frac{1}{m!} \prod_{i=1}^m q^{\alpha_i} \left(\prod_{j=1}^m \partial_{\alpha_j} H_{tb} \right) (\mathbf{K}).$$

From this point on, we will concern ourselves only with the case $n = 2$. We are left with the problem of diagonalizing the expanded TB Hamiltonian followed by the projection onto the appropriate subspace of the eigenbasis, since our interest is to arrive at a spinor description (a Dirac Hamiltonian) of charge carriers on the valence and conduction bands.

We can employ a systematic method which, essentially, consists of treating the higher order terms in the expanded TB Hamiltonian as a perturbation. The method can be outlined as shown in Appendix A.

3.1 Computation of the Dirac Hamiltonian

3.1.1 Taylor expansion of the TB Hamiltonian

The Taylor expansion of the TB Hamiltonian of Eq. (2.14) up to 2nd order reads

$$\begin{aligned} H_{tb}(\tau\mathbf{K} + \mathbf{q}) &= H_{tb}(\tau\mathbf{K}) + H_{\mathbf{q}}^{(1)} + H_{\mathbf{q}}^{(2)} + \mathcal{O}(aq)^3 \\ &= H_{tb}(\tau\mathbf{K}) + q^\mu (\partial_\mu H_{tb})(\tau\mathbf{K}) + \frac{1}{2} q^\mu q^\nu (\partial_\nu \partial_\mu H_{tb})(\tau\mathbf{K}) + \mathcal{O}(aq)^3 \\ &= \begin{pmatrix} \eta_0 & \eta_1 & \eta_2 \\ \eta_1^* & \eta_{11} & \eta_{12} \\ \eta_2^* & \eta_{12}^* & \eta_{22} \end{pmatrix} + a \begin{pmatrix} u_0 & u_1 & u_2 \\ u_1^* & u_{11} & u_{12} \\ u_2^* & u_{12}^* & u_{22} \end{pmatrix} + a^2 \begin{pmatrix} v_0 & v_1 & v_2 \\ v_1^* & v_{11} & v_{12} \\ v_2^* & v_{12}^* & v_{22} \end{pmatrix} + \mathcal{O}(aq)^3, \end{aligned} \tag{3.2}$$

0-th Order

$$\left| \begin{array}{l} \eta_0 = \epsilon_1 - 3t_0 \\ \eta_{11} = \eta_{22} = \epsilon_2 - \frac{3}{2}(t_{11} + t_{22}) \end{array} \right. , \quad \left| \begin{array}{l} \eta_1 = \eta_2 = 0 \\ \eta_{12} = -i\tau 3\sqrt{3}t_{12} \end{array} \right. ,$$

1-st Order

$$\left| \begin{array}{l} u_0 = 0 \\ u_{11} = -\tau \frac{3\sqrt{3}}{4} (t_{22} - t_{11}) q_x, \\ u_{22} = \tau \frac{3\sqrt{3}}{4} (t_{22} - t_{11}) q_x \end{array} \right| \quad \left| \begin{array}{l} u_1 = -\tau \frac{3\sqrt{3}}{2} t_2 q_y - \frac{3}{2} i t_1 q_x \\ u_2 = \tau \frac{3\sqrt{3}}{2} t_2 q_x - \frac{3}{2} i t_1 q_y \\ u_{12} = \tau \frac{3\sqrt{3}}{4} (t_{22} - t_{11}) q_y \end{array} \right.$$

2-nd Order

$$\left| \begin{array}{l} v_0 = \frac{3}{4} t_0 \mathbf{q}^2 \\ v_{11} = \frac{3}{16} [(3t_{11} + t_{22})q_1^2 + (t_{11} + 3t_{22})q_2^2], \\ v_{22} = \frac{3}{16} [(3t_{11} + t_{22})q_2^2 + (t_{11} + 3t_{22})q_1^2] \end{array} \right| \quad \left| \begin{array}{l} v_1 = \frac{3}{4} t_2 q_1 q_2 + i\tau \frac{3\sqrt{3}}{8} t_1 (q_1^2 - q_2^2) \\ v_2 = \frac{3}{8} t_2 (q_1^2 - q_2^2) - i\tau \frac{3\sqrt{3}}{4} t_1 q_1 q_2 \\ v_{12} = -\frac{3}{8} (t_{22} - t_{11}) q_1 q_2 + i\tau \frac{3\sqrt{3}}{4} t_{12} \mathbf{q}^2 \end{array} \right.$$

This result can be obtained simply by first performing transforming coordinates as $\mathbf{k} = \tau 4\pi/(3a) + \mathbf{q}$ and expanding all trigonometric functions up to 2nd order in q_1 and q_2 , making use of the trigonometric identities for the sum of two variables in the argument.

Diagonalization of the TB Hamiltonian at the K -point

The TB Hamiltonian at the $\pm K$ -point is the 0th order term of Eq. (3.2), which reads

$$H_{tb}(\tau \mathbf{K}) = \begin{pmatrix} \epsilon_1 - 3t_0 & 0 & 0 \\ 0 & \epsilon_2 - \frac{3}{2}(t_{11} + t_{22}) & -i\tau 3\sqrt{3}t_{12} \\ 0 & i\tau 3\sqrt{3}t_{12} & \epsilon_2 - \frac{3}{2}(t_{11} + t_{22}) \end{pmatrix}.$$

Solving the eigenproblem is straightforward, yielding

$$\left\{ \begin{array}{ll} |\psi^c(\tau \mathbf{K})\rangle = |\varphi_1^1(\tau \mathbf{K})\rangle = |Y_2^0(\tau \mathbf{K})\rangle & , \quad \varepsilon_c = \epsilon_1 - 3t_0 \\ |\psi^v(\tau \mathbf{K})\rangle = \frac{1}{\sqrt{2}} (|\varphi_2^2(\tau \mathbf{K})\rangle + i\tau |\varphi_1^2(\tau \mathbf{K})\rangle) = |Y_2^{\tau 2}(\tau \mathbf{K})\rangle, & \varepsilon_v = \epsilon_2 - \frac{3}{2}(t_{11} + t_{22}) - 3\sqrt{3}t_{12} \\ |\psi^h(\tau \mathbf{K})\rangle = \frac{1}{\sqrt{2}} (|\varphi_2^2(\tau \mathbf{K})\rangle - i\tau |\varphi_1^2(\tau \mathbf{K})\rangle) = |Y_2^{\tau 2}(\tau \mathbf{K})\rangle, & \varepsilon_h = \epsilon_2 - \frac{3}{2}(t_{11} + t_{22}) + 3\sqrt{3}t_{12} \end{array} \right. . \quad (3.3)$$

The indices c , v and h were attributed on grounds of the results presented in Ref. [1], relatively to the orbital contribution to each band. As shown in the reference, in the neighbourhood of the band edges the lowest unoccupied band (LUB) is largely composed of d_{z^2} orbitals, whereas the highest occupied band (HOB) is predominantly a combination of $d_{x^2-y^2}$ and d_{xy} orbitals. Thus, it is clear that the state belonging in the LUB is that which is equal to the d_{z^2} state. However, it is still indeterminate which of the states spanned by $d_{x^2-y^2}$ and d_{xy} orbitals has an energy closer to and below the LUB, thus belonging in the HOB.

Table 3.1: Energies of states at the K -point and the Fermi energy, gap and inter-band hoppings to 1st order in aq , base on the numerical values of Table 2.3. (Units: eV)

MX_2	ε_c	ε_v	ε_h	ε_F	2Δ	${}_1t_{vc}$	${}_1t_{ch}$	${}_1t_{vh}$
MoS ₂	1.598	-0.065	3.448	0.767	1.663	1.357	0.506	-0.365
WS ₂	1.748	-0.058	3.933	0.845	1.806	1.586	0.383	-0.578
MoSe ₂	1.483	0.047	3.060	0.764	1.436	1.174	0.502	-0.208
WSe ₂	1.564	0.024	3.443	0.794	1.540	1.378	0.408	-0.383

Since there is no intuition regarding the order relation between the different parameters in the model, estimations of the magnitudes of each eigenvalue had to be computed and compared. This was done using the hopping integrals show in Table 2.3. The results are presented in Table 3.1. It is clear that the state spanned by $d_{x^2-y^2}$ and d_{xy} belonging in the HOB is that labeled with the index v in Eq. (3.3). Table 3.1 presents also values for the Fermi energy, gap and the various inter-band effective hoppings to 1st order, which expressions shall be arrived at further on.

The transformation matrix can be inferred from Eq. (3.3), reading

$$U_\tau = \begin{pmatrix} 1 & 0 & 0 \\ 0 & -i\tau/\sqrt{2} & 1/\sqrt{2} \\ 0 & i\tau/\sqrt{2} & 1/\sqrt{2} \end{pmatrix}.$$

Thus, the higher-order matrices in the eigenbasis of $H_{tb}(\mathbf{K}_\tau)$ can be generically written as

$$\begin{aligned} \Sigma^{(m)}(\mathbf{q}) &= U_\tau [H^{(m)}(\mathbf{q})] U_\tau^\dagger \\ &= \begin{pmatrix} h_0 & \frac{1}{\sqrt{2}}(h_2 + i\tau h_1) & \frac{1}{\sqrt{2}}(h_2 - i\tau h_1) \\ \frac{1}{\sqrt{2}}(h_2 + i\tau h_1)^* & \frac{1}{2}(h_{22} + h_{11}) + \tau \text{Im } h_{12} & \frac{1}{2}(h_{22} - h_{11}) - i\tau \text{Re } h_{12} \\ \frac{1}{\sqrt{2}}(h_2 - i\tau h_1)^* & \frac{1}{2}(h_{22} - h_{11}) + i\tau \text{Re } h_{12} & \frac{1}{2}(h_{22} + h_{11}) - \tau \text{Im } h_{12} \end{pmatrix}, \quad h = u, v. \end{aligned} \quad (3.4)$$

3.1.2 1st and 2nd order Perturbation Theory for the spinless TB-Hamiltonian

1st order: massive Dirac Hamiltonian

The perturbation theory analysis outlined in the appendix can now be carried out. Using Eq. (3.4), the 1st order term in the Taylor expansion becomes

$$\Sigma^{(1)}(\mathbf{q}) = a \begin{pmatrix} 0 & {}_1t_{vc}(\tau q_x - iq_y) & {}_1t_{ch}(\tau q_x + iq_y) \\ {}_1t_{vc}(\tau q_x + iq_y) & 0 & {}_1t_{vh}(\tau q_x - iq_y) \\ {}_1t_{ch}(\tau q_x - iq_y) & {}_1t_{vh}(\tau q_x + iq_y) & 0 \end{pmatrix}, \quad (3.5)$$

where the parameters ${}_1t_{vc}$, ${}_1t_{ch}$ and ${}_1t_{vh}$ are the 1st order effective hoppings between the three bands, which read

$${}_1t_{vc} = \frac{3}{2\sqrt{2}}(\sqrt{3}t_2 + t_1), \quad {}_1t_{ch} = \frac{3}{2\sqrt{2}}(\sqrt{3}t_2 - t_1), \quad {}_1t_{vh} = \frac{3\sqrt{3}}{4}(t_{22} - t_{11}), \quad (3.6)$$

Inserting the matrix of Eq. (3.5) in Eq. (A.5), we arrive at the 1st-order effective Hamiltonian:

$$\begin{aligned} H_{eff}^{(1)}(\mathbf{q}) &= P_1 H_0 P_1 + \Sigma_1^{(1)}(\mathbf{q}) \\ &= \begin{pmatrix} \varepsilon_c & 0 \\ 0 & \varepsilon_v \end{pmatrix} + a t_{vc} \begin{pmatrix} 0 & \tau q_x - iq_y \\ \tau q_x + iq_y & 0 \end{pmatrix}. \end{aligned} \quad (3.7)$$

Noting that the Fermi energy is at the mid-point between the maximum of the valence band and minimum of the conduction band, in virtue of the symmetry of the Fermi distribution and electron-hole symmetry, we can rewrite the first term in Eq. (3.7) as

$$\begin{pmatrix} \varepsilon_c & 0 \\ 0 & \varepsilon_v \end{pmatrix} = \varepsilon_F + \begin{pmatrix} \Delta & 0 \\ 0 & -\Delta \end{pmatrix}, \quad \varepsilon_F = \frac{\varepsilon_c + \varepsilon_v}{2}, \quad \Delta = \frac{\varepsilon_c - \varepsilon_v}{2}, \quad (3.8)$$

where 2Δ is the gap between the valence band maximum and the conduction band minimum. Finally, setting the zero of energy to ε_F and introducing the Pauli matrices,

$$\sigma_1 = \begin{pmatrix} 0 & 1 \\ 1 & 0 \end{pmatrix}, \quad \sigma_2 = \begin{pmatrix} 0 & -i \\ i & 0 \end{pmatrix}, \quad \sigma_3 = \begin{pmatrix} 1 & 0 \\ 0 & -1 \end{pmatrix}, \quad \text{where } x_1 = x, x_2 = y, \quad (3.9)$$

we arrive at the Dirac Hamiltonian for low-energy charge carriers

$$H_D(\mathbf{k}) = at(\tau_3 \sigma_1 k_1 + \sigma_2 k_2) + \Delta \sigma_3. \quad (3.10)$$

Here, $t \equiv {}_1t_{vc}$ is the 1st order valence-conduction band effective hopping and the sign τ of the K -point, or valley, has been substituted with a Pauli matrix τ_3 in the space of valley indices. The inequivalent valleys $\pm K$ constitute an additional Hilbert space of the low-energy electrons states, analogous to a spin index. The tensor product $\tau_3 \otimes \sigma_1$ is implied, as well as $\hat{1}_\tau \otimes \sigma_3$ and $\hat{1}_\tau \otimes \sigma_2$. Note that this Hamiltonian is found to 1st order in any monolayer honeycomb lattice with broken inversion-symmetry. Thus, all results obtained using this Hamiltonian are true for any material in the aforementioned symmetry class. Diagonalizing the Hamiltonian

$$H_D(\mathbf{k}) = \begin{pmatrix} \Delta & atk_{\tau+} \\ atk_{\tau-} & -\Delta \end{pmatrix},$$

where $k_{\tau+} = \tau k_1 - ik_2$, with $k_{\tau-} = k_{\tau+}^*$, which obey $k_{\tau-}k_{\tau+} = \mathbf{k}^2$, yields the eigenvalues

$$E_\sigma^{(1)} = \sigma E_{\mathbf{k}} = \sigma \sqrt{\Delta^2 + a^2 t^2 \mathbf{k}^2}, \quad \sigma = \begin{cases} + & , \text{ if } c \\ - & , \text{ if } v \end{cases} \quad (3.11)$$

and the normalized eigenstates

$$|\mathbf{k}, \sigma, \tau\rangle = \frac{atk_{\tau\sigma} |\psi^\sigma(\tau\mathbf{K})\rangle + \sigma(E_{\mathbf{k}} - \Delta) |\psi^{\bar{\sigma}}(\tau\mathbf{K})\rangle}{\sqrt{(E_{\mathbf{k}} - \Delta)^2 + a^2 t^2 \mathbf{k}^2}}, \quad (3.12)$$

with $\bar{\sigma} = -\sigma$ and $\sigma = +$ for the conduction band and $\sigma = -$ for the valence band. In turn, writing $k_{\tau\pm}$ in polar form, so that Eq. (3.10) becomes

$$H_D(\mathbf{k}) = \begin{pmatrix} \Delta & at\mathbf{k} e^{-i\varphi_{\mathbf{k}}} \\ at\mathbf{k} e^{+i\varphi_{\mathbf{k}}} & -\Delta \end{pmatrix}, \quad \mathbf{k} \equiv \|\mathbf{k}\|,$$

and defining the phase $\varphi_{\mathbf{k}}$ and the angle $\theta_{\mathbf{k}}$ as

$$\varphi_{\mathbf{k}} = \arctan\left(\frac{k_2}{k_1}\right), \quad \theta_{\mathbf{k}} = 2 \arctan\left(\frac{E_{\mathbf{k}} - \Delta}{at\mathbf{k}}\right), \quad (3.13)$$

it is possible to rewrite the states of Eq. (3.12) more compactly, as

$$|\mathbf{k}, \sigma, \tau\rangle = \cos \frac{\theta_{\mathbf{k}}}{2} e^{-i\sigma\tau\varphi_{\mathbf{k}}} |\psi^\sigma(\tau\mathbf{K})\rangle + \sigma \sin \frac{\theta_{\mathbf{k}}}{2} |\psi^{\bar{\sigma}}(\tau\mathbf{K})\rangle, \quad (3.14)$$

which is the most general form for the eigenstates of a two-level system. Notice that this parametrization maps each point in the northern hemisphere of the unit 2-sphere S^2 to a pair of states of the two-level system.

Another useful representation of this linear combination is found by noticing that $a^2 t^2 \mathbf{k}^2 = E_{\mathbf{k}}^2 - \Delta^2$, in which case Eq. (3.12) can be rewritten compactly as

$$|\mathbf{k}, \sigma, \tau\rangle = e^{-i\sigma\tau\varphi_{\mathbf{k}}} \sqrt{\frac{1}{2} \left(1 + \frac{\Delta}{E_{\mathbf{k}}}\right)} |\psi^\sigma(\tau\mathbf{K})\rangle + \sigma \sqrt{\frac{1}{2} \left(1 - \frac{\Delta}{E_{\mathbf{k}}}\right)} |\psi^{\bar{\sigma}}(\tau\mathbf{K})\rangle. \quad (3.15)$$

2nd order: Trigonal Warping

The 2nd order term of the effective Hamiltonian has two contributions: one from the 1st order perturbation of the 2nd order term of the Taylor expansion, which will be denoted by $\Sigma_1^{(2)}(\mathbf{q})$, and another from the 2nd order perturbation of the 1st order term of the Taylor expansion, denoted by $\Sigma_2^{(1)}(\mathbf{q})$. Beginning with the former, application of Eq. (3.4) yields

$$\Sigma^{(2)}(\mathbf{q}) = a^2 \begin{pmatrix} \chi_c \mathbf{q}^2 & {}_2 t_{vc} q_{\tau-}^2 & {}_2 t_{ch} q_{\tau+}^2 \\ {}_2 t_{vc} q_{\tau+}^2 & \chi_v \mathbf{q}^2 & {}_2 t_{vh} q_{\tau-}^2 \\ {}_2 t_{ch}^2 q_{\tau-}^2 & {}_2 t_{vh} q_{\tau+}^2 & \chi_h \mathbf{q}^2 \end{pmatrix},$$

where $q_{\tau+} = \tau q_1 - iq_2$, with $q_{\tau-} = q_{\tau+}^*$, and the off-diagonal parameters are the 2nd order effective inter-band hoppings and the diagonal parameters are the contributions to the concavities of each band:

$$\begin{aligned} {}_2 t_{vc} &= \frac{3}{8\sqrt{2}}(t_2 - \sqrt{3}t_1), & {}_2 t_{ch} &= \frac{3}{8\sqrt{2}}(t_2 + \sqrt{3}t_1), & {}_2 t_{vh} &= \frac{3}{16}(t_{22} - t_{11}), \\ \chi_c &= \frac{3}{4}t_0, & \chi_v &= \frac{3}{8}(t_{11} + t_{22} + \sqrt{3}t_{12}), & \chi_h &= \frac{3}{8}(t_{11} + t_{22} - \sqrt{3}t_{12}). \end{aligned} \quad (3.16)$$

Thus, the 1st order perturbation from this term is

$$\Sigma_1^{(2)}(\mathbf{q}) = a^2 \begin{pmatrix} \chi_c \mathbf{q}^2 & {}_2 t_{vc} q_{\tau-}^2 \\ {}_2 t_{vc} q_{\tau+}^2 & \chi_v \mathbf{q}^2 \end{pmatrix}.$$

As for the latter, inserting the 1st order term of Eq. (3.5) in Eq. (A.6) one obtains

$$\begin{aligned} \Sigma_2^{(1)}(\mathbf{q}) &= -\frac{P_1 \Sigma^{(1)} P_h \Sigma^{(1)} P_1}{\varepsilon_h - P_1 H_0 P_1} \\ &= -\begin{pmatrix} \Sigma_{13}^{(1)} \Sigma_{31}^{(1)} / (\varepsilon_h - \varepsilon_c) & \Sigma_{13}^{(1)} \Sigma_{32}^{(1)} / \varepsilon_h \\ \Sigma_{23}^{(1)} \Sigma_{31}^{(1)} / \varepsilon_h & \Sigma_{23}^{(1)} \Sigma_{32}^{(1)} / (\varepsilon_h - \varepsilon_v) \end{pmatrix} = a^2 \begin{pmatrix} \xi_c \mathbf{q}^2 & {}_1 t_{vhc} q_{\tau-}^2 \\ {}_1 t_{vhc} q_{\tau+}^2 & \xi_v \mathbf{q}^2 \end{pmatrix}. \end{aligned}$$

The parameters represent effective hoppings and contributions to the concavities, reading

$${}_1 t_{vhc} = -\frac{({}_1 t_{vh})({}_1 t_{ch})}{\varepsilon_h}, \quad \xi_c = -\frac{({}_1 t_{ch})^2}{\varepsilon_h - \varepsilon_c}, \quad \xi_v = -\frac{({}_1 t_{vh})^2}{\varepsilon_h - \varepsilon_v}. \quad (3.17)$$

Finally, the 2nd order effective Hamiltonian can be written

$$\begin{aligned} H_{eff}^{(2)}(\mathbf{q}) &= H_{eff}^{(1)}(\mathbf{q}) + \Sigma_1^{(2)}(\mathbf{q}) + \Sigma_2^{(1)}(\mathbf{q}) \\ &= \begin{pmatrix} \varepsilon_c & {}_1 t_{vc} q_{\tau+} \\ {}_1 t_{vc} q_{\tau-} & \varepsilon_v \end{pmatrix} + a^2 \begin{pmatrix} (\chi_c + \xi_c) \mathbf{q}^2 & ({}_2 t_{vc} + {}_1 t_{vhc}) q_{\tau-}^2 \\ ({}_2 t_{vc} + {}_1 t_{vhc}) q_{\tau+}^2 & (\chi_v + \xi_v) \mathbf{q}^2 \end{pmatrix} \\ &= \begin{pmatrix} \varepsilon_c + \kappa_c a^2 \mathbf{q}^2 & t a q_{\tau+} + u a^2 q_{\tau-}^2 \\ t a q_{\tau-} + u a^2 q_{\tau+}^2 & \varepsilon_v + \kappa_v a^2 \mathbf{q}^2 \end{pmatrix}, \end{aligned} \quad (3.18)$$

with $\kappa_{v,c} \equiv \chi_{v,c} + \xi_{v,c}$, $t \equiv {}_1 t_{vc}$ and $u \equiv {}_2 t_{vc} + {}_1 t_{vhc}$. Estimations of the relevant 2nd order parameters can be read from Table 3.2. These were obtained using the numerical values of Table 3.1.

It is noteworthy that the contribution from 2nd order perturbation theory is comparable with the contribution from the Taylor expansion, contrary to what would be expected: since the per-

Table 3.2: Band concavity contributions and inter-band hoppings to 2nd order in aq , based on the numerical values of Tables 2.3 and 3.1. (Units: eV)

MX_2	${}_2t_{vc}$	${}_1t_{vhc}$	χ_c	χ_v	ξ_c	ξ_v	u	κ_c	κ_v
MoS_2	-0.0497	0.0536	-0.1380	0.3227	-0.1385	-0.0379	+0.0039	-0.2765	0.2847
WS_2	-0.1183	0.0563	-0.1545	0.3338	-0.0673	-0.0837	-0.0619	-0.2217	0.2501
MoSe_2	-0.0247	0.0341	-0.1410	0.3162	-0.1594	-0.0143	+0.0094	-0.3004	0.3019
WSe_2	-0.0810	0.0454	-0.1553	0.3251	-0.0886	-0.0430	-0.0356	-0.2439	0.2821

turbation theory contribution is due to transitions to a higher-energy band, it should be smaller than the band-intrinsic contribution that results from the Taylor expansion of the tight-binding content of the system. To attain deeper intuition into this behaviour, consider the ratio of the trace of $\Sigma_2^{(1)}(\mathbf{q})$ (perturbation theory) to the trace of $\Sigma_1^{(2)}(\mathbf{q})$ (Taylor expansion) for various MX_2 , which yields

$$\left| \frac{\text{Tr } \Sigma_2^{(1)}(\mathbf{q})}{\text{Tr } \Sigma_1^{(2)}(\mathbf{q})} \right| = \left| \frac{\xi_c + \xi_v}{\chi_c + \chi_v} \right| = \begin{cases} 0.96 & , \text{MoS}_2 \\ 0.84 & , \text{WS}_2 \\ 0.99 & , \text{MoSe}_2 \\ 0.75 & , \text{WSe}_2 \end{cases} .$$

These ratios are, indeed, very close to unity and, therefore, both contributions are of the same order of magnitude. This result can be traced back to four factors:

1. The coefficients on the numerator, from the perturbative contribution, have a structure given by Eq. (3.17). Although the effective hoppings are of the same order of magnitude, there is a noticeable tendency for the conduction band hopping to be greater by factors of the order of unity. This difference is amplified due to the quadratic power, which can be physically traced back to these contributions stemming from the electronic transitions back and forth between bands. On the other hand, the higher-energy band is energetically closer to the conduction band than to the valence band, by a factor of approximately two, which affects the energy scale in the denominator. Indeed, the difference in hopping magnitudes can be seen as a consequence of this energetic proximity as well and, ultimately, this proximity results in the contribution to the conduction band being, generally, greater than the contribution to the valence band, as shown in Table 3.2. Additionally, the magnitude of the relevant hoppings are comparable to those of the band gaps at the K -point;
2. The relation of magnitude is reversed for the contributions from the tight-binding contribution. To understand why, notice the orbital composition of the valence and conduction bands in a vicinity of the K -points. Whereas the conduction band can only afford to have contributions from the hopping between d_{z^2} orbitals, encoded by t_0 , the valence band can have contributions from hoppings to and between the two orbitals d_{xy} and $d_{x^2-y^2}$, given

by t_{11} , t_{22} and t_{12} . This is clear from the structure of the parameters χ_c and χ_v as given in Eq. (3.16). Thus, as it is possible to check in Table 3.2, the contribution to the valence band is, in all cases, distinctly greater than the contribution to the conduction band;

3. One may also notice that the numerical pre-factors attached to the tight-binding contribution reduce substantially the magnitude of these terms. These factors result from the geometric factors attached to the crystal momentum components in the TB Hamiltonian (2.14), and they reflect the fact that electrons cannot hop to a nearest-neighbour lattice site in any arbitrary direction, but only along the directions defined by lattice vectors. This imposes a constraint on electron transport which, naturally, reduces the energetic contribution of the quadratic contribution from the tight-binding content;
4. Additionally, there is a sign difference between the tight-binding contributions, due to $t_0 < 0$ in all cases, which slightly decreases the total magnitude of this contribution. The negative sign of this orbital hopping is, in fact, a consequence of the symmetries of the d_{z^2} orbitals [107].

Diagonalizing the 2nd order Hamiltonian of Eq. (3.18), the spectrum for the valence and conduction bands yield

$$E_\sigma^{(2)} = \varepsilon_F + \kappa_+ a^2 \mathbf{q}^2 + \sigma \sqrt{(\Delta - \kappa_- a^2 \mathbf{q}^2)^2 + (t^2 + u^2 a^2 \mathbf{q}^2) a^2 \mathbf{q}^2 + 2\tau tua^3 \mathbf{q}^3 \cos 3\theta},$$

with ε_F and Δ defined as in Eq. (3.8) and $\kappa_\pm = (\kappa_v \pm \kappa_c)/2$. Note that this dispersion is no longer axially symmetric, as it was in 1st order, due to the the 3rd order term in the square root. It is easy to show that, however, it is invariant under operations of the symmetry group of the lattice, as given in Eq. (2.5), namely, rotations of multiples of $2\pi/3$ and, when conjugated with exchange of valley index, reflections through the angular bisectors. The necessity for the exchange of valley index to preserve invariance reflects the relation between symmetry operations and the equivalence of valleys: equivalent valleys are related by rotations, whereas inequivalent valleys are related by reflections. This breaking of rotational symmetry is known as trigonal warping and, as shown, becomes relevant only in 2nd order of aq .

Taking after Eq. (3.15), we can write down the states in the 2nd order approximation as

$$|\mathbf{k}, \sigma, \tau\rangle = e^{-i\sigma\varphi_k^\tau} \sqrt{\frac{1}{2} \left(1 + \frac{\Delta_k}{E_k^\tau}\right)} |\psi^\sigma(\tau\mathbf{k})\rangle + \sigma \sqrt{\frac{1}{2} \left(1 - \frac{\Delta_k}{E_k^\tau}\right)} |\psi^{\bar{\sigma}}(\tau\mathbf{k})\rangle,$$

where Δ_k , φ_k^τ and E_k^τ read

$$\Delta_k = \Delta - \kappa_- a^2 \mathbf{k}^2, \quad \varphi_k^\tau = \arctan \left(\tau \frac{t \sin \theta - \tau u a k \sin 2\theta}{t \cos \theta + \tau u a k \cos 2\theta} \right),$$

$$E_k^\tau = \sqrt{\Delta_k^2 + (t^2 + u^2 a^2 \mathbf{k}^2) a^2 \mathbf{k}^2 + 2\tau tua^3 \mathbf{k}^3 \cos 3\theta}.$$

3.1.3 1st and 2nd order Perturbation Theory for the SOC-TB Hamiltonian

A perturbative expansion of the spinful TB Hamiltonian can also be obtained. We start by computing the Hamiltonian of Eq. (2.17) at the $\pm K$ -points of the BZ, which reads

$$\begin{aligned} H_{soc}^\alpha(\mathbf{K}_\tau) &= H_{tb}(\mathbf{K}_\tau) + \frac{\alpha\tau\lambda}{2}L_0 \\ &= \begin{pmatrix} \epsilon_1 - 3t_0 & 0 & 0 \\ 0 & \epsilon_2 - \frac{3}{2}(t_{11} + t_{22}) & -i\tau 3\sqrt{3}t_{12} + i\tau\alpha\lambda \\ 0 & i\tau 3\sqrt{3}t_{12} - i\tau\alpha\lambda & \epsilon_2 - \frac{3}{2}(t_{11} + t_{22}) \end{pmatrix}, \end{aligned}$$

where we have introduced the symbol $\alpha = \pm$ to denote the spin index. The inclusion of the valley index in the spin-splitting term is due to the fact that the $+K$ and $-K$ valleys are connected by time reversal. In turn, a time-reversal operation on spin-1/2 states induces spin-flip [109]. Thus, it is necessary to couple the valley index to the spin index. Solving the eigenproblem is straightforward, yielding, similarly to Eq. (3.3),

$$\begin{cases} |\psi^c(\tau\mathbf{K}), \alpha\rangle = |\varphi_1^1(\tau\mathbf{K})\rangle |\alpha\rangle & , \quad \varepsilon_{c,\alpha} = \varepsilon_c \\ |\psi^v(\tau\mathbf{K}), \alpha\rangle = \frac{1}{\sqrt{2}} (|\varphi_2^2(\tau\mathbf{K})\rangle + i\tau |\varphi_1^2(\tau\mathbf{K})\rangle) |\alpha\rangle, & \varepsilon_{v,\alpha} = \varepsilon_v + \alpha\tau\lambda , \\ |\psi^h(\tau\mathbf{K}), \alpha\rangle = \frac{1}{\sqrt{2}} (|\varphi_2^2(\tau\mathbf{K})\rangle - i\tau |\varphi_1^2(\tau\mathbf{K})\rangle) |\alpha\rangle, & \varepsilon_{h,\alpha} = \varepsilon_h - \alpha\tau\lambda \end{cases} \quad (3.19)$$

where the energies ε_c , ε_v and ε_h are the same as in Eq. (3.3). It is immediately evident that the valence band at the K -point becomes spin-split by the amount

$$\Delta\varepsilon_{v,\tau} = \varepsilon_{v,\tau\uparrow} - \varepsilon_{v,\tau\downarrow} = 2\tau\lambda. \quad (3.20)$$

Since the SOC-splitting modifies only diagonal terms in the K -point eigenbasis, the perturbation theory analysis is exactly equal in this case as it was in Sec. 3.1. Thus, the effective Hamiltonian up to 1-st order in perturbation theory can be written as

$$H_{eff}^{(1)}(\mathbf{q}) = \begin{pmatrix} \varepsilon_c & 0 \\ 0 & \varepsilon_v \end{pmatrix} + a_1 t_{vc} \begin{pmatrix} 0 & \tau q_x - iq_y \\ \tau q_x + iq_y & 0 \end{pmatrix} + \alpha\tau\lambda \begin{pmatrix} 0 & 0 \\ 0 & 1 \end{pmatrix}.$$

Separating the first term into the sum of the Fermi energy with the half-gap using Eq. (3.8), introducing Pauli matrices as in Eq. (3.9), to simplify the second and third terms, and replacing the valley and spin indices with appropriate Pauli matrices τ_3 and s_3 , respectively, the Dirac Hamiltonian yields

$$H_D(\mathbf{p}) = at(\tau_3 \sigma_1 k_1 + \sigma_2 k_2) + \Delta \sigma_3 + \lambda \tau_3 (1 - \sigma_3) s_3,$$

(3.21)

where tensor products between operators acting on the different Hilbert spaces are all implied and v_F is the Fermi velocity, as defined in Sec. 3.1.

Upon diagonalization, the Dirac Hamiltonian of Eq. (3.21) yields the eigenvalues

$$E_{c,v}^{\alpha\tau} = \frac{\alpha\tau\lambda}{2} \pm E_{\mathbf{k}} = \frac{\alpha\tau\lambda}{2} \pm \sqrt{(\Delta^{\alpha\tau})^2 + a^2 t^2 \mathbf{k}^2}, \quad \Delta^{\alpha\tau} = \Delta - \frac{\alpha\tau\lambda}{2},$$

associated to the normalized eigenstates

$$|\mathbf{k}, \sigma, \tau, \alpha\rangle = e^{-i\sigma\tau\theta} \sqrt{\frac{1}{2} \left(1 + \frac{\Delta^{\alpha\tau}}{E_{\mathbf{k}}^{\alpha\tau}}\right)} |\psi^\sigma(\tau\mathbf{K}), \alpha\rangle + \sigma \sqrt{\frac{1}{2} \left(1 - \frac{\Delta^{\alpha\tau}}{E_{\mathbf{k}}^{\alpha\tau}}\right)} |\psi^{\bar{\sigma}}(\tau\mathbf{K}), \alpha\rangle, \quad (3.22)$$

Thus, the eigenstates of the spinful Dirac Hamiltonian can be obtained from those of the spinless model through the affine transformations of the half-gap and of the Fermi energy,

$$\Delta \mapsto \Delta^{\alpha\tau} = \Delta - \alpha\tau\lambda/2 \quad \text{and} \quad \varepsilon_F \mapsto \varepsilon_F + \alpha\tau\lambda/2. \quad (3.23)$$

As such, the solutions to the 2nd order Hamiltonian can be readily inferred, yielding, for the spectrum and eigenstates,

$$\begin{aligned} E_{\sigma,\alpha,\tau}^{(2)} &= \varepsilon_F + \frac{\alpha\tau\lambda}{2} + \kappa_+ a^2 \mathbf{k}^2 + \sigma E_{\mathbf{k}}^{\alpha,\tau}, \\ E_{\mathbf{k}}^{\alpha,\tau} &= \sqrt{(\Delta^{\alpha\tau} - \kappa_- a^2 \mathbf{k}^2)^2 + (t^2 + u^2 a^2 \mathbf{k}^2) a^2 \mathbf{k}^2 + 2\tau t u a^3 \mathbf{k}^3 \cos 3\theta}, \end{aligned} \quad (3.24)$$

$$|\mathbf{k}, \sigma, \tau, \alpha\rangle = e^{-i\sigma\varphi_{\mathbf{k}}} \sqrt{\frac{1}{2} \left(1 + \frac{\Delta^{\alpha\tau}}{E_{\mathbf{k}}^{\alpha,\tau}}\right)} |\psi^\sigma(\tau\mathbf{K}), \alpha\rangle + \sigma \sqrt{\frac{1}{2} \left(1 - \frac{\Delta^{\alpha\tau}}{E_{\mathbf{k}}^{\alpha,\tau}}\right)} |\psi^{\bar{\sigma}}(\tau\mathbf{K}), \alpha\rangle. \quad (3.25)$$

3.1.4 Effective masses

It is possible to obtain the effective masses of charge carriers in the valence and conduction bands by expanding the effective Hamiltonians up to quadratic order in q . In this section, m_e refers to the bare mass of the electron and all numerical values used are those of Tables 3.1 and 3.2, of Ref. [1] for material parameters and of Ref. [110] for physical constants.

Spinless

For the 1st order effective Hamiltonian, we find

$$\begin{aligned} E_\sigma^{(1)} &= \varepsilon_F + \sigma \sqrt{\Delta^2 + a^2 t^2 \mathbf{q}^2} \\ &= (\varepsilon_F + \sigma\Delta) + \sigma \frac{1}{2} \frac{a^2 t^2}{\Delta} \mathbf{q}^2 + \mathcal{O}(aq)^3 \quad \frac{m_\sigma^{(1)}}{m_e} = \left(\frac{\hbar^2}{2 m_e a^2} \right) \frac{2\Delta}{t^2}. \\ &= \varepsilon_\sigma + \sigma \frac{\hbar^2 \mathbf{q}^2}{2 m_\sigma^{(1)}} + \mathcal{O}(aq)^3, \end{aligned}$$

Here, electron-hole symmetry is evident: to 1st order, the masses of the valence and conduction bands are equal. It is interesting to note that the 1st order effective mass, in units of the electron mass, is proportional to the fraction of the gap by the square of the effective hopping and that the dimensional pre-factor is simply the energy of an electron in the ground state of an infinite square well of size of the lattice constant a . Numerical values can be read from Table 3.3.

For the 2nd order effective Hamiltonian, we find

$$\begin{aligned} E_\sigma^{(2)} &= \varepsilon_F + \kappa_+ a^2 \mathbf{q}^2 + \sigma \sqrt{\Delta^2 + (t^2 - 2\Delta\kappa_-)a^2 \mathbf{q}^2 + 2\tau tua^3 \mathbf{q}^3 \cos 3\theta + (u^2 + \kappa_-^2)a^4 \mathbf{q}^4} \\ &= (\varepsilon_F + \sigma\Delta) + \sigma \frac{1}{2} \left[\frac{t^2}{\Delta} + \sigma 2(\kappa_+ - \sigma\kappa_-) \right] a^2 \mathbf{q}^2 + \mathcal{O}(aq)^3 \\ &= \varepsilon_\sigma + \sigma \frac{\hbar^2 \mathbf{q}^2}{2 m_\sigma^{(2)}} + \mathcal{O}(aq)^3, \end{aligned}$$

thus, the 2nd order effective masses yield

$$\frac{m_\sigma^{(2)}}{m_e} = \left(\frac{\hbar^2}{2 m_e a^2} \right) \frac{2\Delta}{t^2 + \sigma\kappa_\sigma 2\Delta}. \quad (3.26)$$

The structure of the 2nd order effective mass is similar to the 1st order case, except that the inter-band hopping has a band-dependent correction, proportional to the gap, due to the band concavities, which become relevant at the energy scales of $(aq)^2$. Electron-hole symmetry no longer holds at this energy scale. Numerical values are shown in Table 3.3.

Spinful

Using the superscript $\nu = >, <$, where $>$ stands for $\alpha\tau = +$ and $<$ for $\alpha\tau = -$ (that is, the high-lying and low-lying spin-split branches of the valence band), we can write the effective masses to 1st and 2nd order for the spin. These can be inferred directly from the previous results, by applying the prescriptions of Eq. (3.23), yielding

$$E_{\sigma,\nu}^{(n)} = \varepsilon_{\sigma,\nu} + \sigma \frac{\hbar^2 \mathbf{q}^2}{2 m_{\sigma,\nu}^{(n)}} + \mathcal{O}(aq)^3 \Rightarrow \begin{cases} \frac{m_\sigma^\nu}{m_e} = \left(\frac{\hbar^2}{2 m_e a^2} \right) \frac{2\Delta^\nu}{t^2}, & n = 1 \\ \frac{m_\sigma^\nu}{m_e} = \left(\frac{\hbar^2}{2 m_e a^2} \right) \frac{2\Delta^\nu}{t^2 + \sigma\kappa_\sigma 2\Delta^\nu}, & n = 2 \end{cases}$$

Numerical values are show in Table 3.3, below. Note that the spin-splitting is substantial enough to, in all cases except MoS₂, render the high-lying cone of the valence band less massive than the conduction band.

Table 3.3: Numerical values of the effective masses to both 1st and 2nd order for the conduction band, degenerate valence band and spin-split valence band. (Units: m_e)

$M X_2$	MoS_2		WS_2		MoSe_2		WSe_2	
order	1st	2nd	1st	2nd	1st	2nd	1st	2nd
m_c	0.338	0.401	0.269	0.291	0.359	0.450	0.280	0.312
m_v		0.428		0.316		0.477		0.343
$m_v^>$	0.323	0.405	0.237	0.273	0.336	0.438	0.238	0.283
$m_v^<$	0.353	0.453	0.300	0.360	0.382	0.518	0.321	0.407

3.2 Hall effects in inversion symmetry broken honeycomb lattices

The concept of the Berry phase has found a unifying and fundamental role in the understanding of condensed matter systems, besides all other branches of quantum physics, having proven that phenomena pertaining to the response of electrons to many qualitatively diverse perturbations are, in fact, a consequence of the geometry of Bloch bands, as discussed in Ref. [111].

In the following section, this framework shall be employed to the model derived previously, with the particular focus of arriving at the Hall effects displayed in monolayered TMDCs. This follows closely the arguments and notation presented in Ref. [111]. A study of the quantum adiabatic theorem as the origin of the Berry curvature in solid-state systems, as well as the derivation of relevant expressions, can be found in Appendix B.

3.2.1 Berry connection and Berry curvature

Of a general two-level system

Recovering the results of Sec. 3.1, we have found the Bloch states of the valence and conduction band in the vicinity of the $\pm K$ -points can be described by Eq. (3.14), reading

$$|\mathbf{k}, \sigma, \tau\rangle = \cos \frac{\theta_{\mathbf{k}}}{2} e^{-i\sigma\varphi_{\mathbf{k}}^{\tau}} |\psi^{\sigma}(\tau\mathbf{K})\rangle + \sigma \sin \frac{\theta_{\mathbf{k}}}{2} |\psi^{\bar{\sigma}}(\tau\mathbf{K})\rangle .$$

Note that, without specifying the structures of the angular parameters $\theta_{\mathbf{k}}$ and $\varphi_{\mathbf{k}}$ (and ignoring the valley index τ , for now), these states describe a generic two-level system. Keeping the discussion to the valence band, we have

$$\partial_{\mu} |\mathbf{k}, v, \tau\rangle = e^{i\varphi_{\mathbf{k}}} \left(i \cos \frac{\theta_{\mathbf{k}}}{2} \partial_{\mu} \varphi_{\mathbf{k}} - \frac{1}{2} \sin \frac{\theta_{\mathbf{k}}}{2} \partial_{\mu} \theta_{\mathbf{k}} \right) |\psi^v(\tau\mathbf{K})\rangle - \frac{1}{2} \cos \frac{\theta_{\mathbf{k}}}{2} \partial_{\mu} \theta_{\mathbf{k}} |\psi^c(\tau\mathbf{K})\rangle ,$$

from which, taking the inner product with the original state, we find the Berry connection

$$\mathcal{A}_\mu^v(\mathbf{k}) = i \langle \mathbf{k}, v, \tau | \partial_\mu(\mathbf{k}, v, \tau) \rangle = -\cos^2 \frac{\theta_{\mathbf{k}}}{2} \partial_\mu \varphi_{\mathbf{k}}. \quad (3.27)$$

As a result, the Berry curvature reads

$$\begin{aligned} \Omega_{\mu\nu}^v(\mathbf{k}) &= \partial_\mu \mathcal{A}_\nu^v - \partial_\nu \mathcal{A}_\mu^v \\ &= \frac{1}{2} \varepsilon_{\mu\nu} \sin \theta_{\mathbf{k}} \partial_\alpha \theta_{\mathbf{k}} \partial_\beta \varphi_{\mathbf{k}} \varepsilon^{\alpha\beta}. \end{aligned} \quad (3.28)$$

Furthermore, notice that the pair of contracted tensors in this expression constitutes the Jacobian of the transformation from the parameter space $(k_1, k_2) \in \mathbb{R}^2$ to the region of S^2 charted by $(\theta, \varphi) \in [0, \Theta] \times [0, \Phi]$, where Θ and Φ are model-specific parameters which define the boundary. Assuming that Θ and Φ are independent variables, we can easily compute the Berry phase and extract the Chern number of a two-level system:

$$\begin{aligned} \gamma_v &= \frac{1}{2} \int_{\mathbb{R}^2} dk_1 dk_2 (\partial_1 \theta_{\mathbf{k}} \partial_2 \varphi_{\mathbf{k}} - \partial_2 \theta_{\mathbf{k}} \partial_1 \varphi_{\mathbf{k}}) \sin \theta_{\mathbf{k}} \\ &= \frac{1}{2} \int_0^\Phi d\varphi \int_0^\Theta d\theta \sin \theta \\ &= \Phi \sin^2 \frac{\Theta}{2} = \frac{\Phi}{4\pi} \Omega_\Theta, \end{aligned}$$

where Ω_Θ is the solid-angle defined by a cone of apex angle 2Θ . The Chern number is, thus,

$$c_v = \frac{\Phi}{2\pi} \sin^2 \frac{\Theta}{2}. \quad (3.29)$$

All the expressions derived are valid for any two-level system, since we have not made any assumptions regarding the structure of $\theta_{\mathbf{k}}$ or of $\varphi_{\mathbf{k}}$ or chosen a particular Hamiltonian. Moreover, according to the findings of Sec. B.1.2, the Berry curvature obeys a conservation law given by Eq. (B.15). This conservation law allows us to determine directly the Berry curvature for the conduction band, yielding

$$\sum_n \Omega_{\mu\nu}^n \equiv 0 \Rightarrow \Omega_{\mu\nu}^c = -\Omega_{\mu\nu}^v.$$

Of the massive Dirac Hamiltonian

The low-energy limit of charge carriers on a generic spatial-inversion symmetry broken honeycomb lattice, as pointed out in Sec. 3.1.2, is described by the massive Dirac Hamiltonian of Eq. (3.10), from which we have obtained the dispersion of Eq. (3.11) and the angular parameters of Eq. (3.13):

$$E_{\mathbf{k}} = \sqrt{\Delta^2 + a^2 t^2 \mathbf{k}^2}, \quad \varphi_{\mathbf{k}} = \arctan \left(\frac{k_2}{k_1} \right), \quad \theta_{\mathbf{k}} = 2 \arctan \left(\frac{E_{\mathbf{k}} - \Delta}{at\mathbf{k}} \right).$$

From these relations, we can obtain the identities

$$\begin{aligned}\partial_\mu \varphi_{\mathbf{k}} &= \frac{1}{1 + \left(\frac{k_2}{k_1}\right)^2} \left(\frac{\delta_{2\mu}}{k_1} - \frac{k_2 \delta_{1\mu}}{k_1^2} \right) & \partial_\mu \theta_{\mathbf{k}} &= \frac{1}{1 + \left(\frac{E_{\mathbf{k}} - \Delta}{at\mathbf{k}}\right)^2} \left(\frac{at}{E_{\mathbf{k}}} \frac{k_\mu}{\mathbf{k}} - \frac{E_{\mathbf{k}} - \Delta}{at\mathbf{k}^2} \frac{k_\mu}{\mathbf{k}} \right) \\ &= \frac{1}{k_1^2 + k_2^2} (k_1 \delta_{2\mu} - k_2 \delta_{1\mu}) & &= \frac{atk_\mu}{E_{\mathbf{k}} \mathbf{k}} \frac{a^2 t^2 \mathbf{k}^2 - E_{\mathbf{k}} (E_{\mathbf{k}} - \Delta)}{a^2 t^2 \mathbf{k}^2 + (E_{\mathbf{k}} - \Delta)^2} \\ &= -\frac{\varepsilon_{\mu\alpha} k^\alpha}{\mathbf{k}^2}, & &\stackrel{(*)}{=} \frac{atk\Delta}{E_{\mathbf{k}}^2} \frac{k_\mu}{\mathbf{k}^2},\end{aligned}$$

$$\begin{aligned}\sin \theta_{\mathbf{k}} &= \frac{2 \tan(\theta_{\mathbf{k}}/2)}{1 + \tan^2(\theta_{\mathbf{k}}/2)} \\ &= \frac{2 at\mathbf{k}(E_{\mathbf{k}} - \Delta)}{a^2 t^2 \mathbf{k}^2 + (E_{\mathbf{k}} - \Delta)^2} \\ &\stackrel{(*)}{=} \frac{atk}{E_{\mathbf{k}}},\end{aligned}$$

$$\boxed{\begin{aligned}E_{\mathbf{k}} &= \sqrt{\Delta^2 + a^2 t^2 \mathbf{k}^2} \\ \Leftrightarrow a^2 t^2 \mathbf{k}^2 &= E_{\mathbf{k}}^2 - \Delta^2, \\ \Leftrightarrow (E_{\mathbf{k}} - \Delta)^2 + a^2 t^2 \mathbf{k}^2 &= 2E_{\mathbf{k}}(E_{\mathbf{k}} - \Delta),\end{aligned}}$$

where, in the marked equalities, the boxed identities at the lower right-side corner were used. Hence, the Berry connection becomes

$$\mathcal{A}_\mu^v(\mathbf{k}) = \tau_3 \varepsilon_{\mu\alpha} k^\alpha \left(\frac{\cos \theta_{\mathbf{k}}/2}{\mathbf{k}} \right)^2 = \frac{\tau_3 \varepsilon_{\mu\alpha} k^\alpha a^2 t^2}{(E_{\mathbf{k}} - \Delta)^2 + a^2 t^2 \mathbf{k}^2}, \quad (3.30)$$

whereas the Berry curvature yields

$$\begin{aligned}\Omega_{\mu\nu}^v(\mathbf{k}) &= \frac{1}{2} \varepsilon_{\mu\nu} \tau_3 \frac{atk}{E_{\mathbf{k}}} \left(\frac{atk\Delta}{E_{\mathbf{k}}^2} \frac{k_\alpha}{\mathbf{k}^2} \right) \left(-\frac{\varepsilon_{\beta\gamma} k^\gamma}{\mathbf{k}^2} \right) \varepsilon^{\alpha\beta} \\ &= \varepsilon_{\mu\nu} \tau_3 \frac{a^2 t^2 \Delta}{2 E_{\mathbf{k}}^3},\end{aligned}$$

which is the Berry curvature in a vicinity of the $\pm K$ -points:

$$\boxed{\Omega_{\mu\nu}^v(\mathbf{k}) = \varepsilon_{\mu\nu} \frac{\tau_3}{2} \frac{a^2 t^2}{\Delta^2} \left(1 + \frac{a^2 t^2 \mathbf{k}^2}{\Delta^2} \right)^{-3/2}}. \quad (3.31)$$

3.2.2 Hall conductivity

We now wish to compute the quantum Hall conductivity due to each valley. The most expedite way to do this is to use Eq. (B.36) with Eq. (3.29), noting that, for a two-level massive Dirac Hamiltonian, we have $\Theta = \pi/2$ and $\Phi = 2\pi\tau$. This yields

$$\sigma_H^\tau = \frac{e^2}{h} \frac{\Phi}{2\pi} \sin^2 \frac{\Theta}{2} = \tau_3 \frac{e^2}{2h},$$

which shows that the Chern number of a two-level massive Dirac Hamiltonian has Chern number equal to 1/2.

There is a subtlety regarding the integration that leads up to Eq. (3.29), which is the requirement to take it over the entire real plane. Likewise, Eq. (B.35) requires the integral to be taken over the entire BZ. However, this curvature is only defined in a neighbourhood of the $\pm K$ valleys, therefore, it is expected that the integral of this function would require a cut-off in crystal momentum, to account for the fact that it is obtained under a low-energy, continuum limit approximation. Thus, we are faced with the problem of determining an appropriate momentum cut-off and, if possible, of making sure that the final result does not depend on it, so that it can be taken to infinity and, thus, recover the result of Eq. (3.29).

An energy scale argument

To solve this, it is useful to go to the definition of the Berry curvature in terms of the 1st order adiabatic evolution of quantum states of Sec. B.2. There, it is found that the Berry curvature of a Bloch band can be physically interpreted as the effect of the residual overlap of the band's states with empty states in other bands, due to the transitions induced by the time-variation of the momentum. According to the form of the time-evolved state given by Eq. (B.24), this overlap is inversely proportional to the energy difference between states. Indeed, it is found that the Berry curvature can be written as

$$\Omega_{\mu\nu}^n = i \sum_{m \neq n} \frac{\langle n | \partial_\mu \hat{H} | m \rangle \langle m | \partial_\nu \hat{H} | n \rangle - \langle n | \partial_\nu \hat{H} | m \rangle \langle m | \partial_\mu \hat{H} | n \rangle}{(\varepsilon_n - \varepsilon_m)^2},$$

from Eq. (B.14), showing that it is inversely quadratic dependent on the energy difference.

This aspect of the Berry curvature leads us to state that the contributions to the Berry curvature of the Brillouin Zone are concentrated at the valence-conduction band edges - the $\pm K$ points, in our case - and their immediate vicinity. This means that we can expect Eq. (3.31) to contain all the essential features of the Berry curvature, and that contributions to higher order of k are negligible. Thus, although this result was obtained from an apparently stringent limit, it holds, to a very good approximation, within a broad range of values of k .

In turn, this fact can be translated into the magnitude of the cut-off of the aforementioned integral, in the sense that it can be much larger than one would expect if one were only to consider that the result is derived from a low-energy approximation. Namely, the only condition is that the cut-off keeps the contour of the surface integration from going into the other vertices of the BZ, where it would be necessary to account for contributions from other valleys. These are separated by magnitudes of $4\pi/\sqrt{3}$ from equivalent valleys and of $4\pi/3$ from the inequivalent valley. Therefore, the contour of the integral of the Berry curvature should go no farther than half the magnitudes to the nearest valleys.

Now consider the plots of the Berry curvature of Eq. (3.31) at the $+K$ valley, for various MX_2 ,

shown in Figure 3.1. It is clear that the curvature is very near zero at even half the magnitude separating nearest valleys. Thus, to an excellent approximation, we can make the cut-off go to infinity, since contributions beyond the cut-off are negligible.

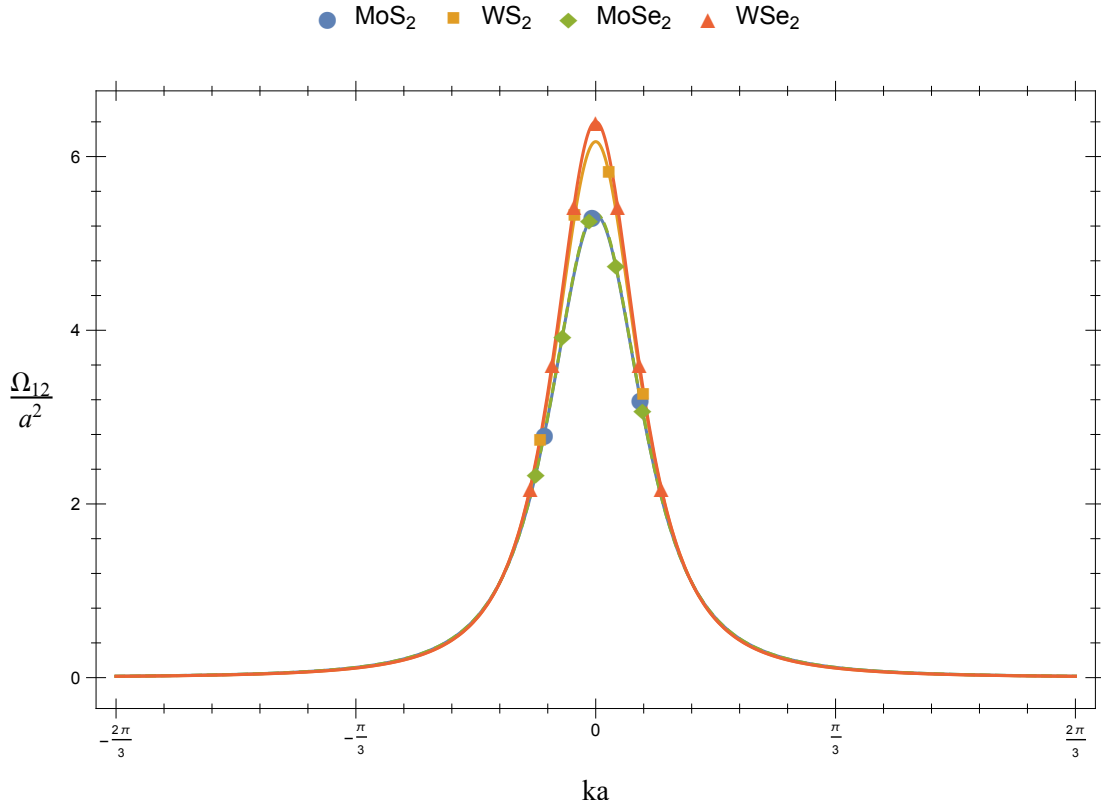


Figure 3.1: Plot of the Berry curvature of Eq. (3.31) in units of the lattice constant a . Values used for the parameters $t \equiv t_{vc}$ and Δ are those of Table 3.1. (Note: The curves for MoS₂ and MoSe₂ coincide).

A topological argument

An alternative argument to circumvent this problem, one which does not invoke the limited width of the curvature, is to notice that the parameters Θ and Φ , the only variables that contain information specific to the model, do not depend on the half-gap Δ . Thus, it should be possible to manipulate the system into closing the gap and reduce the Berry curvature to a sharp peak at the K -point, in which case we would be able to choose an arbitrarily small region of integration that would contain all the curvature of that valley. In turn, this amounts to making the cut-off tend to infinity and the result is, thus, recovered.

The independence of this result on system-specific parameters reflects the topological origin of these quantities. Indeed, in the previous section we managed to compute the Chern number

for any two-level system while containing all the model-specific details to a single number Θ , which, taking after the particular case of the massive Dirac Hamiltonian, we can expect to not depend on any system-specific parameters. Indeed, this means that all systems described by a given family of Hamiltonians, related among each other by variation of parameters, are classified by the same number, or set of numbers, of topological origin. Due to this invariance under continuous deformations (i.e. variation of parameters), these numbers are known as topological invariants.

Considering the foregoing arguments, not only is the use of Eq. (3.29) validated, it is also possible to integrate (3.31) over all momentum space. Introducing the dimensionless vector $\mathbf{y} = at\mathbf{k}/\Delta$ and integrating over the angular part yields

$$\sigma_{\mu\nu}^v = \varepsilon_{\mu\nu}\tau_3 \frac{e^2}{2h} \int_0^{+\infty} d|\mathbf{y}| \frac{1}{(1+|\mathbf{y}|^2)^{3/2}}, \quad (3.32)$$

that is solved simply by making the variable substitution

$$x^2 = \frac{1}{1+|\mathbf{y}|^2}, \quad 0 \leq |\mathbf{y}| < +\infty \Leftrightarrow |\mathbf{y}| = \frac{\sqrt{1-x^2}}{x}, \quad 0 < x \leq 1 \Rightarrow d|\mathbf{y}| = -\frac{dx}{x^2\sqrt{1-x^2}},$$

for which the integral of Eq. (3.32) becomes

$$\int_0^1 dx \frac{x}{\sqrt{1-x^2}} = 1,$$

so that the contribution to the Hall conductivity of the valence band from a Dirac cone indexed by τ is given by

$$\sigma_{\mu\nu}^v = \varepsilon_{\mu\nu}\sigma_H^\tau = \varepsilon_{\mu\nu}\tau_3 \frac{e^2}{2h}. \quad (3.33)$$

Hence, we have recovered the result computed at the very beginning of this section. We can conclude that the Hall conductivity of each Dirac cone is quantized in units of $e^2/(2h)$, with sign determined by the valley index. Before proceeding into further discussion of this effect, note that integration of the Berry curvature over the entire BZ yields a null Chern number, since inequivalent valleys contribute an equal absolute amount of opposite sign.

Taking after the symmetry considerations of Sec. B.1.2, this result is no surprise. Indeed, crystal momentum transforms as $\mathbf{k} \rightarrow -\mathbf{k}$ under parity and under time-reversal, satisfying Eq. (B.16), and the system described by the Hamiltonian of Eq. (2.14) breaks only parity, preserving time-inversion symmetry. Thus, according to Eq. (B.20), the Chern number vanishes for every band of this system and the material is trivial in the topological sense. The fact that the valleys have a non-vanishing Chern number in no way contradicts this, since the Chern number is a global property, accumulated from the Berry curvature over the BZ, meaning that it can be locally non-vanishing, as long as the non-vanishing contributions compensate reciprocally.

Moreover, the existence of an even number of valleys is a fundamental consequence of

defining a gauge theory on a lattice, a result which is encoded in the general chiral fermion doubling theorem [112]. Thus, for any crystalline material with a non-identically vanishing Berry curvature, the sum of the Chern number contributions of the valleys will either vanish or yield an integer multiple of the quantum of conductivity e^2/h .

The valley Hall effect

According to the findings of Sec. B.2, namely, Eqs. (B.29) and (B.32), the Berry curvature of the total parameter-space represents the response of the expectation value of the velocity of particles in Bloch states to the variation of an external parameter. In the particular case that the external parameters couple minimally to momentum, like an electric field through a time-varying vector-potential as in the Hamiltonian of Eq. (B.30), the parameter space reduces to the Brillouin Zone. Thus, the response of Bloch electrons in a material to a linearly weak, spatially uniform electric field depends only on the Berry curvature of the BZ.

Having this in mind, Eq. (3.31) shows a remarkable feature: under the application of an in-plane electric-field, electrons will not only move transversally to its direction, they will also move in opposite directions according to which inequivalent valley they are in, giving rise to a net valley Hall current. This is the valley Hall effect [3].

Although the quantized Hall response vanishes for this class of materials, the existence of a Berry curvature and, thus, the topological features of the valleys, are experimentally observable and have physical consequences. It was first proposed for inversion-symmetry broken graphene [93], where the existence of a Berry curvature would allow charge carriers from each valley to be selectively excited by circularly polarized light. This can be intuitively understood in the sense that the the valleys are connected by time reversal symmetry. Thus, only by interacting with the system with some time-reversal-symmetry breaking perturbation can we obtain differentiated responses from the inequivalent valleys. Exciting charge carriers from a specific valley thus requires breaking time reversal symmetry with circularly polarized light.

The fact that TMDCs, beyond being intrinsically inversion-symmetry broken, have a sizeable spin-splitting, allows excitation of charge carriers polarized in the valley as well as in the spin degrees of freedom. This has been proposed in [3] and experimentally observed in [97].

Part II

Electron-Electron Interactions

Chapter 4

Perturbation Theory and self-energy correction to the electronic structure

This chapter explores corrections to the electronic structure due to the electron-electron interactive problem in TMDCs based on the Hartree-Fock approximation. We will be taking a diagrammatic approach based out of the formulation to be used throughout the remainder of this work, which is the path integral formulation of quantum field theory for quantum statistical mechanics, presented in Appendix C.

4.1 1st order self-energy in the continuum limit

4.1.1 Tight-binding description of electronic interactions

We now consider electron-electron interactions in a tight-binding setting. In order to derive an appropriate general Hamiltonian for this problem, we proceed as in Sec. 2.1.2. Thus, in terms of field operators, the interactive term of the Hamiltonian is

$$\hat{V}_{ee} = \frac{1}{2} \int d^3x \int d^3x' \hat{a}^\dagger(\mathbf{x}) \hat{a}^\dagger(\mathbf{x}') V(\mathbf{x} - \mathbf{x}') \hat{a}(\mathbf{x}') \hat{a}(\mathbf{x}), \quad (4.1)$$

where the potential V is any symmetric potential. Expanding the field operators in Wannier states as Eq. (2.11), the above term becomes

$$\begin{aligned}\hat{V}_{ee} &= \frac{1}{2} \sum_{ii'jj'} U_{\mu\mu'\nu\nu'}^{ii'jj'} \hat{a}_{i\mu}^\dagger \hat{a}_{j\nu}^\dagger \hat{a}_{j'\nu'} \hat{a}_{i'\mu'}, \\ U_{\mu\mu'\nu\nu'}^{ii'jj'} &= \int d^3x \int d^3x' \bar{\phi}_{i\mu}(\mathbf{x}) \bar{\phi}_{j\nu}(\mathbf{x}') \phi_{j'\nu'}(\mathbf{x}') \phi_{i'\mu'}(\mathbf{x}) V(\mathbf{x} - \mathbf{x}').\end{aligned}\quad (4.2)$$

In turn, Fourier transforming to crystal momentum space yields

$$\begin{aligned}\hat{V}_{ee} &= \frac{1}{2} \sum_{\mathbf{k}, \mathbf{k}', \mathbf{q}} \mathcal{V}_{\mathbf{k}, \mathbf{k}'; \mathbf{q}}^{\mu\mu'\nu\nu'} \hat{a}_{\mathbf{k}-\mathbf{q}, \mu}^\dagger \hat{a}_{\mathbf{k}'+\mathbf{q}, \nu}^\dagger \hat{a}_{\mathbf{k}', \nu'} \hat{a}_{\mathbf{k}, \mu'}, \\ \mathcal{V}_{\mathbf{k}, \mathbf{k}'; \mathbf{q}}^{\mu\mu'\nu\nu'} &= \int d^3x \int d^3x' \bar{\varphi}_{\mathbf{k}-\mathbf{q}, \mu}(\mathbf{x}) \bar{\varphi}_{\mathbf{k}'+\mathbf{q}, \nu}(\mathbf{x}') \varphi_{\mathbf{k}', \nu'}(\mathbf{x}') \varphi_{\mathbf{k}, \mu'}(\mathbf{x}) V(\mathbf{x} - \mathbf{x}').\end{aligned}\quad (4.3)$$

A proof for the conservation of momentum in this interaction can be found in Sec. C.3. From Eqs. (2.13) and (4.3) we can write the action of the interacting tight-binding theory as

$$\begin{aligned}S[\bar{\psi}, \psi] &= \int_0^{\beta\hbar} d\tau \sum_{\mathbf{k}} \bar{\psi}_{\mathbf{k}, \alpha}(\tau) (\hbar\partial_\tau + \xi_{\mathbf{k}, \alpha}) \psi_{\mathbf{k}, \alpha}(\tau) \\ &\quad + \frac{1}{2} \int_0^{\beta\hbar} d\tau \sum_{\mathbf{k}, \mathbf{k}', \mathbf{q}} \bar{\psi}_{\mathbf{k}-\mathbf{q}, \mu}(\tau) \bar{\psi}_{\mathbf{k}'+\mathbf{q}, \lambda}(\tau) \mathcal{V}_{\mathbf{k}, \mathbf{k}'; \mathbf{q}}^{\mu\mu'\nu\nu'} \psi_{\mathbf{k}', \lambda'}(\tau) \psi_{\mathbf{k}, \mu'}(\tau) \\ &= \sum_k \bar{\psi}_{k, \alpha} (-i\hbar\omega_n + \xi_{\mathbf{k}, \alpha}) \psi_{k, \alpha} + \frac{1}{2\beta\hbar} \sum_{k, k', q} \bar{\psi}_{k-q, \mu} \bar{\psi}_{k'+q, \lambda} \mathcal{V}_{\mathbf{k}, \mathbf{k}'; \mathbf{q}}^{\mu\mu'\nu\nu'} \psi_{k', \lambda'} \psi_{k, \mu'},\end{aligned}$$

where we defined the bosonic Matsubara frequency $\nu_s = \omega_n - \omega_l = \omega_p - \omega_m$, which is a consequence of the (imaginary) time independence of the Hamiltonian. For notational simplicity, we have defined $\xi_{\mathbf{k}, \alpha} = \varepsilon_{\mathbf{k}, \alpha} - \mu$ and introduced the imaginary-time 4-momenta $k \equiv (i\omega_n, \mathbf{k})$ and $q \equiv (i\nu_n, \mathbf{q})$. Here, the distinction between k and q is merely to keep track of the 4-momenta composing of either fermionic or bosonic Matsubara frequencies. The interaction term is represented by the Feynman diagram of Figure 4.1. Although here we obtain the self-energy correction directly from the diagram, in Sec. C.2 of the Appendix the expression is derived formally, by expanding the exponential of the action in the path integral and employing Wick's theorem, as well as deducing Dyson's equations and its implications in the correction of the electronic

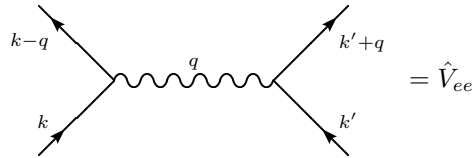


Figure 4.1: Feynman diagram for the electron-electron Coulomb interaction.

structure. This diagram generates two topologically distinct propagators which amount to the Hartree and Fock terms, or direct and exchange terms, respectively. Due to the argument of global neutrality presented in the Sec. C.2, the 1st order contribution to the propagator reduces to the exchange term:

$$\mathcal{G}_{\alpha\beta}^{(1)}(k) = \left[\hat{\mathcal{G}}_0 \hat{\Sigma}^{(1)} \hat{\mathcal{G}}_0 \right]_{\alpha\beta}(k), \quad \Sigma_{\alpha\beta}^{(1)}(k) = -\frac{1}{\beta\hbar^2} \sum_{q,\lambda} \mathcal{V}_{\mathbf{k}+\mathbf{q},\mathbf{k};\mathbf{q}}^{\alpha\lambda\lambda\beta} \mathcal{G}_{0,\lambda}(k+q), \quad (4.4)$$

where $\hat{\Sigma}^{(1)}$ is known as the first-order exchange self-energy operator. This term has a very clear diagrammatic interpretation: considering the diagram of Fig. 4.1, it corresponds to joining two fermionic lines pointing in the same direction from each end of the interaction line, as shown in Fig. 4.2.

Since the potential is time-independent (for instance, the Coulomb potential is instantaneous), we can readily simplify the expression for the self-energy by noting that the summation over Matsubara frequencies involves only the bare propagator. Following the method presented in Sec. C.1.3, the summation yields

$$\sum_s \left[i\nu_s - \left(\frac{\varepsilon_{\mathbf{k}+\mathbf{q}}^\lambda - \mu}{\hbar} - i\omega_n \right) \right]^{-1} = \sum_m \left(i\omega_m - \frac{\varepsilon_{\mathbf{k}+\mathbf{q}}^\lambda - \mu}{\hbar} \right)^{-1} = \frac{\beta\hbar}{e^{\beta(\varepsilon_{\mathbf{k}+\mathbf{q}}^\lambda - \mu)} + 1},$$

where, in the first equality, $i\nu_s + i\omega_n = i\omega_m$ is a fermionic frequency. Substituting into the self-energy, yields

$$\Sigma_{\alpha\beta}(\mathbf{k}) = -\frac{1}{\hbar} \sum_{\mathbf{q},\lambda} \mathcal{V}_{\mathbf{k}+\mathbf{q},\mathbf{k};\mathbf{q}}^{\alpha\lambda\lambda\beta} n_F(\varepsilon_{\mathbf{k}+\mathbf{q}}^\lambda - \mu). \quad (4.5)$$

This result yields two important conclusions: first, the self-energy is independent of the fermionic frequencies, reflecting the instantaneous nature of the interaction; second, in an undoped insulator the only non-negligible contribution is that of the valence band, a result which will be used further on. It is also a very physically reasonable result: the matrix elements of the self-energy are given by the sum over the matrix elements of the interaction over all occupied intermediate states.

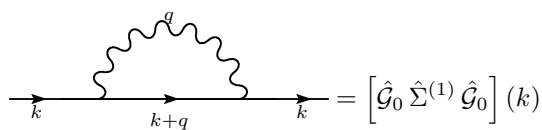


Figure 4.2: Feynman diagram contributing the 1st order exchange self-energy operator.

4.1.2 Evaluation of the matrix elements of the interaction

Computing the self-energy requires evaluating the integral

$$\begin{aligned}\mathcal{V}_{\mathbf{k}+\mathbf{q},\mathbf{k};\mathbf{q}}^{\alpha\lambda\lambda\beta} &= \int d^3x \int d^3r \bar{\varphi}_{\mathbf{k},\alpha}(\mathbf{x}) \bar{\varphi}_{\mathbf{k}+\mathbf{q},\lambda}(\mathbf{x}-\mathbf{r}) \varphi_{\mathbf{k},\beta}(\mathbf{x}-\mathbf{r}) \varphi_{\mathbf{k}+\mathbf{q},\lambda}(\mathbf{x}) V(\mathbf{r}) \\ &= \int d^3x \int d^3r e^{i\mathbf{q}\cdot\mathbf{r}} \bar{u}_{\mathbf{k},\alpha}(\mathbf{x}) \bar{u}_{\mathbf{k}+\mathbf{q},\lambda}(\mathbf{x}-\mathbf{r}) u_{\mathbf{k},\beta}(\mathbf{x}-\mathbf{r}) u_{\mathbf{k}+\mathbf{q},\lambda}(\mathbf{x}) V(\mathbf{r}),\end{aligned}\quad (4.6)$$

where the second equality holds since the integrands are Bloch states. The u functions can be written as

$$u_{\mathbf{k},\alpha}(\mathbf{x}) = \frac{1}{\sqrt{N}} \sum_{\mathbf{R}} g_{\mathbf{k}}^{\alpha}(\mathbf{k}) e^{-i\mathbf{k}\cdot(\mathbf{x}-\mathbf{R})} \phi_i(\mathbf{x}-\mathbf{R}),$$

where a summation over repeated indices is implied and the g functions are obtained from diagonalizing the TB Hamiltonian. The functions ϕ_i , $i \in \{(\mu, j)\}_{\forall \mu, j}$ as defined in Sec. 2.1.2, are the atomic orbitals at each lattice site. Substituting into Eq. (4.6) yields

$$\begin{aligned}\mathcal{V}_{\mathbf{k}+\mathbf{q},\mathbf{k};\mathbf{q}}^{\alpha\lambda\lambda\beta} &= \frac{1}{N^2} \sum_{\mathbf{R}, \mathbf{R}'} \sum_{\mathbf{P}, \mathbf{P}'} \int d^3x \int d^3r \bar{\phi}_i(\mathbf{x}-\mathbf{R}) \phi_{i'}(\mathbf{x}-\mathbf{R}') \bar{\phi}_j(\mathbf{x}-\mathbf{r}-\mathbf{P}) \phi_{j'}(\mathbf{x}-\mathbf{r}-\mathbf{P}') \\ &\quad \times \bar{g}_i^{\alpha}(\mathbf{k}) \bar{g}_j^{\lambda}(\mathbf{k}+\mathbf{q}) g_{j'}^{\beta}(\mathbf{k}) g_{i'}^{\lambda}(\mathbf{k}+\mathbf{q}) e^{i\mathbf{q}\cdot(\mathbf{R}'-\mathbf{P})} e^{i\mathbf{k}\cdot(\mathbf{R}'+\mathbf{P}'-\mathbf{R}-\mathbf{P})} V(\mathbf{r}).\end{aligned}$$

Since we are working the tight-binding approximation, only overlaps between orbitals in the same lattice site are considered non-negligible, so that, in the summations over lattice sites, only the terms $\mathbf{R}' = \mathbf{R}$ and $\mathbf{P}' = \mathbf{P}$ are non-zero. Next, we perform the coordinate transformations $\mathbf{x} \mapsto \mathbf{x} + \mathbf{R}$ and, afterwards, $\mathbf{r} \mapsto \mathbf{r} + \mathbf{R} - \mathbf{P}$, yielding

$$\begin{aligned}\mathcal{V}_{\mathbf{k}+\mathbf{q},\mathbf{k};\mathbf{q}}^{\alpha\lambda\lambda\beta} &= \int d^3x \int d^3r \bar{\phi}_i(\mathbf{x}) \phi_{i'}(\mathbf{x}) \bar{\phi}_j(\mathbf{x}-\mathbf{r}) \phi_{j'}(\mathbf{x}-\mathbf{r}) \\ &\quad \times \bar{g}_i^{\alpha}(\mathbf{k}) \bar{g}_j^{\lambda}(\mathbf{k}+\mathbf{q}) g_{j'}^{\beta}(\mathbf{k}) g_{i'}^{\lambda}(\mathbf{k}+\mathbf{q}) \frac{1}{N^2} \sum_{\mathbf{R}, \mathbf{P}} e^{i\mathbf{q}\cdot(\mathbf{R}-\mathbf{P})} V(\mathbf{r} + \mathbf{R} - \mathbf{P}).\end{aligned}$$

Now, introducing the lattice Fourier transform of V

$$\begin{aligned}v(\mathbf{q}) &= \frac{1}{N} \sum_{\mathbf{r}} e^{i\mathbf{q}\cdot\mathbf{r}} V(\mathbf{r}), \\ V(\mathbf{r}) &= \sum_{\mathbf{q}} e^{-i\mathbf{q}\cdot\mathbf{r}} v(\mathbf{q}),\end{aligned}$$

and using a new integration variable $\mathbf{x}' = \mathbf{x} - \mathbf{r}$ we find

$$\begin{aligned}\mathcal{V}_{\mathbf{k}+\mathbf{q},\mathbf{k};\mathbf{q}}^{\alpha\lambda\lambda\beta} &= \int d^3x e^{i\mathbf{q}\cdot\mathbf{x}} \bar{\phi}_i(\mathbf{x}) \phi_{i'}(\mathbf{x}) \int d^3x' e^{-i\mathbf{q}\cdot\mathbf{x}'} \bar{\phi}_j(\mathbf{x}') \phi_{j'}(\mathbf{x}') \\ &\quad \times \bar{g}_i^{\alpha}(\mathbf{k}) \bar{g}_j^{\lambda}(\mathbf{k}+\mathbf{q}) g_{j'}^{\beta}(\mathbf{k}) g_{i'}^{\lambda}(\mathbf{k}+\mathbf{q}) v(\mathbf{q}).\end{aligned}$$

The integrals involving the orbitals can be approximated by the identity in the orbital indices, multiplied by a function $I(\mathbf{q})$ that is approximately constant and equal to unity [113]. These assumptions are based, respectively, on the orthogonality of the orbital wave-functions and on the fact that these are very localized relatively to the length-scales of the problem. Therefore, we may write the interaction term as

$$\mathcal{V}_{\mathbf{k}+\mathbf{q}, \mathbf{k}; \mathbf{q}}^{\alpha\lambda\beta} = v(\mathbf{q}) F_{\alpha\lambda\beta}(\mathbf{k}, \mathbf{q}),$$

with $F_{\alpha\lambda\beta}(\mathbf{k}, \mathbf{q}) = |I(\mathbf{q})|^2 \sum_{i,j} \bar{g}_i^\alpha(\mathbf{k}) g_i^\lambda(\mathbf{k} + \mathbf{q}) \bar{g}_j^\lambda(\mathbf{k} + \mathbf{q}) g_j^\beta(\mathbf{k}).$

Clearly, the matrix elements of the interaction can be separated into two factors: the Fourier transform of the potential and a “form factor” due to the band structure. Also, it will be useful to concentrate all the \mathbf{k} -dependence of the summation in the potential factor, so that we transform the summation variable as $\mathbf{q} \mapsto \mathbf{q} - \mathbf{k}$. Substituting into Eq. (4.5) yields

$$\Sigma_{\alpha\beta}(\mathbf{k}) = -\frac{1}{\hbar} \sum_{i,j} \bar{g}_i^\alpha(\mathbf{k}) g_j^\beta(\mathbf{k}) \sum_{\mathbf{q}} \sum_{\lambda} \bar{g}_j^\lambda(\mathbf{k}) g_i^\lambda(\mathbf{k}) v(\mathbf{q} - \mathbf{k}) n_F(\varepsilon_{\mathbf{k}}^\lambda - \mu). \quad (4.7)$$

This expression can be further simplified due to the presence of the Fermi-Dirac distribution, so that we can neglect the contribution from the conduction band and safely approximate the contribution in the valence band as $n_F(\varepsilon_{\mathbf{k}}^- - \mu) \simeq 1$. Finally, substituting the summation over crystal momentum with an integration with the prescription

$$\sum_{\mathbf{q}} \rightarrow \frac{N}{\mathcal{A}_{BZ}} \int d^2 q, \quad (4.8)$$

where $\mathcal{A}_{BZ} = (2/\sqrt{3})(2\pi/a)^2 = (2\pi)^2/\mathcal{A}_{uc}$ is the area of the Brillouin Zone. The expression above can thus be rewritten as

$$\Sigma_{\alpha\beta}^\sigma(\mathbf{k}) = -\frac{N}{\mathcal{A}_{BZ}\hbar} \sum_{i,j} \bar{g}_i^{\alpha,\sigma}(\mathbf{k}) g_j^{\beta,\sigma}(\mathbf{k}) \int d^2 q v(\mathbf{k} - \mathbf{q}) \bar{g}_j^{v,\sigma}(\mathbf{q}) g_i^{v,\sigma}(\mathbf{q}), \quad (4.9)$$

where spin indices have been explicitly included for clarity. Note that there is no summation over spin indices in the intermediate states since the Coulomb interaction conserves spin.

Coulomb interaction in the low-energy limit

We are interested in studying electronic interactions in the low-energy limit of the tight-binding model. Working in the low-energy, long-wavelength limit we can replace the summation in the Fourier transform of the potential by an integral with the prescription

$$\sum_{\tilde{\mathbf{R}}} \rightarrow \frac{1}{\mathcal{A}_{uc}} \int d^2 r,$$

where $\mathcal{A}_{uc} = a^2\sqrt{3}/2$ is the area of the unit cell, so that we can write

$$v(\mathbf{q}) = \frac{e^2}{4\pi\varepsilon_r\varepsilon_0} \frac{1}{N\mathcal{A}_{uc}} \lim_{\eta \rightarrow 0^+} \int d^2r \frac{1}{r} e^{i\mathbf{q}\cdot\mathbf{r}} e^{-\eta r},$$

where the parameter η was introduced as a regularization. Transforming to polar coordinates yields

$$\begin{aligned} v(\mathbf{q}) &= \frac{e^2}{4\pi\varepsilon_r\varepsilon_0} \frac{1}{N\mathcal{A}_{uc}} \lim_{\eta \rightarrow 0^+} \int_0^{2\pi} d\theta \int_a^{+\infty} dr e^{-(\eta - iq\cos\theta)r} \\ &= \frac{e^2}{4\pi\varepsilon_r\varepsilon_0} \frac{1}{N\mathcal{A}_{uc}} \lim_{\eta \rightarrow 0^+} \int_0^{2\pi} \frac{d\theta}{\eta - iq\cos\theta} \\ &= \frac{e^2}{4\pi\varepsilon} \frac{1}{N\mathcal{A}_{uc}} \lim_{\eta \rightarrow 0^+} \int_0^{2\pi} d\theta \left(\frac{\eta}{\eta^2 + \mathbf{q}^2 \cos^2\theta} + \frac{iq\cos\theta}{\eta^2 + \mathbf{q}^2 \cos^2\theta} \right) \\ &= \frac{e^2}{4\pi\varepsilon_r\varepsilon_0} \frac{1}{N\mathcal{A}_{uc}} \lim_{\eta \rightarrow 0^+} \frac{2\pi}{\sqrt{\eta^2 + \mathbf{q}^2}} + 0 \\ &= \frac{e^2}{2\varepsilon_r\varepsilon_0} \frac{1}{N\mathcal{A}_{uc}} \frac{1}{|\mathbf{q}|}. \end{aligned}$$

Now, we can apply the states determined in Sec. 3.1 to Eq. (4.6). In their most general form, which is considering band, valley and spin indices and considering states up to the 2nd order approximation, these are given by, according to Eq. (3.25),

$$|\mathbf{k}, \alpha, \tau, \sigma\rangle = e^{-i\alpha\varphi_{\mathbf{k}}^\tau} \sqrt{\frac{1}{2} \left(1 + \frac{\Delta_{\mathbf{k}}^{\sigma\tau}}{E_{\mathbf{k}}^{\sigma,\tau}} \right)} |\psi^\alpha(\tau\mathbf{K}), \sigma\rangle + \alpha \sqrt{\frac{1}{2} \left(1 - \frac{\Delta_{\mathbf{k}}^{\sigma\tau}}{E_{\mathbf{k}}^{\sigma,\tau}} \right)} |\psi^{\bar{\alpha}}(\tau\mathbf{K}), \sigma\rangle. \quad (4.10)$$

Since at the K -points the Bloch states consist of a linear combination of the orbital states d_{z^2} , $d_{x^2-y^2}$ and d_{xy} such that they are exactly proportional to $l = 2$ spherical harmonics (as it is clear by looking at Eqs. (2.2) and (3.3)), the g functions can be substituted by the coefficients of the state written above directly into Eq. (4.9), yielding

$$\begin{aligned} \Sigma_{\alpha\beta}^{\tau,\sigma}(\mathbf{k}) &= -\frac{N}{\mathcal{A}_{BZ}\hbar} \sum_{i,j} \bar{g}_i^{\alpha,\tau,\sigma}(\mathbf{k}) g_j^{\beta,\tau,\sigma}(\mathbf{k}) \int d^2q v(\mathbf{k} - \mathbf{q}) \bar{g}_j^{v,\tau,\sigma}(\mathbf{q}) g_i^{v,\tau,\sigma}(\mathbf{q}) \\ &= -\frac{1}{2\pi\hbar} \frac{e^2}{4\pi\varepsilon_r\varepsilon_0} \sum_{\lambda=+,-} \bar{g}_\lambda^{\alpha,\tau,\sigma}(\mathbf{k}) g_\lambda^{\beta,\tau,\sigma}(\mathbf{k}) \int d^2q \frac{1}{|\mathbf{k} - \mathbf{q}|} |g_\lambda^{v,\tau,\sigma}(\mathbf{q})|^2 \\ &\quad - \frac{1}{2\pi\hbar} \frac{e^2}{4\pi\varepsilon_r\varepsilon_0} \sum_{\lambda=+,-} \bar{g}_\lambda^{\alpha,\tau,\sigma}(\mathbf{k}) g_{-\lambda}^{\beta,\tau,\sigma}(\mathbf{k}) \sum_\gamma \int d^2q \frac{1}{|\mathbf{k} - \mathbf{q}|} \bar{g}_{-\lambda}^{v,\tau,\sigma}(\mathbf{q}) g_\lambda^{v,\tau,\sigma}(\mathbf{q}) \\ &= -\frac{1}{4\pi\hbar} \frac{\alpha\hbar c}{\varepsilon_r a} \sum_{\lambda=+,-} \bar{g}_\lambda^{\alpha,\tau,\sigma}(\mathbf{k}) g_\lambda^{\beta,\tau,\sigma}(\mathbf{k}) \int d^2q \frac{1}{|\mathbf{k} - \mathbf{q}|} \left(1 - \lambda \frac{\Delta_{\mathbf{q}}^{\sigma\tau}}{E_{\mathbf{q}}^{\sigma,\tau}} \right) \\ &\quad + \frac{1}{4\pi\hbar} \frac{\alpha\hbar c}{\varepsilon_r a} \sum_{\lambda=+,-} \bar{g}_\lambda^{\alpha,\tau,\sigma}(\mathbf{k}) g_\lambda^{\beta,\tau,\sigma}(\mathbf{k}) \int d^2q \frac{1}{|\mathbf{k} - \mathbf{q}|} e^{-i\lambda\varphi_{\mathbf{q}}^\tau} \sqrt{1 - \left(\frac{\Delta_{\mathbf{q}}^{\sigma\tau}}{E_{\mathbf{q}}^{\sigma,\tau}} \right)^2}, \end{aligned} \quad (4.11)$$

where $\alpha = e^2/(4\pi\varepsilon_0\hbar c)$ is the fine-structure constant. Here, since we consider only two degrees of freedom of the band index in the continuum limit, we separated the sum over j into two sums over i such that $j = i$ and $j = -i$, and relabeled the summation index λ . Note that there is no summation over valley indices: due to the decay Coulomb potential in the reciprocal space, we can expect the contributions from the inequivalent valley to be negligible. From a different perspective, this amounts to the statement, by hypothesis, that the robustness of the valley indices holds under the non-local Coulomb interaction, in the sense that it is not energetic enough to induce valley transitions. Furthermore, considering the way we previously chose to write the integral, which was to concentrate the \mathbf{k} -dependence on the potential factor, we have

$$|\mathbf{k} - \mathbf{q}| = \sqrt{\mathbf{q}^2 + \mathbf{k}^2 - 2\mathbf{q}\mathbf{k} \cos \theta_{\mathbf{k}-\mathbf{q}}}, \quad \theta_{\mathbf{k}-\mathbf{q}} = \tan \left(\frac{\mathbf{k} \sin \theta_{\mathbf{k}} - \mathbf{q} \sin \theta_{\mathbf{q}}}{\mathbf{k} \cos \theta_{\mathbf{k}} - \mathbf{q} \cos \theta_{\mathbf{q}}} \right).$$

Thus, transforming to polar coordinates in 2-space, the integrals of Eq. (4.11) can be written as

$$f_{\lambda,\Lambda}^{\tau,\sigma}(\mathbf{k}) = \int d^2q \frac{a}{|\mathbf{k} - \mathbf{q}|} \left(1 + \lambda \frac{\Delta_{\mathbf{q}}^{\sigma\tau}}{E_{\mathbf{q}}^{\sigma,\tau}} \right) = \int_0^\Lambda dq \int_0^{2\pi} \frac{d\theta}{2\pi} \frac{aq}{\sqrt{\mathbf{q}^2 + \mathbf{k}^2 - 2\mathbf{q}\mathbf{k} \cos \theta_{\mathbf{k}-\mathbf{q}}}} \left(1 - \lambda \frac{\Delta_{\mathbf{q}}^{\sigma\tau}}{E_{\mathbf{q}}^{\sigma,\tau}} \right)$$

and

$$h_{\lambda,\Lambda}^{\tau,\sigma}(\mathbf{k}) = \int d^2q \frac{a}{|\mathbf{k} - \mathbf{q}|} e^{-i\lambda\varphi_{\mathbf{q}}^\tau} \sqrt{1 - \left(\frac{\Delta_{\mathbf{q}}^{\sigma\tau}}{E_{\mathbf{q}}^{\sigma,\tau}} \right)^2} = \int_0^\Lambda dq \int_0^{2\pi} \frac{d\theta}{2\pi} \frac{a q e^{-i\lambda\varphi_{\mathbf{q}}^\tau}}{\sqrt{\mathbf{q}^2 + \mathbf{k}^2 - 2\mathbf{q}\mathbf{k} \cos \theta_{\mathbf{k}-\mathbf{q}}}} \sqrt{1 - \left(\frac{\Delta_{\mathbf{q}}^{\sigma\tau}}{E_{\mathbf{q}}^{\sigma,\tau}} \right)^2},$$

where the cutoff Λ was introduced in order to account for the fact that there is a high energy cutoff to momentum, ultimately given by the presence of the lattice and the respective 1st BZ. The self-energy can be written compactly as

$$\Sigma_{\alpha\beta}^{\tau,\sigma}(\mathbf{k}) = -\frac{\alpha}{2} \frac{c}{\varepsilon_r a} \sum_\lambda \bar{g}_\lambda^{\alpha,\tau,\sigma}(\mathbf{k}) \left[f_{\lambda,\Lambda}^{\tau,\sigma}(\mathbf{k}) g_\lambda^{\beta,\tau,\sigma}(\mathbf{k}) - h_{\lambda,\Lambda}^{\tau,\sigma}(\mathbf{k}) g_{-\lambda}^{\beta,\tau,\sigma}(\mathbf{k}) \right].$$

We can particularize this general expression for some choices of band, valley and spin indices. For instance, the self-energy of a transitionless propagator yields

$$\begin{aligned} \frac{2\varepsilon_r a}{\alpha c} \hbar \Sigma_{\alpha\alpha}^{\tau,\sigma}(\mathbf{k}) &= -\frac{1}{2} \sum_\lambda f_{\lambda,\Lambda}^{\tau,\sigma}(\mathbf{k}) - \lambda \text{Im} h_{\lambda,\Lambda}^{\tau,\sigma}(\mathbf{k}) \sin \varphi_{\mathbf{k}}^\tau \sqrt{1 - \left(\frac{\Delta_{\mathbf{k}}^{\sigma\tau}}{E_{\mathbf{k}}^{\sigma,\tau}} \right)^2} \\ &\quad - \alpha \left[\frac{1}{2} \sum_\lambda \lambda f_{\lambda,\Lambda}^{\tau,\sigma}(\mathbf{k}) \frac{\Delta_{\mathbf{k}}^{\sigma\tau}}{E_{\mathbf{k}}^{\sigma,\tau}} - \text{Re} h_{\lambda,\Lambda}^{\tau,\sigma}(\mathbf{k}) \cos \varphi_{\mathbf{k}}^\tau \sqrt{1 - \left(\frac{\Delta_{\mathbf{k}}^{\sigma\tau}}{E_{\mathbf{k}}^{\sigma,\tau}} \right)^2} \right], \end{aligned} \quad (4.12)$$

while the off-diagonal terms read

$$\begin{aligned} \frac{2\varepsilon_r a}{\alpha c} \hbar \Sigma_{\alpha\bar{\alpha}}^{\tau,\sigma}(\mathbf{k}) &= \frac{2\varepsilon_r a}{\alpha c} \hbar [\Sigma_{\bar{\alpha}\alpha}^{\tau,\sigma}(\mathbf{k})]^* \\ &= e^{i\alpha\varphi_{\mathbf{k}}^\tau} \frac{1}{2} \sum_{\lambda} \lambda \left[h_{\lambda,\Lambda}^{\tau,\sigma}(\mathbf{k}) e^{i\lambda\varphi_{\mathbf{k}}^\tau} \left(1 + \lambda \frac{\Delta_{\mathbf{q}}^{\sigma\tau}}{E_{\mathbf{q}}^{\sigma,\tau}} \right) + f_{\lambda}^{\tau,\sigma}(\mathbf{k}) \sqrt{1 - \left(\frac{\Delta_{\mathbf{k}}^{\sigma\tau}}{E_{\mathbf{k}}^{\sigma,\tau}} \right)^2} \right] \end{aligned} \quad (4.13)$$

where the \mathbf{k} -dependent coefficients read

$$\begin{aligned} \frac{1}{2} \sum_{\lambda} f_{\lambda,\Lambda}^{\tau,\sigma}(\mathbf{k}) &= 2 \int_0^{\Lambda} dq \int_0^{2\pi} \frac{d\theta}{2\pi} \frac{aq}{\sqrt{\mathbf{q}^2 + \mathbf{k}^2 - 2qk \cos \theta_{\mathbf{k}-\mathbf{q}}}}, \\ \frac{1}{2} \sum_{\lambda} \lambda f_{\lambda,\Lambda}^{\tau,\sigma}(\mathbf{k}) &= - \int_0^{\Lambda} dq \int_0^{2\pi} \frac{d\theta}{2\pi} \frac{aq}{\sqrt{\mathbf{q}^2 + \mathbf{k}^2 - 2qk \cos \theta_{\mathbf{k}-\mathbf{q}}}} \frac{\Delta_{\mathbf{q}}^{\sigma\tau}}{E_{\mathbf{q}}^{\sigma,\tau}}, \\ \text{Re } h_{\lambda,\Lambda}^{\tau,\sigma}(\mathbf{k}) &= \int_0^{\Lambda} dq \int_0^{2\pi} \frac{d\theta}{2\pi} \frac{aq \cos \varphi_{\mathbf{q}}^\tau}{\sqrt{\mathbf{q}^2 + \mathbf{k}^2 - 2qk \cos \theta_{\mathbf{k}-\mathbf{q}}}} \sqrt{1 - \left(\frac{\Delta_{\mathbf{q}}^{\sigma\tau}}{E_{\mathbf{q}}^{\sigma,\tau}} \right)^2}, \\ \lambda \text{Im } h_{\lambda,\Lambda}^{\tau,\sigma}(\mathbf{k}) &= - \int_0^{\Lambda} dq \int_0^{2\pi} \frac{d\theta}{2\pi} \frac{aq \sin \varphi_{\mathbf{q}}^\tau}{\sqrt{\mathbf{q}^2 + \mathbf{k}^2 - 2qk \cos \theta_{\mathbf{k}-\mathbf{q}}}} \sqrt{1 - \left(\frac{\Delta_{\mathbf{q}}^{\sigma\tau}}{E_{\mathbf{q}}^{\sigma,\tau}} \right)^2}. \end{aligned}$$

Clearly, there are no closed solutions for these integrals, and it becomes necessary to resort to numerical methods. Note, however, that numerically determining these integrals, as functions of \mathbf{k} , is not straightforward, due to the obvious singularity resulting from the unscreened Coulomb potential. We can, nonetheless, reach some conclusions by looking only at the simplest case: $\mathbf{k} = 0$.

4.2 Gap renormalization

4.2.1 Undoped system

As consequence of Dyson's equations, the structure of Eq. (C.31) implies that the self-energy renormalizes the spectrum as

$$\mathcal{E}_{\mathbf{k},\lambda,\sigma}^{\tau} = \varepsilon_{\mathbf{k},\lambda,\sigma}^{\tau} + \hbar \text{Re } \Sigma_{\alpha\bar{\alpha}}^{\tau,\sigma}(\mathbf{k}).$$

In particular, this implies that the spin-split band-gaps become renormalized as

$$\begin{aligned} 2\Delta_*^{\sigma\tau} &= \mathcal{E}_{\mathbf{0},c,\sigma}^{\tau} - \mathcal{E}_{\mathbf{0},v,\sigma}^{\tau} \\ &= \varepsilon_{\mathbf{0},c,\sigma}^{\tau} - \varepsilon_{\mathbf{0},v,\sigma}^{\tau} + \hbar \text{Re } [\Sigma_{cc}^{\tau,\sigma}(\mathbf{0}) - \Sigma_{vv}^{\tau,\sigma}(\mathbf{0})] \\ &= 2\Delta^{\sigma\tau} + 2\delta\Delta^{\sigma\tau}, \end{aligned}$$

where the renormalization of the half-gap $\delta\Delta^{\sigma\tau}$ is given by

$$-\frac{\alpha}{2} \frac{\hbar c}{\varepsilon_r a} \frac{1}{2} \sum_{\lambda} \lambda f_{\lambda, \Lambda}^{\sigma, \tau}(\mathbf{0}) = \frac{\alpha}{2} \frac{\hbar c}{\varepsilon_r a} \int_0^{\Lambda} adq \int_0^{2\pi} \frac{d\theta}{2\pi} \frac{\Delta_q^{\sigma\tau}}{E_q^{\sigma, \tau}},$$

which integrand reads

$$\frac{\Delta_q^{\sigma\tau}}{E_q^{\sigma, \tau}} = \frac{\Delta^{\sigma\tau} - \kappa_- a^2 \mathbf{q}^2}{\sqrt{(\Delta^{\sigma\tau} - \kappa_- a^2 \mathbf{q}^2)^2 + (t^2 + u^2 a^2 \mathbf{q}^2) a^2 \mathbf{q}^2 + 2\tau tua^3 \mathbf{q}^3 \cos 3\theta}}, \quad (4.14)$$

based on the 2nd order spectrum for the spinful bands, Eq. (3.24). The divergence due to the Coulomb potential has vanished and the integral shall converge easily. Also, we compute the following results for a cutoff at $\Lambda = 1/a$.

Due spin-splitting at the edge of the valence band, we can define a half-gap $\Delta^>$ for the energetically high-lying branch (spin-up and spin-down in the K and $-K$ valleys, respectively) and, similarly, $\Delta^<$ for the energetically low-lying branch (spin-down and spin-up in the K and $-K$ valleys, respectively), along with the respective renormalization $\delta\Delta^>$ and $\delta\Delta^<$. In turn, this implies a renormalization of the spin-gap $\delta\lambda$. Values for these parameters are shown in Table 4.1.

Table 4.1: Renormalization of the half-band-gaps for the spin-split valence band, for $\varepsilon_r = 1$. The renormalization of the half-spin-gap can be inferred from $\delta\lambda = \delta\Delta^< - \delta\Delta^>$. (Units: eV)

	MX_2	MoS_2	WS_2	$MoSe_2$	WSe_2
$\delta\Delta^>$	1.65	1.58	1.62	1.52	
$\delta\Delta^<$	1.71	1.73	1.71	1.72	

These values are clearly an overestimation: the renormalizations are about twice the value found for the bare gap 2Δ , given in Table 3.1, which are of order ~ 1.5 eV. Such values are not consistent with previous results [22] but, still, are within a reasonable order of magnitude.

This is an indicator that there may, in fact, exist screening effects due to high-energy electrons unaccounted for in this low-energy model. Indeed, although these electrons are unable to effectively screen the potential and cut its long range short, since they are constrained within the Fermi sea, they may provide a substantial increase of the dielectric constant in these materials. Such is the situation in graphene, for instance: for the Fermi level at the Dirac point, the DOS vanishes and the Coulomb interaction is not screened. It turns out, however, that the σ -orbital electrons are responsible for an increased dielectric constant [114]. We can expect this to happen, even more dramatically, in TMDCs: not only do these materials have 11 valence electrons per unit cell, the large atomic number of transition metals means there is a large amount of core electrons in the system, thus possibly yielding a substantial dielectric constant.

Furthermore, this result indicates that electron-electron interactions are an important con-

tribution towards the gap, likely more preponderant than the lattice potential. As such, since electron-electron interactions are susceptible to the dielectric constant of the substrate, we expect a tunable gap. Although the substrate affects also the lattice potential, it is expected to affect the electronic long-range interactions to a larger degree.

4.2.2 Hole-doped system

To discuss the gap renormalization in this case, we must momentarily return to Eq. (4.7),

$$\Sigma_{\alpha\beta}^*(\mathbf{k}, \mu) = -\frac{1}{\hbar} \sum_{i,j} \bar{g}_i^\alpha(\mathbf{k}) g_j^\beta(\mathbf{k}) \sum_{\mathbf{q}} \sum_{\lambda} \bar{g}_j^\lambda(\mathbf{k}) g_i^\lambda(\mathbf{k}) v_s(\mathbf{q} - \mathbf{k}) n_F(\varepsilon_{\mathbf{k}}^\lambda - \mu).$$

We can keep the band summation restricted to the valence band but, since now we have the Fermi level within the valence band, not only will the limits of the summation in crystal momentum become modified, the very Coulomb interaction will become screened, since now we have a non-vanishing DOS at the Fermi level and, thus, charge fluctuations. Within a Thomas-Fermi approximation, the screened Coulomb interaction reads

$$v_s(\mathbf{q}) = \frac{e^2}{2\varepsilon_r \varepsilon_0} \frac{1}{N\mathcal{A}_{uc}} \frac{1}{\mathbf{q} + q_{TF}},$$

where q_{TF} is the Thomas-Fermi vector. This result can be obtained as a static low-energy limit of the random-phase approximation (RPA) [115].

As before, here we shall consider the spin-split valence band, which means that, up to some hole density, only the high-lying cones (spin-up and spin-down in the K and K' valleys, respectively) will acquire charge pockets. This implies that the only DOS contributing to the screening are those of the high-lying cones from the two inequivalent valleys. In fact, in the next chapter we will show that higher doping regimes are, most likely, experimentally inaccessible, so that we can safely make a low-energy approximation for the DOS by using a parabolic approximation of the spectrum at the edge of the valence band. For the high-lying cones, this reads

$$\varepsilon_{\mathbf{k},\uparrow}^A = \varepsilon_{\mathbf{k},\downarrow}^B = \varepsilon_{\mathbf{k}}^> = -\underline{\Delta}^> - \frac{\hbar^2 \mathbf{k}^2}{2m^>},$$

where $-\underline{\Delta}^> = -(\Delta - \lambda)$ is the top of the high-lying cones with the zero of energy at ε_F . In 2D, this spectrum yields a constant DOS which, further on in the next chapter, will be shown to be

$$D^> = \frac{2\pi}{\mathcal{A}_{BZ}} \frac{m^>}{\hbar^2} = \frac{\sqrt{3}}{4\pi} \left(\frac{a}{\hbar} \right)^2 m^>, \quad (4.15)$$

so that the Thomas-Fermi vector is given by

$$q_{TF} = \frac{2e^2}{\varepsilon_r \varepsilon_0} \frac{D^>}{A_{uc}} = \frac{e^2 m^>}{\pi \varepsilon_r \varepsilon_0 \hbar^2},$$

where the factor of 2 in the first equality is due to the multiplicity of valleys. Numerical values are shown in Table 4.2. We can decompose the self-energy into the contribution from the filled band, determined previously, plus a subtractive contribution from the doped holes in the valence band. This reads

$$\Sigma_{\alpha\beta}^*(\mathbf{k}, k_F) = \Sigma_{\alpha\beta}(\mathbf{k}) - \Sigma_{\alpha\beta}(\mathbf{k}, k_F)|_h , \quad (4.16)$$

which holds since, for a filled band, q_{TF} vanishes and the potential is, once again, unscreened. The second term reads, after prescribing summation to integrals,

$$\Sigma_{\alpha\beta}^{\tau,\sigma}(\mathbf{k}, k_F)|_h = -\frac{N}{\mathcal{A}_{BZ}\hbar} \sum_{i,j} \bar{g}_i^{\alpha,\tau,\sigma}(\mathbf{k}) g_j^{\beta,\tau,\sigma}(\mathbf{k}) \int_0^{k_F} dq \int_0^{2\pi} d\theta v_s(\mathbf{k} - \mathbf{q}) \bar{g}_j^{v,\tau,\sigma}(\mathbf{q}) g_i^{v,\tau,\sigma}(\mathbf{q}) ,$$

where k_F , the Fermi momentum, reads

$$k_F = \sqrt{\frac{2m^>(|\mu| - \Delta^>)}{\hbar^2}} .$$

Clearly, we will again arrive at the expressions of Eqs. (4.12) and (4.13) with the difference that now the cutoff is well defined at the Fermi momentum, and that the coefficients f and h are modified due to the Thomas-Fermi vector in the potential. We are now in a position to determine the renormalization of the gap due to hole doping. This reads

$$\begin{aligned} \delta\Delta_h^{\sigma\tau}(k_F) &= \frac{\hbar}{2} \text{Re} [\Sigma_{cc}^{\tau,\sigma}(\mathbf{0}, k_F)|_h - \Sigma_{vv}^{\tau,\sigma}(\mathbf{0}, k_F)|_h] \\ &= \frac{\alpha}{2} \frac{\hbar c}{\varepsilon_r a} \int_0^{k_F} adq \int_0^{2\pi} \frac{d\theta}{2\pi} \frac{q}{q + q_{TF}} \frac{\Delta_q^{\sigma\tau}}{E_q^{\sigma,\tau}} \\ &= \frac{\alpha}{2} \frac{\hbar c}{\varepsilon_r} q_{TF} \int_0^{k_F/q_{TF}} dx \int_0^{2\pi} \frac{d\theta}{2\pi} \frac{x}{1+x} \frac{\Delta_{q_{TF}x}^{\sigma\tau}}{E_{q_{TF}x}^{\sigma,\tau}} . \end{aligned} \quad (4.17)$$

Notice that q_{TF} defines a scale for the density, to which we can assign a low-density regime for $k_F \ll q_{TF}$ and a high-density regime for $k_F \gg q_{TF}$. We then have a threshold between these regimes at $k_F = q_{TF}$ which, in turn, sets the intermediate density ρ_{TF} , given by

$$\begin{aligned} q_{TF} &= \sqrt{\frac{2m^>(|\mu| - \Delta^>)_{TF}}{\hbar^2}} \stackrel{(4.15)}{=} \sqrt{\frac{4\pi D^>(|\mu| - \Delta^>)_{TF}}{\mathcal{A}_{uc}}} = \sqrt{2\pi\rho_{TF}} \\ &\Leftrightarrow \rho_{TF} = \frac{q_{TF}^2}{2\pi} , \end{aligned}$$

where a density ρ , for a Fermi level only below the high-lying cones and within the parabolic approximation, is defined as $\rho = 2D^>(|\mu| - \Delta^>)/\mathcal{A}_{uc}$. Values are shown in Table 4.2. These are computed based on the 2nd order estimates for the effective masses presented in Sec. 3.1.4.

Table 4.2: Thomas-Fermi vector q_{TF} and the associated hole surface density ρ_{TF} in hole-doped TMDCs.

MX_2	MoS_2	WS_2	MoSe_2	WSe_2
$q_{TF} (\text{\AA}^{-1})$	0.306	0.207	0.331	0.214
$\rho_{TF} (\times 10^{16} \text{ cm}^{-2})$	1.49	0.679	1.74	0.726

Though it is not yet clear, in the next chapter we estimate an upper bound for the experimentally realizable hole density by electric field effect, which will be shown to be of order $\sim 10^{16} \text{ cm}^{-2}$. Thus, the high-density regime is experimentally inaccessible and will not be considered, so that we focus on the low density regime $k_F \ll q_{TF}$. This way, we can Taylor expand the integral of Eq. 4.17 in powers of x to 2nd order, since this variable goes up to as much as $k_F/q_{TF} \ll 1$. As such, note that

$$\frac{x}{1+x} \frac{\Delta_{q_{TF}x}^{\sigma\tau}}{E_{q_{TF}x}^{\sigma,\tau}} = x + \mathcal{O}(x^2),$$

yielding, for the gap renormalization $\delta\Delta_h^{\sigma\tau}$,

$$\delta\Delta_h^{\sigma\tau} = \frac{\alpha \hbar c}{4 \varepsilon_r} \frac{k_F^2}{q_{TF}} = \frac{\alpha}{4\varepsilon_r} \frac{hc}{q_{TF}} \rho,$$

which scales linearly with the hole surface density. Note that the result does not depend on $\sigma\tau$ and thus is the same for all cones. Values for the coefficient are presented in Table (4.3)

Table 4.3: Ratio of gap shift to hole surface density $\delta\Delta_h/\rho$ in hole-doped TMDCs, for $\varepsilon_r = 1$. (Units: eV cm²)

MX_2	MoS_2	WS_2	MoSe_2	WSe_2
$\delta\Delta_h/\rho (\times 10^{-14})$	0.0739	0.110	0.0683	0.106

Although these results are reasonable, they are expected to be overestimated, as argued for the renormalization of the gap in the undoped case. Despite the small magnitude, for a density $\sim 10^{14} \text{ cm}^{-2}$, which is indeed small compared to ρ_{TF} , this correction is of the order of the corrections obtained from the 2nd order Hamiltonian in Sec. (3.1.2) and, as such, is expected to be experimentally measurable with such techniques as angle-resolve photoemission spectroscopy. Note also that this contribution is subtractive, according to Eq. (4.16).

Chapter 5

Broken symmetry phases - Hubbard model

This chapter presents the study of a possible broken symmetry phase in TMDCs. Beginning with the discussion of a Hubbard model with intra- and inter-orbital Coulomb repulsion, the low-energy limit is taken in order to peruse the existence of a spin-valley polarized phase in hole-doped TMDCs.

The phase discussed here relies crucially on the strong spin-orbit coupling existent in these systems which, most significantly, induces a sizable spin-splitting at the valence band edge, as analyzed in Sec. 3.1.3.

5.1 General formulation for TMDCs

Starting with the spinful lattice Hamiltonian with an interactive term as in Eq. (4.2) (summation over orbital indices implied),

$$\hat{\mathcal{H}} = \sum_{\langle i,j \rangle} \hat{a}_{i\alpha}^\dagger E_{\alpha\beta}(\mathbf{r}_{ij}) \hat{a}_{j\beta} + \frac{1}{2} \sum_{ii'jj'} U_{\alpha\alpha'\beta\beta'}^{ii'jj'} \hat{a}_{i\alpha}^\dagger \hat{a}_{j\beta}^\dagger \hat{a}_{j'\beta'} \hat{a}_{i'\alpha'}, \quad (5.1)$$

the Hubbard model is obtained by considering only terms which account for on-site, density-density interactions, such that $i = i' = j = j'$, $\alpha = \alpha'$ and $\beta = \beta'$, so that we write $U_{\mu\mu'\nu\nu'}^{ii'jj'} \equiv U_{\alpha\beta} \delta_{ij} \delta_{i'i} \delta_{jj'} \delta_{\alpha\alpha'} \delta_{\beta\beta'}$. Furthermore, we now consider spin and orbital indices separately, and note that the coupling matrix U is implicitly spin-dependent, in virtue of the Pauli exclusion principle. Thus, Eq. (5.1) becomes

$$\hat{\mathcal{H}} = \sum_{\langle i,j \rangle} \sum_{\alpha,\beta,\sigma} \hat{a}_{i,\alpha\sigma}^\dagger E_{\alpha\beta}^\sigma(\mathbf{r}_{ij}) \hat{a}_{j,\beta\sigma} + \frac{1}{2} \sum_i \sum_{\alpha,\beta} \sum_{\sigma,\sigma'} U_{\alpha\beta}^{\sigma\sigma'} \hat{a}_{i,\alpha\sigma}^\dagger \hat{a}_{j,\beta\sigma'}^\dagger \hat{a}_{j',\beta'\sigma'} \hat{a}_{i',\alpha'\sigma}. \quad (5.2)$$

We can rearrange the interactive term into number operators, which yields an additional quadratic term that vanishes identically, in virtue of the Pauli exclusion principle. The rearranged Hamiltonian reads

$$\hat{\mathcal{H}} = \sum_{\langle i,j \rangle} \sum_{\alpha,\beta,\sigma} \hat{a}_{i,\alpha\sigma}^\dagger E_{\alpha\beta}^\sigma(\mathbf{r}_{ij}) \hat{a}_{j,\beta\sigma} + \frac{1}{2} \sum_i \sum_{\alpha,\beta} \sum_{\sigma,\sigma'} U_{\alpha\beta}^{\sigma\sigma'} \hat{n}_{i,\alpha\sigma} \hat{n}_{i,\beta\sigma'}.$$

5.1.1 Intra- and inter-orbital couplings, validity of the Hubbard model

The matrix elements of U have been studied for $3d$ orbitals in the context of manganites, such as in Ref. [116]. In this reference, it is shown that for the 4 parameters composing these matrix elements - U for intra-orbital Coulomb interaction, U' for the inter-orbital Coulomb interaction, J for the inter-orbital exchange interaction and J' for the inter-orbital pair-hopping amplitude - the relations

$$J = J',$$

$$U = U' + 2J,$$

hold for any combination of $3d$ orbitals [116]. Therefore, U accounts for the diagonal elements and U' for the off-diagonal elements (in orbital index space) of the U matrix, so that expanding the interactive term yields

$$\hat{V} = \sum_i \sum_\sigma \left[\left(\frac{U}{2} \sum_\alpha \hat{n}_{i,\alpha\sigma} \hat{n}_{i,\alpha\bar{\sigma}} + \frac{U'}{2} \sum_{\alpha \neq \beta} \hat{n}_{i,\alpha\sigma} \hat{n}_{i,\beta\bar{\sigma}} \right) + \frac{U'}{2} \sum_{\alpha \neq \beta} \hat{n}_{i,\alpha\sigma} \hat{n}_{i,\beta\sigma} \right].$$

Due to the inter-orbital coupling U' , an anti-Hubbard term emerges, since it is possible for parallel-spin electrons on different orbitals to interact on-site, as is clear from the third term. Clearly, this term counters the spin-alignment tendency provided by the Hubbard terms and will depromote the realization of a spin-polarized phase.

Although J is generally much smaller than U [116], it is not entirely negligible, in the sense that $U' < U$ holds but, also, $U' \simeq U$ to a good approximation. We can take advantage of this nuance to study a possible spin-polarized phase in these materials analytically. Since $U' < U$, even if by a slight difference, the Hubbard terms are expected to have a marginal dominance over the anti-Hubbard term, so that we can neglect the latter and write down an effective interaction,

$$\hat{V}_{eff} = \sum_i \sum_\sigma \left(\frac{U}{2} \sum_\alpha \hat{n}_{i,\alpha\sigma} \hat{n}_{i,\alpha\bar{\sigma}} + \frac{U'}{2} \sum_{\alpha \neq \beta} \hat{n}_{i,\alpha\sigma} \hat{n}_{i,\beta\bar{\sigma}} \right)$$

On the other hand, we can make use of $U' \simeq U$ to greatly simplify the analysis, so that the

effective interactive term is rewritten

$$\hat{V}_{eff} \simeq \frac{U}{2} \sum_i \sum_{\sigma} \sum_{\alpha, \beta} \hat{n}_{i,\alpha\sigma} \hat{n}_{i,\beta\bar{\sigma}} = U \sum_i \hat{n}_{i\uparrow} \hat{n}_{i\downarrow},$$

where $\hat{n}_{i\sigma} = \sum_{\alpha} \hat{n}_{i,\alpha\sigma}$ and α stands for a orbital index. Note that the factor $1/2$ cancels since $\hat{n}_{i\downarrow} \hat{n}_{i\uparrow} = \hat{n}_{i\uparrow} \hat{n}_{i\downarrow}$. The price to pay for this approximation scheme is that the critical values yielded by this model are expected to be highly underestimated. However, the resulting Hubbard model contains all the essential physics to account for a possible spin-polarized phase in this class of materials.

5.1.2 Path-integral formulation

Now, we can transform the single-body term to crystal-momentum space, so that the Hamiltonian now reads

$$\hat{\mathcal{H}} = \sum_{\mathbf{k}, \sigma} \hat{\varphi}_{\mathbf{k}, \alpha\sigma}^{\dagger} [H_{tb}(\mathbf{k})]_{\alpha\beta}^{\sigma} \hat{\varphi}_{\mathbf{k}, \beta\sigma} + U \sum_i \hat{n}_{i\uparrow} \hat{n}_{i\downarrow}. \quad (5.2)$$

(Summation over orbital indices is implied.) In turn, the interactive term can be rewritten in a way that clearly discriminates the contributions of the charge and spin densities, by writing

$$\sum_i \hat{n}_{i\uparrow} \hat{n}_{i\downarrow} = \frac{1}{4} \sum_i (\hat{n}_{i\uparrow} + \hat{n}_{i\downarrow})^2 - \frac{1}{4} \sum_i (\hat{n}_{i\uparrow} - \hat{n}_{i\downarrow})^2. \quad (5.3)$$

Due to charge conservation, the first term is surely expected to be unimportant and will be dropped. Moreover, we can identify the second term as the \hat{S}^z angular-momentum operator in a Schwinger-like representation, which we write

$$\hat{S}_i = \sum_{\sigma} \hat{a}_{i,\alpha\sigma}^{\dagger} (\hat{\sigma}_3)_{\sigma\sigma'} \hat{a}_{i,\alpha\sigma'} = \sum_{\alpha} \begin{pmatrix} \hat{a}_{i,\alpha\uparrow} \\ \hat{a}_{i,\alpha\downarrow} \end{pmatrix}^{\dagger} \begin{pmatrix} 1 & 0 \\ 0 & -1 \end{pmatrix} \begin{pmatrix} \hat{a}_{i,\alpha\uparrow} \\ \hat{a}_{i,\alpha\downarrow} \end{pmatrix} = \sum_{\sigma} \sigma \hat{a}_{i,\alpha\sigma}^{\dagger} \hat{a}_{i,\alpha\sigma}.$$

Thus, the Hamiltonian now reads

$$\hat{\mathcal{H}} = \sum_{\mathbf{k}, \sigma} \hat{\varphi}_{\mathbf{k}, \alpha\sigma}^{\dagger} [H_{tb}(\mathbf{k})]_{\alpha\beta}^{\sigma} \hat{\varphi}_{\mathbf{k}, \beta\sigma} - \frac{U}{4} \sum_i (\hat{S}_i)^2.$$

Finally, considering a grand-canonical ensemble, the action reads

$$S[\bar{\varphi}, \varphi] = \int_0^{\beta\hbar} d\tau \left\{ \sum_{\mathbf{k}, \sigma} \bar{\varphi}_{\mathbf{k}, \alpha\sigma} [(\hbar\partial_{\tau} - \mu)\delta_{\alpha\beta} + [H_{tb}(\mathbf{k})]_{\alpha\beta}^{\sigma}] \varphi_{\mathbf{k}, \beta\sigma} - \frac{U}{4} \sum_i \left(\sum_{\sigma} \sigma \bar{\varphi}_{i,\alpha\sigma} \varphi_{i,\alpha\sigma} \right)^2 \right\}.$$

Considering the foregoing action, we can decouple the quartic term by performing a Hubbard-Stratonovich transformation, taking the associated grand-partition function and introducing the

following Gaussian functional integral

$$\begin{aligned} & \prod_i \exp \left[\frac{U}{4\hbar} \int_0^{\beta\hbar} d\tau \left(\sum_{\sigma} \sigma \bar{\varphi}_{i,\alpha\sigma} \varphi_{i,\alpha\sigma} \right)^2 \right] \\ &= \int \mathcal{D}m \prod_i \exp \left(-\frac{U}{4\hbar} \int_0^{\beta\hbar} d\tau m_i^2 - \frac{U}{2\hbar} \int_0^{\beta\hbar} d\tau \sum_{\sigma} \sigma m_i \bar{\varphi}_{i,\alpha\sigma} \varphi_{i,\alpha\sigma} \right), \end{aligned}$$

thus introducing the real bosonic decoupling field m . After transforming the $m\bar{\varphi}\varphi$ term to the crystal-momentum and frequency spaces and defining the imaginary-time 4-momentum $k \equiv (i\omega_n, \mathbf{k})$, the decoupled action reads

$$S[m, \bar{\varphi}, \varphi]/\hbar = \frac{N\beta U}{4} \sum_k |m_k|^2 - \sum_{k,k'} \sum_{\alpha,\beta,\sigma} \bar{\psi}_{k,\alpha\sigma} \left[\left(\hat{\mathcal{G}}_*^{-1} \right)_{k,\alpha\beta}^{\sigma} \delta_{k,k'} - \frac{\sigma U}{2\hbar} m_{k'-k} \delta_{\alpha\beta} \right] \psi_{k',\beta\sigma},$$

where the matrix $\hat{\mathcal{G}}_*^{-1}$ is the inverse of the single-electron Green's function (or bare propagator), given by (in the space of crystal momentum, Matsubara frequencies, orbital and spin indices)

$$\hbar \left(\hat{\mathcal{G}}_*^{-1} \right)_{k,\alpha\beta}^{\sigma} = (i\hbar\omega_n + \mu) \delta_{\alpha\beta} - [H_{tb}(\mathbf{k})]_{\alpha\beta}^{\sigma}.$$

Note that this is not simply the bare propagator of the non-interactive system $\hat{\mathcal{G}}_0$, since the Fermi level is that of the interactive system. The field m is real in lattice space, hence $m_k = \overline{m_{-k}}$. This action is quadratic in the fermionic fields and, thus, integrable, yielding the grand-partition function

$$\begin{aligned} \mathcal{Z} &= \int \mathcal{D}m \int \mathcal{D}(\bar{\psi}, \psi) e^{-S[m, \bar{\varphi}, \varphi]/\hbar} \\ &= \int \mathcal{D}m \exp \left(-\frac{N\beta U}{4} \sum_k |m_k|^2 \right) \det \beta \hbar \left(\hat{\mathcal{G}}_*^{-1} - \frac{U}{2\hbar} \hat{\sigma}_3 \hat{m} \right), \end{aligned}$$

where \hat{m} is such that $m_{k'-k} \delta_{\alpha\beta} = (\hat{m})_{kk',\alpha\beta}$. We can now obtain an effective action in terms of m by exponentiating the determinant and using the general operator identity [117]

$$\ln \det \hat{O} = \text{Tr} \ln \hat{O},$$

yielding

$$S[m]/\hbar = \frac{N\beta U}{4} \sum_k |m_k|^2 - \text{Tr} \ln \beta \hbar \left(\hat{\mathcal{G}}_*^{-1} - \frac{U}{2\hbar} \hat{\sigma}_3 \hat{m} \right). \quad (5.4)$$

We now turn to a low-energy description of the Hubbard interaction in this system, in which the spin-split valence band and spin-valley coupling effects shall be of key importance to the non-trivial physics of a broken-symmetry phase.

5.2 Low-energy theory

Transformation to band indices

Recovering the Hamiltonian of Eq. (5.2),

$$\hat{\mathcal{H}} = \sum_{\mathbf{k},\sigma} \hat{\varphi}_{\mathbf{k},\alpha\sigma}^\dagger [H_{tb}(\mathbf{k})]_{\alpha\beta}^{\sigma} \hat{\varphi}_{\mathbf{k},\beta\sigma} + U \sum_i \hat{n}_{i\uparrow} \hat{n}_{i\downarrow},$$

we now wish to transform it so that a low-energy approximation becomes amenable. It is necessary to transform the Hubbard term to crystal momentum space, yielding

$$U \sum_i \hat{n}_{i\uparrow} \hat{n}_{i\downarrow} = \frac{U}{N} \sum_{\mathbf{q}} \hat{\rho}_{\mathbf{q},\uparrow} \hat{\rho}_{-\mathbf{q},\downarrow},$$

where the real bosonic operators $\{\hat{\rho}_{\mathbf{q},\sigma}\}$ are written in terms of the fermionic operators as

$$\hat{\rho}_{\mathbf{q},\sigma} = \sum_{\mathbf{k}} \hat{\varphi}_{\mathbf{k}+\mathbf{q},\alpha\sigma}^\dagger \hat{\varphi}_{\mathbf{k},\alpha\sigma}, \quad \forall \sigma, \mathbf{q}.$$

This includes diagonalizing the tight-binding Hamiltonian and transforming to band indices which, in turn, allows a simplification: since we are considering a hole-doped, low-energy system, we need only consider the contribution of the valence band. A subtlety arises, though, when transforming the Hubbard term to band indices, since the transformation, albeit unitary, is momentum-dependent. If the transformation is such that

$$\hat{\varphi}_{\mathbf{k},\beta\sigma} = \mathcal{U}_{\mathbf{k},\sigma}^{\beta\nu} \hat{\psi}_{\mathbf{k},\nu\sigma}, \quad \mathcal{U}_{\mathbf{k},\sigma}^\dagger H_{tb}(\mathbf{k}) \mathcal{U}_{\mathbf{k},\sigma} = \text{diag}[\varepsilon_{\mathbf{k},\sigma}^h, \varepsilon_{\mathbf{k},\sigma}^c, \varepsilon_{\mathbf{k},\sigma}^v],$$

where $\{\hat{\psi}_{\mathbf{k},\nu\sigma}\}$ are annihilation operators in the space of band indices, we thus have

$$\hat{\rho}_{\mathbf{q},\sigma} = \sum_{\mathbf{k}} \hat{\varphi}_{\mathbf{k}+\mathbf{q},\alpha\sigma}^\dagger \hat{\varphi}_{\mathbf{k},\beta\sigma} = \sum_{\mathbf{k}} \hat{\psi}_{\mathbf{k}+\mathbf{q},\mu\sigma}^\dagger \left(\mathcal{U}_{\mathbf{k}+\mathbf{q},\sigma}^{\mu\alpha} \right)^* \mathcal{U}_{\mathbf{k},\sigma}^{\alpha\nu} \hat{\psi}_{\mathbf{k},\nu\sigma}.$$

Simplifying this expression requires introducing the low-energy description of the system in the BZ. Thus, we consider states with momentum lying in the vicinity of the valleys K and $K' = -K$ as the primary contribution to the action. It then becomes necessary to introduce sums over valley indices, accounting for contributions from the two inequivalent valleys. Furthermore, this implies that all relevant momenta are of the order of K , which requires $||\mathbf{q}|| \ll K$, so that the relation

$$\mathcal{U}_{\mathbf{k}+\mathbf{q},\sigma}^\dagger \mathcal{U}_{\mathbf{k},\sigma} \simeq \mathcal{U}_{\mathbf{k},\sigma}^\dagger \mathcal{U}_{\mathbf{k},\sigma} = \hat{1}$$

holds to a very good approximation, within a low-energy description. Further on we will work within a mean-field approximation, which implies $\mathbf{q} = 0$ and the relation will hold exactly. Con-

sidering the foregoing arguments, the low-energy Hamiltonian reads

$$\hat{\mathcal{H}} = \sum_{\sigma, \tau} \sum_{\mathbf{k}} \hat{\psi}_{\mathbf{k}, \sigma}^{\tau \dagger} \varepsilon_{\mathbf{k}, \sigma}^{\tau} \hat{\psi}_{\mathbf{k}, \sigma}^{\tau} + \frac{U}{N} \sum_{\tau, \tau'} \sum_{\mathbf{q}} \hat{\rho}_{\mathbf{q}, \uparrow}^{\tau} \hat{\rho}_{-\mathbf{q}, \downarrow}^{\tau'}, \quad (5.5)$$

yielding an action, in the grand-canonical ensemble, given by

$$S[\{\bar{\psi}_{\sigma}^{\tau}, \psi_{\sigma}^{\tau}\}] = \sum_{\sigma, \tau} \sum_k \bar{\psi}_{k, \sigma}^{\tau} (-i\hbar\omega_n + \xi_{\mathbf{k}, \sigma}^{\tau}) \psi_{k, \sigma}^{\tau} + \frac{U}{N\beta\hbar} \sum_{\tau, \tau'} \sum_q \rho_{q, \uparrow}^{\tau} \rho_{-q, \downarrow}^{\tau'}, \quad (5.6)$$

where $\xi_{\mathbf{k}, \sigma}^{\tau} = \varepsilon_{\mathbf{k}, \sigma}^{\tau} - \mu$, $\varepsilon_{\mathbf{k}, \sigma}^{\tau}$ is the low-energy spectrum of the spin-split valence band, τ and τ' are valley indices, and k and q are imaginary-time 4-momenta. The decoupling of the quartic term is taken on the electron densities, introducing an Hubbard-Stratonovich transformation to Eq. (5.6) as is, reading

$$\begin{aligned} & \prod_q \exp \left[-\frac{U}{N\beta\hbar^2} \sum_{\tau, \tau'} \rho_{q, \uparrow}^{\tau} \rho_{-q, \downarrow}^{\tau'} \right] \\ &= \int \mathcal{D}\{\phi_{\sigma}^{\tau}\} \prod_q \exp \left[-N\beta U \sum_{\tau, \tau'} \phi_{q, \uparrow}^{\tau} \phi_{-q, \downarrow}^{\tau'} + \frac{iU}{\hbar} \sum_{\tau, \tau'} (\rho_{q, \uparrow}^{\tau} \phi_{-q, \downarrow}^{\tau'} + \phi_{q, \uparrow}^{\tau} \rho_{-q, \downarrow}^{\tau'}) \right]. \end{aligned}$$

With the new H-S fields, the action reads

$$S[\{\phi_{\sigma}^{\tau}, \bar{\psi}_{\sigma}^{\tau}, \psi_{\sigma}^{\tau}\}]/\hbar = N\beta U \sum_q \sum_{\tau, \tau'} \phi_{q, \uparrow}^{\tau} \phi_{-q, \downarrow}^{\tau'} - \sum_{k, k'} \sum_{\tau, \sigma} \bar{\psi}_{k', \sigma}^{\tau} \left[\left(\hat{\mathcal{G}}_*^{-1} \right)_{k, \sigma}^{\tau} \delta_{k, k'} + \frac{iU}{\hbar} \sum_{\tau'} \phi_{k-k', \bar{\sigma}}^{\tau'} \right] \psi_{k, \sigma}^{\tau}. \quad (5.7)$$

Integrating out the fermionic degrees of freedom yields the ϕ -field effective action

$$S[\{\phi_{\sigma}^{\tau}\}]/\hbar = N\beta U \sum_q \sum_{\tau, \tau'} \phi_{q, \uparrow}^{\tau} \phi_{-q, \downarrow}^{\tau'} - \text{Tr} \ln \beta \hbar \left[\hat{\mathcal{G}}_*^{-1} + \frac{iU}{\hbar} \sum_{\tau'} \hat{\phi}^{\tau'} \right],$$

which, as expected, is structurally similar to the action of Eq. (5.4).

5.2.1 Saddle-point solution

Our interest is determining the critical value of the intra-orbital interaction energy U which onsets a charge imbalance between spin populations of the system and, thus, breaking of time-reversal symmetry. If the system is to have a ground-state which breaks this symmetry, there must exist at least one configuration of the fields $\{\phi_{\sigma}^{\tau}\}$ which is an extremum of the action. Put simply, we will now find

$$\forall \tau, \sigma, \frac{\delta}{\delta \phi_{-q, \sigma}^{\tau}} S[\{\phi_{\sigma}^{\tau}\}] = 0 \quad (5.8)$$

which, in turn, shall yield the critical value U_c , provided the extremum of the action is, in fact, a minimum. In turn, the configuration which minimizes the action is expected to be the dominant contribution to the grand-partition function, in virtue of the structure of the path integral. Carrying out the functional derivatives, noting particularly that

$$\frac{\delta}{\delta\phi_{-q,\sigma}^{\tau}} \sum_{\sigma'} \text{Tr} \ln \beta \hbar \left(\hat{\mathcal{G}}^{-1} \right)_{\sigma'} = \sum_{\sigma', \tau'} \sum_{k', k} \left(\hat{\mathcal{G}} \right)_{k', k, \sigma'}^{\tau'} \left(\frac{\delta}{\delta\phi_{-q,\sigma}^{\tau}} \hat{\mathcal{G}}^{-1} \right)_{k, k', \sigma'}^{\tau'},$$

a general result, valid in virtue of taking the functional derivative of the trace of an operator [117]. We find

$$\phi_{q,\sigma}^{\tau} = \frac{i}{N\beta\hbar} \sum_k \left[\left(\hat{\mathcal{G}}_*^{-1} \right)_{k,\sigma}^{\tau} \delta_{q,0} + \frac{iU}{\hbar} \sum_{\tau'} \phi_{q,\bar{\sigma}}^{\tau'} \right]^{-1}, \quad \forall \tau, \sigma.$$

The solution of this set of equations requires making a physically motivated ansatz. In fact, we can expect a space- and time-independent configuration to minimize the action. As such, we consider the ansatz

$$\phi_{q,\sigma}^{\tau} = i n_{\sigma}^{\tau} \delta_{q,0}, \quad \forall \tau, \sigma.$$

The resulting self-consistent equations are simplified by performing the Matsubara frequency summations, yielding

$$n_{\sigma}^{\tau} = \frac{1}{N} \sum_{\mathbf{k}} n_F \left(\varepsilon_{\mathbf{k},\sigma}^{\tau} - \mu + U \sum_{\tau'} n_{\bar{\sigma}}^{\tau'} \right), \quad \forall \tau, \sigma. \quad (5.9)$$

As expected, the action is stationary for homogeneous H-S fields which solution is the electron densities at each cone. As we will be shown, however, they do not yield a minimum of the action.

Before proceeding, it is imperative to introduce some assumptions. The first is regarding the position of the Fermi level, lowered by hole-doping, and the subsequent shift of the spin-split cones. Namely, we have to consider that the low-lying bands (\uparrow in valley B and \downarrow in valley A) will only be affected by the charge imbalances for some intervals of the Fermi level μ_0 , that is, the Fermi level set at $U = 0$. In fact, we can break this picture down to three regimes:

1. Low doping: down to some level of μ_0 , say μ_A , only the high-lying bands (\uparrow in valley A and \downarrow in valley B) suffer an imbalance.
2. Intermediate doping: from μ_A down to another level μ_B , the \downarrow - A valley will contribute as well, since that valley rises in energy enough to be energetically favourable to lose some of its electrons to \uparrow - A .
3. High doping: \uparrow - B will only come into play for a Fermi level below the maximum of this cone, since its energy is lowered.

For now, our aim is to determine the existence of a spin and valley polarized material, thus it is sufficient to consider a Fermi level for which the low-lying cones remain completely filled. That is, we shall work assuming that $n_{\downarrow}^A = n_{\uparrow}^B$ and that charge imbalance happens solely between the cones \uparrow - A and \downarrow - B , thus taking $n_{\uparrow}^A - n_{\downarrow}^B$ as an order parameter.

The second is regarding the description of the energy spectrum of the low-energy system. More precisely, we consider to be within the range of validity of the parabolic approximation for the valence band. Furthermore, due to the spin-splitting at the edge of the valence band, we distinguish the highest-lying and lowest-lying branches of the spin-split valence band according to the different spin-valley couplings, so that we have, respectively,

$$\varepsilon_{\mathbf{k},\uparrow}^A = \varepsilon_{\mathbf{k},\downarrow}^B = \varepsilon_{\mathbf{k}}^> = -\underline{\Delta}^> - \frac{\hbar^2 \mathbf{k}^2}{2m^>} , \quad \text{and} \quad \varepsilon_{\mathbf{k},\uparrow}^B = \varepsilon_{\mathbf{k},\downarrow}^A = \varepsilon_{\mathbf{k}}^< = -\underline{\Delta}^< - \frac{\hbar^2 \mathbf{k}^2}{2m^<} , \quad (5.10)$$

where the parameters $\underline{\Delta}^{\nu}$, $\nu = >, <$, are related to the spin-split half-gap by

$$\underline{\Delta}^{\nu} = \Delta^{\nu} - \frac{\nu \lambda}{2} = \Delta - \nu \lambda ,$$

where the binary index ν is assigned to positive and negative signs as $\{>, <\} \mapsto \{+, -\}$. Note that these spectra yield constant DOS in 2D,

$$D^{\sigma\tau}(\varepsilon) = D^{\nu}(\varepsilon) \equiv D^{\nu} .$$

Also, in further calculations we will take the zero of energy to be ε_F (the midpoint between the unsplit valence band and the conduction band, as in Eq. (3.8)) so that $\mu < 0$.

Considering the foregoing argument, we use Eqs. (5.9), for the electron densities, and (5.10), for the DOS, to compute the order parameter $n_{\uparrow}^A - n_{\downarrow}^B$, yielding

$$\begin{aligned} n_{\uparrow}^A - n_{\downarrow}^B &= \frac{1}{N} \sum_{\mathbf{k}} \left[n_F \left(\varepsilon_{\mathbf{k},\uparrow}^A - \mu + U \sum_{\tau'} n_{\downarrow}^{\tau'} \right) - n_F \left(\varepsilon_{\mathbf{k},\downarrow}^B - \mu + U \sum_{\tau'} n_{\uparrow}^{\tau'} \right) \right] \\ &= \frac{1}{\mathcal{A}_{BZ}} \int d^2 k \left[n_F \left(\varepsilon_{\mathbf{k},\uparrow}^A - \mu + U \sum_{\tau'} n_{\downarrow}^{\tau'} \right) - n_F \left(\varepsilon_{\mathbf{k},\downarrow}^B - \mu + U \sum_{\tau'} n_{\uparrow}^{\tau'} \right) \right] \\ &= \frac{2\pi}{\mathcal{A}_{BZ}} \frac{m^>}{\hbar^2} \int_0^{\Lambda} \frac{\hbar^2 k dk}{m^>} \left[n_F \left(\varepsilon_{\mathbf{k},\uparrow}^A - \mu + U \sum_{\tau'} n_{\downarrow}^{\tau'} \right) - n_F \left(\varepsilon_{\mathbf{k},\downarrow}^B - \mu + U \sum_{\tau'} n_{\uparrow}^{\tau'} \right) \right] \\ &= D^> \int_{\varepsilon_{\Lambda}^>}^{-\underline{\Delta}^>} d\varepsilon \left[n_F \left(\varepsilon - \mu + U \sum_{\tau'} n_{\downarrow}^{\tau'} \right) - n_F \left(\varepsilon - \mu + U \sum_{\tau'} n_{\uparrow}^{\tau'} \right) \right] \\ &\stackrel{T \rightarrow 0}{=} D^> \int_{\mu - U \sum_{\tau'} n_{\uparrow}^{\tau'}}^{\mu - U \sum_{\tau'} n_{\downarrow}^{\tau'}} d\varepsilon = D^> U \left(\sum_{\tau'} n_{\uparrow}^{\tau'} - \sum_{\tau'} n_{\downarrow}^{\tau'} \right) \\ &= D^> U (n_{\uparrow}^A - n_{\downarrow}^B) \end{aligned} \quad (5.11)$$

$$\Rightarrow (1 - D^> U) (n_{\uparrow}^A - n_{\downarrow}^B) = 0 . \quad (5.12)$$

According to this, $n_{\uparrow}^A - n_{\downarrow}^B = 0$ except for $D^>U = 1$. Although the equation suggests the inexistence of a broken-symmetry phase, the singular behaviour for a fixed value of U suggests otherwise. This is an indicator that the extremum of S does not correspond to a minimum in the broken-symmetry phase and that we must approach the problem from a different standpoint.

We will, however, make use of the solution arrived at here, which amounts to the saddle-point solution of the action, valid for the normal phase. But before proceeding, we derive an additional result, which relates the Fermi level μ for $U \neq 0$ and the Fermi level of the non-interactive system μ_0 , in virtue of charge conservation. This reads

$$\begin{aligned} n &= n_{\uparrow}^A + n_{\uparrow}^B + n_{\downarrow}^A + n_{\downarrow}^B \\ &= 2D^>(\mu_0 - \varepsilon_{\Lambda}^>) + 2D^<(-\Delta^< - \varepsilon_{\Lambda}^<) \\ &\stackrel{(5.9)}{=} 2D^> \left(\mu - \frac{U}{2} \sum_{\tau, \sigma} n_{\sigma}^{\tau} - \varepsilon_{\Lambda}^> \right) + 2D^<(-\Delta^< - \varepsilon_{\Lambda}^<), \end{aligned} \quad (5.13)$$

where, in the second equality, the electron densities in the non-interactive system were used, $\varepsilon_{\Lambda}^>, \varepsilon_{\Lambda}^< < 0$ are cone-dependent cutoffs and n is the total electron density. Noting that, in the normal phase, the following relations hold

$$\sum_{\sigma} n_{\sigma}^A = \sum_{\sigma} n_{\sigma}^B = \sum_{\tau} n_{\uparrow}^{\tau} = \sum_{\tau} n_{\downarrow}^{\tau} = \frac{n}{2}, \quad (5.14)$$

we arrive at

$$\mu = \mu_0 + \frac{Un}{2}. \quad (5.15)$$

This relation holds for the normal phase as well as for the broken symmetry phase in the low doping regime, but not for any other, as will be shown further on. Note that due to the constancy of the DOS and, therefore, simplicity of the integrals for $T \rightarrow 0$, from now on most computations involving electron densities will be written directly, as in Eq. (5.13).

5.2.2 Action expansion

Consider again the Hubbard-Stratonovich action of Eq (5.7)

$$S[\{\phi_{\sigma}^{\tau}, \bar{\psi}_{\sigma}^{\tau}, \psi_{\sigma}^{\tau}\}]/\hbar = N\beta U \sum_q \sum_{\tau, \tau'} \phi_{q, \uparrow}^{\tau} \phi_{-q, \downarrow}^{\tau'} - \sum_{k, k'} \sum_{\tau, \sigma} \bar{\psi}_{k', \sigma}^{\tau} \left[\left(\hat{\mathcal{G}}_*^{-1} \right)_{k, \sigma}^{\tau} \delta_{k', k} + \frac{iU}{\hbar} \sum_{\tau'} \phi_{k-k', \bar{\sigma}}^{\tau'} \right] \psi_{k, \sigma}^{\tau}.$$

We now introduce an ansatz for the ϕ -fields such that

$$\phi_{q, \sigma}^{\tau} = i\bar{n}_{\sigma}^{\tau} \delta_{q, 0} + \delta\phi_{q, \sigma}^{\tau}, \quad \forall \tau, \sigma. \quad (5.16)$$

Here, $\{\bar{n}_{\sigma}^{\tau}\}$ are the saddle-point solutions for the normal phase - the electron densities at each cone in the normal phase - perturbed by a contribution $\delta\phi_{q, \sigma}^{\tau}$ for which, by hypothesis, $|\delta\phi_{q, \sigma}^{\tau}| \ll$

\bar{n}_σ^τ holds. Absorbing the saddle-point contribution into the inverse of the propagator $\hat{\mathcal{G}}_*$, we arrive at the bare propagator in the non-interactive system $\hat{\mathcal{G}}_0$,

$$\hbar \left(\hat{\mathcal{G}}_0^{-1} \right)_{k,\sigma}^\tau = i\hbar\omega_n - \varepsilon_{\mathbf{k},\sigma}^\tau + \mu - U \sum_{\tau'} n_\sigma^{\tau'} = i\hbar\omega_n - \varepsilon_{\mathbf{k},\sigma}^\tau + \mu_0,$$

where Eqs. (5.14) and (5.15) were used in the second equality. Integrating out the fermionic fields,

$$S[\{\delta\phi_\sigma^\tau\}]/\hbar = N\beta U \sum_q \sum_{\tau,\tau'} (i\bar{n}_\uparrow^\tau \delta_{q,0} + \delta\phi_{q,\uparrow}^\tau) (i\bar{n}_\downarrow^{\tau'} \delta_{q,0} + \delta\phi_{-q,\downarrow}^{\tau'}) - \text{Tr} \ln \left[\beta \hbar \left(\hat{\mathcal{G}}_0^{-1} + \frac{iU}{\hbar} \sum_\tau \delta\hat{\phi}^\tau \right) \right], \quad (5.17)$$

factoring out the bare propagator and simplifying the quadratic term in virtue of Eq. (5.14), we obtain the grand-partition function

$$\mathcal{Z} = \mathcal{Z}_0 \int \mathcal{D}\{\delta\phi_\sigma^\tau\} e^{-S'[\{\delta\phi_\sigma^\tau\}]/\hbar}, \quad (5.18)$$

where \mathcal{Z}_0 is the grand-partition function of the non-interactive system and the new ϕ -field action S' reads

$$\begin{aligned} S'[\{\delta\phi_\sigma^\tau\}]/\hbar &= -N\beta U \left(\frac{n}{2} \right)^2 + N\beta U \frac{in}{2} \sum_q \sum_\tau (\delta\phi_{q,\uparrow}^\tau + \delta\phi_{-q,\downarrow}^\tau) \\ &\quad + N\beta U \sum_q \sum_{\tau,\tau'} \delta\phi_{q,\uparrow}^\tau \delta\phi_{-q,\downarrow}^{\tau'} - \text{Tr} \ln \left[1 + \frac{iU}{\hbar} \hat{\mathcal{G}}_0 \sum_\tau \delta\hat{\phi}^\tau \right]. \end{aligned}$$

Now, due to the magnitude of the perturbations $\{\delta\phi_{q,\sigma}^\tau\}$ relatively to the electron densities $\{n_\sigma^\tau\}$, hypothesized previously, it is possible to obtain the action up to quadratic order in $\delta\phi$ by Taylor expanding the fermionic contribution of the action which, in virtue of the trace, reads

$$\begin{aligned} F[\{\delta\phi_\sigma^\tau\}] &= \text{Tr} \ln \left[1 + \frac{iU}{\hbar} \hat{\mathcal{G}}_0 \sum_{\tau'} \delta\hat{\phi}^{\tau'} \right] = \\ &= \frac{iU}{\hbar} \sum_{\sigma,\tau} \sum_{k,k'} \left(\hat{\mathcal{G}}_0 \right)_{k,k'}^{\tau,\sigma} \left(\sum_{\tau'} \delta\hat{\phi}^{\tau'} \right)_{k',k}^{\bar{\sigma}} \\ &\quad + \frac{1}{2} \left(\frac{U}{\hbar} \right)^2 \sum_{\sigma,\tau} \sum_{k,k',q,q'} \left(\hat{\mathcal{G}}_0 \right)_{k,k'}^{\tau,\sigma} \left(\sum_{\tau'} \delta\hat{\phi}^{\tau'} \right)_{k',q'}^{\bar{\sigma}} \left(\hat{\mathcal{G}}_0 \right)_{q',q}^{\tau,\sigma} \left(\sum_{\tau'} \delta\hat{\phi}^{\tau'} \right)_{q,k}^{\bar{\sigma}}. \end{aligned} \quad (5.19)$$

Note that $\left(\hat{\mathcal{G}}_0 \right)_{k',k}^{\tau,\sigma} = \left(\hat{\mathcal{G}}_0 \right)_{k,\sigma}^\tau \delta_{k',k}$ and $\left(\sum_{\tau'} \delta\hat{\phi}^{\tau'} \right)_{k',k}^{\bar{\sigma}} = \sum_{\tau'} \delta\phi_{k-k',\bar{\sigma}}^{\tau'}$. Note also that, within the validity of the parabolic approximation, this expansion is exact, as shown in Sec. D.2 of Appendix D. We now make an ansatz for the decoupling fields ϕ , imposing space- and time-homogeneity

$$\delta\phi_{q,\sigma}^\tau \equiv i\eta_\sigma^\tau \delta_{q,0}, \forall \tau, \sigma. \quad (5.20)$$

This ansatz is variational, in the sense that the solution will be determined in virtue of minimization of the action: equivalently to the motivation of Eq. (5.8), the structure of the path integral Eq. (5.18) is such that the solutions which minimize the action constitute the dominant contribution to the grand-partition function.

Why is this approach necessary, considering it is founded essentially on the same principle as the previous one? Eq. (5.12) suggests that the saddle-point solution fails to account for a minimum in the broken symmetry phase, so that we must take a slightly wider look at the action in the vicinity of the transition. Indeed, this approach will allow for a more intricate manipulation of the action, essentially by including constraints due to conservation laws unaccounted for so far.

Eq. (5.19) then becomes

$$F(\{\eta_\sigma^\tau\})/\hbar = -\frac{U}{\hbar} \sum_{\sigma,\tau} \sum_k \frac{\sum_{\tau'} \eta_{\sigma}^{\tau'}}{i\omega_n - \varepsilon_{\mathbf{k},\sigma}^\tau + \mu_0} - \frac{1}{2} \left(\frac{U}{\hbar} \right)^2 \sum_{\sigma,\tau} \sum_k \left(\frac{\sum_{\tau'} \eta_{\sigma}^{\tau'}}{i\omega_n - \varepsilon_{\mathbf{k},\sigma}^\tau + \mu_0} \right)^2. \quad (5.21)$$

We can perform the Matsubara frequency integrations, yielding

$$F(\{\eta_\sigma^\tau\})/\hbar = -\beta U \sum_{\sigma} \sum_{\tau'} \eta_{\sigma}^{\tau'} \sum_{\mathbf{k},\tau} n_F(\varepsilon_{\mathbf{k},\sigma}^\tau - \mu_0) - \frac{\beta U^2}{2} \sum_{\sigma} \left(\sum_{\tau'} \eta_{\sigma}^{\tau'} \right)^2 \sum_{\mathbf{k},\tau} \frac{\partial n_F(\varepsilon_{\mathbf{k},\sigma}^\tau - \mu_0)}{\partial \varepsilon_{\mathbf{k},\sigma}^\tau}, \quad (5.22)$$

where the derivative of the Fermi distribution in the second term appears in virtue of taking the residue of a second-order pole [118]. Replacing summations we have, for the 1st order and 2nd order terms, respectively,

$$\begin{aligned} & \sum_{\sigma} \sum_{\tau'} \eta_{\sigma}^{\tau'} \sum_{\mathbf{k},\tau} n_F(\varepsilon_{\mathbf{k},\sigma}^\tau - \mu_0) = \\ & \stackrel{T \rightarrow 0}{=} N \left[D^> (\mu_0 - \varepsilon_{\Lambda}^>) - D^< (\Delta^< + \varepsilon_{\Lambda}^<) \right] \sum_{\tau} \eta_{\sigma}^{\tau} \stackrel{(5.13)}{=} N \frac{n}{2} \sum_{\tau,\sigma} \eta_{\sigma}^{\tau}, \end{aligned} \quad (5.23)$$

$$\begin{aligned} & \sum_{\sigma} \left(\sum_{\tau'} \eta_{\sigma}^{\tau'} \right)^2 \sum_{\mathbf{k},\tau} \frac{\partial n_F(\varepsilon_{\mathbf{k},\sigma}^\tau - \mu_0)}{\partial \varepsilon_{\mathbf{k},\sigma}^\tau} = \\ & \stackrel{T \rightarrow 0}{=} -N \left[D^> \int_{-\varepsilon_{\Lambda}^>}^{-\Delta^>} d\varepsilon \delta(\mu_0 - \varepsilon) + D^< \int_{-\varepsilon_{\Lambda}^<}^{-\Delta^<} d\varepsilon \delta(\mu_0 - \varepsilon) \right] \sum_{\sigma} \left(\sum_{\tau'} \eta_{\sigma}^{\tau'} \right)^2 \\ & = -ND^> \sum_{\sigma} \left(\sum_{\tau'} \eta_{\sigma}^{\tau'} \right)^2, \end{aligned} \quad (5.24)$$

We can now use charge conservation to impose a constraint on the variational parameters $\{\eta_\sigma^\tau\}$. Retrieving again the fermionic propagator from the effective action of Eq. (5.17), applying the

ansatz of Eq. (5.20) yields

$$\hbar \left(\hat{\mathcal{G}}^{-1} \right)_{k,\sigma}^{\tau} = i\hbar\omega_n - \varepsilon_{\mathbf{k},\sigma}^{\tau} + \mu_0 - U \sum_{\tau'} \eta_{\sigma}^{\tau'} .$$

This is, in fact, the propagator in the broken symmetry phase, which implies that the non-interactive electronic bands become modified by a spin-dependent shift, reading

$$\varepsilon_{\mathbf{k},\sigma}^{\tau} = \varepsilon_{\mathbf{k},\sigma}^{\tau} + U \sum_{\tau'} \eta_{\sigma}^{\tau'} = \varepsilon_{\mathbf{k},\sigma}^{\tau} - \frac{\sigma U}{2} \sum_{\tau',\sigma'} \sigma' \eta_{\sigma'}^{\tau'} + \frac{U}{2} \sum_{\tau',\sigma'} \eta_{\sigma'}^{\tau'} , \quad (5.25)$$

which shall be referred to as magnetic bands (or cones). The second equality is obtained in virtue of

$$\sum_{\tau'} \eta_{\sigma}^{\tau'} = \frac{1}{2} \sum_{\tau',\sigma'} \eta_{\sigma'}^{\tau'} - \frac{\sigma}{2} \sum_{\tau',\sigma'} \sigma' \eta_{\sigma'}^{\tau'} .$$

Using this result to compute electron densities in the interactive system, we can now compare the cone fillings between the non-interactive and the interactive system, setting a constraint to the parameters $\{\eta_{\sigma}^{\tau}\}$ in virtue of charge conservation. This reads

$$\begin{aligned} n &= 2D^>(\mu_0 - \varepsilon_{\Lambda}^>) + 2D^<(-\Delta^< - \varepsilon_{\Lambda}^<) \\ &= D^> \left(\mu_0 - U \sum_{\tau} \eta_{\downarrow}^{\tau} - \varepsilon_{\Lambda}^> \right) + D^> \left(\mu_0 - U \sum_{\tau} \eta_{\uparrow}^{\tau} - \varepsilon_{\Lambda}^> \right) \\ &\quad + 2D^<(-\Delta^< - \varepsilon_{\Lambda}^<), \\ &\Rightarrow \boxed{\sum_{\tau,\sigma} \eta_{\sigma}^{\tau} = 0} , \end{aligned} \quad (5.26)$$

rendering the 1st order term of the fermionic contribution of the expanded action, Eq. (5.22), vanishing. Moreover, note that

$$\sum_{\sigma} \left(\sum_{\tau'} \eta_{\sigma}^{\tau'} \right)^2 = \left(\sum_{\tau,\sigma} \eta_{\sigma}^{\tau} \right)^2 - 2 \sum_{\tau,\tau'} \eta_{\uparrow}^{\tau} \eta_{\downarrow}^{\tau'} , \quad (5.27)$$

holds for the 2nd order term and, in turn

$$\begin{aligned} \sum_{\tau,\tau'} \eta_{\uparrow}^{\tau} \eta_{\downarrow}^{\tau'} &= \frac{1}{4} \left(\sum_{\tau,\sigma} \eta_{\sigma}^{\tau} \right)^2 - \frac{1}{4} \left(\sum_{\tau,\sigma} \sigma \eta_{\sigma}^{\tau} \right)^2 \\ &\Rightarrow \sum_{\sigma} \left(\sum_{\tau'} \eta_{\sigma}^{\tau'} \right)^2 = \frac{1}{2} \left(\sum_{\tau,\sigma} \eta_{\sigma}^{\tau} \right)^2 + \frac{1}{2} \left(\sum_{\tau,\sigma} \sigma \eta_{\sigma}^{\tau} \right)^2 , \end{aligned} \quad (5.28)$$

so that the fermionic contribution reads

$$F(\{\eta_\sigma^\tau\})/\hbar = N\beta U D^> U \left(\sum_{\tau,\sigma} \frac{\sigma \eta_\sigma^\tau}{2} \right)^2,$$

yielding, for the total action,

$$\begin{aligned} S'(\{\eta_\sigma^\tau\})/\hbar &= -N\beta U \left(\frac{n}{2} \right)^2 - N\beta U \frac{n}{2} \sum_{\tau,\sigma} \eta_\sigma^\tau - N\beta U \sum_{\tau,\tau'} \eta_\uparrow^\tau \eta_\downarrow^{\tau'} - N\beta D^> U^2 \left(\sum_{\tau,\sigma} \frac{\sigma \eta_\sigma^\tau}{2} \right)^2 \\ &= N\beta U (1 - D^> U) \left(\sum_{\tau,\sigma} \frac{\sigma \eta_\sigma^\tau}{2} \right)^2 - N\beta U \left(\frac{n}{2} \right)^2, \end{aligned}$$

where, in the second equality, Eqs. (5.26) and (5.28) were used. Finally, recovering that $\eta_\downarrow^A = \eta_\uparrow^B = 0$ holds - accounting for the fact that, in the low doping regime, the \downarrow -A and \uparrow -B are not affected by charge imbalance - yields

$$\frac{S'(\xi)}{N\beta \hbar U} = \frac{S'(\{\eta_\sigma^\tau\})}{N\beta \hbar U} + \left(\frac{n}{2} \right)^2 = (1 - D^> U) \left(\frac{\xi}{2} \right)^2, \quad (5.29)$$

where $\xi = \sum_{\tau,\sigma} \sigma \eta_\sigma^\tau = \eta_\uparrow^A - \eta_\downarrow^B$. Note that, for $D^> U > 1$, the action is minimized by maximizing the variational parameter ξ and, thus, charge imbalance becomes non-vanishing. This implies the existence of a broken symmetry phase, wherein the hole-doped system becomes spontaneously spin and valley polarized, provided that the on-site Coulomb interaction energy is greater than the critical value

$$\boxed{U_c = \frac{1}{D^>}},$$

with the DOS $D^>$ given by, according to the fourth equality of Eq. (5.11),

$$D^> = \frac{2\pi}{\mathcal{A}_{BZ}} \frac{m^>}{\hbar^2} = \frac{\sqrt{3}}{4\pi} \left(\frac{a}{\hbar} \right)^2 m^>, \quad (5.30)$$

where $\mathcal{A}_{BZ} = (2/\sqrt{3})(2\pi/a)^2$ is the area of the Brillouin Zone and $m^>$ is the effective mass of charge carriers in the high-lying cones of the spin-split valence band, as given by Eq. (3.26). As expected, the onset of the phase transition is defined by a Stoner criterion. Values of $D^>$ and U_c for the different TMDCs are shown in Table 5.1.

Table 5.1: DOS of the high-lying cones $D^>$ and critical value U_c for the various TMDCs - low doping. (Units: eV)

MX_2	MoS_2	WS_2	$MoSe_2$	WSe_2
$D^> (-1)$	0.0745	0.0503	0.0876	0.0565
U_c	13.4	19.9	11.4	17.7

These appear to be higher than current estimates for the interaction strength, ranging in $2 \div 10$ eV [119], especially for W compounds. There are reasons to believe, however, that the strength of the on-site Coulomb interaction (or, put simply, of the Hubbard coupling) might cover these critical values, based on studies carried out for graphene [114], where the energy of the partially screened on-site Coulomb interaction is found to be 9.3 eV. TMDCs, in turn, due to their richer electronic structure, are expected to have significantly larger values for the Coulomb interaction, so that these values do not stand to compromise the realization of this phase.

Note, also, that the values used for the effective mass are an estimate, since they are obtained from the non-interacting, undoped electronic structure and, as such, are not accurate for the system studied here.

Failure of the saddle-point solution: charge conservation

This result accounts for the findings from the saddle-point solution: indeed, for $U = U_c$ the action is flat and, trivially, the order parameter is arbitrary, and for $U > U_c$ the action inverts its concavity, so that its extremum is actually a maximum in the broken symmetry phase.

In this sense, the action derived so far is not physical, since it implies that charge imbalance would increase unboundedly to minimize the action. The minimum of the action must then be fixed by charge conservation. In turn, charge conservation imposes that the cone $\uparrow\text{-}A$ can only be filled up to its capacity, which reads, for the spin density $n_\uparrow^A - n_\downarrow^B$,

$$\begin{aligned} n_\uparrow^A - n_\downarrow^B &= D^> \left(\int_{\varepsilon_\Lambda^>}^{-\Delta^>} d\varepsilon - \int_{\varepsilon_\Lambda^>}^{\mu_0 - \frac{U}{2}\xi} d\varepsilon \right) \\ &= D^> \int_{\mu_0 - \frac{U}{2}\xi}^{-\Delta^>} d\varepsilon \\ &= \frac{D^>U}{2}\xi - D^>(\Delta^> + \mu_0), \end{aligned}$$

On the other hand, charge imbalance in the magnetic cones is given by

$$\begin{aligned} n_\uparrow^A - n_\downarrow^B &= D^> \int d\varepsilon \left[n_F \left(\varepsilon - \mu_0 - \frac{U\xi}{2} \right) - n_F \left(\varepsilon - \mu_0 + \frac{U\xi}{2} \right) \right] \\ &= \int_{\mu_0 - \frac{U}{2}\xi}^{\mu_0 + \frac{U}{2}\xi} d\varepsilon \\ &= D^>U\xi. \end{aligned}$$

Equating, we arrive at a constraint for the parameter ξ , reading

$$\frac{D^>U}{2}\xi + D^>(\Delta^> + \mu_0) = 0. \quad (5.31)$$

Note that the filling constraint of Eq. (5.31) is equivalent to imposing directly that the top of

the \uparrow -A cone coincides with the Fermi level, that is,

$$-\underline{\Delta}^> = \mu_0 + \frac{U\xi}{2},$$

and, as will be shown, directly yields the mean-field solution in the broken symmetry phase, which we call ξ_U . Now, we introduce this constraint in the unphysical action of Eq. (5.29) using a Lagrange multiplier λ , which is promptly eliminated by variating ξ ,

$$\delta \left\{ S'(\xi) - \lambda \left[\frac{D^>U}{2}\xi + D^>(\underline{\Delta}^> + \mu_0) \right] \right\} = 0 \Rightarrow \lambda = N\beta U \frac{1 - D^>U}{D^>U} \xi.$$

Substituting back, we arrive at the physical action,

$$\boxed{\frac{\mathcal{S}(\xi)}{N\beta\hbar U} = - \left(\frac{U}{U_c} - 1 \right) \left(\xi_U - \frac{\xi}{2} \right) \frac{\xi}{2}, \quad U > U_c, \xi > 0.} \quad (5.32)$$

This is the most general form of the action, up to second order of the variational order parameter ξ , valid for all doping regimes. The extremum of \mathcal{S} is then given by

$$\boxed{\frac{\partial \mathcal{S}}{\partial \xi}(\xi_U) = 0 \Leftrightarrow \xi_U = 2 \frac{|\mu_0| - \underline{\Delta}^>}{U}, \quad U > U_c}, \quad (5.33)$$

which, clearly, is a minimum in the broken symmetry phase $U > U_c$:

$$\frac{\partial^2 \mathcal{S}}{\partial \xi^2} = \frac{N\beta U}{2} \left(\frac{U}{U_c} - 1 \right) > 0.$$

Figure 5.1 depicts the physical picture for this transition, in terms of the cones in the magnetic bands. Additionally, it is possible to determine μ_A , the Fermi level down to which the \downarrow -A cone remains completely filled, according to the condition $n_\uparrow^B = n_\downarrow^A$ for $\xi = \xi_U$. This condition reads

$$n_\uparrow^B - n_\downarrow^A = D^< \int_{\mu_A - U\xi_U/2}^{-\underline{\Delta}^<} d\varepsilon = 0 \Leftrightarrow |\mu_A| = \frac{\underline{\Delta}^> + \underline{\Delta}^<}{2} = \Delta.$$

Furthermore, the magnetization density (i.e. spin density) yields

$$m = n_\uparrow^A - n_\downarrow^B = D^>U\xi_U = 2D^>(|\mu_0| - \underline{\Delta}^>), \quad (5.34)$$

which, as expected, is equal to the hole density $p = 2D^>(|\mu_0| - \underline{\Delta}^>)$, meaning that all charge transferred to the \uparrow -A cone originates from the \downarrow -B cone, as required by charge conservation. Indeed, considering the conservation law Eq. (5.26) and that $\eta_\downarrow^A = \eta_\uparrow^B = 0$ holds, in this regime,

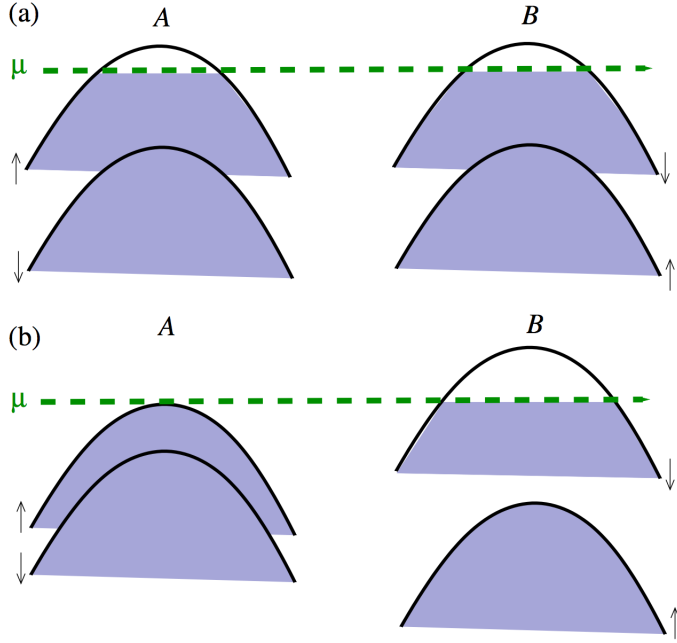


Figure 5.1: Magnetic bands, according to Eq. 5.25, for (a) the normal phase, $D > U < 1$, and (b) the magnetic phase, $D > U > 1$. In (b) we have assumed $\xi > 0$.

we can determine the solutions $\eta_{\uparrow,U}^A$ and $\eta_{\downarrow,U}^B$ in the broken symmetry phase, yielding

$$\eta_{\uparrow,U}^A = -\eta_{\downarrow,U}^B = \frac{|\mu_0| - \Delta^>}{U}. \quad (5.35)$$

These solutions confirm our ansatz: they are proportional (by a factor of $D > U$) to the variation of charge density in each cone and, indeed, such a variation is smaller in magnitude than the total charge density of a cone.

Finally, note that the same results obtained with the formalism used can be obtained using a variational mean-field approach based on the Gibbs-Bogoliubov-Feynman inequality, as discussed in Sec. D.1 of Appendix D.

5.2.3 Anomalous Hall effect in the spin-valley-polarized phase

This phase has physical implications beyond magnetism, in virtue of being not only spin polarized but also valley polarized.

For instance, in Sec. 3.2.1 we went over how the existence of a Berry curvature allowed charge carriers in inequivalent valleys to be selectively excited by breaking time reversal symmetry with circularly polarized light. Here, however, the system spontaneously breaks time-reversal symmetry, so that a time-reversal symmetry breaking external perturbation is no longer

needed. This should be clear from Fig. 5.1: due to depletion of charge carriers in a given valley, the other valley will have its charge carriers energetically closer to the conduction band, at the distance of the band gap. Thus, shining properly tuned light is enough to excite valley-polarized charge carriers.

Moreover, the topological character of the Dirac cones has direct and observable consequence. As discussed in Sec. 3.2.1, the expression for the valley Hall conductivity was derived and revealed that this class of materials is topologically trivial, manifested in the fact that contributions of both valleys cancel out identically. However, in a valley-polarized phase, that will no longer be the case, and an anomalous Hall effect can be expected. To see this, we retrieve the expression of the Berry curvature, Eq. (3.31), written for the spin-split valence band,

$$\Omega_{\mu\nu}^{\sigma\tau}(\mathbf{k}) = \varepsilon_{\mu\nu} \frac{\tau}{2} \frac{a^2 t^2}{(\Delta^{\sigma\tau})^2} \left[1 + \frac{a^2 t^2 \mathbf{k}^2}{(\Delta^{\sigma\tau})^2} \right]^{-3/2}, \quad (5.36)$$

and the general expression for the anomalous Hall conductivity, Eq. (B.37), written for the magnetic bands,

$$\sigma_{\mu\nu}^v = \frac{e^2}{\hbar} \sum_{\sigma,\tau} \int \frac{d^2 k}{(2\pi)^2} n_F \left(\varepsilon_{\mathbf{k},\sigma}^\tau - \mu_0 - \sigma \frac{U\xi_U}{2} \right) \Omega_{\mu\nu}^{\sigma,\tau}.$$

The contributions from the low-lying cones cancel identically, keeping only contributions from the imbalanced high-lying cones. Taking the $T \rightarrow 0$ limit for the Fermi distribution,

$$\sigma_{\mu\nu}^v = \frac{e^2}{\hbar} \frac{m^>}{\hbar^2} \int_{\mu_0 - U\xi_U/2}^{-\Delta^>} dE \frac{\varepsilon_{\mu\nu}}{2} \frac{a^2 t^2}{(\Delta^>)^2} \left[1 - \frac{2m^>a^2}{\hbar^2} \left(\frac{t}{\Delta^>} \right)^2 (E + \Delta^>) \right]^{-3/2}.$$

The integral can be solved directly, yielding

$$\begin{aligned} \sigma_{\mu\nu}^v &= \varepsilon_{\mu\nu} \frac{e^2}{2\hbar} \frac{1}{\sqrt{1 - \frac{2m^>a^2}{\hbar^2} \left(\frac{t}{\Delta^>} \right)^2 (E + \Delta^>)}} \Bigg|_{E=\Delta^>-2|\mu_0|}^{E=-\Delta^>} \\ &= \varepsilon_{\mu\nu} \frac{e^2}{2\hbar} \left[1 - \frac{1}{\sqrt{1 + \frac{8\pi D^>}{\sqrt{3}} \left(\frac{t}{\Delta^>} \right)^2 (|\mu_0| - \Delta^>)}} \right], \end{aligned} \quad (5.37)$$

where Eqs. (5.30) and (5.34) were used to substitute for the band mass in terms of the DOS. Furthermore, noting that the second term in the square root is essentially the magnetization density, Eq. 5.34, and assuming that the system is doped only slightly below the maximum of the high-lying cones, we can expand the square root to 1st order, yielding

$$\frac{2h\sigma_{AH}^v}{e^2} = 1 - \left[1 + \frac{4\pi}{\sqrt{3}} \left(\frac{t}{\Delta^>} \right)^2 m \right]^{-\frac{1}{2}} = \frac{2\pi}{\sqrt{3}} \left(\frac{t}{\Delta^>} \right)^2 m + \mathcal{O}(m^2), \quad (5.38)$$

with $\sigma_{\mu\nu}^v = \varepsilon_{\mu\nu}\sigma_{AH}^v$. This phase displays a valence band anomalous Hall response linear in the magnetization density, for small doping. Not only is this conductivity transversal, it implies also a spin-polarized response, which can be inferred from Figure 5.1: while the contributions from the spin-up cones cancel, the contributions from the spin-down cones do not, and ultimately the resulting conductivity stems from this imbalance. Note also that there is an additional longitudinal conductivity, due to the charge pocket in the high-lying spin-down cone. As such, this response will be spin polarized, as well.

Experimental realization

The existence of an anomalous Hall conductivity in the broken symmetry phase provides an experimentally accessible test to its realization. There is, however, a limitation regarding the doping capacity, in the sense that not all doping regimes may be experimentally accessible due to fundamentally physical limitations.

Due to the geometry of 2D materials, such as single-layered TMDCs, it is possible to induce charge carriers by electric field effect. That is, setting up the single-layer to be one of the plates of a parallel plane capacitor, thus applying an external electric field E . This is the electric field inside the parallel plane capacitor, which is known to be

$$E = \frac{e\rho}{\varepsilon},$$

where $e > 0$ is the absolute electron charge, ρ is the hole surface density and ε the permittivity of the medium. This implies a gate voltage such that $V_g = E l$, where l is the inter-plane distance. The set-up consists, essentially, of the capacitor composed of the single-layered TMDC and of a wafer of Si^+ . The inter-planar medium is a SiO_2 wafer of dielectric constant $\varepsilon_r = 3.9$ and with a typical thickness $l \sim 300 \text{ nm}$ [120]. A schematic is shown in Figure 5.2.

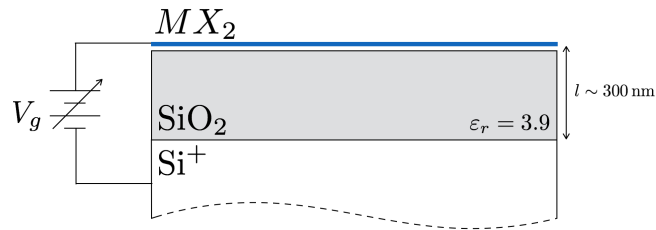


Figure 5.2: Schematic of the electric-field effect apparatus.

Although this method has the advantage of inducing charge carriers without introducing disorder in the system, it has a limitation regarding the scale of the gate voltage and, thus, of the in-plane electric field, since beyond a certain threshold the material sample, as well as the medium, will be ionized and, ultimately, annihilated. The upper bound for this threshold is set in terms of the ionizing electric field magnitude for hydrogen. The magnitude of this electric field

can be estimated by

$$E_H = \frac{e}{4\pi\epsilon_0 a_0^2},$$

where a_0 is the Bohr radius. In turn, this implies a hole surface density and a gate voltage respectively given by

$$\rho_H = \frac{\epsilon_r}{4\pi a_0^2} = 1.11 \times 10^{16} \text{ cm}^{-2}, \quad V_{g,H} = \frac{el}{4\pi\epsilon_0 a_0^2} = 1.54 \times 10^5 \text{ V},$$

where ϵ_r is the relative permittivity of the medium. We have previously determined the thresholds μ_A and μ_B for the onset of the intermediate and high doping regimes, respectively,

$$|\mu_A| = \Delta, \quad |\mu_B| = \underline{\Delta}^< = \Delta + \lambda.$$

Within the validity of the parabolic approximation, the relation between hole surface density ρ and the Fermi level μ_0 is given by

$$\rho = \frac{2D^>(|\mu_0| - \underline{\Delta}^>)}{\mathcal{A}_{uc}},$$

where $\mathcal{A}_{uc} = a^2\sqrt{3}/2$ is the area of the unit cell. Note that the terms in numerator are the number of holes per unit cell (which have, so far, been referred to simply as densities). We can thus estimate the threshold μ_A in terms of hole surface density by

$$\rho_A = \frac{2D^>\lambda}{\mathcal{A}_{uc}}.$$

Numerical values for this threshold are shown in Table 5.2.

Table 5.2: Hole surface density ρ_A for the intermediate threshold for the different TMDCs. (Units: cm^{-2})

MX_2	MoS_2	WS_2	MoSe_2	WSe_2
$\rho_A (\times 10^{15})$	1.23	2.41	1.66	2.69

Clearly, these values are only one order of magnitude below the order of ρ_H , so that we can expect the intermediate and high doping regimes to be experimentally untenable. However, it is interesting, if only academically, to get a sense of the physics of the two further doping regimes, to which we now proceed.

5.3 Dependence on the Fermi level

As discussed earlier, the cones which are affected by charge imbalance depend on the Fermi level μ_0 , and we have shown that the thresholds

$$|\mu_A| = \Delta, \quad |\mu_B| = \underline{\Delta}^< = \Delta + \lambda,$$

hold, respectively, for the cases in which the \downarrow -A cone is shifted above the Fermi level and in which the Fermi level is below the maximum of the \uparrow -B cone. Despite the different physics in each regime, we can expect the differences to be merely quantitative, as we will show. Nonetheless, some remarks are in order.

The first is regarding the validity of the parabolic approximation: we can expect this approximation to break down, for the high-lying cones, as we go lower in the Fermi level. For the present cases, which are experimentally inaccessible and, thus, of less general interest, our intention is only to check how observables and system parameters - such as the critical parameter, the anomalous Hall conductivity the magnetization density - behave along the various doping regimes, so that we keep to the parabolic approximation, for simplicity.

Note, however, that we could get more accurate results without going beyond an analytical treatment, for instance, by correcting the constant DOS with a higher-order term obtained from the exact spectrum for the 2nd order low-energy, Eq. (3.24), as derived in Sec. 3.1.

The second is regarding the validity of the expansion of the action, Eq. (5.19): as the Fermi level is lowered, the charge variations may become comparable to the total charge in each cone, while, on the other hand, we have shown that the mean-field solutions for the variational ansatz Eq. (5.20) are, essentially, the charge variations in each cone. This may break down the 2nd order approximation of the action. In principle, this can be circumvented by expanding to higher-order but, as shown in Sec. D.2, higher-order terms of the expansion are vanishing for a constant DOS. This only reinforces the necessity of correcting the DOS with higher-order terms in order to accurately account for the intermediate and high doping regimes.

The third is regarding the charge conservation laws in this system: In the previous case we have assumed Eq. (5.15) to hold, an assumption that proved to be right. Indeed, the physics in the low doping regime is rather simple: the charge transferred from the upwards shifted cone is identically the same as the charge transferred to the downwards shifted one, so that any shift of the Fermi level identically cancels, remaining the same as in the normal phase. This assumption yielded a simpler, more direct conservation law, given by Eq. (5.26),

$$\sum_{\tau,\sigma} \eta_\sigma^\tau = 0.$$

After studying the previous case, we have confirmed that these parameters are proportional to the charge density variation in each cone, so that this equation has a very simple, intuitive interpretation: charge density variations must total to zero. It is easy to understand that this

condition must hold for all regimes, so that we discard Eq. (5.15) and substitute it with the relaxed condition

$$\mu - \frac{Un}{2} = \mu_0 + \delta\mu, \quad (5.39)$$

where $\delta\mu$ is a variational parameter representing a shift of the Fermi level, thus promoting Eq. (5.26) as the central conservation law.

Why, though, need we introduce Eq. (5.39)? Consider, for instance, the intermediate case, in which there is charge imbalance between two spin-down cones, \downarrow -A and \downarrow -B, and one spin-up cone, \uparrow -A. The spin-up cone will accommodate charge from two cones, contributions which we have no *a priori* information on. Thus, for the increased contribution (relatively to the low doping regime) from the spin-down cones not to exceed the capacity of the spin-up cone (and violating charge conservation), the Fermi level is forced to increase, which will be determined by the distribution of charge obtained from minimization of the action constrained to the capacity of the cones, as carried out previously.

It might appear worrisome that we can no longer substitute $\hat{\mathcal{G}}_*$ for $\hat{\mathcal{G}}_0$ in the H-S action, Eq. (5.7), after applying the ansatz Eq. (5.16), namely, regarding the computation of the 1st and 2nd order contributions of the fermionic action, Eq. (5.19). There is, however, a condition regarding that computation which we needed not worry about previously, as it was identically satisfied: since the action is expanded around the saddle-point solution, all coefficients are computed in that solution, that is, in the normal phase, for which $\delta\mu = 0$ holds, so that the propagator in the expanded part of Eq. (5.19) is effectively the bare one. Thus, although it is true that we cannot carry out the aforementioned substitution, all subsequent computations can be carried out identically.

Finally, given that Eq. (5.26) holds, the magnetic bands Eq (5.25) reduce to

$$\mathcal{E}_{\mathbf{k},\sigma}^{\tau} = \varepsilon_{\mathbf{k},\sigma}^{\tau} - \frac{\sigma U}{2} \sum_{\tau',\sigma'} \sigma' \eta_{\sigma'}^{\tau'}.$$

5.3.1 Intermediate doping regime: $\mu_B < \mu_0 < \mu_A$

For the intermediate case, in which, besides the high-lying cones, only the \downarrow -A cone is affected by charge imbalance, we find the following relation between the shift of the Fermi level $\delta\mu$ and the variational spin density $\sum_{\tau,\sigma} \sigma \eta_{\sigma}^{\tau}$, in virtue of charge conservation,

$$\begin{aligned} n &= 2D^>(\mu_0 - \varepsilon_{\Lambda}^>) + 2D^<(-\underline{\Delta}^< - \varepsilon_{\Lambda}^<) \\ &= D^> \left(\mu_0 + \delta\mu + \frac{U}{2} \sum_{\tau,\sigma} \sigma \eta_{\sigma}^{\tau} - \varepsilon_{\Lambda}^> \right) + D^> \left(\mu_0 + \delta\mu - \frac{U}{2} \sum_{\tau,\sigma} \sigma \eta_{\sigma}^{\tau} - \varepsilon_{\Lambda}^> \right) \\ &\quad + D^<(-\underline{\Delta}^< - \varepsilon_{\Lambda}^<) + D^< \left(\mu_0 + \delta\mu - \frac{U}{2} \sum_{\tau,\sigma} \sigma \eta_{\sigma}^{\tau} - \varepsilon_{\Lambda}^< \right) \end{aligned}$$

$$\Rightarrow (2D^> + D^<) \delta\mu = D^< U \sum_{\tau,\sigma} \frac{\sigma \eta_\sigma^\tau}{2} - D^< (\underline{\Delta}^< - |\mu_0|) . \quad (5.40)$$

The fermionic contribution is the same as Eqs. (5.23) and (5.24),

$$F = \frac{1}{2} N \beta U D^> U \sum_{\sigma} \left(\sum_{\tau'} \eta_{\sigma}^{\tau'} \right)^2 .$$

Note that the 1st order term vanishes identically, in virtue of charge conservation, Eq. (5.26). As before, using Eqs. (5.27) and (5.28) to decouple the variational parameters in the quadratic order terms, we can write the unphysical action as

$$\frac{S'(\xi)}{N \beta U} = (1 - D^> U) \left(\frac{\xi}{2} \right)^2 ,$$

where, noting that only $\eta_{\uparrow}^B = 0$ in this regime, ξ is given by

$$\xi = \sum_{\tau,\sigma} \sigma \eta_{\sigma}^{\tau} = \eta_{\uparrow}^A - \eta_{\downarrow}^A - \eta_{\downarrow}^B .$$

It is clear that the critical value for the Hubbard coupling constant within the intermediate doping regime is again given by

$$\boxed{U_c = \frac{1}{D^>}},$$

the same as the low doping case, which numerical values are shown in Table 5.1. In turn, applying the filling constraint for the \uparrow -A cone which, in this regime, reads

$$\begin{aligned} -\underline{\Delta}^> &= \mu_0 + \delta\mu + \frac{U\xi}{2} \\ &= \mu_0 - \frac{D^< (\underline{\Delta}^< - |\mu_0|)}{2D^> + D^<} + \frac{D^> + D^<}{2D^> + D^<} U\xi , \end{aligned}$$

yielding the mean-field solution

$$\boxed{\xi_U = \frac{2}{U} \frac{D^> (|\mu_0| - \underline{\Delta}^>) + D^< \lambda}{D^> + D^<}}.$$

This regime yields a magnetization in the broken symmetry phase given by

$$\begin{aligned} m &= D^> \int_{-\mu_A^*}^{-\underline{\Delta}^>} d\varepsilon + D^< \int_{-\mu_A^*}^{-\underline{\Delta}^<} d\varepsilon \\ &= 2D^> \frac{D^> (|\mu_0| - \underline{\Delta}^>) + D^< \lambda}{D^> + D^<} + 2D^< \frac{D^> (|\mu_0| - \underline{\Delta}^>) - D^> \lambda}{D^> + D^<} \\ &= 2D^> (|\mu_0| - \underline{\Delta}^>) , \end{aligned}$$

which is the same as for the low doping regime, and the anomalous Hall conductivity reads

$$\begin{aligned} & \frac{2h\sigma_{AH}^v}{e^2} \\ &= \frac{1}{\sqrt{1 - \frac{2\pi}{\sqrt{3}} \left(\frac{t}{\Delta^>}\right)^2 D^> (E + \underline{\Delta}^>)}} \Bigg|_{E=-\mu_A^*}^{E=-\underline{\Delta}^>} - \frac{1}{\sqrt{1 - \frac{2\pi}{\sqrt{3}} \left(\frac{t}{\Delta^<}\right)^2 D^< (E + \underline{\Delta}^<)}} \Bigg|_{E=-\mu_A^*}^{E=-\underline{\Delta}^<} \\ &= \left[1 + \frac{4\pi D^<}{\sqrt{3}} \left(\frac{t}{\Delta^<} \right)^2 \frac{D^>(|\mu_0| - \Delta)}{D^> + D^<} \right]^{-\frac{1}{2}} - \left[1 + \frac{4\pi D^>}{\sqrt{3}} \left(\frac{t}{\Delta^>} \right)^2 \left(\lambda + \frac{D^>(|\mu_0| - \Delta)}{D^> + D^<} \right) \right]^{-\frac{1}{2}}, \end{aligned}$$

where the parameter μ_A^* is given by

$$\mu_A^* = |\mu_0| + \frac{D^<(\underline{\Delta}^< - |\mu_0|)}{2D^> + D^<} + \frac{2D^>}{2D^> + D^<} \frac{D^>(|\mu_0| - \underline{\Delta}^>) + D^<\lambda}{D^> + D^<}.$$

Note that the conductivity is, indeed, continuous with the conductivity in the low doping regime, though the 1st derivative is not. Finally, the shift of the Fermi level in the broken symmetry phase $\delta\mu_*$ is given by

$$\begin{aligned} \delta\mu_* &= \frac{D^<}{2D^> + D^<} \frac{U\xi_U}{2} - \frac{D^<(\underline{\Delta}^< - |\mu_0|)}{2D^> + D^<} \\ &= \frac{2D^<(|\mu_0| - \Delta)}{D^> + D^<} > 0, \end{aligned}$$

which, noting that Δ is the threshold μ_A , is a measure of how much the system goes into the intermediate regime: the more the cones become asymmetrically imbalanced, in the manner discussed in these section's preliminaries, the greater the compensation of the Fermi level.

5.3.2 High doping regime: $\mu_0 < \mu_B$

The high doping regime, in which all cones are affected by charge imbalance, we find the following relation between for the shift of the Fermi level $\delta\mu$, in virtue of charge conservation,

$$\begin{aligned} n &= 2D^>(\mu_0 - \varepsilon_\Lambda^>) + 2D^<(\mu_0 - \varepsilon_\Lambda^<) \\ &= D^> \left(\mu_0 + \delta\mu + \frac{U}{2} \sum_{\tau,\sigma} \sigma\eta_\sigma^\tau - \varepsilon_\Lambda^> \right) + D^> \left(\mu_0 + \delta\mu - \frac{U}{2} \sum_{\tau,\sigma} \sigma\eta_\sigma^\tau - \varepsilon_\Lambda^> \right) \\ &\quad + D^<(-\underline{\Delta}^< - \varepsilon_\Lambda^<) + D^< \left(\mu_0 + \delta\mu - \frac{U}{2} \sum_{\tau,\sigma} \sigma\eta_\sigma^\tau - \varepsilon_\Lambda^< \right) \\ &\Rightarrow (2D^> + D^<) \delta\mu = D^< U \sum_{\tau,\sigma} \frac{\sigma\eta_\sigma^\tau}{2} - D^<(|\mu_0| - \underline{\Delta}^<). \end{aligned} \tag{5.41}$$

All computations proceed identically to the previous cases. For the fermionic contribution we now find

$$F = \frac{1}{2} N\beta U (D^> + D^<)U \sum_{\sigma} \left(\sum_{\tau'} \eta_{\sigma}^{\tau'} \right)^2,$$

yielding an action

$$\frac{S'(\xi)}{N\beta U} = [1 - (D^> + D^<)U] \left(\frac{\xi}{2} \right)^2,$$

with ξ given by

$$\xi = \sum_{\tau, \sigma} \sigma \eta_{\sigma}^{\tau} = \eta_{\uparrow}^A + \eta_{\uparrow}^B - \eta_{\downarrow}^A - \eta_{\downarrow}^B,$$

so that, in the high doping regime, the critical value of U is given by

$$U_c = \frac{1}{D^> + D^<}.$$

Numerical values are shown in Table 5.3.

Table 5.3: Critical value U_c for the various TMDCs - high doping. (Units: eV)

—	MoS ₂	WS ₂	MoSe ₂	WSe ₂
$D^> \left(\text{--}^1 \right)$	0.0745	0.0503	0.0876	0.0565
$D^< \left(\text{--}^1 \right)$	0.0833	0.0663	0.1037	0.0813
U_c	6.33	8.57	5.23	7.25

These are significantly smaller, but of the same order of magnitude, than the values for the lower doping regimes, justified by the greater DOS due to the imbalance in the low-lying cones.

The filling constraint for the \uparrow -A cone now reads

$$\begin{aligned} -\underline{\Delta}^> &= \mu_0 + \delta\mu + \frac{U\xi}{2} \\ &= \mu_0 - \frac{D^<(|\mu_0| - \underline{\Delta}^<)}{2D^> + D^<} + \frac{D^> + D^<}{2D^> + D^<} U\xi, \end{aligned}$$

yielding the mean-field solution

$$\xi_U = \frac{2}{U} \frac{D^>(|\mu_0| - \underline{\Delta}^>) + D^<(|\mu_0| - \underline{\Delta}^<) + D^<\lambda}{D^> + D^<}.$$

We can finally compute the magnetization density, the anomalous Hall conductivity in this regime

and the shift of the Fermi level. The former yields

$$\begin{aligned}
m &= D^> \int_{-\mu_B^*}^{-\Delta^>} d\varepsilon + D^< \int_{-\mu_B^*}^{-\Delta^<} d\varepsilon \\
&= 2D^> \frac{D^>(|\mu_0| - \underline{\Delta}^>) + D^<(|\mu_0| - \underline{\Delta}^<) + D^<\lambda}{D^> + D^<} + 2D^< \frac{D^>(|\mu_0| - \underline{\Delta}^>) + D^<(|\mu_0| - \underline{\Delta}^<) - D^>\lambda}{D^> + D^<} \\
&= 2D^>(|\mu_0| - \underline{\Delta}^>) + 2D^<(|\mu_0| - \underline{\Delta}^<),
\end{aligned}$$

where μ_B^* is given by

$$\mu_B^* = |\mu_0| + \frac{D^<(|\mu_0| - \underline{\Delta}^<)}{2D^> + D^<} + \frac{2D^>}{2D^> + D^<} \frac{D^>(|\mu_0| - \underline{\Delta}^>) + D^<(|\mu_0| - \underline{\Delta}^<) + D^<\lambda}{D^> + D^<}.$$

As for the anomalous Hall conductivity, we find

$$\begin{aligned}
\frac{2h\sigma_{AH}^v}{e^2} &= \frac{1}{\sqrt{1 - \frac{2\pi}{\sqrt{3}} \left(\frac{t}{\Delta^>}\right)^2 D^> (E + \underline{\Delta}^>)}} \Bigg|_{E=-\mu_B^*}^{E=-\underline{\Delta}^>} \\
&\quad - \frac{1}{\sqrt{1 - \frac{2\pi}{\sqrt{3}} \left(\frac{t}{\Delta^<}\right)^2 D^< (E + \underline{\Delta}^<)}} \Bigg|_{E=-\mu_B^*}^{E=-\underline{\Delta}^<} \\
&= \left[1 + \frac{4\pi D^<}{\sqrt{3}} \left(\frac{t}{\Delta^<} \right)^2 \left(|\mu_0| - \underline{\Delta}^< + \frac{D^>\lambda}{D^> + D^<} \right) \right]^{-\frac{1}{2}} \\
&\quad - \left[1 + \frac{4\pi D^>}{\sqrt{3}} \left(\frac{t}{\Delta^>} \right)^2 \left(|\mu_0| - \underline{\Delta}^< + \frac{2D^> + D^<}{D^> + D^<} \lambda \right) \right]^{-\frac{1}{2}},
\end{aligned}$$

which is continuous with the conductivity in the intermediate doping regime. Finally, the shift of the Fermi level in the broken symmetry phase reads

$$\begin{aligned}
\delta\mu_* &= \frac{D^<}{2D^> + D^<} \frac{U\xi_U}{2} - \frac{D^<(|\mu_0| - \underline{\Delta}^<)}{2D^> + D^<} \\
&= \frac{2D^<\lambda}{D^> + D^<} > 0.
\end{aligned}$$

Chapter 6

Conclusions and future work

As proposed at the beginning of this work, we have managed to take a simplified model of the band structure, which presents an excellent approximation within a low-energy theory, and employed it to study some consequences of the electron interactions which, even if not entirely accurate within our framework, have shown some of the physics at play in the many-body setting of these systems.

A group theoretical framework for tight-binding

By basing the discussion on the discrete symmetries of the system at hand, this method stands as an effective, intuitive and elegant way of constructing the tight-binding Hamiltonian. In this particular case, it does not yield an accurate description of the band structure across the whole BZ since it is an effective model which considers only 3 of the 11 orbitals per unit cell. However, since the valence and conduction band edges are composed exclusively of these 3 orbitals [1], it provides a low-energy theory very accurately while avoiding complications due to an increased number of orbitals. This has, thus, proved to be a good strategy to set-up a low-energy theory.

Self-energy correction

Despite the simplicity of the Hartree-Fock approximation for the self-energy, the numerical treatment of the results did not present a straight-forward problem, largely due to the divergences associated to the unscreened Coulomb potential. Furthermore, the cutoff dependence presented, itself, a challenge, since many of the results proved to be very sensitive to its variation.

Attenuating the dependence on the cutoff of these results is, probably, the primary step to improve our analysis, since it affects even the relatively simple case we managed to further into. A proposed way to do this is to make the computation self-consistent: compute the self-energy, determine the correction to the spectrum and plug the corrected spectrum back in to compute the next iteration of the self-energy, until convergence is achieved. This approach, despite

indicated for eliminating or, at least, attenuating the sensitivity towards the cutoff, requires being able to compute the full self-energy within a range of momenta, a technical difficulty which will require a solution of its own.

Either way, despite having restricted ourselves to the simplest possible problem, that of computing the gap renormalization, the results were telling: for the undoped case we found that not only the renormalized gap is sensitive to the dielectric constant of the material or of the substrate, but also that the TMDCs must have a substantial dielectric constant due to the high-energy valence and core electrons of the transition metals, unaccounted for in the low-energy model; the hole doped case has a well-defined (independent of cutoff) contribution, linear in the hole density, but still depends on the result of the undoped case.

Note that obtaining accurate estimates for the self-energy correction is not only an end in itself, but is also of great importance for improving the accuracy of the quantitative results of the Hubbard model, especially the corrections in the hole doped case.

Broken symmetry phases - Hubbard model

As noted in the text, the approximations taken to arrive at the effective Hubbard model used may have rendered much of the quantitative predictions inaccurate. However, the physics described should hold, as well as the existence of an anomalous Hall conductivity in this phase, making for an experimentally accessible test of its realization.

Despite the apparently large values for the critical parameters, there is no reason to believe that the strength of the Hubbard coupling in TMDCs does not cover these values. One must note, though, that mean-field is known to systematically underestimate critical parameters and that we have discarded the anti-Hubbard term in building the effective model used, so that the values found are most likely underestimated.

We believe it is possible to carry out a more accurate mean-field treatment of the full Hubbard model (including the anti-Hubbard term) in these systems without going beyond an analytical approach. Although, to start with, we are faced with the problem of having 3 bands coupled to 2 spin degrees of freedom, a dimensionality which most likely renders the subsequent matricial manipulations intractable, the fact is that the valence band, at its edge, is composed solely of orbitals d_{xy} and $d_{x^2-y^2}$, thus effectively reducing the dimensionality of the problem. This, along with other reasonable approximations, is expected to make the problem analytically tractable while yielding more accurate results and physics.

It might as well be worthwhile to go beyond the parabolic approximation, even within the low doping regime. Although the quantitative corrections are expected to not be significative, it might be interesting to look at the physics yielded by a 4th order term, namely, regarding the existence of meta-stable solutions. Of course, all analytical results are to be corroborated with results from numerical simulations of the system.

Bibliography

- [1] Gui-Bin Liu, Wen-Yu Shan, Yugui Yao, Wang Yao, and Di Xiao. Three-band tight-binding model for monolayers of group-vib transition metal dichalcogenides. *Phys. Rev. B*, 88:085433, Aug 2013. (document), 2, 2.1.1, 2.1, 2.1.2, 2.3, 3.1.1, 3.1.4, 6
- [2] K. S. Novoselov, D. Jiang, F. Schedin, T. J. Booth, V. V. Khotkevich, S. V. Morozov, and A. K. Geim. Two-dimensional atomic crystals. *Proceedings of the National Academy of Sciences of the United States of America*, 102(30):10451–10453, 07 2005. (document), 1.1, 1.1, 1.3
- [3] Di Xiao, Gui-Bin Liu, Wanxiang Feng, Xiaodong Xu, and Wang Yao. Coupled spin and valley physics in monolayers of mos_2 and other group-vi dichalcogenides. *Phys. Rev. Lett.*, 108:196802, May 2012. (document), 1.1, 1.3, 1.3, 1.2, 1.3, 1.3, 1.3, 1.4, 3.2.2
- [4] L. D. Landau. Zur theorie der phasenumwandlungen ii. *Phys. Z. Sowjetunion*, (11):26–35, 1937. 1.1
- [5] R. E. Peierls. Quelques proprietes typiques des corps solides. *Ann. I. H. Poincare*, (5):177–222, 1935. 1.1
- [6] N. D. Mermin and H. Wagner. Absence of ferromagnetism or antiferromagnetism in one- or two-dimensional isotropic heisenberg models. *Phys. Rev. Lett.*, 17:1133–1136, Nov 1966. 1.1
- [7] N. D. Mermin. Crystalline order in two dimensions. *Phys. Rev.*, 176:250–254, Dec 1968. 1.1
- [8] N Goldenfeld. *Lectures on phase transitions and the renormalization group*. Addison-Wesley, Advanced Book Program, Reading, Mass., 1992. 1.1
- [9] A. K. Geim and K. S. Novoselov. The rise of graphene. *Nat Mater*, 6(3):183–191, 03 2007. 1.1
- [10] J A Venables, G D T Spiller, and M Hanbucken. Nucleation and growth of thin films. *Reports on Progress in Physics*, 47(4):399, 1984. 1.1, 1.3

- [11] J. W. Evans, P. A. Thiel, and M. C. Bartelt. Morphological evolution during epitaxial thin film growth: Formation of 2d islands and 3d mounds. *Surface Science Reports*, 61(1–2):1–128, 4 2006. 1.1, 1.3
- [12] K. S. Novoselov, A. K. Geim, S. V. Morozov, D. Jiang, Y. Zhang, S. V. Dubonos, I. V. Grigorieva, and A. A. Firsov. Electric field effect in atomically thin carbon films. *Science*, 306(5696):666–669, 10 2004. 1.1
- [13] Andrey K. Geim and Allan H. MacDonald. Graphene: Exploring Carbon Flatland. *Physics Today*, 60, 2007. 1.1
- [14] M. S. Dresselhaus and G. Dresselhaus. Intercalation compounds of graphite. *Adv. Phys.*, (51):1–186, 2002. 1.1
- [15] T. A. Land, T. Michely, R. J. Behm, J. C. Hemminger, and G. Comsa. Stm investigation of single layer graphite structures produced on pt(111) by hydrocarbon decomposition. *Surf. Sci.*, (264):261–270, 1992. 1.1
- [16] A. et al. Nagashima. Electronic states of monolayer graphite formed on tic(111) surface. *Surf. Sci.*, (291):93–98, 1993. 1.1
- [17] A. J. van Bommel, J. E. Crombeen, and A. van Tooren. Leed and auger electron observations of the sic(0001) surface. *Surf. Sci.*, (48):463–472, 1975. 1.1
- [18] I. Forbeaux, J.-M. Thelin, and J. M. Debever. Heteroepitaxial graphite on 6h-sic(0001): Interface formation through conduction-band electronic structure. *Phys. Rev. B*, (58):16396–16406, 1998.
- [19] C. et al. Berger. Ultrathin epitaxial graphite: 2d electron gas properties and a route toward graphene-based nanoelectronics. *J. Phys. Chem. B*, (108):19912–19916, 2004. 1.1
- [20] A. H. Castro Neto, F. Guinea, N. M. R. Peres, K. S. Novoselov, and A. K. Geim. The electronic properties of graphene. *Rev. Mod. Phys.*, 81:109–162, Jan 2009. 1.1, 1.2, 1.2
- [21] Graphene is not alone. *Nat Nano*, 7(11):683–683, 11 2012. 1.1, 1.3, 1.3
- [22] Rafael Roldán, Jose A. Silva-Guillén, M. Pilar López-Sancho, Francisco Guinea, Emmanuel Cappelluti, and Pablo Ordejón. Electronic properties of single-layer and multi-layer transition metal dichalcogenides MX₂ (M = Mo, W and X = S, Se). *Annalen der Physik*, 526(9-10):347–357, 2014. 1.3, 1.3, 1.3, 1.3b, 1.3, 1.3, 1.3, 4.2.1
- [23] Deep Jariwala, Vinod K. Sangwan, Lincoln J. Lauhon, Tobin J. Marks, and Mark C. Hersam. Emerging device applications for semiconducting two-dimensional transition metal dichalcogenides. *ACS Nano*, 8(2):1102–1120, 2014. PMID: 24476095.

- [24] H. Ochoa and R. Roldán. Spin-orbit-mediated spin relaxation in monolayer mos₂. *Phys. Rev. B*, 87:245421, Jun 2013.
- [25] Kin Fai Mak, Changgu Lee, James Hone, Jie Shan, and Tony F. Heinz. Atomically thin MoS₂: A new direct-gap semiconductor. *Phys. Rev. Lett.*, 105:136805, Sep 2010. 1.3, 1.3
- [26] B. Radisavljevic, A. Radenovic, J. Brivio, V. Giacometti, and A. Kis. Single-layer MoS₂ transistors. *Nat Nano*, 6(3):147–150, 03 2011. 1.3
- [27] Qing Hua Wang, Kourosh Kalantar-Zadeh, Andras Kis, Jonathan N. Coleman, and Michael S. Strano. Electronics and optoelectronics of two-dimensional transition metal dichalcogenides. *Nat Nano*, 7(11):699–712, 11 2012. 1.2, 1.3, 1.3
- [28] M. A. Cazalilla, H. Ochoa, and F. Guinea. Quantum spin hall effect in two-dimensional crystals of transition-metal dichalcogenides. *Phys. Rev. Lett.*, 113:077201, Aug 2014. 1.1, 1.3, 1.3
- [29] D. C. Elias, R. V. Gorbachev, A. S. Mayorov, S. V. Morozov, A. A. Zhukov, P. Blake, L. A. Ponomarenko, I. V. Grigorieva, K. S. Novoselov, F. Guinea, and A. K. Geim. Dirac cones reshaped by interaction effects in suspended graphene. *Nat Phys*, 7(9):701–704, 09 2011. 1.2
- [30] Yuanbo Zhang, Tsung-Ta Tang, Caglar Girit, Zhao Hao, Michael C. Martin, Alex Zettl, Michael F. Crommie, Y. Ron Shen, and Feng Wang. Direct observation of a widely tunable bandgap in bilayer graphene. *Nature*, 459(7248):820–823, 06 2009. 1.2
- [31] Song-Lin Li, Hisao Miyazaki, Hidefumi Hiura, Chuan Liu, and Kazuhito Tsukagoshi. Enhanced logic performance with semiconducting bilayer graphene channels. *ACS Nano*, 5(1):500–506, 2015/01/19 2010. 1.2
- [32] Eduardo V. Castro, K. S. Novoselov, S. V. Morozov, N. M. R. Peres, J. M. B. Lopes dos Santos, Johan Nilsson, F. Guinea, A. K. Geim, and A. H. Castro Neto. Biased bilayer graphene: Semiconductor with a gap tunable by the electric field effect. *Phys. Rev. Lett.*, 99:216802, Nov 2007. 1.2
- [33] Ming-Wei Lin, Cheng Ling, Yiyang Zhang, Hyeun Joong Yoon, Mark Ming-Cheng Cheng, Luis A Agapito, Nicholas Kioussis, Noppi Widjaja, and Zhixian Zhou. Room-temperature high on/off ratio in suspended graphene nanoribbon field-effect transistors. *Nanotechnology*, 22(26):265201, 2011. 1.2
- [34] Xiaolin Li, Xinran Wang, Li Zhang, Sangwon Lee, and Hongjie Dai. Chemically derived, ultrasmooth graphene nanoribbon semiconductors. *Science*, 319(5867):1229–1232, 2008.

- [35] Melinda Y. Han, Barbaros Özyilmaz, Yuanbo Zhang, and Philip Kim. Energy band-gap engineering of graphene nanoribbons. *Phys. Rev. Lett.*, 98:206805, May 2007. 1.2
- [36] Richard Balog, Bjarke Jorgensen, Louis Nilsson, Mie Andersen, Emile Rienks, Marco Bianchi, Mattia Fanetti, Erik Laegsgaard, Alessandro Baraldi, Silvano Lizzit, Zeljko Sljivancanin, Flemming Besenbacher, Bjork Hammer, Thomas G. Pedersen, Philip Hofmann, and Liv Hornekaer. Bandgap opening in graphene induced by patterned hydrogen adsorption. *Nat Mater*, 9(4):315–319, 04 2010. 1.2
- [37] N. M. R. Peres, F. Guinea, and A. H. Castro Neto. Coulomb interactions and ferromagnetism in pure and doped graphene. *Phys. Rev. B*, 72:174406, Nov 2005. 1.2
- [38] J. González, F. Guinea, and M. A. H. Vozmediano. Marginal-fermi-liquid behavior from two-dimensional coulomb interaction. *Phys. Rev. B*, 59:R2474–R2477, Jan 1999. 1.2
- [39] Eduardo V. Castro, N. M. R. Peres, T. Stauber, and N. A. P. Silva. Low-density ferromagnetism in biased bilayer graphene. *Phys. Rev. Lett.*, 100:186803, May 2008. 1.2
- [40] M. M. Ugeda, I. Brihuega, F. Guinea, and J. M. Gómez-Rodríguez. Missing atom as a source of carbon magnetism. *Phys. Rev. Lett.*, 104:096804, Mar 2010. 1.2
- [41] Vitor M Pereira, F Guinea, JMB Lopes Dos Santos, NMR Peres, and AH Castro Neto. Disorder induced localized states in graphene. *Physical review letters*, 96(3):036801, 2006. 1.2
- [42] R. R. Nair, M. Sepioni, I-Ling Tsai, O. Lehtinen, J. Keinonen, A. V. Krasheninnikov, T. Thomson, A. K. Geim, and I. V. Grigorieva. Spin-half paramagnetism in graphene induced by point defects. *Nat Phys*, 8(3):199–202, 03 2012. 1.2
- [43] Oleg V. Yazyev. Magnetism in disordered graphene and irradiated graphite. *Phys. Rev. Lett.*, 101:037203, Jul 2008. 1.2
- [44] Rahul Nandkishore, L. S. Levitov, and A. V. Chubukov. Chiral superconductivity from repulsive interactions in doped graphene. *Nat Phys*, 8(2):158–163, 02 2012. 1.2
- [45] Dmitri K. Efetov and Philip Kim. Controlling electron-phonon interactions in graphene at ultrahigh carrier densities. *Phys. Rev. Lett.*, 105:256805, Dec 2010. 1.2
- [46] B. Andrei Bernevig, Taylor L. Hughes, and Shou-Cheng Zhang. Quantum spin hall effect and topological phase transition in hgte quantum wells. *Science*, 314(5806):1757–1761, 12 2006. 1.2
- [47] Y. L. Chen, J. G. Analytis, J. H. Chu, Z. K. Liu, S. K. Mo, X. L. Qi, H. J. Zhang, D. H. Lu, X. Dai, Z. Fang, S. C. Zhang, I. R. Fisher, Z. Hussain, and Z. X. Shen. Experimental realization of a three-dimensional topological insulator, bi₂te₃. *Science*, 325(5937):178–181, 07 2009.

- [48] D. Hsieh, D. Qian, L. Wray, Y. Xia, Y. S. Hor, R. J. Cava, and M. Z. Hasan. A topological dirac insulator in a quantum spin hall phase. *Nature*, 452(7190):970–974, 04 2008.
- [49] Liang Fu, C. L. Kane, and E. J. Mele. Topological insulators in three dimensions. *Phys. Rev. Lett.*, 98:106803, Mar 2007.
- [50] Y Xia, Dong Qian, David Hsieh, L Wray, A Pal, Hsin Lin, Arun Bansil, DHYS Grauer, YS Hor, RJ Cava, et al. Observation of a large-gap topological-insulator class with a single dirac cone on the surface. *Nature Physics*, 5(6):398–402, 2009. 1.2
- [51] Xiao-Liang Qi and Shou-Cheng Zhang. Topological insulators and superconductors. *Rev. Mod. Phys.*, 83:1057–1110, Oct 2011. 1.2, 1.3, 1.3
- [52] M. Z. Hasan and C. L. Kane. Colloquium : Topological insulators. *Rev. Mod. Phys.*, 82:3045–3067, Nov 2010. 1.2
- [53] C. L. Kane and E. J. Mele. Quantum spin hall effect in graphene. *Phys. Rev. Lett.*, 95:226801, Nov 2005. 1.2
- [54] Hongki Min, JE Hill, Nikolas A Sinitsyn, BR Sahu, Leonard Kleinman, and Allan H MacDonald. Intrinsic and rashba spin-orbit interactions in graphene sheets. *Physical Review B*, 74(16):165310, 2006. 1.2
- [55] Yugui Yao, Fei Ye, Xiao-Liang Qi, Shou-Cheng Zhang, and Zhong Fang. Spin-orbit gap of graphene: First-principles calculations. *Physical Review B*, 75(4):041401, 2007. 1.2
- [56] J. A. Wilson and A. D. Yoffe. The transition metal dichalcogenides discussion and interpretation of the observed optical, electrical and structural properties. *Advances in Physics*, 18(73):193–335, 2015/01/08 1969. 1.3
- [57] A D Yoffe. Layer compounds. *Annual Review of Materials Science*, 3(1):147–170, 2015/01/08 1973.
- [58] L. F. Mattheiss. Band structures of transition-metal-dichalcogenide layer compounds. *Phys. Rev. B*, 8:3719–3740, Oct 1973.
- [59] A. D. Yoffe. Low-dimensional systems: quantum size effects and electronic properties of semiconductor microcrystallites (zero-dimensional systems) and some quasi-two-dimensional systems. *Advances in Physics*, 42(2):173–262, 2015/01/08 1993. 1.3
- [60] E. Cappelluti, R. Roldán, J. A. Silva-Guillén, P. Ordejón, and F. Guinea. Tight-binding model and direct-gap/indirect-gap transition in single-layer and multilayer mos₂. *Phys. Rev. B*, 88:075409, Aug 2013. 1.3, 1.3
- [61] Z. Y. Zhu, Y. C. Cheng, and U. Schwingenschlögl. Giant spin-orbit-induced spin splitting in two-dimensional transition-metal dichalcogenide semiconductors. *Phys. Rev. B*, 84:153402, Oct 2011. 1.3

- [62] Jonathan N. Coleman, Mustafa Lotya, Arlene O'Neill, Shane D. Bergin, Paul J. King, Umar Khan, Karen Young, Alexandre Gaucher, Sukanta De, Ronan J. Smith, Igor V. Shvets, Sunil K. Arora, George Stanton, Hye-Young Kim, Kangho Lee, Gyu Tae Kim, Georg S. Duesberg, Toby Hallam, John J. Boland, Jing Jing Wang, John F. Donegan, Jaime C. Grunlan, Gregory Moriarty, Aleksey Shmeliov, Rebecca J. Nicholls, James M. Perkins, Eleanor M. Grieveson, Koenraad Theuwissen, David W. McComb, Peter D. Nellist, and Valeria Nicolosi. Two-dimensional nanosheets produced by liquid exfoliation of layered materials. *Science*, 331(6017):568–571, 02 2011. 1.3
- [63] Ronan J. Smith, Paul J. King, Mustafa Lotya, Christian Wirtz, Umar Khan, Sukanta De, Arlene O'Neill, Georg S. Duesberg, Jaime C. Grunlan, Gregory Moriarty, Jun Chen, Jiazhao Wang, Andrew I. Minett, Valeria Nicolosi, and Jonathan N. Coleman. Large-scale exfoliation of inorganic layered compounds in aqueous surfactant solutions. *Advanced Materials*, 23(34):3944–3948, 2011.
- [64] Kai-Ge Zhou, Nan-Nan Mao, Hang-Xing Wang, Yong Peng, and Hao-Li Zhang. A mixed-solvent strategy for efficient exfoliation of inorganic graphene analogues. *Angewandte Chemie International Edition*, 50(46):10839–10842, 2011.
- [65] Peter May, Umar Khan, J. Marguerite Hughes, and Jonathan N. Coleman. Role of solubility parameters in understanding the steric stabilization of exfoliated two-dimensional nanosheets by adsorbed polymers. *The Journal of Physical Chemistry C*, 116(20):11393–11400, 2015/01/10 2012. 1.3
- [66] Rabin Bissessur, Joy Heising, and Wakgari Hirpo. Toward pillared layered metal sulfides. intercalation of the chalcogenide clusters $\text{Co}_6\text{q}_8(\text{pr}_3)_6$ ($\text{q} = \text{s}, \text{se}$, and te and $\text{r} = \text{alkyl}$) into MoS_2 . *Chemistry of Materials*, 8(2):318–320, 2015/01/10 1996. 1.3
- [67] Per Joensen, R. F. Frindt, and S. Roy Morrison. Single-layer MoS_2 . *Materials Research Bulletin*, 21(4):457–461, 4 1986.
- [68] Minoru Osada and Takayoshi Sasaki. Exfoliated oxide nanosheets: new solution to nanoelectronics. *Journal of Materials Chemistry*, 19(17):2503–2511, 2009.
- [69] Goki Eda, Hisato Yamaguchi, Damien Voiry, Takeshi Fujita, Mingwei Chen, and Manish Chhowalla. Photoluminescence from chemically exfoliated MoS_2 . *Nano Letters*, 11(12):5111–5116, 2015/01/10 2011.
- [70] Zhiyuan Zeng, Zongyou Yin, Xiao Huang, Hai Li, Qiyuan He, Gang Lu, Freddy Boey, and Hua Zhang. Single-layer semiconducting nanosheets: High-yield preparation and device fabrication. *Angewandte Chemie International Edition*, 50(47):11093–11097, 2011. 1.3
- [71] Yi-Hsien Lee, Xin-Quan Zhang, Wenjing Zhang, Mu-Tung Chang, Cheng-Te Lin, Kai-Di Chang, Ya-Chu Yu, Jacob Tse-Wei Wang, Chia-Seng Chang, Lain-Jong Li, and Tsung-

- Wu Lin. Synthesis of large-area mos₂ atomic layers with chemical vapor deposition. *Advanced Materials*, 24(17):2320–2325, 2012. 1.3
- [72] Yongjie Zhan, Zheng Liu, Sina Najmaei, Pulickel M. Ajayan, and Jun Lou. Large-area vapor-phase growth and characterization of mos₂ atomic layers on a sio₂ substrate. *Small*, 8(7):966–971, 2012.
- [73] Keng-Ku Liu, Wenjing Zhang, Yi-Hsien Lee, Yu-Chuan Lin, Mu-Tung Chang, Ching-Yuan Su, Chia-Seng Chang, Hai Li, Yumeng Shi, Hua Zhang, Chao-Sung Lai, and Lain-Jong Li. Growth of large-area and highly crystalline mos₂ thin layers on insulating substrates. *Nano Letters*, 12(3):1538–1544, 2015/01/10 2012.
- [74] Jing-Kai Huang, Jiang Pu, Chang-Lung Hsu, Ming-Hui Chiu, Zhen-Yu Juang, Yung-Huang Chang, Wen-Hao Chang, Yoshihiro Iwasa, Taishi Takenobu, and Lain-Jong Li. Large-area synthesis of highly crystalline wse₂ monolayers and device applications. *ACS nano*, 8(1):923–930, 2013. 1.3
- [75] Yiya Peng, Zhaoyu Meng, Chang Zhong, Jun Lu, Weichao Yu, Zhiping Yang, and Yitai Qian. Hydrothermal synthesis of mos₂ and its pressure-related crystallization. *Journal of Solid State Chemistry*, 159(1):170–173, 2001. 1.3
- [76] A. K. Geim and I. V. Grigorieva. Van der waals heterostructures. *Nature*, 499(7459):419–425, 07 2013. 1.3
- [77] J. T. Ye, Y. J. Zhang, R. Akashi, M. S. Bahramy, R. Arita, and Y. Iwasa. Superconducting dome in a gate-tuned band insulator. *Science*, 338(6111):1193–1196, 11 2012. 1.3, 1.3a
- [78] Kouji Taniguchi, Akiyo Matsumoto, Hidekazu Shimotani, and Hidenori Takagi. Electric-field-induced superconductivity at 9.4k in a layered transition metal disulphide mos₂. *App. Phys. Lett.*, 101:042603, 2012. 1.3
- [79] R. Roldán, E. Cappelluti, and F. Guinea. Interactions and superconductivity in heavily doped mos₂. *Phys. Rev. B*, 88:054515, Aug 2013. 1.3
- [80] Noah FQ Yuan, Kin Fai Mak, and KT Law. Possible topological superconducting phases of mos₂. *arXiv preprint arXiv:1405.3519*, 2014. 1.3
- [81] S. Mathew, K. Gopinadhan, T. K. Chan, X. J. Yu, D. Zhan, L. Cao, A. Rusydi, M. B. H. Breese, S. Dhar, Z. X. Shen, T. Venkatesan, and John T. L. Thong. Magnetism in mos₂ induced by proton irradiation. *Applied Physics Letters*, 101(10):–, 2012. 1.3
- [82] Sang Wook Han, Young Hun Hwang, Seon-Ho Kim, Won Seok Yun, J. D. Lee, Min Gyu Park, Sunmin Ryu, Ju Sang Park, Dae-Hwang Yoo, Sang-Pil Yoon, Soon Cheol Hong, Kwang S. Kim, and Young S. Park. Controlling ferromagnetic easy axis in a layered mos₂ single crystal. *Phys. Rev. Lett.*, 110:247201, Jun 2013. 1.3

- [83] Hannu-Pekka Komsa, Jani Kotakoski, Simon Kurasch, Ossi Lehtinen, Ute Kaiser, and Arkady V. Krasheninnikov. Two-dimensional transition metal dichalcogenides under electron irradiation: Defect production and doping. *Phys. Rev. Lett.*, 109:035503, Jul 2012. 1.3
- [84] Andres Castellanos-Gomez, Rafael Roldán, Emmanuele Cappelluti, Michele Buscema, Francisco Guinea, Herre S. J. van der Zant, and Gary A. Steele. Local strain engineering in atomically thin mos₂. *Nano Letters*, 13(11):5361–5366, 2015/01/09 2013. 1.3
- [85] Shengjun Yuan, Rafael Roldán, M. I. Katsnelson, and Francisco Guinea. Effect of point defects on the optical and transport properties of mos₂ and ws₂. *Phys. Rev. B*, 90:041402, Jul 2014. 1.3
- [86] Tianxing Ma, Feiming Hu, Zhongbing Huang, and Hai-Qing Lin. Controllability of ferromagnetism in graphene. *Applied Physics Letters*, 97(11):112504, 2010. 1.3
- [87] Andres Castellanos-Gomez, Menno Poot, Gary A. Steele, Herre S. J. van der Zant, Nicolás Agraït, and Gabino Rubio-Bollinger. Elastic properties of freely suspended mos₂ nanosheets. *Advanced Materials*, 24(6):772–775, 2012. 1.3
- [88] F. Guinea, M. I. Katsnelson, and A. K. Geim. Energy gaps and a zero-field quantum hall effect in graphene by strain engineering. *Nat Phys*, 6(1):30–33, 01 2010. 1.3
- [89] N. Levy, S. A. Burke, K. L. Meaker, M. Panlasigui, A. Zettl, F. Guinea, A. H. Castro Neto, and M. F. Crommie. Strain-induced pseudo-magnetic fields greater than 300 tesla in graphene nanobubbles. *Science*, 329(5991):544–547, 07 2010. 1.3
- [90] M. A. H. Vozmediano, M. I. Katsnelson, and F. Guinea. Gauge fields in graphene. *Physics Reports*, 496(4–5):109–148, 11 2010. 1.3
- [91] A. Rycerz, J. Tworzydlo, and C. W. J. Beenakker. Valley filter and valley valve in graphene. *Nat Phys*, 3(3):172–175, 03 2007. 1.3
- [92] Di Xiao, Wang Yao, and Qian Niu. Valley-contrasting physics in graphene: Magnetic moment and topological transport. *Phys. Rev. Lett.*, 99:236809, Dec 2007. 1.3
- [93] Wang Yao, Di Xiao, and Qian Niu. Valley-dependent optoelectronics from inversion symmetry breaking. *Phys. Rev. B*, 77:235406, Jun 2008. 1.3, 3.2.2
- [94] Fan Zhang, Jeil Jung, Gregory A. Fiete, Qian Niu, and Allan H. MacDonald. Spontaneous quantum hall states in chirally stacked few-layer graphene systems. *Phys. Rev. Lett.*, 106:156801, Apr 2011. 1.3
- [95] S. Gwo and C. K. Shih. Site-selective imaging in scanning tunneling microscopy of graphite: The nature of site asymmetry. *Phys. Rev. B*, 47:13059–13062, May 1993. 1.3

- [96] Hualing Zeng, Junfeng Dai, Wang Yao, Di Xiao, and Xiaodong Cui. Valley polarization in mos₂ monolayers by optical pumping. *Nat Nano*, 7(8):490–493, 08 2012. 1.3
- [97] K. F. Mak, K. L. McGill, J. Park, and P. L. McEuen. The valley hall effect in mos₂ transistors. *arXiv:1403.5039.*, 2014. 1.3, 3.2.2
- [98] Kin Fai Mak, Keliang He, Jie Shan, and Tony F. Heinz. Control of valley polarization in monolayer mos₂ by optical helicity. *Nat Nano*, 7(8):494–498, 08 2012. 1.3
- [99] H. Ochoa, F. Guinea, and V. I. Fal'ko. Spin memory and spin-lattice relaxation in two-dimensional hexagonal crystals. *Phys. Rev. B*, 88:195417, Nov 2013. 1.3
- [100] Aaron M Jones, Hongyi Yu, Nirmal J Ghimire, Sanfeng Wu, Grant Aivazian, Jason S Ross, Bo Zhao, Jiaqiang Yan, David G Mandrus, Di Xiao, et al. Optical generation of excitonic valley coherence in monolayer wse₂. *Nature nanotechnology*, 8(9):634–638, 2013. 1.3
- [101] Jason S Ross, Sanfeng Wu, Hongyi Yu, Nirmal J Ghimire, Aaron M Jones, Grant Aivazian, Jiaqiang Yan, David G Mandrus, Di Xiao, Wang Yao, et al. Electrical control of neutral and charged excitons in a monolayer semiconductor. *Nature communications*, 4:1474, 2013.
- [102] Kin Fai Mak, Keliang He, Changgu Lee, Gwan Hyoung Lee, James Hone, Tony F. Heinz, and Jie Shan. Tightly bound trions in monolayer mos₂. *Nat Mater*, 12(3):207–211, 03 2013. 1.3
- [103] Alexey Chernikov, Timothy C. Berkelbach, Heather M. Hill, Albert Rigosi, Yilei Li, Ozgur Burak Aslan, David R. Reichman, Mark S. Hybertsen, and Tony F. Heinz. Exciton binding energy and nonhydrogenic rydberg series in monolayer ws₂. *Phys. Rev. Lett.*, 113:076802, Aug 2014. 1.3
- [104] Tawinan Cheiwchanchamnangij and Walter R. L. Lambrecht. Quasiparticle band structure calculation of monolayer, bilayer, and bulk mos₂. *Phys. Rev. B*, 85:205302, May 2012. 1.3
- [105] Ashwin Ramasubramaniam. Large excitonic effects in monolayers of molybdenum and tungsten dichalcogenides. *Phys. Rev. B*, 86:115409, Sep 2012.
- [106] Timothy C. Berkelbach, Mark S. Hybertsen, and David R. Reichman. Microscopic theory of singlet exciton fission. iii. crystalline pentacene. *The Journal of Chemical Physics*, 141(7):–, 2014. 1.3
- [107] W. A. Harrison. *Solid State Theory*. Dover Publications, 1980. 2.1.1, 4
- [108] M. Hamermesh. *Group Theory and Its Application to Physical Problems*. Addison Wesley Series in Physics. Addison Wesley, 1962. 2.1.1
- [109] JJ Sakurai. *Modern Quantum Mechanics (Revised Edition)*. Addison Wesley, 09 1993. 2.2.1, 3.1.3, B.1.2, B.1.2

- [110] K. A. Olive and Particle Data Group. Review of particle physics. *Chinese Physics C*, 38(9):090001, 2014. 3.1.4
- [111] Di Xiao, Ming-Che Chang, and Qian Niu. Berry phase effects on electronic properties. *Rev. Mod. Phys.*, 82:1959–2007, Jul 2010. 3.2, B.1.2, B.1.2, B.2.3
- [112] H. B. Nielsen and M. Ninomiya. A no-go theorem for regularizing chiral fermions. *Physics Letters B*, 105(2–3):219–223, 10 1981. 3.2.2
- [113] Kenneth W. K. Shung. Dielectric function and plasmon structure of stage-1 intercalated graphite. *Physical Review B*, 34(2):979–993, 07 1986. 4.1.2
- [114] T. O. Wehling, E. Şaşioğlu, C. Friedrich, A. I. Lichtenstein, M. I. Katsnelson, and S. Blügel. Strength of effective coulomb interactions in graphene and graphite. *Physical Review Letters*, 106(23):236805–, 06 2011. 4.2.1, 5.2.2
- [115] G. D. Mahan. *Many-Particle Physics*. Springer, 2000. 4.2.2
- [116] Elbio Dagotto, Takashi Hotta, and Adriana Moreo. Colossal magnetoresistant materials: the key role of phase separation. *Physics Reports*, 344(1–3):1–153, 4 2001. 5.1.1
- [117] A. Altland and B. D. Simons. *Condensed Matter Field Theory*. Cambridge University Press, 2010. 5.1.2, 5.2.1, C.1, C.2.2
- [118] Pedro Girão. *Introdução à Análise Complexa, Séries de Fourier e Equações Diferenciais*. IST Press, 2014. 5.2.2, D.2
- [119] R. Roldán, E. Cappelluti, and F. Guinea. Interactions and superconductivity in heavily doped mos₂. *Physical Review B*, 88(5):054515–, 08 2013. 5.2.2
- [120] Eduardo V Castro, K S Novoselov, S V Morozov, N M R Peres, J M B Lopes dos Santos, Johan Nilsson, F Guinea, A K Geim, and A H Castro Neto. Electronic properties of a biased graphene bilayer. *Journal of Physics: Condensed Matter*, 22(17):175503, 2010. 5.2.3
- [121] M. V. Berry. Quantal phase factors accompanying adiabatic changes. *Proceedings of the Royal Society of London A: Mathematical, Physical and Engineering Sciences*, 392(1802):45–57, 03 1984. B.1.1
- [122] M. Nakahara. *Geometry, Topology and Physics, Second Edition*. Taylor & Francis, 2003. B.1.2
- [123] F. D. M. Haldane. Berry curvature on the fermi surface: Anomalous hall effect as a topological fermi-liquid property. *Phys. Rev. Lett.*, 93:206602, Nov 2004. B.2.3, B.2.3
- [124] A. L. Fetter and J. D. Walecka. *Quantum theory of many-particle systems*. McGraw-Hill, 1971. C.1, C.2.1, C.2.1, C.2.2

- [125] Eduardo Fradkin. *Field theories of condensed matter systems*. Number 82. Addison Wesley Publishing Company, 1991. C.1
- [126] Herbert Callen. *Thermodynamics and an Introduction to Thermostatistics*. Wiley, 09 1985. D.1
- [127] R. P. Feynman. *Statistical Mechanics: A Set Of Lectures*. Westview Press, 1998. D.1

Appendix A

Perturbation theory for the tight-binding Hamiltonian

Diagonalization of the K -point Hamiltonian

Firstly, diagonalize the 0th-order term in the expanded TB Hamiltonian, $H_{tb}(\mathbf{K})$. The eigenvalues will be the energy of the highest states in the HOB, the energy of the lowest states in the LUB and the energies of the highest or lowest states of the remaining bands, which are expected to be energetically distant from the HOB and the LUB. The eigenvectors will yield the basis states for the energy bands at the K point, from which a subspace shall be used to carry out the perturbative treatment of the 1st-order term. This can be written

$$H_{tb}(\mathbf{K}) |\psi^n\rangle = \varepsilon_n |\psi^n\rangle : \quad |\psi^n\rangle = \sum_{j,\mu} U_{n,j\mu} |\varphi_\mu^j(\mathbf{K})\rangle , \quad |\psi^n\rangle \equiv |\psi^n(\mathbf{K})\rangle , \quad n = v, c, h .$$

where U is the transformation matrix, necessarily unitary, from the original basis to the eigenbasis. Thus, the 0th-order term is, in its eigenbasis,

$$H_0 \equiv U H_{tb}(\mathbf{K}) U^\dagger = \begin{pmatrix} \varepsilon_c & 0 & 0 \\ 0 & \varepsilon_v & 0 \\ 0 & 0 & \varepsilon_h \end{pmatrix} .$$

Now we can write the perturbation in the basis of the band states at the K -point. Hence, the total Hamiltonian at the K -point in the basis of the band states is

$$H_{\mathbf{K}}(\mathbf{q}) = U H_{tb}(\mathbf{K} + \mathbf{q}) U^\dagger = H_0 + \sum_{m=1}^n \Sigma^{(m)}(\mathbf{q}) + \mathcal{O}(aq)^{n+1} , \quad \Sigma^{(m)}(\mathbf{q}) \equiv U [H^{(m)}(\mathbf{q})] U^\dagger .$$

Subspace Projectors

We wish to obtain an effective Hamiltonian for the $v - c$, or low-energy, subspace. However, the perturbation Σ may be general, in the sense that we cannot expect it to be block-diagonal relatively to the low-energy subspace. Indeed, we must expect that the perturbation will mix states of the subspace with other states. However, we should expect also that this only happens for high enough energies, that is, when the energy of the perturbations is enough to cause transitions to states with energies that deviate substantially from the energy scale of the states in the subspace.

This argument sets the ground to carry out a perturbation theory analysis. To that end, define the projectors P_1 , to the subspace of the valence and conduction bands, and P_2 , the subspace of the remaining bands, such that

$$\begin{aligned} P_1 &= P_v + P_c = |\psi^v\rangle\langle\psi^v| + |\psi^c\rangle\langle\psi^c|, \\ P_2 &= \sum_h P_h = \sum_h |\psi^h\rangle\langle\psi^h|. \end{aligned}$$

Consider $|\varphi\rangle$ an eigenstate of the full Hamiltonian $H_{\mathbf{K}}$

$$H_{\mathbf{K}}|\varphi\rangle = E|\varphi\rangle,$$

which can be rewritten as

$$(E - H_0)|\varphi\rangle = \Sigma|\varphi\rangle, \quad \Sigma \equiv \sum_{k=1}^n \Sigma^{(k)}(\mathbf{q}). \quad (\text{A.1})$$

Applying the projectors P_1 and P_h to the left of Eq. (A.1), noting that they project onto subspaces of the eigenbasis of H_0 , and making use of the projective property $P_i P_j = P_i \delta_{ij}$, we arrive at the coefficient of $|\varphi\rangle$ on each subspace

$$P_1|\varphi\rangle = (E - P_1 H_0 P_1)^{-1} P_1 \Sigma|\varphi\rangle = \left(\frac{P_v}{E - \varepsilon_v} + \frac{P_c}{E - \varepsilon_c} \right) \Sigma|\varphi\rangle, \quad (\text{A.2})$$

$$P_h|\varphi\rangle = \frac{P_h \Sigma}{E - \varepsilon_h} |\varphi\rangle \Rightarrow P_2|\varphi\rangle = \sum_h \frac{P_h \Sigma}{E - \varepsilon_h} |\varphi\rangle. \quad (\text{A.3})$$

Thus, considering energies such that $E \sim \varepsilon_v, \varepsilon_c$ and provided that the energy of the perturbation obeys $E - \varepsilon_v, E - \varepsilon_c \ll E - \varepsilon_h$, the denominator of Eq. (A.2) will be much smaller than that of Eq. (A.3) and it must hold that

$$|\langle\varphi|P_1|\varphi\rangle| \gg |\langle\varphi|P_2|\varphi\rangle|. \quad (\text{A.4})$$

This result allows Eq. (A.2) to be expanded in a perturbation series. Note, however, that this argument may not apply to a basis of arbitrary dimension, since the sum involved in P_2 may

render the associated coefficient non-negligible relatively to the coefficient associated to P_1 .

Perturbation Series

In order to develop the perturbation series, a decomposition of identity $\hat{1} = P_1 + P_2$ is introduced in Eq. (A.2), so that

$$\begin{aligned} P_1 |\varphi\rangle &= (E - P_1 H_0 P_1)^{-1} P_1 \Sigma(P_1 + P_2) |\varphi\rangle \\ &\stackrel{(A.4)}{=} (E - P_1 H_0 P_1)^{-1} P_1 \Sigma P_1 |\varphi\rangle + \mathcal{O}(P_2), \\ (E - P_1 H_0 P_1) P_1 |\varphi\rangle &= P_1 \Sigma P_1 P_1 |\varphi\rangle \\ E P_1 |\varphi\rangle &= (P_1 H_0 P_1 + P_1 \Sigma P_1) P_1 |\varphi\rangle, \end{aligned}$$

which implies that, to 1st-order, the effective Hamiltonian in $v - c$ subspace is

$$H_{\text{eff}}^{(1)} = P_1 H_0 P_1 + P_1 \Sigma P_1. \quad (\text{A.5})$$

The effective Hamiltonian to 1st-order was obtained by expanding $P_1 |\varphi\rangle$ to 0th-order in the coefficient of P_2 . In turn, by introducing a decomposition of identity in Eq. (A.3) we find

$$\begin{aligned} P_2 |\varphi\rangle &= \sum_h \frac{P_h \Sigma}{\varepsilon_{c,v} - \varepsilon_h} (P_1 + P_2) |\varphi\rangle \\ &= \sum_h \frac{P_h \Sigma P_1}{\varepsilon_{c,v} - \varepsilon_h} |\varphi\rangle + \mathcal{O}(P_2^2), \end{aligned}$$

where E was written as the symbol $\varepsilon_{c,v}$ since we are considering energies $E \sim \varepsilon_c, \varepsilon_v$. This result allows Eq. (A.2) to be expanded up to 1st-order in the coefficient P_2 in terms of P_1 :

$$P_1 |\varphi\rangle = (E - P_1 H_0 P_1)^{-1} P_1 \Sigma \left(P_1 + \sum_h \frac{P_h \Sigma P_1}{P_1 H_0 P_1 - \varepsilon_h} \right) P_1 |\varphi\rangle + \mathcal{O}(P_2^2).$$

This result implies that the effective Hamiltonian up to 2nd-order is

$$H_{\text{eff}}^{(2)} = P_1 H_0 P_1 + P_1 \Sigma P_1 - \sum_h \frac{P_1 \Sigma P_h \Sigma P_1}{\varepsilon_h - P_1 H_0 P_1}, \quad (\text{A.6})$$

where the symbol $\varepsilon_{c,v}$ has been substituted with $P_1 H_0 P_1$, the operator H_0 projected on the P_1 subspace. It is worthwhile noticing that taking the expectation value of Eq. (A.6) on the states of the $v - c$ subspace yields indeed the usual spectrum obtained from time-independent perturbation theory:

$$E_n^{(2)}=\left\langle \varphi_n\right|H_{eff}^{(2)}\left|\varphi_n\right\rangle =\varepsilon_n+\left\langle \varphi_n\right|\Sigma\left|\varphi_n\right\rangle -\sum_{h\neq n}\frac{\left|\left\langle \varphi_h\right|\Sigma\left|\varphi_n\right\rangle \right|^2}{\varepsilon_h-\varepsilon_n},\qquad n=v,c.$$

Appendix B

Quantum adiabatic theorem and Berry curvature

B.1 Adiabatic time evolution of a quantum system

Consider a Hamiltonian depending on time through a set of parameters $\{P^\mu(t)\}$ and its instantaneous, non-degenerate eigenbasis, which read

$$H(\mathbf{P}) |\tilde{n}(\mathbf{P})\rangle = \varepsilon_n(\mathbf{P}) |\tilde{n}(\mathbf{P})\rangle, \quad \mathbf{P} \equiv \mathbf{P}(t). \quad (\text{B.1})$$

Note, however that this equation does not uniquely determine the basis, since it allows the functions to be multiplied by a \mathbf{Q} -dependent phase factor, i.e. to make a gauge choice. Moreover, a quantum system initially in an eigenstate $|n(\mathbf{P}(0))\rangle$ will remain as an instantaneous eigenstate of the Hamiltonian $H(\mathbf{P})$ under adiabatic evolution. Here, adiabatic is understood as in the thermodynamic definition: that the system evolves slowly enough so that the system can adapt to the new configuration at each instant. This amounts to saying that the rate of change of the system parameters $\mathbf{P}(t)$ is negligible, $\dot{\mathbf{P}} \rightarrow 0$. This is the content of the quantum adiabatic theorem, which is proven next.

B.1.1 Quantum adiabatic theorem

Suppose that the state $|\psi(t)\rangle$ obeys the Schrödinger with the \mathbf{P} -dependent Hamiltonian of Eq. (B.1)

$$i\hbar \partial_t |\psi(t)\rangle = H(\mathbf{P}(t)) |\psi(t)\rangle.$$

Expanding in the instantaneous eigenbasis of the Hamiltonian

$$|\psi(t)\rangle = \sum_n \exp\left(-\frac{i}{\hbar} \int_0^t dt' \varepsilon_n(t')\right) a_n(t) |\tilde{n}(t)\rangle, \quad |\tilde{n}(t)\rangle \equiv |\tilde{n}(\mathbf{P}(t))\rangle \text{ and } \varepsilon_n(t) \equiv \varepsilon_n(\mathbf{P}(t)),$$

and inserting in the Schrödinger equation finds, for the coefficients $a_n(t)$,

$$\dot{a}_n(t) = - \sum_m a_m(t) \langle \tilde{n}(t) | \partial_t | \tilde{m}(t) \rangle \exp\left\{-\frac{i}{\hbar} \int_0^t dt' [\varepsilon_m(t') - \varepsilon_n(t')]\right\}. \quad (\text{B.2})$$

Now, writing $\partial_t = \partial_t Q^\mu \partial_\mu$, $\mu = 1, 2, \dots, \dim(\mathbf{P})$, since the states depend on time through the parameters \mathbf{P} , we introduce the adiabatic approximation, which is equivalent to stating that $Q_{,t}^\mu \rightarrow 0$. To 0-th order, Eq. (B.2) reads

$$\dot{a}_n(t) = \mathcal{O}(Q_{,t}^\mu) \Rightarrow \dot{a}_n^{(0)}(t) = 0. \quad (\text{B.3})$$

Then, if at time $t = 0$ the state of the quantum system is the n th instantaneous eigenstate, which is to say $a_n(0) = 1$, then it will remain in that state throughout the time evolution of the system, which is to say $a_n^{(0)}(t) = 1$ in virtue of Eq. (B.3). For the argument that follows next, it is not necessary to go further than the 0th order approximation. Nevertheless, the 1st order approximation has important consequences and shall be explored later on.

Gauge freedom

We now return to the point made earlier on that, indeed, the eigenstates $|\tilde{n}(t)\rangle$ are defined up to a \mathbf{P} -dependent phase factor. More succinctly, each of them has an associated gauge freedom. Considering thus the result of the 0-th order adiabatic approximation, the following ansatz is introduced

$$|\psi_0(t)\rangle_n - \mathcal{O}(Q_{,t}) \equiv |n(\mathbf{P}(t)), t\rangle = \exp\left(-\frac{i}{\hbar} \int_0^t dt' \varepsilon_n(t')\right) e^{i\gamma_n(t)} |n(\mathbf{P}(t))\rangle. \quad (\text{B.4})$$

Inserting it in the Schrödinger equation

$$\begin{aligned} i\hbar \partial_t |n(\mathbf{P}(t)), t\rangle &= H(\mathbf{P}(t)) |n(\mathbf{P}(t)), t\rangle \\ \Rightarrow [\varepsilon_n(\mathbf{P}(t)) - \hbar \dot{\gamma}_n(t)] |n(\mathbf{P}(t))\rangle + i\hbar \partial_t |n(\mathbf{P}(t))\rangle &= \varepsilon_n(\mathbf{P}(t)) |n(\mathbf{P}(t))\rangle, \end{aligned}$$

and left-multiplying by $\langle n(\mathbf{P}(t))|$ yields

$$[\varepsilon_n(\mathbf{P}(t)) - \hbar \dot{\gamma}_n(t)] + i\hbar \langle n(\mathbf{P}(t)) | \partial_t | n(\mathbf{P}(t)) \rangle = \varepsilon_n(\mathbf{P}(t)) \Rightarrow \gamma_n(t) = i \int_0^t ds \langle n(\mathbf{P}(s)) | \partial_s | n(\mathbf{P}(s)) \rangle.$$

Finally, writing $\partial_s = \partial_s P^\mu \partial_\mu$ as before, the above integral becomes

$$\gamma_n[\Gamma] = \int_{\Gamma} dP^\mu \mathcal{A}_\mu^n, \quad (\text{B.5})$$

where Γ is the path in parameter-space traced out by the system going from $\mathbf{P}(0)$ to $\mathbf{P}(t)$ and the integrand is the Berry connection (or vector potential)

$$\boxed{\mathcal{A}_\mu^n(\mathbf{P}) = i \langle n(\mathbf{P}) | \partial_\mu | n(\mathbf{P}) \rangle}. \quad (\text{B.6})$$

Thus, the quantity of Eq. (B.5) appears as an additional phase in the adiabatic evolution of a quantum system. Despite this fact, since the rise of quantum mechanics and until the work by Berry [121], this phase had been disregarded in the study of quantum dynamics, since its elimination amounts to a gauge transformation. Indeed, $\mathcal{A}_\mu^n(\mathbf{P})$ is gauge-dependent, so that

$$|n(\mathbf{P})\rangle \rightarrow e^{i\zeta(\mathbf{P})} |n(\mathbf{P})\rangle \quad \text{and} \quad \mathcal{A}_\mu^n(\mathbf{P}) \rightarrow \mathcal{A}_\mu^n(\mathbf{P}) - \partial_\mu \zeta(\mathbf{P}),$$

where $\zeta(\mathbf{P})$ is an arbitrary smooth function. Thus, an appropriate choice of the gauge function can eliminate $\gamma_n(t)$, leaving only the dynamic phase, rendering it unobservable.

B.1.2 Berry phase and Berry curvature

However, if the path considered is cyclical, so that $\mathbf{P}(0) = \mathbf{P}(t)$, γ_n becomes gauge-invariant and, therefore, observable. Note that, in this case, the time-dependence is no longer essential. It is the path traced out by the parameters, rather than their time dependence, that determines this quantity. Hence, it can be written

$$\boxed{\gamma_n[\Gamma] = \oint_{\Gamma} dP^\mu \mathcal{A}_\mu^n = \int_{\Sigma} dP^\mu dP^\nu \Omega_{\mu\nu}^n}, \quad (\text{B.7})$$

where the second equality results from Stokes' Theorem. This quantity is known as Berry (or geometric) phase. Here, Σ is a surface in parameter-space such that $\Gamma = \partial\Sigma$ and $\Omega_{\mu\nu}^n$ is the Berry curvature tensor, which is a gauge-invariant field or, put more succinctly, a gauge-field, reading

$$\boxed{\Omega_{\mu\nu}^n = \partial_\mu \mathcal{A}_\nu^n - \partial_\nu \mathcal{A}_\mu^n}. \quad (\text{B.8})$$

This expression can be recast in a vector form, using a Levi-Civita symbol

$$\Omega_{\mu\nu}^n = \varepsilon_{\mu\nu\alpha} \Omega^{n\alpha} \Leftrightarrow \Omega^{n\alpha} = \frac{1}{3} \varepsilon^{\mu\nu\alpha} \partial_\mu \mathcal{A}_\nu^n. \quad (\text{B.9})$$

The Berry phase γ_n has the remarkable property that it may be proportional to an integer, i.e. quantized. This happens when parameter-space is periodic in all coordinates and the surface Σ is the whole parameter-space.

This result relies crucially on the fact that, although states along $\partial\Sigma$ are identified, in virtue of periodicity, they can differ by a phase. Thus, there is a Berry phase accumulation when tracing a path over $\partial\Sigma$, but this is not the phase of Eq. (B.5): this gauge dependent contribution vanishes, in virtue of periodicity. However, since the path is closed, the final state the path arrives at is the initial state. Since the phase must then be equal to unity, this imposes a condition on the Berry phase:

$$\boxed{\gamma_n = 2\pi c_n, \quad c_n \in \mathbb{Z}}, \quad (\text{B.10})$$

where c_n is known as the first Chern number of the n -th band. Note that we made no reference to the specificity of the physical system when arguing this result. Indeed, the only condition is the periodicity of the parameter space and, thus, of the Hamiltonian. This is, therefore, a characteristic of the topological structure of the mapping between the parameter-space spanned by $\{P^\mu\}$ and the states $|n(\mathbf{P})\rangle$ [111]. An intuitive but more detailed discussion of this result can be found in Ref. [111]. A more rigorous but accessible discussion can be found in Ref. [122].

Note that the Berry curvature, unlike the Berry phase, does not require the system to evolve along a closed loop in parameter-space in order to be a well-defined, observable quantity: it is an intrinsically local quantity, defined at each point in parameter-space. In this sense, the curvature is a more fundamental quantity than the phase.

Symmetries of the Berry curvature

Some important symmetries and conservation laws of the Berry curvature can be obtained directly from its definition. To see this, note that Eq. (B.8) can be rewritten as

$$-i\Omega_{\mu\nu}^n = \partial_\mu \langle n | \partial_\nu n \rangle - \partial_\nu \langle n | \partial_\mu n \rangle = \langle \partial_\mu n | \partial_\nu n \rangle - \langle \partial_\nu n | \partial_\mu n \rangle. \quad (\text{B.11})$$

Taking the first equality, one can introduce a decomposition of identity such that

$$\sum_{m \neq n} |m\rangle\langle m| = \hat{1} - |n\rangle\langle n|, \quad (\text{B.12})$$

and using the identity for the matrix element of the parameter-differentiated Hamiltonian

$$\langle n | \partial_\mu \hat{H} | m \rangle = \delta_{nm} \partial_\mu \varepsilon_n + (\varepsilon_n - \varepsilon_m) \langle \partial_\mu n | m \rangle, \quad (\text{B.13})$$

one obtains the following useful expression for the Berry curvature

$$\Omega_{\mu\nu}^n = i \sum_{m \neq n} \frac{\langle n | \partial_\mu \hat{H} | m \rangle \langle m | \partial_\nu \hat{H} | n \rangle - \langle n | \partial_\nu \hat{H} | m \rangle \langle m | \partial_\mu \hat{H} | n \rangle}{(\varepsilon_n - \varepsilon_m)^2}. \quad (\text{B.14})$$

A conservation law becomes apparent from this expression. Rearranging terms and summing over n results in an identically vanishing quantity:

$$\sum_n \Omega_{\mu\nu}^n \equiv 0. \quad (\text{B.15})$$

This is the local conservation law of the Berry curvature [111].

Consider now the spatial-inversion (parity) and time-reversal operators, denoted by $\hat{\mathcal{P}}$ and $\hat{\mathcal{T}}$, respectively, and a system in which the parameters \mathbf{P} transform, under both $\hat{\mathcal{P}}$ and $\hat{\mathcal{T}}$, as

$$\hat{O}\mathbf{P}\hat{O}^\dagger = -\mathbf{P}, \quad \hat{O} = \hat{\mathcal{P}}, \hat{\mathcal{T}}. \quad (\text{B.16})$$

In order to determine the behaviour of the Berry curvature under these operations, we are going to use the elementary theorem that, if the Hamiltonian is invariant under a transformation, then the transformed eigenstates are also eigenstates of the Hamiltonian. As a corollary, if the energy spectrum is non-degenerate - as is the case we are considering - a symmetry operation maps an eigenstate into itself:

$$\hat{O}|n\rangle = |n\rangle. \quad (\text{B.17})$$

There is a subtle point regarding the time-reversal operator that must be taken account of, which is that it is anti-unitary: for states $|m'\rangle$ and $|n'\rangle$ obtained through time-reversal of the states $|m\rangle$ and $|n\rangle$, respectively, one has [109]

$$\langle m' | n' \rangle = \langle m | \hat{\mathcal{T}}^\dagger \hat{\mathcal{T}} | n \rangle = \langle m | n \rangle^* = \langle n | m \rangle. \quad (\text{B.18})$$

We are now in a position to determine what we have set out to. We first consider a system with time-reversal symmetry. Thus, using the expression of Eq. (B.11), we find

$$\begin{aligned} -i\Omega_{\mu\nu}^n(\mathbf{P}) &= \langle \partial_\mu n | \partial_\nu n \rangle - \langle \partial_\nu n | \partial_\mu n \rangle \\ &= (\partial_\mu |n\rangle)^\dagger (\partial_\nu |n\rangle) - (\partial_\nu |n\rangle)^\dagger (\partial_\mu |n\rangle) \\ &\stackrel{(\text{B.17})}{=} \left(\partial_\mu \hat{\mathcal{T}} |n\rangle \right)^\dagger \left(\partial_\nu \hat{\mathcal{T}} |n\rangle \right) - \left(\partial_\nu \hat{\mathcal{T}} |n\rangle \right)^\dagger \left(\partial_\mu \hat{\mathcal{T}} |n\rangle \right) \\ &\stackrel{(\text{B.16})}{=} (-1)^2 \left(\hat{\mathcal{T}} \partial_\mu |n\rangle \right)^\dagger \left(\hat{\mathcal{T}} \partial_\nu |n\rangle \right) - (-1)^2 \left(\hat{\mathcal{T}} \partial_\nu |n\rangle \right)^\dagger \left(\hat{\mathcal{T}} \partial_\mu |n\rangle \right) \\ &= (\partial_\mu |n\rangle)^\dagger \hat{\mathcal{T}}^\dagger \hat{\mathcal{T}} (\partial_\nu |n\rangle) - (\partial_\nu |n\rangle)^\dagger \hat{\mathcal{T}}^\dagger \hat{\mathcal{T}} (\partial_\mu |n\rangle) \\ &\stackrel{(\text{B.18})}{=} \langle \partial_\nu n | \partial_\mu n \rangle - \langle \partial_\mu n | \partial_\nu n \rangle \\ &= i\Omega_{\mu\nu}^n(-\mathbf{P}) \\ &\Leftrightarrow \Omega_{\mu\nu}^n(\mathbf{P}) \stackrel{\mathcal{T}}{=} -\Omega_{\mu\nu}^n(-\mathbf{P}). \end{aligned}$$

For a system with spatial-inversion symmetry the proof follows similarly except for the sixth

equality, since $\hat{\mathcal{P}}$ is simply a unitary operator [109]. Therefore, we have

$$\Omega_{\mu\nu}^n(\mathbf{P}) \stackrel{\mathcal{P}}{=} \Omega_{\mu\nu}^n(-\mathbf{P}).$$

Far-reaching conclusions can be obtained from these results. First, a system with both spatial-inversion and time-reversal symmetry has an identically vanishing Berry curvature:

$$\Omega_{\mu\nu}^n(\mathbf{P}) \stackrel{\mathcal{T}}{=} -\Omega_{\mu\nu}^n(-\mathbf{P}) \stackrel{\mathcal{P}}{=} -\Omega_{\mu\nu}^n(\mathbf{P}) \equiv 0. \quad (\text{B.19})$$

Second, a system can only have a non-vanishing Chern number if the system breaks time-reversal symmetry without breaking spatial-inversion symmetry:

$$\begin{aligned} \gamma_n[\partial\Sigma] &= \int_{\Sigma} dP^\mu dP^\nu \Omega_{\mu\nu}^n(\mathbf{P}) \\ &= (-1)^2 \int_{\Sigma} dP^\mu dP^\nu \Omega_{\mu\nu}^n(-\mathbf{P}) \\ &\stackrel{\mathcal{T}}{=} - \int_{\Sigma} dP^\mu dP^\nu \Omega_{\mu\nu}^n(\mathbf{P}) \\ &= -\gamma_n[\partial\Sigma] \\ &\equiv 0. \end{aligned} \quad (\text{B.20})$$

Moreover, although it may appear that the Berry curvature is merely an intermediate result in the computation of the Berry phase, that is only the case in a picture as the one used to derive Eq. (B.7), in which parameters evolve passively with time. Once the parameters are taken as dynamical variables, however, the Berry curvature reveals direct effects. In order to explore the deeper consequences of the Berry curvature in the dynamics of Bloch electrons, we must consider the perturbative effect of the remaining eigenstates on the evolution of the unperturbed eigenstate n . This amounts to taking the adiabatic approximation up to 1st order in $P_{,t}^\mu$.

B.1.3 1st order adiabatic approximation

Recovering the adiabatic argument, we now expand the time-evolved quantum state $|\psi(t)\rangle$ in terms of the eigenstates $|n(\mathbf{P}(t))\rangle$, so that it can be written

$$|\psi(t)\rangle = \sum_n a_n(t) |n(\mathbf{P}(t)), t\rangle. \quad (\text{B.21})$$

The equivalent to Eq. (B.2) under this gauge choice reads

$$\partial_t \left(e^{i\gamma_n(t)} a_n(t) \right) = - \sum_m e^{i\gamma_m(t)} a_m(t) \langle n(t) | \partial_t |m(t)\rangle \exp \left\{ -\frac{i}{\hbar} \int_0^t dt' [\varepsilon_m(t') - \varepsilon_n(t')] \right\}. \quad (\text{B.22})$$

Recovering the result of Eq. (B.3) to 0-th order, we have $a_n^{(0)}(t) = 1$ and $a_m^{(0)}(t) = 0$, $m \neq n$, yielding

$$\dot{a}_n^{(1)}(t) = -i\dot{\gamma}_n(t) - \langle n(t) | \partial_t | n(t) \rangle = 0 \Rightarrow a_n^{(1)}(t) = 1,$$

$$\partial_t \left(e^{i\gamma_m(t)} a_m^{(1)}(t) \right) = -e^{i\gamma_n(t)} \langle m(t) | \partial_t | n(t) \rangle \exp \left\{ -\frac{i}{\hbar} \int_0^t dt' [\varepsilon_n(t') - \varepsilon_m(t')] \right\}, \quad m \neq n,$$

where, in the first line, Eq. (B.5) was used along with the relation $\partial_t = \partial_t P^\mu \partial_\mu$. Integrating by parts the second line up to 1-st order in $Q_{,t}^\mu$, we arrive at

$$a_m^{(1)}(t) = -i\hbar \frac{\langle m(t) | \partial_t | n(t) \rangle}{\varepsilon_n(t) - \varepsilon_m(t)} \exp i \left\{ \gamma_n(t) - \gamma_m(t) - \frac{1}{\hbar} \int_0^t dt' [\varepsilon_n(t') - \varepsilon_m(t')] \right\} + \mathcal{O}(P_{,t}^2), \quad (\text{B.23})$$

and inserting in the state of Eq. (B.21), we arrive at the time-evolved state of the quantum system up to 1-st order in the adiabatic approximation:

$$|\psi_1(t)\rangle_n = \sum_j a_j^{(1)}(t) |j(\mathbf{P}(t)), t\rangle + \mathcal{O}(P_{,t}^2)$$

$$= e^{i\gamma_n(t)} \exp \left(-\frac{i}{\hbar} \int_0^t dt' \varepsilon_n(t') \right) \left(|n(t)\rangle - i\hbar \sum_{m \neq n} \frac{\langle m(t) | \partial_t | n(t) \rangle}{\varepsilon_n(t) - \varepsilon_m(t)} |m(t)\rangle \right) + \mathcal{O}(P_{,t}^2). \quad (\text{B.24})$$

This result is valid for any set of non-degenerate instantaneous eigenstates which depend on time through a set of parameters P^μ . The index n of the ket of the total state denotes that the initial state is n and, thus, its dominant component.

From now on, focus shall be given to a particular parameter-space: the Brillouin Zone.

B.2 Bloch bands and Hall effects

B.2.1 Brillouin zone as a parameter space

Consider non-interacting electrons in a Bloch band. The single-electron Hamiltonian in configuration-space reads

$$H = \frac{\hat{\mathbf{p}}^2}{2m} + V(\mathbf{r}), \quad (\text{B.25})$$

where $V(\mathbf{r} + \mathbf{R}) = V(\mathbf{r})$ is the lattice potential and \mathbf{R} is a lattice vector. The periodicity of the potential induces a periodic boundary condition on electron states and endows them with a crystal momentum $\hbar\mathbf{q}$, belonging in the Brillouin Zone. This is simply Bloch's theorem:

$$\langle \mathbf{r} + \mathbf{R} | n'(\mathbf{q}) \rangle = e^{i\mathbf{q} \cdot \mathbf{R}} \langle \mathbf{r} | n'(\mathbf{q}) \rangle.$$

Since \mathbf{q} is a good quantum number, the Brillouin Zone constitutes an appropriate parameter-space on which to employ the formalism of the Berry curvature. However, we must first transform H so that it becomes \mathbf{q} -dependent and, additionally, make sure that the eigenstates after the transformation are contained in the Hilbert space of the Bloch bands within the Brillouin Zone. This is achieved with the following transformation:

$$H(\mathbf{q}) = e^{-i\mathbf{q}\cdot\mathbf{r}} H e^{i\mathbf{q}\cdot\mathbf{r}} = \frac{(\hat{\mathbf{p}} + \hbar\mathbf{q})^2}{2m} + V(\mathbf{r}),$$

$$\langle \mathbf{r} | n(\mathbf{q}) \rangle = e^{-i\mathbf{q}\cdot\mathbf{r}} \langle \mathbf{r} | n'(\mathbf{q}) \rangle \Rightarrow \langle \mathbf{r} + \mathbf{R} | n(\mathbf{q}) \rangle = \langle \mathbf{r} | n(\mathbf{q}) \rangle.$$

The transformed eigenstates are simply the cell-periodic part of the original Bloch states. The strict boundary condition of the second line ensures that all eigenstates are within the same Hilbert space. Therefore, it is possible to take the Brillouin Zone as the parameter-space of the Hamiltonian $H(\mathbf{q})$ with eigenbasis $\{|n(\mathbf{q})\rangle\}$.

B.2.2 Velocity under adiabatic evolution

Consider now a Hamiltonian with separate dependence on \mathbf{q} and on time through other set of parameters $\mathbf{P}(t)$. The (\mathbf{q}, t) -dependent velocity operator is given by

$$\hat{v}_\mu(\mathbf{q}, t) = e^{-i\mathbf{q}\cdot\hat{\mathbf{r}}} \hat{r}_{\mu,t} e^{i\mathbf{q}\cdot\hat{\mathbf{r}}} = -\frac{i}{\hbar} e^{-i\mathbf{q}\cdot\hat{\mathbf{r}}} [\hat{r}_\mu, \hat{H}(t)] e^{i\mathbf{q}\cdot\hat{\mathbf{r}}} = \frac{1}{\hbar} [\hat{H}(\mathbf{q}, t), \hat{r}_\mu] = \frac{\partial \hat{H}(\mathbf{q}, t)}{\hbar \partial q^\mu},$$

from which we obtain the diagonal matrix element of the velocity operator in the adiabatically evolved state of Eq. (B.24):

$$\begin{aligned} v_\mu^n(\mathbf{q}, t) &= \langle \psi_1(t) | \hat{v}_\mu(\mathbf{q}, t) | \psi_1(t) \rangle_{nn} \\ &= \frac{\langle n | \partial_\mu \hat{H} | n \rangle}{\hbar} - \sum_{m \neq n} \frac{i}{\varepsilon_n - \varepsilon_m} \left[\langle n | \partial_\mu \hat{H} | m \rangle \langle m | \partial_t n \rangle - \langle \partial_t n | m \rangle \langle m | \partial_\mu \hat{H} | n \rangle \right] + \mathcal{O}(P_{,t}^2) \\ &= \frac{\partial \varepsilon_n(\mathbf{q}, t)}{\hbar \partial q^\mu} - i [\langle \partial_\mu n | \partial_t n \rangle - \langle \partial_t n | \partial_\mu n \rangle] + \mathcal{O}(P_{,t}^2), \end{aligned} \tag{B.26}$$

where, in the third equality, the identities of Eqs. (B.13) and (B.12) were used. Finally, dropping higher-order terms and identifying the second term in the third equality with the Berry curvature, through Eq. (B.11), Eq. (B.26) reads

$$v_\mu^n(\mathbf{q}, t) = \frac{\partial \varepsilon_n(\mathbf{q}, t)}{\hbar \partial q^\mu} - \Omega_{\mu t}^n. \tag{B.27}$$

This result provides some insight into the physical meaning of the Berry curvature: electrons in the n -th Bloch band will suffer a perturbation due to empty states in the remaining Bloch bands, to which electrons in the n -th band can transition induced by the adiabatic variation of the external parameters. It is this residual overlap of the time-evolved n -th band state with empty

states in other bands that makes the anomalous term emerge. This anomalous term is identified with the Berry curvature which, in turn, is identified with a curvature of the parameter-space: the Brillouin Zone compounded with the external time-dependent parameter-space.

It is possible to further write Eq. (B.27), by making explicit the dependence on the external parameters $\mathbf{P}(t)$, which reads

$$v_\mu^n(\mathbf{q}, t) = \frac{\partial \varepsilon_n(\mathbf{q}, t)}{\hbar \partial q^\mu} - P_{,t}^a \Omega_{\mu a}^n \stackrel{(B.9)}{=} \frac{\partial \varepsilon_n(\mathbf{q}, t)}{\hbar \partial q^\mu} - \varepsilon_{\mu a \beta} P_{,t}^a \Omega^{n \beta}, \quad (B.28)$$

where the index of the $\mathbf{P}(t)$ was chosen to be latin as a reminder that the corresponding derivative within the Berry curvature is relatively to \mathbf{P} and not to \mathbf{q} . Further insight is obtained by noticing that

$$\frac{\delta v_\mu^n(\mathbf{q})}{\delta P_{,t}^a} = -\Omega_{\mu a}^n. \quad (B.29)$$

As shall be found later on, the Berry curvature tensor represents a linear response of Bloch electrons to the variation of the time derivative of the external parameters.

B.2.3 Bloch electrons in an electric field

In order to study the effect of an uniform electric field \mathbf{E} in the system of Bloch bands, consider a time-dependent, spatially uniform vector-potential $\mathbf{A}(t)$ entering in the Hamiltonian of Eq. (B.25) through the minimal-coupling prescription of the momentum, $\hat{\mathbf{p}} \rightarrow \hat{\mathbf{p}} - e\mathbf{A}(t)$. After the transformation into the Brillouin Zone, the new (\mathbf{q}, t) -dependent Hamiltonian reads

$$H(\mathbf{q}, t) = \frac{1}{2m} \left[\hat{\mathbf{p}} + \hbar \left(\mathbf{q} - \frac{e}{\hbar} \mathbf{A}(t) \right) \right]^2 + V(\mathbf{r}) = H \left(\mathbf{q} - \frac{e}{\hbar} \mathbf{A}(t) \right). \quad (B.30)$$

We can apply Eq. (B.28) to study the electron transport induced by such an electric field. We find

$$v_\mu^n(\mathbf{q}, \mathbf{A}) = \bar{v}_\mu^n + E^a \Omega_{\mu a}^n(\mathbf{q}, \mathbf{A}), \quad \Omega_{\mu a}^n(\mathbf{q}, \mathbf{A}) = i \left[\left\langle \frac{\partial n}{\partial q^\mu} \middle| \frac{\partial n}{\partial A^a} \right\rangle - \left\langle \frac{\partial n}{\partial A^a} \middle| \frac{\partial n}{\partial q^\mu} \right\rangle \right], \quad (B.31)$$

where \bar{v}_μ^n is just the Hamiltonian contribution. The parameter-dependence of this expression can be simplified by noticing that it is possible to define a gauge-invariant momentum, which is simply the total mechanical momentum of the system,

$$\mathbf{k} = \mathbf{q} - \frac{e}{\hbar} \mathbf{A}(t) \Rightarrow d\mathbf{k} = d\mathbf{q} - \frac{e}{\hbar} d\mathbf{A} \Rightarrow \begin{cases} \frac{\partial}{\partial q^\mu} &= \frac{\partial}{\partial k^\mu} \\ \frac{\partial}{\partial A^a} &= -\frac{e}{\hbar} \frac{\partial}{\partial k^a} \end{cases}.$$

From this, Eq. (B.31) can be rewritten as

$$v_\mu^n(\mathbf{k}) = \frac{\partial \varepsilon_n(\mathbf{k})}{\hbar \partial k^\mu} - \frac{e}{\hbar} E^\nu \Omega_{\mu\nu}^n(\mathbf{k}), \quad (\text{B.32})$$

where the latin index was dropped as both derivatives are relative to the crystal momentum \mathbf{k} .

Quantum anomalous Hall effect

Assuming now that the system is an insulator, i.e. that the Fermi level is in the gap and the BZ is completely occupied, it is possible to define a total current density due to electrons in the valence band by

$$j_\mu^v = -\frac{e}{N \mathcal{A}_{uc}} \sum_{\mathbf{k}} v_\mu^v(\mathbf{k}), \quad (\text{B.33})$$

where N is the number of unit cells in the system and \mathcal{A}_{uc} the area of the unit cell. Replacing the sum with an integration over the entire BZ,

$$\sum_{\mathbf{k}} \rightarrow \frac{N}{\mathcal{A}_{BZ}} \int_{BZ} d^d k, \quad (\text{B.34})$$

where \mathcal{A}_{BZ} is the d -volume of the Brillouin Zone. Note that $\mathcal{A}_{BZ} \mathcal{A}_{uc} = (2\pi)^d$. Then, the first term in Eq. (B.32) vanishes under integration in virtue of the symmetry of the BZ, being left with

$$j_\mu^v = E^\nu \frac{e^2}{\hbar} \int_{BZ} \frac{d^d k}{(2\pi)^d} \Omega_{\mu\nu}^v,$$

which, taking after Eq. (B.29), implies that the total conductivity of the material is given by

$$\sigma_{\mu\nu}^v = \frac{e^2}{\hbar} \int_{BZ} \frac{d^d k}{(2\pi)^d} \Omega_{\mu\nu}^v. \quad (\text{B.35})$$

This is the Hall conductivity associated to the quantum anomalous Hall effect. Important conclusion can be drawn from this result. First, although the system is an insulator, there will be a finite response if the system breaks time-reversal symmetry. Second, the Berry curvature tensor is anti-symmetric, thus the conductivity has vanishing longitudinal components. Third, it vanishes identically for dimensions greater than 2, hence the restriction of Eq. (B.35) to $d = 2$. Fourth, according to Eqs. (B.7) and (B.10), it can be written as:

$$\sigma_{\mu\nu}^v = \varepsilon_{\mu\nu} \sigma_{AH} = \varepsilon_{\mu\nu} \frac{e^2}{h} \frac{\gamma_v}{2\pi} = \varepsilon_{\mu\nu} \frac{e^2 c_v}{h}, \quad (\text{B.36})$$

where c_v is the Chern number of the valence band and σ_{AH} is the coefficient of this anomalous Hall conductivity. Most importantly, since the integration is performed over the entire BZ, the

Chern number is an integer and this Hall conductivity is quantized in units of e^2/h , hence quantum anomalous Hall conductivity. This final result is equivalent to stating that the most general and fundamental condition for the existence of a quantum Hall effect is the non-vanishing of the Chern number of a band.

Anomalous Hall effect

In case the system is a metal or a doped insulator, so that the Fermi level lies within a partially filled band, it is necessary to account for the distribution of states. The summation of Eq. (B.33) includes only occupied states which, after the substitution of Eq. (B.34), translates into the inclusion of the Fermi-Dirac distribution in the integrand. Therefore, the anomalous contribution to the Hall conductivity reads

$$\sigma_{\mu\nu}^n = \frac{e^2}{\hbar} \int_{BZ} \frac{d^d k}{(2\pi)^d} n_F(\varepsilon_n(\mathbf{k}) - \mu) \Omega_{\mu\nu}^n, \quad (\text{B.37})$$

where n_F is the Fermi-Dirac distribution. Note that this quantity is no longer quantized. It may also appear that this result has to take into account the physics in the bulk of the BZ, contrary to the principles of the Fermi-liquid theory [111]. However, this conclusion can be shown to be untrue and that, indeed, this integral depends only on the Fermi surface.

The proof of this is considerably simpler in 2D than in 3D. A general proof in 3D can be found in Ref. [123]. Fortunately, it is the former that we are interested in. Particularizing thus to $d = 2$ and integrating by parts, Eq. (B.37) yields

$$\begin{aligned} \sigma_{\mu\nu}^n &= \frac{e^2}{\hbar} \int_{BZ} \frac{d^2 k}{(2\pi)^2} (\mathcal{A}_\mu^n \partial_\nu n_F - A_\nu^n \partial_\mu n_F) \\ &= -\frac{e^2}{\hbar} \int_{BZ} \frac{d^2 k}{(2\pi)^2} \delta(\mu - \varepsilon_n(\mathbf{k})) (\mathcal{A}_\mu^n \partial_\nu \varepsilon_n - A_\nu^n \partial_\mu \varepsilon_n), \end{aligned} \quad (\text{B.38})$$

where we made use of the fact that, for physically relevant temperatures, the Fermi-Dirac distribution reduces, within good approximation, to the Heaviside function as $n_F(\varepsilon_n(\mathbf{k}) - \mu) = \theta(\mu - \varepsilon_n(\mathbf{k}))$, where μ is the Fermi level. Eq. (B.38) means the conductivity depends only on some quantity integrated on the level surface of the dispersion at the Fermi level or, put more succinctly, on the Fermi surface. Indeed, it can be shown that Eq. (B.38) yields [123]

$$\sigma_{\mu\nu}^n = \varepsilon_{\mu\nu} \frac{e^2}{2\pi\hbar} \oint_{FS} dk^\alpha \mathcal{A}_\alpha^n.$$

(B.39)

This result shows that, at least in 2D, the anomalous Hall conductivity is a Fermi surface property, consisting essentially of the Berry phase accumulated along the Fermi level of the dispersion of the n -th band. Note that, since the region of integration does not cover the entire BZ, this conductivity is not quantized.

Appendix C

Perturbation theory for the electron propagator, self-energy correction

C.1 Path Integral approach to Statistical Quantum Mechanics

The central problem of equilibrium quantum statistical mechanics is computing the partition function \mathcal{Z} of the grand-canonical ensemble, given by

$$\mathcal{Z} = e^{-\beta F} = \text{Tr} e^{-\beta \hat{K}} = \sum_{\{n_i\}} \langle \dots n_i \dots | e^{-\beta \hat{K}} | \dots n_i \dots \rangle , \quad (\text{C.1})$$

where $\hat{K} = \hat{H} - \mu \hat{N}$, the summation is over every possible configuration and the states are the total number states given by the tensor product of occupation number states of every state accessible to the system. The free energy F is defined thermodynamically as [124]

$$dF = -SdT - PdV - Nd\mu , \quad (\text{C.2})$$

where S is entropy, T temperature, P pressure, V volume, N is the expected value of the total particle number and μ is the chemical potential. Clearly, the approach using occupation number states renders the problem intractable for the general many-body problem, which leads us to introduce coherent states. In turn, the use of coherent states lends itself naturally to the construction of the path integral, allowing the grand-partition function to be rewritten as

$$\mathcal{Z} = \int \prod_i \mathcal{D}(\bar{\psi}_i, \psi_i) e^{-\frac{1}{\hbar} S[\bar{\psi}, \psi]} , \quad (\text{C.3})$$

where i stands symbolically for any set quantum number of the system and S is the action in imaginary time, a functional of fermionic or bosonic fields, which reads

$$S[\bar{\psi}, \psi] = \int_0^{\beta\hbar} d\tau \left[\sum_i \bar{\psi}_i(\tau) \hbar \partial_\tau \psi_i(\tau) + K(\bar{\psi}, \psi) \right], \quad (\text{C.4})$$

with $K(\bar{\psi}, \psi)$ the normal ordered matrix element of \hat{K} in the holomorphic representation of coherent states:

$$K(\bar{\psi}, \psi) = \frac{\langle \psi | \hat{K}(\hat{a}^\dagger, \hat{a}) | \psi \rangle}{\langle \psi | \mathbb{1} | \psi \rangle}. \quad (\text{C.5})$$

Eqs. (C.4) and (C.5) thus provide a prescription to go from the grand-canonical Hamiltonian to the action in imaginary time.

Additionally, the construction of the path integral implies that the bosonic or fermionic states have a periodicity or anti-periodicity, respectively, of $\beta\hbar$ in imaginary time. It is thus natural to introduce a Fourier transform of these states which complies with the (anti-)periodicity of the fields,

$$\begin{aligned} \psi_i(\tau) &= \frac{1}{\sqrt{\beta\hbar}} \sum_n e^{-i\omega_n \tau} \psi_{in}, & \omega_n &= \begin{cases} \frac{2\pi}{\beta\hbar} n & \text{Bosonic} \\ \frac{2\pi}{\beta\hbar} (n + \frac{1}{2}) & \text{Fermionic} \end{cases}, \\ \psi_{in} &= \frac{1}{\sqrt{\beta\hbar}} \int_0^{\beta\hbar} d\tau e^{i\omega_n \tau} \psi_i(\tau), \end{aligned} \quad (\text{C.6})$$

where the ω_n are known as Matsubara frequencies. Comprehensive derivations and discussions of the construction of the path integral can be found in references such as [117] and [125].

C.1.1 Grand-partition function of a non-interacting theory

Consider a second-quantized Hamiltonian describing a fermionic or bosonic free or, interchangeably, non-interacting theory written in its eigenbasis

$$\hat{H} = \hat{H}_0 + \sum_\alpha (\bar{\eta}_\alpha \hat{a}_\alpha + \hat{a}_\alpha^\dagger \eta_\alpha), \quad \hat{H}_0 = \sum_\alpha \varepsilon_\alpha \hat{a}_\alpha^\dagger \hat{a}_\alpha,$$

where α is any set of quantum numbers which identifies each state and where the sources $\bar{\eta}_\alpha$ and η_α have been introduced in order to ease future computations. Using Eqs. (C.5) and (C.4), we arrive at the action in imaginary time of this Hamiltonian

$$S[\bar{\psi}, \psi] = \int_0^{\beta\hbar} d\tau \sum_\alpha [\bar{\psi}_\alpha(\tau) (\hbar \partial_\tau + \varepsilon_\alpha - \mu) \psi_\alpha(\tau) + \bar{\eta}_\alpha(\tau) \psi_\alpha(\tau) + \bar{\psi}_\alpha(\tau) \eta_\alpha(\tau)].$$

Taking the Fourier transform of the fields, the action becomes

$$S[\bar{\psi}, \psi] = \sum_\alpha \sum_n [\bar{\psi}_{\alpha n} (-i\hbar\omega_n + \varepsilon_\alpha - \mu) \psi_{\alpha n} + \bar{\eta}_{\alpha n} \psi_{\alpha n} + \bar{\psi}_{\alpha n} \eta_{\alpha n}],$$

and it is easy to see that this coordinate transformation induces a Jacobian such that

$$\mathcal{D}(\bar{\psi}_\alpha, \psi_\alpha) = \prod_n (\beta\hbar)^{-\nu} d(\bar{\psi}_{\alpha n}, \psi_{\alpha n}).$$

Thus, the field integral in Eq. (C.3) becomes

$$\begin{aligned} \mathcal{Z}(\bar{\eta}, \eta) &= \int \prod_\alpha \prod_n (\beta\hbar)^{-\nu} d(\bar{\psi}_{\alpha n}, \psi_{\alpha n}) \exp \left\{ -\frac{1}{\hbar} \sum_\alpha \sum_n [\bar{\psi}_{\alpha n} (-i\hbar\omega_n + \varepsilon_\alpha - \mu) \psi_{\alpha n} + \bar{\eta}_{\alpha n} \psi_{\alpha n} + \bar{\psi}_{\alpha n} \eta_{\alpha n}] \right\} \\ &= \prod_\alpha \prod_n (\beta\hbar)^{-\nu} \int d(\bar{\psi}_{\alpha n}, \psi_{\alpha n}) \exp \left\{ -\frac{1}{\hbar} [\bar{\psi}_{\alpha n} (-i\hbar\omega_n + \varepsilon_\alpha - \mu) \psi_{\alpha n} + \bar{\eta}_{\alpha n} \psi_{\alpha n} + \bar{\psi}_{\alpha n} \eta_{\alpha n}] \right\} \\ &= \prod_\alpha \prod_n [\beta(-i\hbar\omega_n + \varepsilon_\alpha - \mu)]^{-\nu} \exp \left\{ -\frac{1}{\hbar} \frac{\bar{\eta}_{\alpha n} \eta_{\alpha n}}{-i\hbar\omega_n + \varepsilon_\alpha - \mu} \right\}, \end{aligned} \quad (\text{C.7})$$

where the integrations were solved directly by completing the square and performing Gaussian integrations, since the action is diagonal. Setting the sources to zero yields the grand-partition function of the free theory:

$$\mathcal{Z}_0 = \mathcal{Z}(0, 0) = \prod_\alpha \prod_n [\beta(-i\hbar\omega_n + \varepsilon_\alpha - \mu)]^{-\nu}, \quad (\text{C.8})$$

and, according to Eq. (C.1), the source-dependent free energy of the non-interacting system is given by

$$F(\bar{\eta}, \eta) = -\frac{1}{\beta} \ln \mathcal{Z}(\bar{\eta}, \eta) = \sum_{\alpha, n} \left\{ \frac{\nu}{\beta} \ln [\beta(-i\hbar\omega_n + \varepsilon_\alpha - \mu)] + \frac{1}{\beta\hbar} \frac{\bar{\eta}_{\alpha n} \eta_{\alpha n}}{-i\hbar\omega_n + \varepsilon_\alpha - \mu} \right\}. \quad (\text{C.9})$$

Clearly, for a generic basis, partition function from Eq. (C.8) would be written as

$$\mathcal{Z}_0 = \det [\beta(-i\hbar\hat{\omega} + \hat{K})]^{-\nu}, \quad (\text{C.10})$$

where $\hat{\omega} = (\omega_n \delta_{nm})_{\forall n, m}$ and the determinant is taken upon the total space of the quantum numbers and of the Matsubara frequencies.

C.1.2 Green's functions - bare propagator

The propagators are given by the imaginary time Green's functions, defined as

$$\begin{aligned} G_{\alpha\beta}(\tau, \tau') &= \langle T_\tau \hat{a}_\alpha(\tau) \hat{a}_\beta^\dagger(\tau') \rangle \\ &= \theta(\tau - \tau') \langle \hat{a}_\alpha(\tau) \hat{a}_\beta^\dagger(\tau') \rangle + \nu \theta(\tau' - \tau) \langle \hat{a}_\beta^\dagger(\tau') \hat{a}_\alpha(\tau) \rangle \end{aligned} \quad (\text{C.11})$$

where the symbol T_τ is the (imaginary-)time ordering operator and θ is the Heaviside step function defined as

$$\theta(x) = \begin{cases} 1, & x > 0 \\ 1/2, & x = 0 \\ 0, & x < 0 \end{cases}. \quad (\text{C.12})$$

The imaginary-time dependent operators are written in the Heisenberg representation

$$\hat{a}_\alpha(\tau) = \hat{\mathcal{U}}_H(0, \tau) \hat{a}_\alpha \hat{\mathcal{U}}_H(\tau, 0), \quad \hat{a}_\beta^\dagger(\tau) = \hat{\mathcal{U}}_H(0, \tau) \hat{a}_\beta^\dagger \hat{\mathcal{U}}_H(\tau, 0), \quad (\text{C.13})$$

where the imaginary time evolution operator $\hat{\mathcal{U}}(\tau, 0)$ obeys the equation of movement

$$\hbar \partial_\tau \hat{\mathcal{U}}_H(\tau, 0) = -\hat{K}(\tau) \hat{\mathcal{U}}_H(\tau, 0) \quad \text{which implies} \quad \hat{\mathcal{U}}_H(\tau, 0) = T_\tau \exp \left\{ -\frac{1}{\hbar} \int_0^\tau d\tau' \hat{K}(\tau') \right\}. \quad (\text{C.14})$$

Clearly, solutions of this equation satisfy the group property

$$\hat{\mathcal{U}}_H(\tau, \tau') \hat{\mathcal{U}}_H(\tau', 0) = \hat{\mathcal{U}}_H(\tau, 0), \quad (\text{C.15})$$

particularly, they admit an inverse

$$1 = \hat{\mathcal{U}}_H(0, 0) = \hat{\mathcal{U}}_H(0, \tau) \hat{\mathcal{U}}_H(\tau, 0) = [\hat{\mathcal{U}}_H(\tau, 0)]^{-1} \hat{\mathcal{U}}_H(\tau, 0) = \hat{\mathcal{U}}_H(0, \tau) [\hat{\mathcal{U}}_H(0, \tau)]^{-1},$$

justifying the way we wrote Eq. (C.13). As a final remark, note that, unlike in real time, $\hat{a}_\beta^\dagger(\tau) \neq [\hat{a}_\beta(\tau)]^\dagger$.

Now, we are interested in the Fourier transform of Eq. (C.11)

$$\mathcal{G}_{\alpha\beta}(i\omega_n, i\omega_m) = \frac{1}{\beta\hbar} \int_0^{\beta\hbar} d\tau \int_0^{\beta\hbar} d\tau' e^{i\omega_n \tau} G_{\alpha\beta}(\tau, \tau') e^{-i\omega_m \tau'},$$

and, particularly, in cases in which the system is homogeneous in imaginary time, meaning $G_{\alpha\beta}(\tau, \tau') \equiv G_{\alpha\beta}(\tau - \tau')$. Substituting in the equation above, and transforming variables as $\tau \rightarrow \tau - \tau'$ and $\tau' \rightarrow \tau'$, it can be written

$$\begin{aligned} \mathcal{G}_{\alpha\beta}(i\omega_n, i\omega_m) &= \int_{-\beta\hbar}^{+\beta\hbar} d(\tau - \tau') e^{i\omega_n(\tau - \tau')} G_{\alpha\beta}(\tau - \tau') \frac{1}{\beta\hbar} \int_0^{\beta\hbar} d\tau' e^{i(\omega_n - \omega_m)\tau'} \\ &= 2 \mathcal{G}_{\alpha\beta}(i\omega_n) \delta_{nm}, \end{aligned}$$

where the Fourier transform of the time-homogenous propagator was defined as

$$G_{\alpha\beta}(\tau) = \frac{1}{\beta\hbar} \sum_n e^{-i\omega_n \tau} \mathcal{G}_{\alpha\beta}(i\omega_n), \quad \mathcal{G}_{\alpha\beta}(i\omega_n) = \frac{1}{2} \int_{-\beta\hbar}^{+\beta\hbar} d\tau e^{i\omega_n \tau} G_{\alpha\beta}(\tau). \quad (\text{C.16})$$

As expected, the Fourier transform of the propagator of a time homogenous system is diagonal in frequency-space. Moreover, the propagator is time-homogeneous if the Hamiltonian is time-independent. To see this, consider Eq. (C.13) and, for instance, the first term of Eq. (C.11). We have

$$\begin{aligned}
\langle \hat{a}_\alpha(\tau) \hat{a}_\beta^\dagger(\tau') \rangle &= \text{Tr} e^{-\beta(\hat{K}-\Omega)} \hat{\mathcal{U}}_H(0, \tau) \hat{a}_\alpha \hat{\mathcal{U}}_H(\tau, 0) \hat{\mathcal{U}}_H(0, \tau') \hat{a}_\beta^\dagger \hat{\mathcal{U}}_H(\tau', 0) \\
&= \text{Tr} \hat{\mathcal{U}}_H(\tau', 0) e^{-\beta(\hat{K}-\Omega)} \hat{\mathcal{U}}_H(0, \tau) \hat{a}_\alpha \hat{\mathcal{U}}_H(\tau, 0) \hat{\mathcal{U}}_H(0, \tau') \hat{a}_\beta^\dagger \\
&= \text{Tr} e^{-\beta(\hat{K}-\Omega)} \hat{\mathcal{U}}_H(\tau', 0) \hat{\mathcal{U}}_H(0, \tau) \hat{a}_\alpha \hat{\mathcal{U}}_H(\tau, 0) \hat{\mathcal{U}}_H(0, \tau') \hat{a}_\beta^\dagger \\
&\stackrel{(C.15)}{=} \text{Tr} e^{-\beta(\hat{K}-\Omega)} \hat{\mathcal{U}}_H(\tau', \tau) \hat{a}_\alpha \hat{\mathcal{U}}_H(\tau, \tau') \hat{a}_\beta^\dagger \\
&= \langle \hat{a}_\alpha(\tau - \tau') \hat{a}_\beta^\dagger(0) \rangle.
\end{aligned}$$

Clearly, the third equality is valid if and only if the Hamiltonian \hat{K} commutes with itself at every instant, a condition that is satisfied if \hat{K} is imaginary-time independent, in which case $\hat{\mathcal{U}}_H$ has the simple form

$$\hat{\mathcal{U}}_H(\tau, 0) = e^{-\tau \hat{K}/\hbar}.$$

Now, applying the second equality of Eq. (C.16) to Eq. (C.11) in the time-homogeneous case yields

$$\begin{aligned}
2\mathcal{G}_{\alpha\beta}(i\omega_n) &= \int_0^{+\beta\hbar} d\tau e^{i\omega_n\tau} \langle \hat{a}_\alpha(\tau) \hat{a}_\beta^\dagger(0) \rangle + \nu \int_{-\beta\hbar}^0 d\tau e^{i\omega_n\tau} \langle \hat{a}_\beta^\dagger(0) \hat{a}_\alpha(\tau) \rangle \\
&= \int_0^{+\beta\hbar} d\tau e^{i\omega_n\tau} \langle \hat{a}_\alpha(\tau) \hat{a}_\beta^\dagger(0) \rangle + \nu \int_0^{+\beta\hbar} d\tau' e^{-i\omega_n\tau'} \langle \hat{a}_\beta^\dagger(\tau') \hat{a}_\alpha(0) \rangle \\
&= \sqrt{\beta\hbar} \langle \hat{c}_\alpha(i\omega_n) \hat{c}_\beta^\dagger(0) \rangle + \nu \sqrt{\beta\hbar} \langle \hat{c}_\beta^\dagger(i\omega_n) \hat{c}_\alpha(0) \rangle \\
&= \sum_m \left[\langle \hat{c}_\alpha(i\omega_n) \hat{c}_\beta^\dagger(i\omega_m) \rangle + \nu \langle \hat{c}_\beta^\dagger(i\omega_n) \hat{c}_\alpha(i\omega_m) \rangle \right],
\end{aligned}$$

where the Fourier transform of the creation and annihilation operators were defined as

$$\hat{a}_\alpha(\tau) = \frac{1}{\sqrt{\beta\hbar}} \sum_m e^{-i\omega_n\tau} \hat{c}_\alpha(i\omega_m), \quad \hat{c}_\alpha(i\omega_n) = \frac{1}{\sqrt{\beta\hbar}} \int_0^{\beta\hbar} d\tau e^{i\omega_n\tau} \hat{a}_\alpha(\tau).$$

Computing ensemble averages in the general case is highly non-trivial and is the subject of perturbation theory, which shall be developed later on. However, it is easy to compute them

exactly in the case of a free-theory. For the first term, we have

$$\begin{aligned}
\langle \hat{c}_\alpha(i\omega_n) \hat{c}_\beta^\dagger(i\omega_m) \rangle_0 &= \frac{\int \prod_{n,\sigma} d(\bar{\psi}_{\sigma n}, \psi_{\sigma n}) e^{-\frac{1}{\hbar} S_0[\bar{\psi}, \psi]} \psi_{\alpha n} \bar{\psi}_{\beta m}}{\int \prod_{n,\sigma} d(\bar{\psi}_{\sigma n}, \psi_{\sigma n}) e^{-\frac{1}{\hbar} S_0[\bar{\psi}, \psi]}} \\
&= \frac{\nu \hbar^2}{\mathcal{Z}(\bar{\eta}, \eta)} \frac{\partial^2 \mathcal{Z}(\bar{\eta}, \eta)}{\partial \bar{\eta}_{\alpha n} \partial \eta_{\beta m}} \Big|_{\bar{\eta}, \eta=0} \\
&= \nu \hbar^2 \left[\frac{\partial^2 \ln \mathcal{Z}(\bar{\eta}, \eta)}{\partial \bar{\eta}_{\alpha n} \partial \eta_{\beta m}} - \frac{\partial \ln \mathcal{Z}(\bar{\eta}, \eta)}{\partial \bar{\eta}_{\alpha n}} \frac{\partial \ln \mathcal{Z}(\bar{\eta}, \eta)}{\partial \eta_{\beta m}} \right]_{\bar{\eta}, \eta=0} \\
&\stackrel{(C.9)}{=} -\frac{\hbar \delta_{\alpha\beta} \delta_{nm}}{-i\hbar\omega_n + \varepsilon_\alpha - \mu} = \langle \hat{c}_\alpha(i\omega_n) \hat{c}_\alpha^\dagger(i\omega_n) \rangle_0 \delta_{\alpha\beta} \delta_{nm}.
\end{aligned}$$

The second term can be obtained simply by commuting the fields in the first equality of the above equation, meaning

$$\begin{aligned}
\langle \hat{c}_\beta^\dagger(i\omega_m) \hat{c}_\alpha(i\omega_n) \rangle_0 &= \nu \langle \hat{c}_\alpha(i\omega_n) \hat{c}_\beta^\dagger(i\omega_m) \rangle_0 = \nu \langle \hat{c}_\alpha(i\omega_m) \hat{c}_\beta^\dagger(i\omega_n) \rangle_0 = \langle \hat{c}_\beta^\dagger(i\omega_n) \hat{c}_\alpha(i\omega_m) \rangle_0 \\
&\Rightarrow \langle \hat{c}_\beta^\dagger(i\omega_n) \hat{c}_\alpha(i\omega_m) \rangle_0 = -\frac{\nu \hbar \delta_{\alpha\beta} \delta_{nm}}{-i\hbar\omega_n + \varepsilon_\alpha - \mu},
\end{aligned}$$

where the second equality is in virtue of the diagonality of the ensemble average. Thus, we arrive at the bare propagator in the frequency domain:

$$\boxed{\mathcal{G}_{0,\alpha\beta}(i\omega_n) = \frac{\delta_{\alpha\beta}}{i\omega_n - \omega_\alpha}}, \quad (\text{C.17})$$

whereas the imaginary time free propagator is obtained by taking the inverse Fourier transform

$$G_{0,\alpha\beta}(\tau) = \frac{\delta_{\alpha\beta}}{\beta\hbar} \sum_n \frac{e^{-i\omega_n\tau}}{i\omega_n - \omega_\alpha}, \quad (\text{C.18})$$

where we defined $\hbar\omega_\alpha = \varepsilon_\alpha - \mu$. From Eq. (C.10) it is clear that the bare propagator is related to the free energy of the non-interacting theory as

$$F_0 = \frac{\nu}{\beta} \text{Tr} \ln [\beta \hbar \hat{\mathcal{G}}_0^{-1}], \quad (\text{C.19})$$

where the trace is taken upon the space of the quantum numbers and of the Matsubara frequencies. Moreover, the action can be written as

$$S[\bar{\psi}, \psi] = -\Psi^\dagger \hat{\mathcal{G}}_0^{-1} \Psi,$$

where $\Psi = (\psi_{\alpha n})_{\forall \alpha, n}$ is a column-vector.

C.1.3 Matsubara frequency sums

So far, we have encountered two quantities that require computing a summation over Matsubara frequencies: the free energy F_0 and the propagator $G_{0,\alpha\beta}(\tau)$. Although the free energy could have been easily computed by taking the trace over Fock space (which is tractable in a non-interacting theory) and the time domain propagator could be obtained by analyzing the equations of motion of the creation and destruction operators (a straightforward exercise in the time-independent case), it is instructive to compute them by evaluating the sums, which are of the form

$$S = \sum_n h(\omega_n).$$

To carry this out, notice that the fermionic or bosonic Matsubara frequencies are poles of either of the following functions $g_\nu : \mathbb{C} \rightarrow \mathbb{C}$,

$$g_\nu(z) = \frac{\beta\hbar}{e^{\beta\hbar z} - \nu}, \text{ or, alternatively, } g_\nu(z) = \frac{\beta\hbar}{2} \left[\coth \left(\frac{\beta\hbar z}{2} \right) \right]^\nu,$$

each pole with residue equal to ν , so that the summation S can be written as

$$S = \sum_n h(\omega_n) = \nu \sum_n \operatorname{Res}[h(-iz)g(z)]_{z=i\omega_n} = \frac{\nu}{2\pi i} \oint_\gamma dz h(-iz) g(z), \quad (\text{C.20})$$

where γ is any contour enclosing the poles of g .

The standard procedure consists of considering a narrow contour along the imaginary axis that encloses every pole, assumed to close at $z \rightarrow \pm i\infty$. Now, as long as the product hg decays faster than $|z|^{-1}$, it is possible to expand this contour to an infinitely large circle. Assuming that h has a set of isolated poles $\{z_k\}$, the expanded contour will enclose each of these poles around a vicinity of each of them, while the integral along the contour at infinity will vanish. This argument yields

$$S = \frac{\nu}{2\pi i} \oint_\gamma dz h(-iz) g(z) = -\nu \sum_k \operatorname{Res}[h(-iz)g(z)]_{z=z_k}, \quad (\text{C.21})$$

where the minus sign appears due to the circulation of the contour enclosing each pole being of opposite direction (clockwise) to the circulation of the original contour (counter-clockwise).

We shall begin by computing the free energy F_0 for the free theory. From Eq. (C.8), we have

$$F_0 = \sum_\alpha F_{0,\alpha} = \sum_\alpha \sum_n \frac{\nu}{\beta} \ln[\beta\hbar(-i\omega_n + \omega_\alpha)],$$

where we defined $\hbar\omega_\alpha = \varepsilon_\alpha - \mu$. Applying the procedure outlined above, we have

$$\frac{\nu}{\beta} \sum_n \ln[\beta\hbar(-i\omega_n + \omega_\alpha)] = \frac{\hbar}{2\pi i} \oint_\gamma dz \frac{\ln[\beta\hbar(\omega_\alpha - z)]}{e^{\beta\hbar z} - \nu}.$$

The integrand has not isolated poles but rather a branch cut along the region $\{z \in \mathbb{C} : \omega_\alpha \leq \operatorname{Re} z < +\infty, \operatorname{Im} z = 0\}$. The product of the integrands decays more rapidly than $|z|^{-1}$ and the contour can be expanded so that it encloses the branch cut, without crossing it. Since the integral on the complex plane vanishes, the contour integral reduces to an integral along the real axis with an appropriate regularization, which amounts to avoiding the branch cut on the real axis. This integral can be written

$$F_{0,\alpha} = \lim_{\delta \rightarrow 0^+} \frac{1}{2\pi i \beta} \int_{-\infty}^{+\infty} dx (e^x - \nu)^{-1} [\ln(\beta \hbar \omega_\alpha - x^+) - \ln(\beta \hbar \omega_\alpha - x^-)] ,$$

where $x = \operatorname{Re} \beta \hbar z$ and $x^\pm = x \pm i\delta$. Clearly, the integral vanishes everywhere along the real axis except on the vicinity of the branch cut. Under the limit, it is safe to say that $g(x^\pm/\beta \hbar) = g(x/\beta \hbar)$ since this function is continuous across the cut. Moreover, noting that $(e^x - \nu)^{-1} = \nu \partial_x \ln(1 - \nu e^{-x})$, we integrate by parts, yielding

$$F_{0,\alpha} = - \lim_{\delta \rightarrow 0^+} \frac{\nu}{2\pi i \beta} \int_{-\infty}^{+\infty} dx \ln(1 - \nu e^{-x}) \left(\frac{1}{x^+ - \beta \hbar \omega_\alpha} - \frac{1}{x^- - \beta \hbar \omega_\alpha} \right) .$$

Thus, using the Cauchy principal value

$$\lim_{\delta \rightarrow 0^+} \frac{1}{y \pm i\delta} = \lim_{\delta \rightarrow 0^+} \frac{y}{y^2 + \delta^2} \mp i \lim_{\delta \rightarrow 0^+} \frac{\delta}{y^2 + \delta^2} = P \frac{1}{y} \mp i\pi \delta(y) , \quad (\text{C.22})$$

we arrive at the result

$$F_{0,\alpha} = \frac{\nu}{\beta} \int_{-\infty}^{+\infty} dx \ln(1 - \nu e^{-x}) \delta(x - \beta \hbar \omega_\alpha) = \frac{\nu}{\beta} \ln(1 - \nu e^{-\beta(\varepsilon_\alpha - \mu)}) ,$$

and the free energy F_0 of a non-interacting system is given by

$$F_0 = \frac{\nu}{\beta} \sum_\alpha \ln(1 - \nu e^{-\beta(\varepsilon_\alpha - \mu)}) . \quad (\text{C.23})$$

Now, according to Eq. (C.2), the expected value of the total number of particles is minus the variation of the free energy with respect to the chemical potential, so that we find

$$N = - \left. \frac{\partial F_0}{\partial \mu} \right|_{T,V} = \sum_\alpha \frac{1}{e^{\beta(\varepsilon_\alpha - \mu)} - \nu} = \sum_\alpha n_\nu(\varepsilon_\alpha - \mu) , \quad (\text{C.24})$$

where $n_\nu(\varepsilon_\alpha - \mu)$ is the expectation value of the number of particles in the state labeled by α , i.e. the Bose-Einstein function for $\nu = +$ and the Fermi-Dirac function for $\nu = -$.

Consider now Eq. (C.18). We begin by noting that the propagator has two parts, in virtue of the time ordering operator. Thus, we can write

$$G_{0,\alpha}(\tau) = \frac{1}{\beta\hbar} \sum_n \frac{e^{-i\omega_n\tau}}{i\omega_n - \omega_\alpha} = \frac{1}{\beta\hbar} \left[\sum_n \frac{e^{-i\omega_n\tau}}{i\omega_n - \omega_\alpha} \theta(\tau) + \sum_n \frac{e^{-i\omega_n\tau}}{i\omega_n - \omega_\alpha} \theta(-\tau) \right], \quad (\text{C.25})$$

noting that $1 = \theta(\tau) + \theta(-\tau)$, $\forall \tau \in \mathbb{R}$, with the Heaviside function as defined in Eq. C.12. Applying the procedure outline above, we find, for each term

$$\begin{aligned} & \frac{1}{\beta\hbar} \sum_n \frac{e^{-i\omega_n\tau}}{i\omega_n - \omega_\alpha} \theta(\tau) && \frac{1}{\beta\hbar} \sum_n \frac{e^{-i\omega_n\tau}}{i\omega_n - \omega_\alpha} \theta(-\tau) \\ &= -\frac{1}{\beta\hbar} \sum_n \frac{e^{i\omega_n\tau}}{i\omega_n + \omega_\alpha} \theta(\tau) && = \frac{1}{\beta\hbar} \sum_n \frac{e^{i\omega_n(-\tau)}}{i\omega_n - \omega_\alpha} \theta(-\tau) \\ &= -\frac{\nu}{2\pi i} \oint_{\gamma} dz \frac{1}{e^{\beta\hbar z} - \nu} \frac{e^{z\tau}}{z + \omega_\alpha} \theta(\tau) && = \frac{\nu}{2\pi i} \oint_{\gamma} dz \frac{1}{e^{\beta\hbar z} - \nu} \frac{e^{z(-\tau)}}{z - \omega_\alpha} \theta(-\tau) \\ &= -\frac{\nu}{\nu - e^{-\beta\hbar\omega_\alpha}} e^{-\omega_\alpha\tau} \theta(\tau) && = -\frac{\nu}{e^{\beta\hbar\omega_\alpha} - \nu} e^{-\omega_\alpha\tau} \theta(-\tau). \end{aligned}$$

The last equality of both equations is valid since the integrand does decay more rapidly than $|z|^{-1}$, so that we can expand the contour infinitely: as $|z| \rightarrow \infty$, in the left half-plane we have $e^{z|\tau|}/(e^{\beta\hbar z} - \nu) \rightarrow -\nu e^{z|\tau|} \rightarrow 0$, whereas in the right half-plane we have $e^{z|\tau|}/(e^{\beta\hbar z} - \nu) \rightarrow e^{z(|\tau|-\beta\hbar)} \rightarrow 0$, since $\tau \in]-\beta\hbar, +\beta\hbar[$.

Therefore, the total free propagator in imaginary time domain can be written as

$$G_{0,\alpha\beta}(\tau - \tau') = -\nu \left[\frac{\theta(\tau' - \tau)}{e^{\beta\hbar\omega_\alpha} - \nu} + \frac{\theta(\tau - \tau')}{\nu - e^{-\beta\hbar\omega_\alpha}} \right] e^{-\omega_\alpha(\tau - \tau')}.$$

Transforming imaginary time as $0 < \tau - \tau' \rightarrow \tau - \tau' - \beta\hbar < 0$ and $0 > \tau - \tau' \rightarrow \tau - \tau' + \beta\hbar > 0$, since $(\tau - \tau') \in]-\beta\hbar, +\beta\hbar[$, the propagator transforms as

$$G_{0,\alpha}(\tau - \tau' \pm \beta\hbar) = \nu G_{0,\alpha}(\tau - \tau'),$$

displaying the necessary (anti-)periodicity. Additionally, it can be written in terms of the expected occupation number n_ν as

$$G_{0,\alpha}(\tau - \tau') = -[\theta(\tau - \tau') + \nu n_\nu(\varepsilon_\alpha - \mu)] e^{-\omega_\alpha(\tau - \tau')}.$$

C.2 Green's functions - Perturbation Theory

We now wish to compute the propagator for an interactive system. However, it is impossible to obtain an exact solution as in Sec. C.1.2. Instead, we shall develop perturbation theory.

The principle is that, since it is impossible to obtain a closed form of the functional integrals, the exponential of the action is expanded in a power series. For instance, the grand-partition

function is formally written as

$$\begin{aligned}
\mathcal{Z} &= \int \mathcal{D}(\bar{\psi}, \psi) \exp \left\{ -(S_0[\bar{\psi}, \psi] + S_V[\bar{\psi}, \psi])/\hbar \right\} \\
&= \int \mathcal{D}(\bar{\psi}, \psi) \exp \left\{ -S_0[\bar{\psi}, \psi]/\hbar \right\} \sum_{n=0}^{+\infty} \frac{1}{n!} (-S_V[\bar{\psi}, \psi]/\hbar)^n \\
&= \mathcal{Z}_0 \left[1 + \sum_{n=1}^{+\infty} \left(\frac{-1}{\beta \hbar^2} \right)^n \frac{1}{2^n n!} \left\langle \left(\Psi^\dagger \Psi^\dagger \hat{\mathcal{V}} \Psi \Psi \right)^n \right\rangle_0 \right] \\
&= \mathcal{Z}_0 + \sum_{n=1}^{+\infty} \mathcal{Z}^{(n)},
\end{aligned}$$

where \mathcal{Z}_0 is the grand-partition function of the non-interacting system and $\langle \dots \rangle_0$ is the expectation value taken over the non-interacting ensemble. In turn, the propagator shall be given by

$$\begin{aligned}
\mathcal{G}_{\alpha\beta}(k, k') &= \langle \psi_k^\alpha \bar{\psi}_{k'}^\beta \rangle \\
&= \frac{\langle \psi_k^\alpha \bar{\psi}_{k'}^\beta \rangle_0 + \sum_{n=1}^{+\infty} (-\beta \hbar^2)^{-n} \frac{1}{2^n n!} \left\langle \left(\Psi^\dagger \Psi^\dagger \hat{\mathcal{V}} \Psi \Psi \right)^n \psi_k^\alpha \bar{\psi}_{k'}^\beta \right\rangle_0}{1 + \sum_{n=1}^{+\infty} (-\beta \hbar^2)^{-n} \frac{1}{2^n n!} \left\langle \left(\Psi^\dagger \Psi^\dagger \hat{\mathcal{V}} \Psi \Psi \right)^n \right\rangle_0} \\
&= \mathcal{G}_{0,\alpha}(k) \delta_{\alpha\beta} \delta_{k,k'} + \sum_{n=1}^{+\infty} \mathcal{G}_{\alpha\beta}^{(n)}(k, k').
\end{aligned} \tag{C.26}$$

C.2.1 1st order contribution to the propagator

For now, we are interested in taking perturbation theory for the propagator up to 1st order. Expanding the denominator yields

$$\begin{aligned}
\mathcal{G}_{\alpha\beta}(k, k') &= \frac{\langle \psi_k^\alpha \bar{\psi}_{k'}^\beta \rangle_0 - \frac{1}{2\beta\hbar^2} \left\langle \Psi^\dagger \Psi^\dagger \hat{\mathcal{V}} \Psi \Psi \psi_k^\alpha \bar{\psi}_{k'}^\beta \right\rangle_0 + (\dots)}{1 - \frac{1}{2\beta\hbar^2} \left\langle \Psi^\dagger \Psi^\dagger \hat{\mathcal{V}} \Psi \Psi \right\rangle_0 + (\dots)} \\
&= \left(\langle \psi_k^\alpha \bar{\psi}_{k'}^\beta \rangle_0 - \frac{1}{2\beta\hbar^2} \langle \Psi^\dagger \Psi^\dagger \hat{\mathcal{V}} \Psi \Psi \psi_k^\alpha \bar{\psi}_{k'}^\beta \rangle_0 \right) \\
&\quad \times \left(1 + \frac{1}{2\beta\hbar^2} \langle \Psi^\dagger \Psi^\dagger \hat{\mathcal{V}} \Psi \Psi \rangle_0 \right) + (\dots) \\
&= \langle \psi_k^\alpha \bar{\psi}_{k'}^\beta \rangle_0 - \frac{1}{2\beta\hbar^2} \left(\langle \Psi^\dagger \Psi^\dagger \hat{\mathcal{V}} \Psi \Psi \psi_k^\alpha \bar{\psi}_{k'}^\beta \rangle_0 - \langle \psi_k^\alpha \bar{\psi}_{k'}^\beta \rangle_0 \langle \Psi^\dagger \Psi^\dagger \hat{\mathcal{V}} \Psi \Psi \rangle_0 \right) + (\dots) \\
&= \mathcal{G}_{0,\alpha}(k) \delta_{\alpha\beta} \delta_{k,k'} + \mathcal{G}_{\alpha\beta}^{(1)}(k, k') + (\dots).
\end{aligned}$$

We now consider the 1st order term of the propagator, which is given by

$$\begin{aligned} \mathcal{G}_{\alpha\beta}^{(1)}(k, k') = & \\ = \frac{-1}{2\beta\hbar^2} \sum_{p,p',q} \mathcal{V}_{\mathbf{p},\mathbf{p}';\mathbf{q}}^{\mu\mu'\nu\nu'} & [\langle \bar{\psi}_{p-q,\mu} \bar{\psi}_{p'+q,\lambda} \psi_{p',\lambda'} \psi_{p,\mu'} \psi_{k,\alpha} \bar{\psi}_{k',\beta} \rangle_0 \\ - \langle \psi_{k,\alpha} \bar{\psi}_{k',\beta} \rangle_0 \langle \bar{\psi}_{p-q,\mu} \bar{\psi}_{p'+q,\lambda} \psi_{p',\lambda'} \psi_{p,\mu'} \rangle_0] \end{aligned} \quad (\text{C.27})$$

We now make use of a fundamental result known as the finite-temperature Wick's theorem, which states that the expected value of any even number of fields in a non-interacting ensemble (therefore, with a quadratic action) can be expanded as a sum over all the products of the expected values of field pairings [124]. Thus, our six-field and four-field correlation functions can be written as a sum of products of two-field correlation functions in the non-interacting ensemble or, put succinctly, bare propagators. We now apply the foregoing theorem to Eq. C.27, yielding

$$\begin{aligned} \mathcal{G}_{\alpha\beta}^{(1)}(k, k') = & \\ = -\frac{1}{2\beta\hbar^2} \sum_{p,p',q} \mathcal{V}_{\mathbf{p},\mathbf{p}';\mathbf{q}}^{\mu\mu'\nu\nu'} & \\ \times \{ \langle \psi_{k,\alpha} \bar{\psi}_{p-q,\mu} \rangle_0 [\langle \psi_{p,\mu'} \bar{\psi}_{p'+q,\lambda} \rangle_0 \langle \psi_{p',\lambda'} \bar{\psi}_{k',\beta} \rangle_0 - \langle \psi_{p',\lambda'} \bar{\psi}_{p'+q,\lambda} \rangle_0 \langle \psi_{p,\mu'} \bar{\psi}_{k',\beta} \rangle_0] \\ + \langle \psi_{k,\alpha} \bar{\psi}_{p'+q,\lambda} \rangle_0 [\langle \psi_{p',\lambda'} \bar{\psi}_{p-q,\mu} \rangle_0 \langle \psi_{p,\mu'} \bar{\psi}_{k',\beta} \rangle_0 - \langle \psi_{p,\mu'} \bar{\psi}_{p-q,\mu} \rangle_0 \langle \psi_{p',\lambda'} \bar{\psi}_{k',\beta} \rangle_0] \} & \\ + Z_{\alpha\beta}^{(1)}(k, k') - Z_{\alpha\beta}^{(1)}(k, k') & \\ = -\frac{1}{2\beta\hbar^2} \sum_{p,p',q} \mathcal{V}_{\mathbf{p},\mathbf{p}';\mathbf{q}}^{\mu\mu'\nu\nu'} & \\ \times \{ \mathcal{G}_{0,\alpha}(k) \delta_{\alpha\mu} \delta_{k,p-q} [\mathcal{G}_{0,\lambda}(p) \delta_{\lambda\mu'} \delta_{p,p'+q} \mathcal{G}_{0,\beta}(k') \delta_{\beta\lambda'} \delta_{k',p'} - \mathcal{G}_{0,\lambda}(p') \delta_{\lambda\lambda'} \delta_{p',p'+q} \mathcal{G}_{0,\beta}(k') \delta_{\beta\mu'} \delta_{k',p}] \\ + \mathcal{G}_{0,\alpha}(k) \delta_{\alpha\lambda} \delta_{k,p'+q} [\mathcal{G}_{0,\lambda}(p') \delta_{\lambda\mu'} \delta_{p',p-q} \mathcal{G}_{0,\beta}(k') \delta_{\beta\mu'} \delta_{k',p} - \mathcal{G}_{0,\mu}(p) \delta_{\mu\mu'} \delta_{p,p-q} \mathcal{G}_{0,\beta}(k') \delta_{\beta\lambda'} \delta_{k',p'}] \} & \\ \Rightarrow \mathcal{G}_{\alpha\beta}^{(1)}(k, k') & \\ = \frac{\delta_{k,k'}}{2\beta\hbar^2} \mathcal{G}_{0,\alpha}(k) \left[\mathcal{V}_{\mathbf{k},\mathbf{k};\mathbf{0}}^{\alpha\beta\lambda\lambda} \sum_p \mathcal{G}_{0,\lambda}(p) + \mathcal{V}_{\mathbf{k},\mathbf{k};\mathbf{0}}^{\mu\mu\alpha\beta} \sum_p \mathcal{G}_{0,\mu}(p) \right. & \\ \left. - \sum_q \mathcal{V}_{\mathbf{k}+\mathbf{q},\mathbf{k};\mathbf{q}}^{\alpha\lambda\lambda\beta} \mathcal{G}_{0,\lambda}(k+q) - \sum_q \mathcal{V}_{\mathbf{k},\mathbf{k}-\mathbf{q};\mathbf{q}}^{\mu\beta\alpha\mu} \mathcal{G}_{0,\mu}(k-q) \right] \mathcal{G}_{0,\beta}(k) & \end{aligned} \quad (\text{C.28})$$

In this derivation, the minus signs arise due to the permutations of fermion fields required to realize the pairings. (Evidently, these signs would not arise in the case of bosonic fields.) The last two terms, labeled $Z_{\alpha\beta}^{(1)}(k, k')$, are identical and cancel each other. They are written as

$$\begin{aligned}
Z_{\alpha\beta}^{(1)}(k, k') &= \\
&= \langle \psi_{k,\alpha} \bar{\psi}_{k',\beta} \rangle_0 [\langle \psi_{p,\mu'} \bar{\psi}_{p-q,\mu} \rangle_0 \langle \psi_{p',\lambda'} \bar{\psi}_{p'+q,\lambda} \rangle_0 - \langle \psi_{p',\lambda'} \bar{\psi}_{p-q,\mu} \rangle_0 \langle \psi_{p,\mu'} \bar{\psi}_{p'+q,\lambda} \rangle_0] \\
&= \mathcal{G}_{0,\alpha}(k) \delta_{\alpha\beta} [\delta_{k,k'} \mathcal{G}_{0,\mu}(p) \delta_{\mu\mu'} \delta_{p,p-q} \mathcal{G}_{0,\lambda}(p') \delta_{\lambda\lambda'} \delta_{p',p'+q} - \mathcal{G}_{0,\mu}(p') \delta_{\mu\lambda'} \delta_{p',p-q} \mathcal{G}_{0,\lambda}(p) \delta_{\lambda\mu'} \delta_{p,p'+q}] \\
&= \frac{1}{\beta\hbar^2} \mathcal{G}_{0,\alpha}(k) \delta_{\alpha\beta} \delta_{k,k'} \left[\sum_{p,p'} \mathcal{V}_{\mathbf{p},\mathbf{p}';\mathbf{0}}^{\mu\mu\lambda\lambda} \mathcal{G}_{0,\mu}(p) \mathcal{G}_{0,\lambda}(p') - \sum_{p,q} \mathcal{V}_{\mathbf{p},\mathbf{p}-\mathbf{q};\mathbf{q}}^{\mu\lambda\lambda\mu} \mathcal{G}_{0,\mu}(p-q) \mathcal{G}_{0,\lambda}(p) \right].
\end{aligned}$$

These represent disconnected processes, since the interaction does not depend on external indices and, thus, does not connect with the external propagator. We can infer that this result is generalizable to any order in perturbation theory, since the disconnected terms are cancelled by a term that results from expanding the denominator in Eq. (C.26). Therefore, the propagator can be more succinctly written as

$$\mathcal{G}_{\alpha\beta}(k, k') = \langle \psi_{k,\alpha} \bar{\psi}_{k',\beta} \rangle_0 + \sum_{n=1}^{+\infty} \left(-\frac{1}{\beta\hbar^2} \right)^n \frac{1}{2n!!} \left\langle \left(\Psi^\dagger \Psi^\dagger \hat{V} \Psi \Psi \right)^n \psi_{k,\alpha} \bar{\psi}_{k',\beta} \right\rangle_0^c, \quad (\text{C.29})$$

where $\langle \dots \rangle^c$ is the connected correlation function or cumulant. This result is a consequence of the linked cluster theorem [124].

Moreover, there is a clear similarity among the non-vanishing terms with the same sign, in Eq. (C.28). By looking at the structure of the interaction matrix elements (presented in the main body) it becomes clear that both terms of each of those pairs are, in fact, the same and, thus, represent the same process. We have

$$\begin{aligned}
\mathcal{V}_{\mathbf{k},\mathbf{k};\mathbf{0}}^{\alpha\beta\lambda\lambda} &= \int d^3x \int d^3x' \bar{\varphi}_{\mathbf{k},\alpha}(\mathbf{x}) \bar{\varphi}_{\mathbf{k},\lambda}(\mathbf{x}') \varphi_{\mathbf{k},\lambda}(\mathbf{x}') \varphi_{\mathbf{k},\beta}(\mathbf{x}) V(\mathbf{x} - \mathbf{x}') \\
&= \int d^3x' \int d^3x \bar{\varphi}_{\mathbf{k},\lambda}(\mathbf{x}') \bar{\varphi}_{\mathbf{k},\alpha}(\mathbf{x}) \varphi_{\mathbf{k},\beta}(\mathbf{x}) \varphi_{\mathbf{k},\lambda}(\mathbf{x}') V(\mathbf{x}' - \mathbf{x}) \\
&= \mathcal{V}_{\mathbf{k},\mathbf{k};\mathbf{0}}^{\lambda\lambda\alpha\beta}
\end{aligned}$$

and

$$\begin{aligned}
\sum_{\mathbf{q}} \mathcal{V}_{\mathbf{k}+\mathbf{q},\mathbf{k};\mathbf{q}}^{\alpha\lambda\lambda\beta} &= \sum_{\mathbf{q}} \int d^3x \int d^3x' \bar{\varphi}_{\mathbf{k},\alpha}(\mathbf{x}) \bar{\varphi}_{\mathbf{k}+\mathbf{q},\lambda}(\mathbf{x}') \varphi_{\mathbf{k},\beta}(\mathbf{x}') \varphi_{\mathbf{k}+\mathbf{q},\lambda}(\mathbf{x}) V(\mathbf{x} - \mathbf{x}') \\
&= \sum_{\mathbf{q}} \int d^3x' \int d^3x \bar{\varphi}_{\mathbf{k}+\mathbf{q},\lambda}(\mathbf{x}') \bar{\varphi}_{\mathbf{k},\alpha}(\mathbf{x}) \varphi_{\mathbf{k}+\mathbf{q},\lambda}(\mathbf{x}) \varphi_{\mathbf{k},\beta}(\mathbf{x}') V(\mathbf{x}' - \mathbf{x}) \\
&= \sum_{\mathbf{q}} \mathcal{V}_{\mathbf{k},\mathbf{k}+\mathbf{q};-\mathbf{q}}^{\lambda\beta\alpha\lambda} = \sum_{\mathbf{q}} \mathcal{V}_{\mathbf{k},\mathbf{k}-\mathbf{q};+\mathbf{q}}^{\lambda\beta\alpha\lambda},
\end{aligned}$$

so that, finally, we arrive at the 1st order contribution to the propagator

$$\mathcal{G}_{\alpha\beta}^{(1)}(k) = \frac{1}{\beta\hbar^2} \mathcal{G}_{0,\alpha}(k) \left[\mathcal{V}_{\mathbf{k},\mathbf{k};\mathbf{0}}^{\alpha\beta\lambda\lambda} \sum_p \mathcal{G}_{0,\lambda}(p) - \sum_q \mathcal{V}_{\mathbf{k}+\mathbf{q},\mathbf{k};\mathbf{q}}^{\alpha\lambda\lambda\beta} \mathcal{G}_{0,\lambda}(k+q) \right] \mathcal{G}_{0,\beta}(k),$$

The diagonality of the propagator in conjugate space was clear from the outset: the interaction conserves crystal momentum (it is spatially homogeneous) and the Hamiltonian is independent of time, as previously stated, which, in turn, implies conservation of energy. However, unlike the bare propagator, it does not conserve band index: the interaction can, in principle, induce band transitions.

The two terms in brackets are known as the direct and exchange terms or, alluding to the Hartree-Fock approximation, the Hartree and Fock terms, respectively. It is then clear that the 1st order contribution to the propagator amounts to the Hartree-Fock approximation.

Looking at the structure of the interaction factor, it is clear that the first term corresponds a density-density interaction and, thus, of classical nature. Note that this term is irrelevant, since such a repulsive interaction between electrons is compensated by the attractive interaction of positive charges in the background which, in our case, amounts to the lattice. More importantly, this is true for any order of perturbation theory [124]. Since the assertion that the electron-electron repulsive interaction is cancelled by the electron-ion attractive interaction is valid for any globally homogeneous system we will not consider it for the remainder of this work.

C.2.2 Dyson's equations, self-energy correction of the bare propagator

As it is, our treatment yields merely an additive term to the bare propagator, a manifestly perturbative result. However, in a many-body setting, it is not reasonable to assume that the interaction is weak enough to only be relevant up to first-order in perturbation theory. Indeed, the process described above may have relevant contributions to all orders of the perturbative expansion. This problem is circumvented to a great extent by introducing Dyson's Equations [117, 124].

Although we are not aiming for a formal proof, we can present the following diagrammatic argument: since the n th order of the perturbative expansion is represented by the sum of the diagrams resulting from every connected combination of n interaction diagrams of Fig. 4.1 (in the main text), each order will contain a term that corresponds to the n -fold multiplication of the diagram of Fig. 4.2. For instance, to 2nd order, this diagram is

$$\begin{array}{c} \text{Diagram: } \text{A horizontal line with two wavy lines attached to it.} \\ = \hat{\mathcal{G}}_0 \hat{\Sigma} \hat{\mathcal{G}}_0 \hat{\Sigma} \hat{\mathcal{G}}_0 . \end{array}$$

Now, even though there are different processes contributing to propagator at higher orders, we assume that this is the most important contribution, since it is the only non-vanishing contribution to leading order. Therefore, we approximate Eq. (C.29) by restricting the summation to the class of diagrams that correspond to the self-energy of Eq. (4.4). Diagrammatically, it reads

$$\begin{array}{c} \text{Diagram: } \text{A horizontal line with two wavy lines attached to it, followed by a plus sign, then another horizontal line with two wavy lines attached to it, followed by a plus sign, and so on.} \\ = \dots + \dots + \dots + \dots , \end{array}$$

which, equationally, translates to

$$\hat{\mathcal{G}} = \hat{\mathcal{G}}_0 + \hat{\mathcal{G}}_0 \hat{\Sigma} \hat{\mathcal{G}}_0 + \hat{\mathcal{G}}_0 \hat{\Sigma} \hat{\mathcal{G}}_0 \hat{\Sigma} \hat{\mathcal{G}}_0 + \hat{\mathcal{G}}_0 \hat{\Sigma} \hat{\mathcal{G}}_0 \hat{\Sigma} \hat{\mathcal{G}}_0 \hat{\Sigma} \hat{\mathcal{G}}_0 + \dots$$

Although the summation involved in this equation is infinite, it also has a remarkable structure: it is recursive, yielding a self-consistent equation

$$\begin{aligned} \hat{\mathcal{G}} &= \hat{\mathcal{G}}_0 + \hat{\mathcal{G}}_0 \hat{\Sigma} \left[\hat{\mathcal{G}}^0 + \hat{\mathcal{G}}_0 \hat{\Sigma} \hat{\mathcal{G}}_0 + \hat{\mathcal{G}}_0 \hat{\Sigma} \hat{\mathcal{G}}_0 \hat{\Sigma} \hat{\mathcal{G}}_0 + \dots \right] \\ &= \hat{\mathcal{G}}_0 + \hat{\mathcal{G}}_0 \hat{\Sigma} \hat{\mathcal{G}}. \end{aligned} \quad (\text{C.30})$$

This is an instance of what is known as Dyson's Equations. Strictly speaking, the self-energy operator in Dyson's Equations takes into account every diagram that is not one-particle reducible. However, such an approach is analytically intractable, so that it is a common approach to approximate it by the contribution from the first-order exchange process, in virtue of the physically motivated argument presented above. Now, solving Eq. (C.30) in order to $\hat{\mathcal{G}}$ yields

$$\hat{\mathcal{G}}_{\alpha\beta}(\mathbf{k}, i\omega_n) = \left[\hat{\mathcal{G}}_0^{-1} - \hat{\Sigma} \right]_{\alpha\beta}^{-1}(\mathbf{k}, i\omega_n). \quad (\text{C.31})$$

For instance, considering a generic conduction-valence band system, without valley or spin indices, the propagator as the form

$$\begin{aligned} \hat{\mathcal{G}} &= \begin{pmatrix} \mathcal{G}_{0,c}^{-1} - \Sigma_{cc} & -\Sigma_{cv} \\ -\Sigma_{vc} & \mathcal{G}_{0,v}^{-1} - \Sigma_{vv} \end{pmatrix}^{-1} \\ &= \frac{1}{(\mathcal{G}_{0,c}^{-1} - \Sigma_{cc})(\mathcal{G}_{0,v}^{-1} - \Sigma_{vv}) - \Sigma_{vc}\Sigma_{cv}} \begin{pmatrix} \mathcal{G}_{0,v}^{-1} - \Sigma_{vv} & \Sigma_{cv} \\ \Sigma_{vc} & \mathcal{G}_{0,c}^{-1} - \Sigma_{cc} \end{pmatrix}. \end{aligned}$$

C.3 Conservation of crystal momentum from the Coulomb potential

Although we have written the interaction term in crystal momentum space directly, it is worthwhile going over the proof that the class of interactions considered conserves, indeed, crystal momentum. Note that crystal momentum states are Bloch states, i.e.

$$\varphi_{\mathbf{k},\mu}(\mathbf{x}) = e^{i\mathbf{k}\cdot\mathbf{x}} u_{\mathbf{k},\mu}(\mathbf{x}), \quad u_{\mathbf{k},\mu}(\mathbf{x} + \mathbf{R}) = u_{\mathbf{k},\mu}(\mathbf{x}),$$

$\forall \mathbf{x}, \mathbf{k}, \mu$ and \mathbf{R} a lattice vector. Moreover, consider an additional crystal momentum \mathbf{q}' and substitute the integral over all space by an integral over the unit cell summed over all lattice

sites, i.e. $\mathbf{x} = \mathbf{y} + \mathbf{R}$. We thus find

$$\begin{aligned}
& \mathcal{V}_{\mathbf{k}, \mathbf{k}'; \mathbf{q}, \mathbf{q}'}^{\mu\mu' \nu\nu'} \\
&= \sum_{\mathbf{R}, \mathbf{R}'} \int d^3y \int d^3y' e^{-i(\mathbf{k}-\mathbf{q}) \cdot (\mathbf{y}+\mathbf{R})} e^{-i(\mathbf{k}'+\mathbf{q}') \cdot (\mathbf{y}'+\mathbf{R}')} e^{i\mathbf{k}' \cdot (\mathbf{y}'+\mathbf{R}')} e^{i\mathbf{k} \cdot (\mathbf{y}+\mathbf{R})} \\
&\times \bar{u}_{\mathbf{k}-\mathbf{q}, \mu}(\mathbf{y}+\mathbf{R}) \bar{u}_{\mathbf{k}'+\mathbf{q}', \nu}(\mathbf{y}'+\mathbf{R}') u_{\mathbf{k}', \nu'}(\mathbf{y}'+\mathbf{R}') u_{\mathbf{k}, \mu'}(\mathbf{y}+\mathbf{R}) V(\mathbf{y}-\mathbf{y}'+\mathbf{R}-\mathbf{R}') \\
&= \sum_{\mathbf{R}} e^{i(\mathbf{q}-\mathbf{q}') \cdot \mathbf{R}} \int d^3y \sum_{\tilde{\mathbf{R}}} \int d^3y' e^{i\mathbf{q}' \cdot \tilde{\mathbf{R}}} e^{i(\mathbf{q} \cdot \mathbf{y} - \mathbf{q}' \cdot \mathbf{y}')} \times \bar{u}_{\mathbf{k}-\mathbf{q}, \mu}(\mathbf{y}) \bar{u}_{\mathbf{k}'+\mathbf{q}', \nu}(\mathbf{y}') u_{\mathbf{k}', \nu'}(\mathbf{y}') u_{\mathbf{k}, \mu'}(\mathbf{y}) V(\mathbf{y}-\mathbf{y}'+\tilde{\mathbf{R}}) \\
&= \delta_{\mathbf{q}, \mathbf{q}'} \sum_{\mathbf{R}} \int d^3y \sum_{\tilde{\mathbf{R}}} \int d^3y' e^{i\mathbf{q} \cdot (\mathbf{y}-\mathbf{y}')} e^{i\mathbf{q} \cdot \tilde{\mathbf{R}}} \times \bar{u}_{\mathbf{k}-\mathbf{q}, \mu}(\mathbf{y}) \bar{u}_{\mathbf{k}'+\mathbf{q}, \nu}(\mathbf{y}') u_{\mathbf{k}', \nu'}(\mathbf{y}') u_{\mathbf{k}, \mu'}(\mathbf{y}) V(\mathbf{y}-\mathbf{y}'+\tilde{\mathbf{R}}) \\
&= \delta_{\mathbf{q}, \mathbf{q}'} \sum_{\mathbf{R}} \int d^3y \bar{u}_{\mathbf{k}-\mathbf{q}, \mu}(\mathbf{y}) u_{\mathbf{k}, \mu'}(\mathbf{y}) \times \sum_{\tilde{\mathbf{R}}} \int d^3y'' e^{i\mathbf{q} \cdot \mathbf{y}''} e^{i\mathbf{q} \cdot \tilde{\mathbf{R}}} \bar{u}_{\mathbf{k}'+\mathbf{q}, \nu}(\mathbf{y}-\mathbf{y}'') u_{\mathbf{k}', \nu'}(\mathbf{y}-\mathbf{y}'') V(\mathbf{y}''+\tilde{\mathbf{R}}) \\
&= \delta_{\mathbf{q}, \mathbf{q}'} \int d^3x \bar{u}_{\mathbf{k}-\mathbf{q}, \mu}(\mathbf{x}) u_{\mathbf{k}, \mu'}(\mathbf{x}) \int d^3r e^{i\mathbf{q} \cdot \mathbf{r}} \bar{u}_{\mathbf{k}'+\mathbf{q}, \nu}(\mathbf{x}-\mathbf{r}) u_{\mathbf{k}', \nu'}(\mathbf{x}-\mathbf{r}) V(\mathbf{r}) \\
&= \delta_{\mathbf{q}, \mathbf{q}'} \int d^3x \int d^3r e^{i\mathbf{q} \cdot \mathbf{r}} \bar{u}_{\mathbf{k}-\mathbf{q}, \mu}(\mathbf{x}) \bar{u}_{\mathbf{k}'+\mathbf{q}, \nu}(\mathbf{x}-\mathbf{r}) u_{\mathbf{k}', \nu'}(\mathbf{x}-\mathbf{r}) u_{\mathbf{k}, \mu'}(\mathbf{x}) V(\mathbf{r}) \\
&= \delta_{\mathbf{q}, \mathbf{q}'} \mathcal{V}_{\mathbf{k}, \mathbf{k}'; \mathbf{q}, \mathbf{q}'}^{\mu\mu' \nu\nu'}.
\end{aligned}$$

Appendix D

The Gibbs-Bogoliubov-Feynman inequality and the Hubbard-Stratonovich action approaches to the mean-field problem

D.1 Mean-field from a variational free energy using the Gibbs-Bogoliubov-Feynman inequality

The variational method is built upon the so called Gibbs-Bogoliubov-Feynman inequality (see Refs. [126] and [127] for derivations),

$$\Omega \leq \langle \hat{\mathcal{H}} \rangle_{MF} - T\mathcal{S}_{MF} - \mu\langle \hat{N} \rangle_{MF}, \quad (\text{D.1})$$

where Ω is the system's grand canonical potential, T is the temperature, μ is the chemical potential, and $\langle \cdots \rangle_{MF}$ and \mathcal{S}_{MF} are respectively the thermal average and the entropy for any thermal distribution $\rho_{MF} = \exp(-\beta\hat{\mathcal{H}}_{MF})$. We have used \hat{N} as the operator for the total number of particles, where as usual we assume the commutation $[\hat{\mathcal{H}}, \hat{N}] = 0$ to hold. The equality in Eq. (D.1) is realized only when $\hat{\mathcal{H}}_{MF} = \hat{\mathcal{H}}$, and thus we can use this inequality as a variational principle to get, from a given family of simpler (non-interacting) Hamiltonians $\hat{\mathcal{H}}_{MF}$, the one that

better describes the system. Noting that,

$$\Omega_{MF} = \langle \hat{\mathcal{H}}_{MF} \rangle_{MF} - T\mathcal{S}_{MF} - \mu \langle \hat{\mathcal{N}} \rangle_{MF}, \quad (\text{D.2})$$

it is usual to rewrite Eq. (D.1) as,

$$\Omega \leq \Omega_{MF} + \langle \hat{\mathcal{H}} - \hat{\mathcal{H}}_{MF} \rangle_{MF}. \quad (\text{D.3})$$

We have $\langle \hat{\mathcal{N}} \rangle \equiv N_e$, where N_e is the number of fermions in the system. It is then appropriate to work in the canonical ensemble. Owing to the thermodynamic relation $\Omega \simeq \mathcal{F} - \mu \langle \hat{\mathcal{N}} \rangle$, valid in the thermodynamic limit, we can write the following inequality for the free energy \mathcal{F} ,

$$\mathcal{F} \leq \mathcal{F}_{MF} + \langle \hat{\mathcal{H}} - \hat{\mathcal{H}}_{MF} \rangle_{MF} \equiv F, \quad (\text{D.4})$$

where

$$\mathcal{F}_{MF} = \Omega_{MF} + \mu N_e, \quad (\text{D.5})$$

with μ such that $N_e = \langle \hat{\mathcal{N}} \rangle_{MF}$. Equation (D.4) defines the functional F , which has to be minimized with respect to some mean field parameter defining the family of simpler models we are probing.

Recovering the Hamiltonian of Eq. (5.5),

$$\hat{\mathcal{H}} = \sum_{\sigma, \tau} \sum_{\mathbf{k}} \hat{\psi}_{\mathbf{k}, \sigma}^{\tau \dagger} \varepsilon_{\mathbf{k}, \sigma}^{\tau} \hat{\psi}_{\mathbf{k}, \sigma}^{\tau} + \frac{U}{2N} \sum_{\tau, \tau'} \sum_{\mathbf{q}} \hat{\rho}_{\mathbf{q}, \sigma}^{\tau} \hat{\rho}_{-\mathbf{q}, \bar{\sigma}}^{\tau'},$$

we decouple in the direct channel, yielding the mean-field Hamiltonian

$$\hat{\mathcal{H}}_{MF} = \hat{\mathcal{H}}_0 + \frac{U}{2N} \sum_{\tau, \tau'} \sum_{\sigma, \mathbf{q}} \hat{\rho}_{\mathbf{q}, \sigma}^{\tau} \phi_{-\mathbf{q}, \bar{\sigma}}^{\tau'}, \quad (\text{D.6})$$

and determine $\phi_{\mathbf{q}, \sigma}^{\tau}$ such that F , given by Eq. D.4, is minimized,

$$\phi_{\mathbf{q}, \sigma}^{\tau} \rightarrow \phi_{\mathbf{q}, \sigma}^{\tau} + \delta \phi_{\mathbf{q}, \sigma}^{\tau} \Rightarrow \delta F = \delta \mathcal{F}_{MF} + \delta \langle \hat{\mathcal{H}} - \hat{\mathcal{H}}_{MF} \rangle_{MF} = 0. \quad (\text{D.7})$$

The bilinearity of the mean-field Hamiltonian, Eq. (D.6), guarantees we can apply Wick's theorem to compute $\langle \hat{\mathcal{H}} \rangle_{MF}$, namely,

$$\begin{aligned} \langle \hat{\rho}_{\mathbf{q}, \uparrow}^{\tau} \hat{\rho}_{-\mathbf{q}, \downarrow}^{\tau'} \rangle_{MF} &= \sum_{\mathbf{k}, \mathbf{k}'} \langle \hat{\psi}_{\mathbf{k}+\mathbf{q}, \uparrow}^{\tau \dagger} \hat{\psi}_{\mathbf{k}, \uparrow}^{\tau} \hat{\psi}_{\mathbf{k}-\mathbf{q}, \downarrow}^{\tau' \dagger} \hat{\psi}_{\mathbf{k}, \downarrow}^{\tau'} \rangle_{MF} \\ &= \sum_{\mathbf{k}, \mathbf{k}'} \langle \hat{\psi}_{\mathbf{k}+\mathbf{q}, \uparrow}^{\tau \dagger} \hat{\psi}_{\mathbf{k}, \uparrow}^{\tau} \rangle_{MF} \langle \hat{\psi}_{\mathbf{k}-\mathbf{q}, \downarrow}^{\tau' \dagger} \hat{\psi}_{\mathbf{k}, \downarrow}^{\tau'} \rangle_{MF} - \sum_{\mathbf{k}, \mathbf{k}'} \langle \hat{\psi}_{\mathbf{k}+\mathbf{q}, \uparrow}^{\tau \dagger} \hat{\psi}_{\mathbf{k}, \downarrow}^{\tau'} \rangle_{MF} \langle \hat{\psi}_{\mathbf{k}-\mathbf{q}, \downarrow}^{\tau' \dagger} \hat{\psi}_{\mathbf{k}, \uparrow}^{\tau} \rangle_{MF} \\ &= \langle \hat{\rho}_{\mathbf{q}, \uparrow}^{\tau} \rangle_{MF} \langle \hat{\rho}_{-\mathbf{q}, \downarrow}^{\tau'} \rangle_{MF}, \end{aligned}$$

where the second equality yields in virtue of conservation of the s_z spin component in the mean-field Hamiltonian. Thus,

$$\delta\langle\hat{\mathcal{H}} - \hat{\mathcal{H}}_{MF}\rangle_{MF} = \frac{U}{2N} \sum_{\tau, \tau'} \sum_{\sigma, \mathbf{q}} \left\{ [\langle\hat{\rho}_{\mathbf{q}, \sigma}^\tau\rangle_{MF} - \phi_{\mathbf{q}, \sigma}^\tau] \delta\langle\hat{\rho}_{-\mathbf{q}, \bar{\sigma}}^{\tau'}\rangle_{MF} - \delta\phi_{\mathbf{q}, \sigma}^\tau \langle\hat{\rho}_{-\mathbf{q}, \bar{\sigma}}^{\tau'}\rangle_{MF} \right\}.$$

On the other hand,

$$\delta e^{-\beta\mathcal{F}_{MF}} = -\beta e^{-\beta\mathcal{F}_{MF}} \delta\mathcal{F}_{MF} = \delta\text{Tr } e^{-\beta\hat{\mathcal{H}}_{MF}} \Leftrightarrow \delta\mathcal{F}_{MF} = -\frac{1}{\beta} \frac{\delta\text{Tr } e^{-\beta\hat{\mathcal{H}}_{MF}}}{\text{Tr } e^{-\beta\hat{\mathcal{H}}_{MF}}},$$

whereas, for a general Hamiltonian H , we have

$$\begin{aligned} \text{Tr } e^{-\beta(H+\delta H)} &= \text{Tr } \sum_{n=0}^{\infty} \frac{(-\beta)^n}{n!} (H + \delta H)^n \\ &= \text{Tr } \left[1 + \sum_{n=1}^{\infty} \frac{(-\beta)^n}{n!} \left(H^n + \sum_{m=0}^{n-1} H^m \delta H H^{n-1-m} \right) + \mathcal{O}(\delta H^2) \right] \\ &= \text{Tr } e^{-\beta H} + \text{Tr } \sum_{n=1}^{\infty} \frac{(-\beta)^n}{n!} \sum_{m=0}^{n-1} H^{n-1} \delta H \\ &= \text{Tr } e^{-\beta H} + \text{Tr } \sum_{n=1}^{\infty} \frac{(-\beta)^n}{(n-1)!} H^{n-1} \delta H \\ &= \text{Tr } e^{-\beta H} - \beta \text{Tr } [e^{-\beta H} \delta H], \end{aligned}$$

thus yielding

$$\delta\text{Tr } e^{-\beta H} = \text{Tr } e^{-\beta(H+\delta H)} - \text{Tr } e^{-\beta H} = -\beta \text{Tr } [e^{-\beta H} \delta H],$$

so that

$$\delta\mathcal{F}_{MF} = \frac{\text{Tr } [e^{-\beta\hat{\mathcal{H}}_{MF}} \delta\hat{\mathcal{H}}_{MF}]}{\text{Tr } e^{-\beta\hat{\mathcal{H}}_{MF}}} = \frac{U}{N} \sum_{\tau, \tau'} \sum_{\sigma, \mathbf{q}} \delta\phi_{\mathbf{q}, \sigma}^\tau \langle\hat{\rho}_{-\mathbf{q}, \bar{\sigma}}^{\tau'}\rangle_{MF} = .$$

Combining results yields, for the variation of the free energy,

$$\delta F = \frac{U}{N} \sum_{\tau, \tau'} \sum_{\sigma, \mathbf{q}} [\langle\hat{\rho}_{\mathbf{q}, \sigma}^\tau\rangle_{MF} - \phi_{\mathbf{q}, \sigma}^\tau] \delta\langle\hat{\rho}_{-\mathbf{q}, \bar{\sigma}}^{\tau'}\rangle_{MF} = 0,$$

which implies

$$\phi_{\mathbf{q}, \sigma}^\tau = \langle\hat{\rho}_{\mathbf{q}, \uparrow}^\tau\rangle_{MF} = \sum_{\mathbf{k}, \mathbf{k}'} \langle\hat{\psi}_{\mathbf{k}+\mathbf{q}, \uparrow}^{\tau\dagger} \hat{\psi}_{\mathbf{k}, \uparrow}^\tau\rangle_{MF},$$

so that the mean-field Hamiltonian reads

$$\hat{\mathcal{H}}_{MF} = \sum_{\sigma, \tau} \sum_{\mathbf{k}, \mathbf{q}} \hat{\psi}_{\mathbf{k}+\mathbf{q}, \sigma}^{\tau\dagger} \left[\varepsilon_{\mathbf{k}, \sigma}^\tau \delta_{\mathbf{q}, \mathbf{0}} + U \sum_{\tau'} n_{-\mathbf{q}, \bar{\sigma}}^{\tau'} \right] \hat{\psi}_{\mathbf{k}, \sigma}^\tau, \quad (\text{D.8})$$

where the $\{n_{\mathbf{q},\sigma}^{\tau}\}$ are given by

$$n_{\mathbf{q},\sigma}^{\tau} = \frac{1}{N} \langle \hat{\rho}_{\mathbf{q},\sigma}^{\tau} \rangle_{MF} = \frac{1}{N} \sum_{\mathbf{k}} \langle \hat{\psi}_{\mathbf{k}+\mathbf{q},\sigma}^{\tau\dagger} \hat{\psi}_{\mathbf{k},\sigma}^{\tau} \rangle_{MF}.$$

Keeping the discussion to spatially homogenous solutions, we have

$$n_{\mathbf{q},\sigma}^{\tau} = n_{\sigma}^{\tau} \delta_{\mathbf{q},\mathbf{0}}, \quad (\text{D.9})$$

which yields a mean-field Hamiltonian and a set of mean-field equations respectively given by

$$\begin{aligned} \hat{\mathcal{H}}_{MF} &= \sum_{\sigma,\tau} \sum_{\mathbf{k}} \hat{\psi}_{\mathbf{k},\sigma}^{\tau\dagger} \left[\varepsilon_{\mathbf{k},\sigma}^{\tau} + U \sum_{\tau'} n_{\sigma}^{\tau'} \right] \hat{\psi}_{\mathbf{k},\sigma}^{\tau}, \\ n_{\sigma}^{\tau} &= \frac{1}{N} \sum_{\mathbf{k}} \langle \hat{\psi}_{\mathbf{k},\sigma}^{\tau\dagger} \hat{\psi}_{\mathbf{k},\sigma}^{\tau} \rangle_{MF} = \frac{1}{N} \sum_{\mathbf{k}} \langle \hat{n}_{\mathbf{k},\sigma}^{\tau} \rangle_{MF}. \end{aligned} \quad (\text{D.10})$$

Since the mean-fields Hamiltonian is diagonal, we have

$$\langle \hat{n}_{\mathbf{k},\sigma}^{\tau} \rangle_{MF} = n_F \left(\varepsilon_{\mathbf{k},\sigma}^{\tau} - \mu + U \sum_{\tau'} n_{\sigma}^{\tau'} \right),$$

thus yielding the mean-field equations

$$n_{\sigma}^{\tau} = \frac{1}{N} \sum_{\mathbf{k}} n_F \left(\varepsilon_{\mathbf{k},\sigma}^{\tau} - \mu + U \sum_{\tau'} n_{\sigma}^{\tau'} \right), \quad \forall \tau, \sigma,$$

which are exactly the same as Eq. (5.9), obtained in the main text using the imaginary-time action in the path integral formalism. As we saw there, this approach is unable to yield a solution for the broken symmetry phase and we must resort to other methods, namely, by looking at the structure of the free energy itself.

According to Eqs. (D.2) and (D.5)

$$\mathcal{F}_{MF} = \langle \hat{\mathcal{H}}_{MF} \rangle_{MF} - T \mathcal{S}_{MF},$$

and, thus, for $T \rightarrow 0$, the free energy is identically equal to the internal energy E . However, we can no longer assume the $\{n_{0,\sigma}^{\tau}\}$ to be densities. Rather, the internal energy will now be a functional of some set of variational parameters, which can be specified by correcting the ansatz of Eq. (D.9) as

$$n_{\mathbf{q},\sigma}^{\tau} = (\bar{n}_{\sigma}^{\tau} + \eta_{\sigma}^{\tau}) \delta_{\mathbf{q},\mathbf{0}}, \quad (\text{D.11})$$

similarly to the ansatz Eq. (5.16) and (5.20) proposed in the main text, where $\{\eta_{\sigma}^{\tau}\}$ are variational parameters and $\{\bar{n}_{\sigma}^{\tau}\}$ are the electron densities in the normal phase. The internal energy thus

reads

$$E(\{\eta_\sigma^\tau\}) = \sum_{\tau, \sigma} \sum_{\mathbf{k}} \epsilon_{\mathbf{k}, \sigma}^\tau \langle n_{\mathbf{k}, \sigma}^\tau \rangle_{MF} + \frac{U}{N} \sum_{\tau, \tau'} \sum_{\mathbf{q}} \langle \rho_{\mathbf{q}, \uparrow}^\tau \rangle_{MF} \langle \rho_{-\mathbf{q}, \downarrow}^{\tau'} \rangle_{MF}.$$

The averages are computed in the mean-field ensemble of Hamiltonian Eq. (D.8) with the ansatz Eq. (D.11). Thus, we have

$$\begin{aligned} \langle n_{\mathbf{k}, \sigma}^\tau \rangle_{MF} &= n_F \left(\varepsilon_{\mathbf{k}, \sigma}^\tau - \mu + U \sum_{\tau'} \bar{n}_{\bar{\sigma}}^{\tau'} + U \sum_{\tau'} \eta_{\bar{\sigma}}^{\tau'} \right) \\ &= n_F \left(\varepsilon_{\mathbf{k}, \sigma}^\tau - \mu_0 - \delta\mu - \frac{\sigma U}{2} \sum_{\tau', \sigma'} \sigma' \eta_{\sigma'}^{\tau'} \right), \end{aligned}$$

where the second equality holds since Eqs (5.14), (5.26) and (5.39), derived in the main text,

$$\begin{aligned} \sum_{\sigma} \bar{n}_{\sigma}^A &= \sum_{\sigma} \bar{n}_{\sigma}^B = \sum_{\tau} \bar{n}_{\uparrow}^{\tau} = \sum_{\tau} \bar{n}_{\downarrow}^{\tau} = \frac{n}{2}, \\ \sum_{\tau, \sigma} \eta_{\sigma}^{\tau} &= 0, \quad \mu - \frac{U n}{2} = \mu_0 + \delta\mu, \end{aligned}$$

hold. Also,

$$\begin{aligned} \langle \rho_{\mathbf{q}, \sigma}^\tau \rangle_{MF} &= \sum_{\mathbf{k}} \langle \hat{\psi}_{\mathbf{k}+\mathbf{q}, \sigma}^{\tau\dagger} \hat{\psi}_{\mathbf{k}, \sigma}^\tau \rangle_{MF} \\ &= \sum_{\mathbf{k}} \langle n_{\mathbf{k}, \sigma}^\tau \rangle_{MF} \delta_{\mathbf{q}, \mathbf{0}} \\ &= \sum_{\mathbf{k}} n_F \left(\varepsilon_{\mathbf{k}, \sigma}^\tau - \mu_0 - \delta\mu - \frac{\sigma U}{2} \sum_{\tau', \sigma'} \sigma' \eta_{\sigma'}^{\tau'} \right) \delta_{\mathbf{q}, \mathbf{0}}. \end{aligned}$$

At $T \rightarrow 0$ and within the parabolic approximation, similarly to the procedure in the main text, we have

$$\begin{aligned} \langle \rho_{\mathbf{0}, \sigma}^\tau \rangle_{MF} &= N \int_{\varepsilon_\Lambda^{\sigma\tau}}^{-\Delta^{\sigma\tau}} d\varepsilon D^{\sigma\tau}(\varepsilon) n_F \left(\varepsilon - \mu_0 - \delta\mu - \frac{\sigma U}{2} \sum_{\tau', \sigma'} \sigma' \eta_{\sigma'}^{\tau'} \right) \\ &= N D^{\sigma\tau} \left[\min \left(\mu_0 + \delta\mu + \frac{\sigma U}{2} \sum_{\tau', \sigma'} \sigma' \eta_{\sigma'}^{\tau'}, -\Delta^{\sigma\tau} \right) - \varepsilon_\Lambda^{\sigma\tau} \right], \end{aligned}$$

and, for the single-body term,

$$\begin{aligned} \sum_{\mathbf{k}} \epsilon_{\mathbf{k},\sigma}^{\tau} \langle n_{\mathbf{k},\sigma}^{\tau} \rangle_{MF} &= N \int_{\varepsilon_{\Lambda}^{\sigma\tau}}^{-\Delta^{\sigma\tau}} d\varepsilon D^{\sigma\tau}(\varepsilon) \varepsilon n_F \left(\varepsilon - \mu_0 - \delta\mu - \frac{\sigma U}{2} \sum_{\tau',\sigma'} \sigma' \eta_{\sigma'}^{\tau'} \right) \\ &= \frac{1}{2} ND^{\sigma\tau} \left[\min \left(\mu_0 + \delta\mu + \frac{\sigma U}{2} \sum_{\tau',\sigma'} \sigma' \eta_{\sigma'}^{\tau'}, -\Delta^{\sigma\tau} \right)^2 - (\varepsilon_{\Lambda}^{\sigma\tau})^2 \right], \end{aligned}$$

so that the internal energy reads

$$\begin{aligned} E(\{\eta_{\sigma}^{\tau}\}) &= \frac{N}{2} \sum_{\sigma,\tau} D^{\sigma\tau} \left[\min \left(\mu_0 + \delta\mu + \frac{\sigma U}{2} \sum_{\tau',\sigma'} \sigma' \eta_{\sigma'}^{\tau'}, -\Delta^{\sigma\tau} \right)^2 - (\varepsilon_{\Lambda}^{\sigma\tau})^2 \right] \\ &\quad + NU \sum_{\tau,\tau'} D^{\uparrow\tau} \left[\min \left(\mu_0 + \delta\mu + \frac{U}{2} \sum_{\tau'',\sigma} \sigma \eta_{\sigma}^{\tau''}, -\Delta^{\uparrow\tau} \right) - \varepsilon_{\Lambda}^{\uparrow\tau} \right] \\ &\quad \times D^{\downarrow\tau'} \left[\min \left(\mu_0 + \delta\mu - \frac{U}{2} \sum_{\tau'',\sigma} \sigma \eta_{\sigma}^{\tau''}, -\Delta^{\downarrow\tau'} \right) - \varepsilon_{\Lambda}^{\downarrow\tau'} \right]. \end{aligned}$$

We keep this discussion to the low-doping regime described in the main text, in which case the internal energy reads

$$\begin{aligned} E(\xi) &= \frac{N}{2} \left\{ D^> \left[\left(\mu_0 + \frac{U\xi}{2} \right)^2 + \left(\mu_0 - \frac{U\xi}{2} \right)^2 - 2(\varepsilon_{\Lambda}^>)^2 \right] + 2D^< [(\Delta^<)^2 - (\varepsilon_{\Lambda}^<)^2] \right\} \\ &\quad + NU \left\{ (D^>)^2 \left(\mu_0 + \frac{U\xi}{2} - \varepsilon_{\Lambda}^> \right) \left(\mu_0 - \frac{U\xi}{2} - \varepsilon_{\Lambda}^> \right) \right. \\ &\quad \left. + [D^< (\Delta^< + \varepsilon_{\Lambda}^<)]^2 - 2D^> D^< (\mu_0 - \varepsilon_{\Lambda}^>) (\Delta^< + \varepsilon_{\Lambda}^<) \right\}, \end{aligned}$$

where $\xi = \eta_{\uparrow}^A - \eta_{\downarrow}^B$ and we have $\delta\mu = 0$ for the low doping regime. After some algebra, the expression above simplifies to

$$\begin{aligned} E(\xi) &= \frac{N}{4} \left\{ D^> U^2 \xi^2 + 4D^> [(\mu_0)^2 - (\varepsilon_{\Lambda}^>)^2] + 4D^< [(\Delta^<)^2 - (\varepsilon_{\Lambda}^<)^2] \right\} \\ &\quad + NU \left\{ (D^>)^2 \left[(\mu_0 - \varepsilon_{\Lambda}^>)^2 - \left(\frac{U\xi}{2} \right)^2 \right] \right. \\ &\quad \left. + [D^> (\mu_0 - \varepsilon_{\Lambda}^>) - D^< (\Delta^< + \varepsilon_{\Lambda}^<)]^2 - [D^> (\mu_0 - \varepsilon_{\Lambda}^>)]^2 \right\}, \end{aligned}$$

and we can write

$$E(\xi) - E(0) = \frac{1}{4} ND^> U^2 (1 - D^> U) \xi^2,$$

with $E(0)$ a ξ -independent term given by

$$E(0) = NU \left(\frac{n}{2} \right)^2 - N \{ D^> [(\varepsilon_\Lambda^>)^2 - (\mu_0)^2] + D^< [(\varepsilon_\Lambda^<)^2 - (\Delta^<)^2] \} .$$

Clearly, this approach yields qualitatively equal results to the expansion of the imaginary-time action: for $D^>U > 1$ the system will maximize charge imbalance. The mean-field solution of ξ , corresponding to filling the \uparrow -A cone, will be the same as Eq. (5.33).

D.2 Perturbative expansion of the fermionic term in the Hubbard-Stratonovich action

In the main text, we have derived an effective ϕ -field action from the H-S action Eq. (5.7) which, after making the appropriate ansatz, Eqs. (5.16) and (5.20) and expanding, yields

$$F[\{\delta\phi_\sigma^\tau\}] = \text{Tr} \ln \left[1 + \frac{iU}{\hbar} \hat{\mathcal{G}}_0 \sum_{\tau'} \delta\hat{\phi}^{\tau'} \right] = \sum_{n=1}^{+\infty} \frac{(-1)^{n-1}}{n} \left(\frac{iU}{\hbar} \right)^n \sum_{\sigma, \tau} \sum_{k_1 \dots k_{2n}} \prod_{m=1}^{2n-1} \left(\hat{\mathcal{G}}_0 \right)_{k_m, k_{m+1}}^{\tau, \sigma} \left(\sum_{\tau'} \delta\hat{\phi}^{\tau'} \right)_{k_{m+1}, k_{m+2}}^{\bar{\sigma}}, \quad (\text{D.12})$$

with $k_{2n+1} = k_1$. We have $\left(\hat{\mathcal{G}}_0 \right)_{k_m, k_{m+1}}^{\tau, \sigma} = \left(\hat{\mathcal{G}}_0 \right)_{k_m, \sigma}^\tau \delta_{k_m, k_{m+1}}$ and $\left(\sum_{\tau'} \delta\hat{\phi}^{\tau'} \right)_{k_{m+1}, k_{m+2}}^{\bar{\sigma}} = \sum_{\tau'} \delta\phi_{k_{m+2}-k_{m+1}, \bar{\sigma}}^{\tau'} = \sum_{\tau'} i\eta_{\bar{\sigma}}^{\tau'} \delta_{k_{m+1}, k_{m+2}}$, where the last equality is the homogeneity assumption. We find

$$\begin{aligned} F(\{\eta_\sigma^\tau\}) &= \sum_{n=1}^{+\infty} \frac{(-1)^{n-1}}{n} \sum_{\sigma, \tau} \left(-\frac{U}{\hbar} \sum_{\tau'} \eta_{\bar{\sigma}}^{\tau'} \right)^n \sum_{k_1 \dots k_{2n}} \prod_{m=1}^{2n-1} \left(\hat{\mathcal{G}}_0 \right)_{k_m, \sigma}^\tau \delta_{k_m, k_{m+1}} \delta_{k_{m+1}, k_{m+2}} \\ &= - \sum_{n=1}^{+\infty} \frac{1}{n} \left(\frac{U}{\hbar} \right)^n \sum_{\sigma, \tau} \left(\sum_{\tau'} \eta_{\bar{\sigma}}^{\tau'} \right)^n \sum_{k_1 \dots k_n} \prod_{m=1}^{n-1} \left(\hat{\mathcal{G}}_0 \right)_{k_m, \sigma}^\tau \delta_{k_m, k_{m+1}} \\ &= - \sum_{n=1}^{+\infty} \frac{1}{n} \left(\frac{U}{\hbar} \right)^n \sum_{\sigma, \tau} \left(\sum_{\tau'} \eta_{\bar{\sigma}}^{\tau'} \right)^n \sum_k \left[\left(\hat{\mathcal{G}}_0 \right)_{k, \sigma}^\tau \right]^n \\ &= - \sum_{n=1}^{+\infty} \frac{1}{n} \left(\frac{U}{\hbar} \right)^n \sum_{\sigma, \tau} \sum_k \left(\frac{\sum_{\tau'} \eta_{\bar{\sigma}}^{\tau'}}{i\omega_n - \varepsilon_{\mathbf{k}, \sigma}^\tau + \mu_0} \right)^n. \end{aligned}$$

Taking the Matsubara frequency sums, and according to Cauchy's integral formula [118],

$$F(\{\eta_\sigma^\tau\}) = -\beta U \sum_{n=1}^{+\infty} \frac{U^{n-1}}{n!} \sum_{\sigma, \tau} \left(\sum_{\tau'} \eta_{\bar{\sigma}}^{\tau'} \right)^n \sum_{\mathbf{k}} \left(\frac{\partial}{\partial \varepsilon_{\mathbf{k}, \sigma}^\tau} \right)^{n-1} n_F(\varepsilon_{\mathbf{k}, \sigma}^\tau - \mu_0).$$

Prescribing crystal momentum summations to the appropriate integral and noting that, in the $T \rightarrow 0$ limit, $n_F(\varepsilon - \mu_0) \rightarrow \theta(\mu_0 - \varepsilon)$,

$$\begin{aligned} F(\{\eta_\sigma^\tau\}) &= -N\beta U \sum_{\sigma, \tau'} \eta_{\bar{\sigma}}^{\tau'} \sum_\tau \int_{\varepsilon_\Lambda^{\sigma\tau}}^{-\Delta^{\sigma\tau}} d\varepsilon D^{\sigma\tau}(\varepsilon) n_F(\varepsilon_{\mathbf{k},\sigma}^\tau - \mu_0) \\ &\quad - N\beta U \sum_{n=2}^{+\infty} \frac{U^{n-1}}{n!} \sum_\sigma \left(\sum_{\tau'} \eta_{\bar{\sigma}}^{\tau'} \right)^n (-1)^{n-1} \sum_\tau \int_{\varepsilon_\Lambda^{\sigma\tau}}^{-\Delta^{\sigma\tau}} d\varepsilon D^{\sigma\tau}(\varepsilon) \delta^{(n-2)}(\mu_0 - \varepsilon), \end{aligned}$$

and that, for any well-behaved test function f , $\delta^{(n-2)}[f] = (-1)^{n-2} \delta[f^{(n-2)}] = (-1)^{n-2} f^{(n-2)}(0)$, provided that $\mu_0 > \varepsilon_\Lambda^>$, we find

$$\frac{F(\{\eta_\sigma^\tau\})}{N\beta U} = -\frac{n}{2} \sum_{\sigma, \tau} \eta_\sigma^\tau + \sum_{n=2}^{+\infty} \frac{U^{n-1}}{n!} \sum_\sigma \left(\sum_{\tau'} \eta_{\bar{\sigma}}^{\tau'} \right)^n \sum_\nu \theta(-\varepsilon - \Delta^\nu) \left(\frac{d}{d\varepsilon} \right)^{n-2} D^\nu(\varepsilon) \Big|_{\varepsilon=\mu_0},$$

where $\nu \in \{>, <\}$ stands for the cone index defined earlier. Using the charge conservation law Eq. 5.26,

$$\sum_{\sigma, \tau} \eta_\sigma^\tau = 0,$$

yields, for terms of 2nd and higher orders,

$$\begin{aligned} \sum_\sigma \left(\sum_\tau \eta_\sigma^\tau \right)^n &= \frac{1}{2^n} \sum_{\sigma'} \left(\sum_{\tau, \sigma} \eta_\sigma^\tau - \sigma' \sum_{\tau, \sigma} \sigma \eta_\sigma^\tau \right)^n \\ &= \frac{1}{2^n} \sum_{\sigma'} (-\sigma')^n \left(\sum_{\tau, \sigma} \sigma \eta_\sigma^\tau \right)^n \\ &\stackrel{n \text{ even}}{=} \frac{1}{2^{n-1}} \left(\sum_{\tau, \sigma} \sigma \eta_\sigma^\tau \right)^n. \end{aligned}$$

Thus, all odd-power terms vanish and we can write

$$\frac{F(\{\eta_\sigma^\tau\})}{N\beta U} = \sum_{n=1}^{c+1} \frac{1}{(2n)!} \left(\frac{U}{2} \right)^{2n-1} \left(\sum_{\tau, \sigma} \sigma \eta_\sigma^\tau \right)^{2n} \sum_\nu \theta(-\varepsilon - \Delta^\nu) \left(\frac{d}{d\varepsilon} \right)^{2n-2} D^\nu(\varepsilon) \Big|_{\varepsilon=-|\mu_0|}.$$

where $c = \lfloor k/2 \rfloor$ if C^k is the differentiability class of $\{D^\nu\}$ and with $\lfloor \cdot \rfloor$ the floor function, assuming $c = +\infty$ if $\{D^\nu\}$ are C^∞ . Within the mean-field approximation and for a homogenous solution, this is the most general expression for the expansion of the fermionic term of the H-S action. Now, within the range of validity of the parabolic approximation, as expressed by Eq. (5.10), we have $D^\nu(\varepsilon) \equiv D^\nu, \forall \nu$, so that all terms above 2nd order vanish, yielding

$$\frac{F(\{\eta_\sigma^\tau\})}{N\beta U} = \sum_\nu \theta(|\mu_0| - \Delta^\nu) D^\nu \frac{U}{4} \left(\sum_{\tau, \sigma} \sigma \eta_\sigma^\tau \right)^2.$$